FLUID EVOLUTION DURING METAMORPHISM AND UPLIFT OF THE MASSIVE SULFIDE DEPOSITS AT DUCKTOWN, TENNESSEE, U.S.A.

by

Donald Lewis Hall

Dissertation submitted to the Faculty of the
Virginia Polytechnic Institute and State University
in partial fulfillment of the requirements of the degree of

DOCTOR OF PHILOSOPHY
in
Geology

APPROVED:

Robert J. Bodnar, Chairman

James R. Craig

David A. Hewitt

J. Donald Rimstidt

David J. Wesolowski

July, 1989
Blacksburg, Virginia

FLUID EVOLUTION DURING METAMORPHISM AND UPLIFT OF THE MASSIVE SULFIDE DEPOSITS AT DUCKTOWN, TENNESSEE, U. S. A.

by

Donald Lewis Hall Jr.

Committee Chairman: Robert J. Bodnar

Geological Sciences

(ABSTRACT)

The Ducktown mining district, located in the southeastern corner of Tennessee within the Blue Ridge Province of the southern Appalachians, contains some of the largest metamorphosed pyrrhotite-pyrite-rich massive sulfide deposits in the Appalachian-Caledonian orogen. Oxygen isotope temperatures of 530±20°C are consistent with previous estimates based on mineral thermobarometers (540±40°C; 6-7 kb) suggesting that minerals attained oxygen isotopic equilibrium during peak metamorphism and underwent little retrograde exchange. Fluid inclusion and petrologic data do not support the previous interpretation that low $\delta^{18}O$ zones near orebodies are synmetamorphic, rather, a premetamorphic origin is indicated. Integrated fluid/rock ratios were low enough during and after metamorphism that premetamorphic spatial variations in $\delta^{18}O$ were retained. However, hydrogen and carbon isotopes were homogenized throughout the area during or before metamorphism. The low $\delta^{18}O$ zones surrounding the

orebodies appear to have formed during sea-floor hydrothermal activity associated with ore deposition. The $\delta^{18}O$ value of the fluid responsible for ore deposition, assuming a temperature of 300°C, is calculated to be -1 to +2 per mil, consistent with the interpretation that the ore fluid was modified seawater.

Calculation of theoretical C-O-H-S fluid speciation suggests that the fluid in equilibrium with clinopyroxene-bearing rocks was essentially $H_2O + CO_2$ with $XCO_2 = 0.10$. However, primary fluid inclusions located in clinopyroxene contain significant quantities of CH_4. This discrepancy is explained by hydrogen diffusion into primary fluid inclusions and subsequent conversion of CO_2 to CH_4 during uplift in response to an fH_2 gradient between inclusion and matrix fluids. Low δD values of primary fluid inclusions are consistent with diffusive addition of isotopically light hydrogen after trapping.

Secondary inclusions in metamorphic quartz record a complex uplift history involving a variety of fluids in the C-O-H-N-salt system. Isochores calculated for these inclusions constrain the uplift path to have been initially concave toward the temperature axis. Over the pressure range 2.3 to 1.0 kb the uplift path became nearly isothermal at 215±20°C. Immiscible H_2O-CH_4-N_2-NaCl fluids present during the isothermal stage of the uplift history were derived during Alleghanian thrusting by expulsion of pore fluids and maturation of organic matter in lower plate sedimentary rocks proposed to underlie the deposits. Average uplift rates of 0.1 mm/yr are suggested by the uplift path and available geochronologic data.

ACKNOWLEDGEMENTS

First, I would like to thank my parents and who (in spite of their better judgement) supported my decision to (1) continue my seemingly indefinite unemployment and (2) leave a place where the sun shines 360 days a year for a place where the temperature and relative humidity are the same number. All things considered, it wasn't a bad trade - I received a daughter and a degree out of the deal.

I owe a great deal to my advisor Bob Bodnar who taught me how to be a successful contributor to the scientific community and gave me free reign to pursue my interests in various unrelated aspects of fluid inclusion research.

suggested this project to me and I thank him for allowing me to get involved with one of his pet ore deposits. A great debt is owed who permitted me and other Bodnarians to use (at times ransack) his hydrothermal equipment. has been a source of many fruitful discussions and his constant good humor is appreciated. I would also like to thank and for teaching me how to use isotope extraction lines, for helping me interpret isotope data and for putting up with me during my stay at Oak Ridge. and contributed valuable discussions to this project.

This research would not have been possible without the generosity of the Tennessee Chemical Co. and , who allowed me to collect samples from the orebodies. donated his valuable time by introducing me to the deposit and discussing various aspects of this project.

who studied the distribution and compositions of silicate, oxide and sulfide minerals at Ducktown for his Ph.D. lent me his thesis thin section

collection for fluid inclusion reconnaissance. drafted many figures for me over the last four years, suffered through my ignorance of photography, and fixed and made things, and kindly helped with microprobe analyses.

My stay here has been made more bearable by other friends I have met. Their contributions to this project are too many to enumerate. I have collaborated with on most of the projects that I have been involved with, and his friendship will endure long after we both leave this place. , one of the most thoughtful people I have ever met, has been a source of information, home cooking, elbow grease, and he climbs well. I have had many stimulating discussions with Matt on subjects in metamorphic petrology and structural geology. I learned about placer gold from and collaboration with him is the only claim I have to studying an economic mineral deposit. who can rebuild a Z-car from parts no bigger than your thumb, can also turn a computer program as large as a tractor trailer into several sheets of paper that accomplish the same task. helped me develop some of the computer programs that were used to do speciation calculations. Other friends who have lent support, good humor, outrageous behavior, etc., are

and

and , and .

Finally, the biggest debt is owed my wife who left her family and a productive career to work in a grocery store. She has done more than her share of the work to-date in raising our new daughter , and if not for her unselfishness I would never have attempted this degree.

TABLE OF CONTENTS

LIST OF FIGURES

LIST OF TABLES

CHAPTER I

INTRODUCTION

Metamorphosed pyrrhotite-pyrite-rich massive sulfide deposits, some of the largest and best studied of which are located at Ducktown, Tennessee, occur throughout the Appalachians (Fig. 1). The Ducktown mining district is located in the southeast corner of Tennessee (N35 01 lat. and W084 26 long.) in the Blue Ridge Province of the Southern Appalachians (Fig. 1). The eight orebodies, which comprise the deposit, vary from massive to disseminated but consist on average of 65 vol% massive sulfide and 35 vol% gangue. Massive sulfide ranges from pyrrhotite-rich to pyrite-rich but consists in general of 60 vol% pyrrhotite, 30 vol% pyrite, 4 vol% chalcopyrite, 4 vol% sphalerite and 2 vol% magnetite (Magee, 1968). The host rocks are dominantly metagraywackes and quartz-mica schists with lesser quartzite, metaconglomerate and calc-silicate hornfels. Several lithologies have been recorded only near the orebodies, including chlorite schist, containing dominantly chlorite; muscovite schist consisting dominantly of fine grained muscovite; biotite schist; plagioclase-rich rock and spessartine-rich rock. Similar lithologies have been recorded near other metamorphosed massive sulfides (e.g., Gair & Slack, 1984) and have been interpreted to represent either metamorphosed volcaniclastic rocks, or metamorphosed equivalents of alteration zones and exhalites typically found around unmetamorphosed volcanogenic massive sulfide deposits (Henry, Craig & Gilbert, 1979; Gair & Slack, 1984).

It is now generally accepted that the massive sulfides were deposited

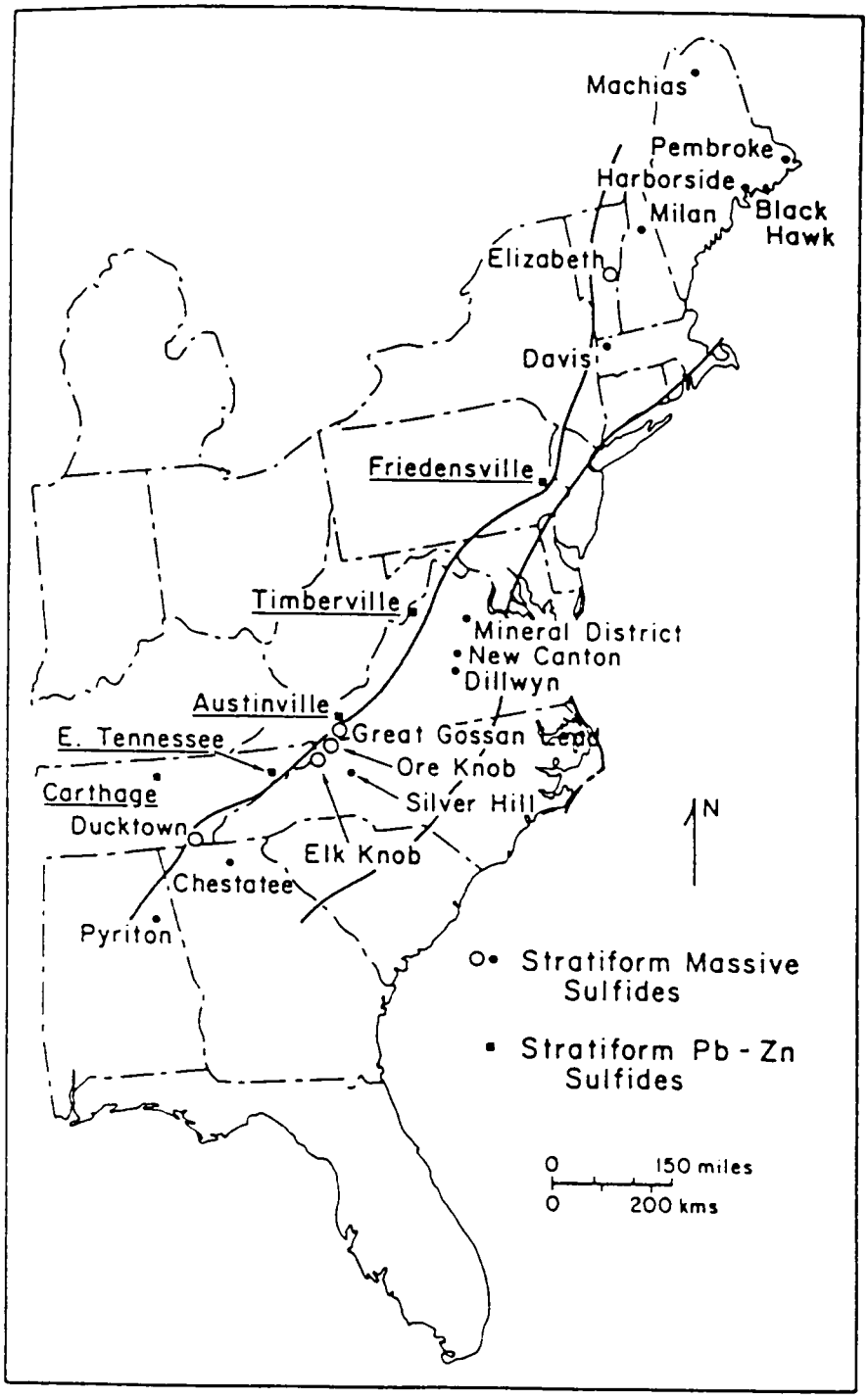

Figure 1. Index map of the eastern U. S. showing the locations of stratiform massive sulfide ore deposits in the Appalachians. Open circles are Ducktown-type stratiform massive sulfide deposits. From Craig (1983).

syngenetically with enclosing sediments during sea-floor hydrothermal activity (Mauger, 1972; Addy, 1973; Nesbitt, 1979; this study). Consequently, they are classified as volcanogenic massive sulfide (VMS) deposits, although some aspects of their genesis are not clear. The orebodies at Ducktown exhibit important similarities to active seafloor hydrothermal deposits, such as are forming in the Red Sea and Guaymas Basin, to younger, relatively undisturbed VMS deposits such as the Kuroko and Besshi deposits, and to older massive sulfide deposits such as the Jerome deposit.

The Ducktown orebodies and their host rocks have undergone polyphase regional metamorphism associated with the closing of the Iapetus ocean during the Paleozoic (Rankin, 1975). At least five episodes of deformation and three episodes of metamorphism have been recognized (Holcombe, 1973; Addy & Ypma, 1977). Pressure-temperature conditions of peak metamorphism have been estimated to be 6-7 kb and 500-580°C (Nesbitt & Essene, 1982; Brooker, Craig & Rimstidt, 1987).

Despite the importance of these ores and their long history of exploitation, many questions remain unanswered regarding their origin and their behavior during metamorphism. Many of these questions could be addressed if the temporal and spatial chemical evolution history of fluids attending burial, metamorphism and uplift of these deposits were known. The presence of these orebodies may exert fundamental controls on fluid composition during metamorphism and hence affect the stabilities and compositions of various silicate minerals (Popp, Gilbert & Craig, 1977; Tso, Gilbert & Craig, 1979). The Appalachian deposits, as well as their Caledonian equivalents, show

many similarities in mineralogy, chemistry, occurrence and metamorphic grade, suggesting that a comprehensive study of fluid evolution in one deposit would be applicable to others as well.

To date, no detailed fluid inclusion studies have been conducted on this important class of ore deposit. The Ducktown deposits provide an excellent opportunity for studying the fluids in metamorphosed massive sulfide ores because large fluid inclusions suitable for study are found in and around the orebodies, and because several recent detailed geologic and geochemical studies have provided a sound basis for understanding the relationship between the ores and adjacent rocks and for interpreting the fluid inclusion data. Fluid inclusions provide one of the best tools available for determining properties of fluids associated with various geologic processes, and can provide valuable information on the nature of fluids attending metamorphism of Ducktown and other massive sulfide deposits in the Appalachians. While mineral equilibria can sometimes be used to define the mole fractions or fugacities of some species in the fluid, notably H_2O, CO_2, O_2 and S_2, other important constituents, such as Na, K, Ca, and CH_4 and H_2S are not adequately constrained by mineral equilibria alone. Studies of fluid inclusions may provide more detailed fluid composition data and may be more sensitive to temporat/spatial variations in fluid composition as compared with fluid compositions obtained from mineral equilibria calculations.

The study of fluid inclusions in metamorphic rocks has contributed substantially to understanding the P-V-T-X properties of fluids in the crust and upper mantle. Despite the advancements however, such studies often

produce results that are difficult to reconcile with other petrologic constraints. Among the potential problems associated with fluid inclusion studies of medium to high grade metamorphic rocks are the small size and general lack of usable fluid inclusions in samples (Roedder, 1984). The fluid inclusions present are frequently texturally secondary and it is often impossible to relate a given plane of inclusions to a particular phase of metamorphism or deformation. Hence, they cannot be unambiguously compared to results obtained from mineral equilibria. Pressure differentials between inclusion and host due to non-isochoric uplift paths may result in internal overpressures which exceed the strength of the host crystal causing decrepitation of parent inclusions and formation of satellite inclusions in "decrepitation clusters" (Swanenberg, 1980). The primary factor influencing decrepitation in a given mineral is the size (volume) of the inclusion (Bodnar, Binns & Hall, 1989) and an inverse relationship between inclusion size and density (homogenization temperature) should be observed. Sterner & Bodnar (1989) have shown that internal underpressures can result in density increases and formation of "implosion haloes".

Although diffusion of oxygen and hydrogen through minerals is well documented (e.g., Muelenbachs and Kushiro, 1974; Giletti and Anderson, 1975; Giletti and Yund, 1984; Giletti, Semet & Yund, 1978; Kronenberg, Kirby, Aines & Rossman, 1986) and the possibility of inclusion "leakage" via diffusion (e.g., of hydrogen) has long been suspected (e.g., Roedder & Skinner, 1968), only recently has experimental evidence for compositional changes in fluid inclusions as a result of diffusion been forthcoming. Pasteris & Wanamaker (1988) demonstrated that oxygen diffusion into and out of

CO_2-rich fluid inclusions in San Carlos olivine could be effected by annealing at 1000°-1400°C. The direction of diffusion was consistent with the fO_2 gradient between the inclusions and the controlled external environment. Sterner, Hall & Bodnar (1988b) and Hall, Sterner & Bodnar (1989) have shown that diffusive loss of molecular water from synthetic fluid inclusions in natural quartz can occur at 825°C and may be important in some metamorphic rocks such as isothermally uplifted granulites. If saline aqueous inclusions are present in samples from these geologic environments, an inverse relationship between inclusion size and salinity should be recognized. In addition, selective loss of water from carbonic fluid inclusions may explain the presence of nearly pure CO_2 inclusions in these terranes. Recently, CO_2-CH_4-H_2-H_2O fluid inclusions have been produced by diffusion of hydrogen into CO_2-H_2O inclusions at 650-825°C (D. L. Hall, S. M. Sterner & R. J. Bodnar, unpublished data). It has been postulated that this mechanism may explain significant CH_4 contents in some CO_2-rich fluid inclusion from granulites (Hall & Bodnar, 1989).

A common problem in metamorphic fluid inclusion studies is the apparent lack of agreement between inclusion compositions and theoretical calculations of fluid speciation. Speciation calculations, usually conducted for the C-O-H±S system, have been used to constrain metamorphic fluid compositions at given P-T-fO_2-fS_2-a_C conditions (French, 1966; Eugster & Skippen, 1967; Holloway, 1977; Ohmoto & Kerrick, 1977) and have demonstrated that systematic changes in speciation are to be expected as the above intensive parameters change. These changes are qualitatively corroborated by metamorphic mineral assemblages sensitive to fluid

composition and by some, but certainly not all, fluid inclusion studies . In some cases the contradiction may be related to non-synchronaeity of inclusion formation and peak metamorphism or to errors in P-T estimates of metamorphism. In other instances there appears to be no reason why calculated and observed compositions should not agree (Casquet, 1986; Kreulen, 1987; Thomas & Spooner, 1988). Suggested explanations for the discrepancies include: 1) uncertainties associated with the calculation of C-O-H-S fluid equilibria, estimation of P-T-fO_2-fS_2-a_C conditions of metamorphism, and estimation of fluid inclusion compositions; 2) continued re-equilibration of fluid species within inclusions during cooling and decompression of the metamorphic terrane (Dubessy, 1984); 3) trapping of a fluid that is out of equilibrium with the surrounding rocks; 4) selective trapping of one phase of an immiscible fluid (Mullis, 1979); and 5) post-trapping diffusive loss of fluid constituents (e.g., H_2, O_2, H_2O) from inclusions during uplift.

The first part of this study reports on fluid inclusions associated with the metamorphosed massive sulfide deposits at Ducktown, Tennessee, U.S.A. In addition to deducing P-T-X relationships in fluid inclusions, the inclusions were examined for evidence of post-trapping volumetric or compositional re-equilibration. Data from fluid inclusions are combined with tectonic and geochronologic data to put the uplift path into an absolute time framework and to derive average uplift rates. In the second part of this study, the compositions of primary fluid inclusions, which occur in clinopyroxene, are compared to C-O-H-S fluid speciation calculations and a model for hydrogen diffusion into primary fluid inclusions is presented to explain the

discrepancies between calculated and observed fluid compositions. In the third part of this study, C-O isotope data on quartz and calcite from the Cherokee and Calloway ore bodies, carbon isotope data from primary and secondary graphite from the ore zones and country rocks, and C-O-H isotope data from primary and secondary fluid inclusions are combined with the previous silicate C-O-H isotope data of Addy and Ypma (1977), more recent information on the fractionation of oxygen between metamorphic minerals, new insights on the origin of Ducktown-type deposits, and the conclusions reached during the other two parts of the study to develop a model for fluid evolution during metamorphism and uplift of this deposit.

REFERENCES

Addy, S. K., 1973. The problem of ore genesis at Ducktown, Tennessee. Interpretation of stable isotopes ($^{18}O/^{16}O$, $^{13}C/^{12}C$ and D/H), microprobe, and textural data. Ph.D. thesis, Columbia Univ., New York.

Addy, S. K. & Ypma, P. J. M., 1977. Origin of massive sulfide deposits at Ducktown, Tennessee: An oxygen, carbon, and hydrogen isotope study. *Economic Geology*, **72**,1245-1268.

Bodnar, R. J., Binns, P. R. & Hall, D. L., 1989. Synthetic fluid inclusions. VI. Quantitative evaluation of the decrepitation behavior of fluid inclusions in quartz at one atmosphere confining pressure. *Journal of Metamorphic Geology*, **6**, 229-242.

Brooker, D. D., Craig, J. R. & Rimstidt, J. D., 1987. Ore metamorphism and pyrite porphyroblast development at the Cherokee Mine, Ducktown, Tennessee. *Economic Geology*, **82**, 72-86.

Casquet, C., 1986. C-O-H-N fluids in quartz segregations from a major ductile shear zone: the Berzosa fault, Spanish Central System. *Journal of Metamorphic Geology*, **4**, 117-130.

Craig, J. R., 1983. Metamorphic features in Appalachian massive sulfides. *Mineralogical Magazine*, **47**, 515-525.

Dubessy, J., 1984. Simulation des equilibres chimiques dans le systeme COH. Consequences methodologiques pour les inclusions fluides. *Bull. Mineral.*, **107**, 155-168.

Eugster, H. P. & Skippen, G. B., 1967. Igneous and metamorphic reactions involving gas equilibria. In *Researches in Geochemistry, II* (ed Abelson, P. H.). New York, John Wiley and Sons, 942-520.

French, B. M., 1966. Some geological implications of equilibrium between graphite and a C-H-O gas phase at high temperatures and pressures. *Reviews of Geophysics*, **4**, 223-253.

Gair, J. E. & Slack, J. F., 1984. Deformation, geochemistry, and origin of massive sulfide deposits, Gossan Lead District, Virginia. *Economic Geology*, **79**, 1483-1520.

Giletti, B. J. & Anderson, T. F., 1975. Studies in diffusion, II. Oxygen in phlogopite mica. *Earth and Planetary Science Letters*, **28**, 225-238.

Gilletti, B. J. & Yund, R. A., 1984. Oxygen diffusion in quartz. *Journal of Geophysical Research*, **89**, 4039-4046.

Giletti, B. J., Semet, M. P. & Yund, R. A., 1978. Studies in diffusion, III. Oxygen in feldspars, an ion microprobe determination. *Geochimica et Cosmochimica Acta*, **42**, 45-57.

Hall, D. L. & Bodnar, R. J., 1989. Methane in fluid inclusions from granulites: A product of hydrogen diffusion?. *Geochimica et Cosmochimica Acta* (in review).

Hall, D. L., Sterner, S. M. & Bodnar, R. J., 1989. Fluid inclusions in regional metamorphic rocks: experimental evidence for post-entrapment volumetric and compositional modifications (abstr.). *10th European Current Research on Fluid Inclusions, Royal School of Mines, Imperial College, University of London*, 44.

Henry, D. K.. Craig, J. R. & Gilbert, M. C., 1979. Ore mineralogy of the Great Gossan Lead, Virginia. *Economic Geology*, **74**, 645-656.

Holcombe, R. J., 1973. Mesoscopic and microscopic analysis of deformation and metamorphism near Ducktown, Tennessee. Ph. D. Thesis, Stanford University, 225 p.

Holloway, J. R., 1977. Fugacity and activity of molecular species in supercritical fluids. In *Thermodynamics in Geology* (ed Fraser, D. G.). Dordrecht, D. Reidel Publishing Company, 161-181.

Kreulen, R., 1987. Thermodynamic calculations of the C-O-H system applied to fluid inclusions: Are fluid inclusions unbiased samples of ancient fluids? *Chemical Geology*, **61**, 59-64.

Kronenberg, A. K., Kirby, S. H., Aines, R. D. & Rossman, G. R., 1986. Solubility and diffusional uptake of hydrogen in quartz at high water pressures: Implications for hydrolytic weakening. *Journal of Geophysical Research*, **91**, 12723-12744.

Magee, M., 1968. Geology and ore deppsits of the Ducktown district, Tennessee. In *Ore deposits of the United States: 1933-1967* (ed Ridge, J. D.). *American Institute of Mining, Metallurgical, and Petroleum Engineers, Inc.*, 207-241.

Mauger, R. L., 1972. A sulfur isotope study of the Ducktown Tennessee District, U.S.A. *Economic Geology*, **67**, 497-510.

Muelenbachs, K. & Kushiro, I., 1974. Oxygen isotope exchange and equilibrium of silicates with CO_2 and O_2. *Carnegie Institute Washington, D. C., Yearbook*, **73**, 232-236.

Mullis, J., 1979. The system methane-water as a geologic thermometer and barometer from the external part of the Central Alps. *Bulletin de Mineralogie*, **102**, 526-536.

Nesbitt, B. E., 1979. Regional metamorphism of the Ducktown, Tennessee massive sulfides and adjoining portions of the Blue Ridge Province. Ph. D Thesis. Univerisity of Michigan, 216 p.

Nesbitt, B. E. & Essene, E. J., 1982. Metamorphic thermometry and barometry of a portion of the southern Blue Ridge province. *American Journal of Science*, **282**, 701-729.

Ohmoto, H. & Kerrick, D., 1977. Devolatilization equilibria in graphitic systems. *American Journal of Science*, **277**, 1013-1044.

Pasteris, J. D. & Wanamaker, B. J., 1988. Laser raman microprobe analysis of experimentally re-equilibrated fluid inclusions in olivine: Some implications for mantle fluids. *American Mineralogist*, **73**, 1074-1088.

Popp, R. D., Gilbert, M. C. & Craig, J. R., 1977. Stability of Fe-Mg amphiboles with respect to sulfur fugacity. *American Mineralogist*, **62**, 13-20.

Rankin, D. W., 1975. The continental margin of eastern North America in the Southern Appalchians: the opening and closing of the proto-Atlantic ocean. *American Journal of Science*, **275-A**, 298-336.

Roedder, E., 1984. *Fluid inclusions*. Mineralogical Society of America, Reviews in Mineralogy, **12**, 644 p.

Roedder, E. & Skinner, B. J., 1968. Experimental evidence that fluid inclusions do not leak. *Economic Geology*, **63**, 715-730.

Sterner, S. M. & Bodnar, R. J., 1989. Synthetic fluid inclusions - VII. Re-equilibration of fluid inclusions in quartz during laboratory-simulated burial and uplift. *Journal of Metamorphic Geology*,**7**, 243-260.

Sterner, S. M., Hall, D. L. & Bodnar, R. J., 1988. Post-entrapment compositional changes in fluid inclusions: Experimental evidence for water diffusion in quartz (abstr.). *Geological Society of America Abstracts with Programs*, **20**, A100.

Swanenberg, H. E. C., 1980. Fluid inclusions in high-grade metamorphic rocks from S. W. Norway. *Geologica Ultraiectina, Univ. Utrecht.*, **25**, 147p.

Thomas, A. V. & Spooner, E. T. C., 1988. Fluid inclusions in the system H_2O-CH_4-NaCl-CO_2 from metasomatic tourmaline within the border unit of the Tanco zoned granitic pegmatite, S. E. Manitoba. *Geochimica et Cosmochimica Acta*, **52**, 1065-1076.

Tso, J. L., Gilbert, M. C. & Craig, J. R., 1979. Sulfidation of synthetic biotite. *American Mineralogist*, **64**, 304-316.

CHAPTER II

CONSTRAINTS FROM FLUID INCLUSIONS

INTRODUCTION

Metamorphosed pyrrhotite-pyrite-rich massive sulfide deposits, some of the largest and best studied of which are located at Ducktown, Tennessee, occur throughout the Appalachian-Caledonian orogen (Fig. 1). Despite the importance of these ores and their long history of exploitation, many questions remain unanswered regarding their origin and their behavior during metamorphism. Many of these questions could be addressed if the temporal and spatial chemical evolution history of fluids attending burial, metamorphism and uplift of these deposits were known. The presence of these orebodies may exert fundamental controls on fluid composition during metamorphism and hence affect the stabilities and compositions of various silicate minerals (Popp, Gilbert & Craig, 1977; Tso, Gilbert & Craig, 1979).

The Appalachian deposits, as well as their Caledonian equivalents, show many similarities in mineralogy, chemistry, occurrence and metamorphic grade, suggesting that a comprehensive study of fluid evolution in one deposit would be applicable to others as well. Fluid inclusions provide one of the best tools available for determining properties of fluids associated with various geologic processes, and can provide valuable information on the nature of fluids attending metamorphism of Ducktown and other massive sulfide deposits in the Appalachians. While mineral equilibria can sometimes be used to define the mole fractions or fugacities of some species in the fluid,

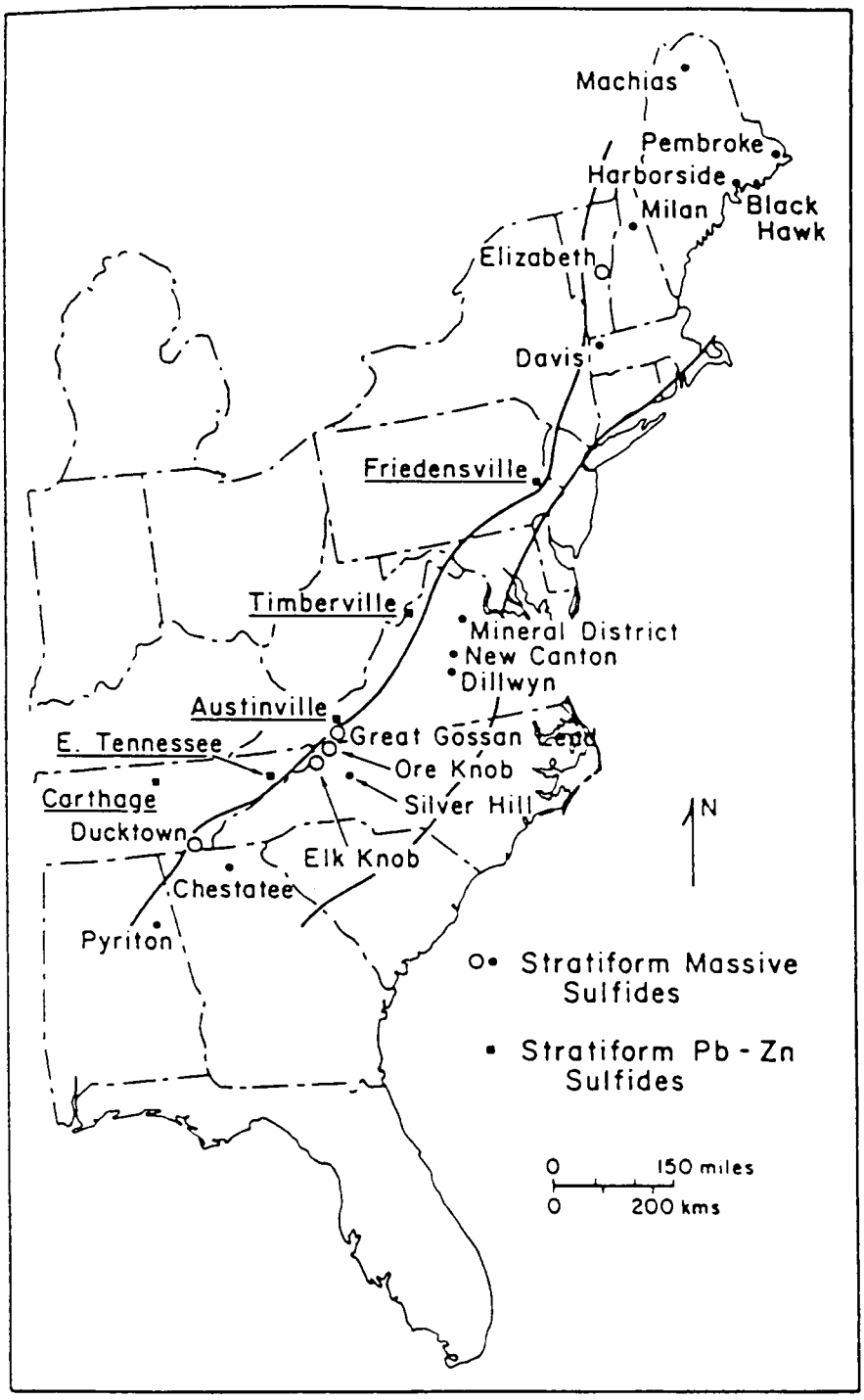

Figure 1. Index map of the eastern U. S. showing the locations of stratiform massive sulfide ore deposits in the Appalachians. Open circles are Ducktown-type stratiform massive sulfide deposits. From Craig (1983).

notably H_2O, CO_2, O_2 and S_2, other important constituents, such as Na, K, Ca, and CH_4 and H_2S are not adequately constrained by mineral equilibria alone. Studies of fluid inclusions may provide more detailed fluid composition data and may be more sensitive to temporat/spatial variations in fluid composition as compared with fluid compositions obtained from mineral equilibria calculations.

To date, no detailed fluid inclusion studies have been conducted on this important class of ore deposit. The Ducktown deposits provide an excellent opportunity for studying the fluids in metamorphosed massive sulfide ores because large fluid inclusions suitable for study are found in and around the orebodies, and because several recent detailed geologic and geochemical studies have provided a sound basis for understanding the relationship between the ores and adjacent rocks and for interpreting the fluid inclusion data. This study reports on fluid inclusions associated with this deposit. In addition to deducing P-T-X relationships in fluid inclusions, the inclusions were studied to see if they show evidence of post-trapping volumetric or compositional re-equilibration. Data from fluid inclusions are combined with tectonic and geochronologic data to put the uplift path into an absolute time framework and to derive average uplift rates.

The study of fluid inclusions in metamorphic rocks has contributed substantially to understanding the P-V-T-X properties of fluids in the crust and upper mantle. Despite the advancements however, such studies often produce results that are difficult to reconcile with other petrologic constraints. Among the potential problems associated with fluid inclusion studies of medium to high grade metamorphic rocks are the small size and general lack

of usable fluid inclusions in samples (Roedder, 1984). The fluid inclusions present are frequently texturally secondary and it is often impossible to relate a given plane of inclusions to a particular phase of metamorphism or deformation. Hence, they cannot be unambiguously compared to results obtained from mineral equilibria. Pressure differentials between inclusion and host due to non-isochoric uplift paths may result in internal overpressures which exceed the strength of the host crystal causing decrepitation of parent inclusions and formation of satellite inclusions in "decrepitation clusters" (Swanenberg, 1980). The primary factor influencing decrepitation in a given mineral is the size (volume) of the inclusion (Bodnar, Binns & Hall, 1989) and an inverse relationship between inclusion size and density (homogenization temperature) should be observed. Sterner & Bodnar (1989) have shown that internal underpressures can result in density increases and formation of "implosion haloes".

Although diffusion of oxygen and hydrogen through minerals is well documented (e.g., Muelenbachs and Kushiro, 1974; Giletti and Anderson, 1975; Giletti and Yund, 1984; Giletti, Semet & Yund, 1978; Kronenberg, Kirby, Aines & Rossman, 1986) and the possibility of inclusion "leakage" via diffusion (e.g. of hydrogen) has long been suspected (e.g., Roedder & Skinner, 1968), only recently has experimental evidence for compositional changes in fluid inclusions as a result of diffusion been forthcoming. Pasteris & Wanamaker (1988) demonstrated that oxygen diffusion into and out of CO_2-rich fluid inclusions in San Carlos olivine could be effected by annealing at 1000°-1400°C. The direction of diffusion was consistent with the fO_2 gradient between the inclusions and the controlled external environment.

Sterner, Hall & Bodnar (1988b) and Hall, Sterner & Bodnar (1989) have shown that diffusive loss of molecular water from synthetic fluid inclusions in natural quartz can occur at 825°C and may be important in some metamorphic rocks such as isothermally uplifted granulites. If saline aqueous inclusions are present in such situations, an inverse relationship between inclusion size and salinity should be recognized. In addition, selective loss of water from carbonic fluid inclusions may explain the presence of nearly pure CO_2 inclusions in these terranes. Recently, CO_2-CH_4-H_2-H_2O fluid inclusions have been produced by diffusion of hydrogen into CO_2-H_2O inclusions at 825°C (D. L. Hall, S. M. Sterner & R. J. Bodnar, unpublished data). This process has been postulated as a mechanism to explain significant CH_4 contents in some CO_2-rich fluid inclusion from granulites (Hall & Bodnar, 1989).

A common problem in metamorphic fluid inclusion studies is the apparent lack of agreement between inclusion compositions and theoretical calculations of fluid speciation. Speciation calculations, usually conducted for the C-O-H±S system, have been used to constrain metamorphic fluid compositions at given P-T-fO_2-fS_2-a_C conditions (French, 1966; Eugster & Skippen, 1967; Holloway, 1977; Ohmoto & Kerrick, 1977) and have demonstrated that systematic changes in speciation are to be expected as the above intensive parameters change. These changes are qualitatively corroborated by metamorphic mineral assemblages sensitive to fluid composition and by some, but certainly not all, fluid inclusion studies . In some cases the contradiction may be related to non-synchronaeity of inclusion formation and peak metamorphism or to errors in P-T estimates of

metamorphism. In other instances there is no apparent reason why calculated and observed compositions should not agree (Casquet, 1986; Kreulen, 1987; Thomas & Spooner, 1988). Suggested explanations for the discrepancies include: 1) uncertainties associated with the calculation of C-O-H-S fluid equilibria, estimation of P-T-fO_2-fS_2-a_C conditions of metamorphism, and estimation of fluid inclusion compositions; 2) continued reaction of fluid species within inclusions during cooling and decompression of the metamorphic terrane (Dubessy, 1984); 3) trapping of a fluid that is out of equilibrium with the surrounding rocks; 4) selective trapping of one phase of an immiscible fluid (Mullis, 1979); and 5) post-trapping diffusive loss of fluid constituents (e.g., H_2, O_2, H_2O) from inclusions during uplift.

GEOLOGICAL SETTING

The Ducktown mining district is located in the southeast corner of Tennessee (N35 01 lat. and W084 26 long.) in the Blue Ridge Province of the Southern Appalachians (Fig. 1). Eight major orebodies ranging in size from 250,000 to 70,000,000 tons (180,000,000 tons total) are contained within the Late Precambrian Copperhill Formation of the Great Smoky Group within the Ocoee Series (Fig. 2). Detailed stratigraphic studies have been conducted by Emmons & Laney (1926), Magee (1968) and Holcombe (1973). The orebodies are located within one to three stratigraphic horizons but are difficult to correlate due to the effects of deformation (Fig. 2). The host rocks are dominantly metagraywackes and quartz-mica schists with lesser quartzite, metaconglomerate and calc-silicate hornfels. The latter contains

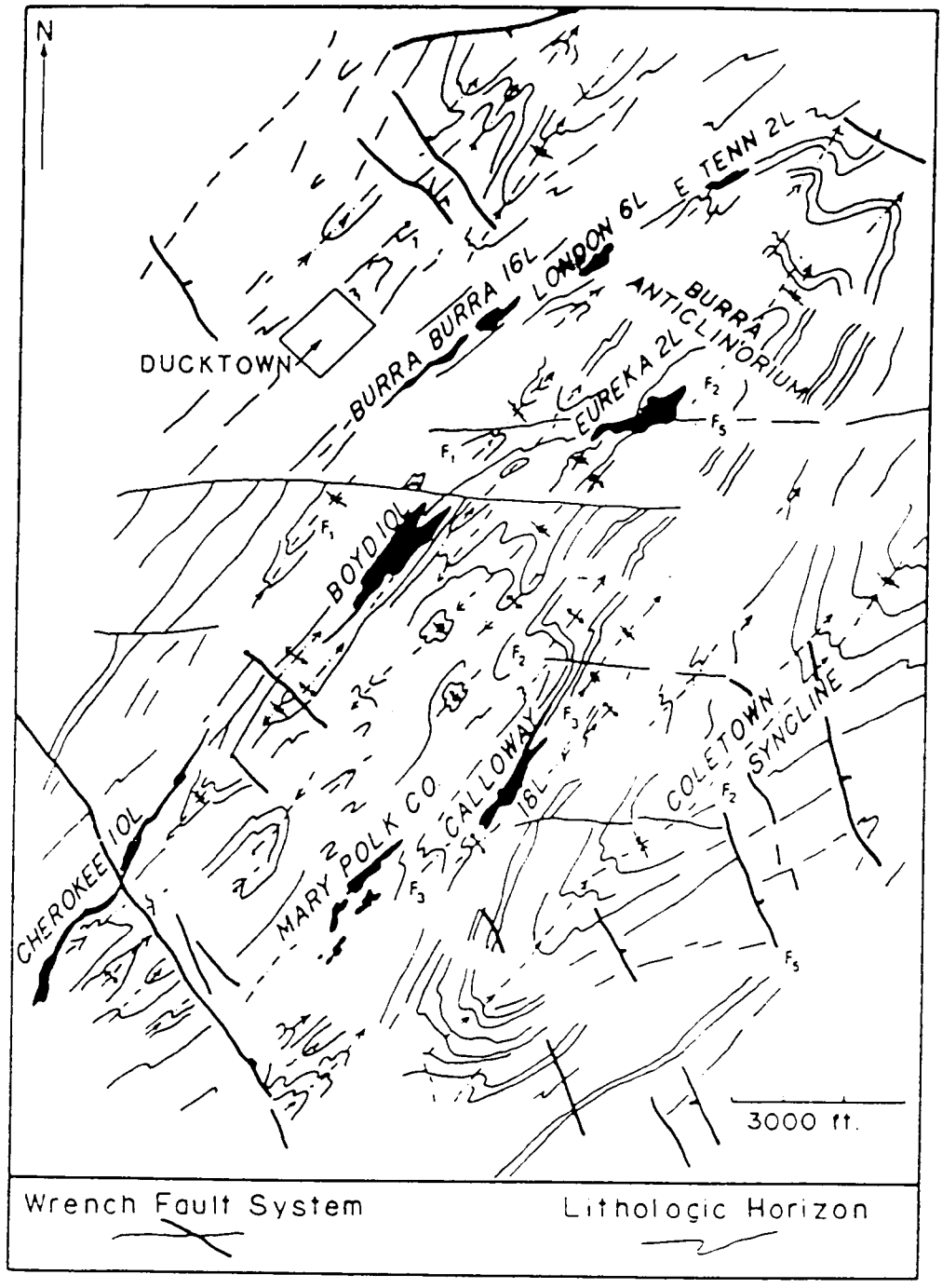

Figure 2. Detailed structural map of the Ducktown mining district showing the distribution of the orebodies (black) and lithologic units (thin lines). Also shown are megascopic structural features. F1-F5 correspond to the deformation events shown in Figure 3. (From Addy & Ypma, 1977).

plagioclase, quartz, calcite, clinozoisite, hornblende, garnet and sphene, occurs as irregular podlike masses within metagraywacke, and may represent metamorphosed calcareous concretions (Hadley & Goldsmith, 1963). In addition, several lithologies have been recorded only near the orebodies, including chlorite schist, containing dominantly chlorite; muscovite schist consisting dominantly of fine grained muscovite; biotite schist; plagioclase-rich rock and spessartine-rich rock. Similar lithologies have been recorded near other metamorphosed massive sulfides (e.g., Gair & Slack, 1984) and have been interpreted to represent either metamorphosed volcaniclastic rocks, or metamorphosed equivalents of the alteration zones and exhalites which are typically found around unmetamorphosed volcanogenic massive sulfide deposits (Henry, Craig & Gilbert, 1979; Gair & Slack, 1984).

The orebodies vary from massive to disseminated but consist on average of 65 vol% massive sulfide and 35 vol% gangue. The massive sulfide ranges from pyrrhotite-rich to pyrite-rich but consists in general of 60 vol% pyrrhotite, 30 vol% pyrite, 4 vol% chalcopyrite, 4 vol% sphalerite and 2 vol% magnetite (Magee, 1968). Other reported metallic phases include galena, molybdenite, tetrahedrite, native bismuth, cubanite, stannite, bornite, rutile and ilmenite. Traces of gold and silver have been reported from assays but the mineralogic hosts for these metals remain unknown as no discrete precious-metal-bearing phase has ever been reported. Assays of samples from ore zones average 35.4 wt% Fe, 24.3 wt% S, 1.04 wt% Cu, and 0.89 wt% Zn (Slater, 1982). Gangue minerals include tremolite-actinolite, cummingtonite, biotite, muscovite, stilpnomelane, chlorite, quartz, calcite, dolomite, rhodochrosite,

talc, clinopyroxene, plagioclase, garnet, epidote group minerals, anhydrite and rhodonite.

The Ocoee Series consists of at least 12 km of marine clastic rocks deposited in a large, rapidly subsiding basin while adjacent areas were being uplifted (Rodgers, 1972). The Great Smoky Group, within which the massive sulfides were deposited, represents deep water turbidites with source areas to the northeast (Hadley, 1970). Evidence for cogenetic volcanism during sedimentation of the Ocoee Series is sparse, as little volcanic or volcaniclastic material is recognized in the statigraphic record (Rankin, 1976). Rankin (1975) has suggested that the absence of volcanic rocks in the Ocoee reflects deposition in a series of grabens to the west (cratonward) of the actual opening of the Precambrian Iapetus ocean. Thus, no *in situ* production of oceanic crust occurred within these grabens. However, amphibolite bodies that have been found have been interpreted to be metamorphosed synsedimentary diabase sills and dikes. These amphibolites have the geochemical signature of olivine tholeiites and are thought to have been emplaced during intracratonic rifting in the early stages of development of Iapetus (Lawson & Misra, 1985).

The Ducktown orebodies and their host rocks have undergone polyphase regional metamorphism associated with the closing of Iapetus during the Paleozoic (Rankin, 1975). Holcombe (1973) and Addy & Ypma (1977) have recognized at least five episodes of deformation (F1-F5) and three episodes of metamorphism (M1-M3) (Fig. 3). The M1-F1 event, which reached garnet grade and produced large open folds in lower grade areas and tight isoclinal folds in higher grade areas, occurred during the Taconic orogeny (480-440

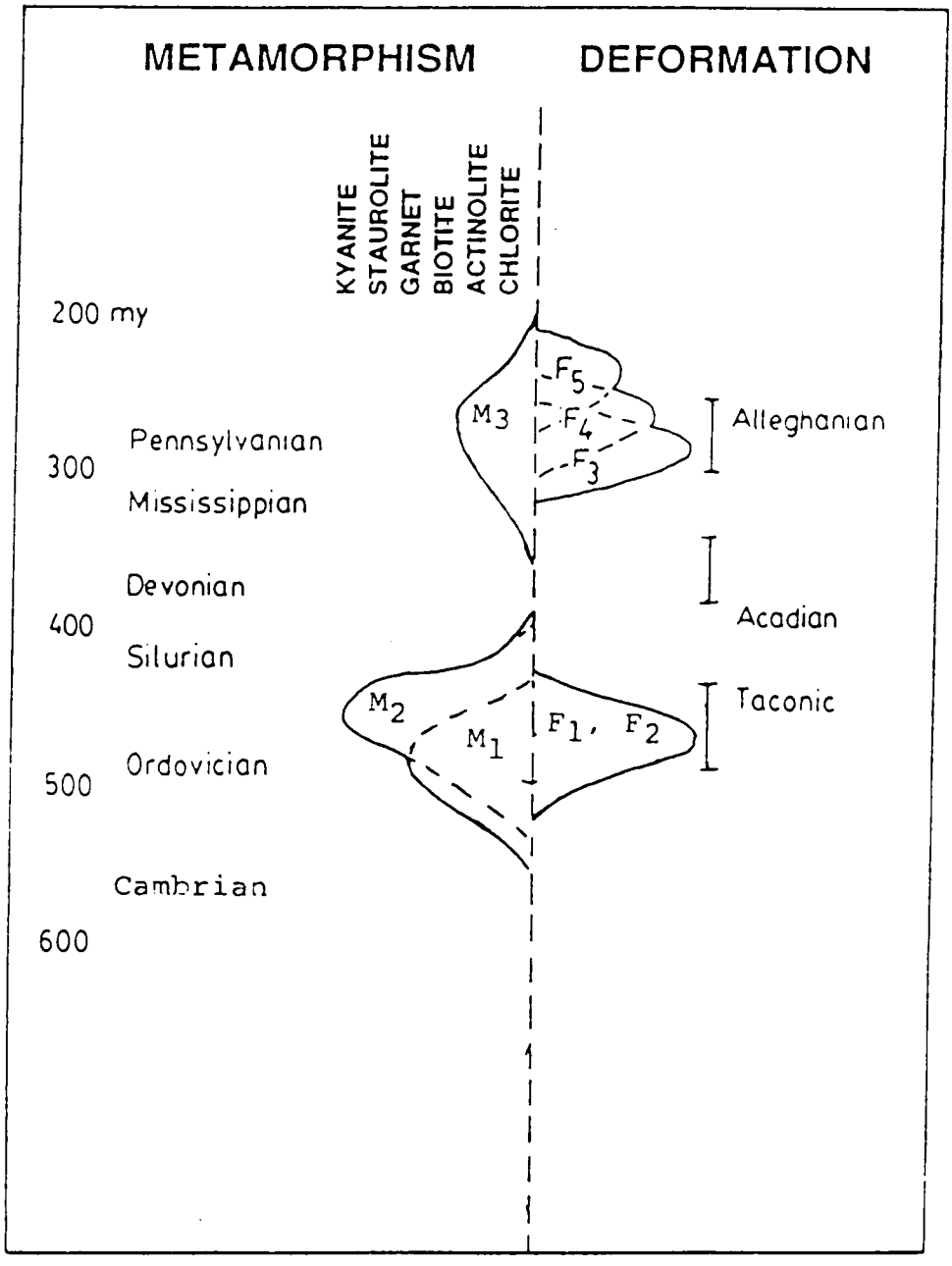

Figure 3.Schematic diagram showing the sequence of deformation and metamorphism (Modified after Addy & Ypma, 1977).

m.a.). Axial planes strike north-northeast and dip 30°-35° southeast (Holcombe, 1973). The M2 metamorphic event attained staurolite-kyanite grade and was interpreted by Addy & Ypma (1977) to have occurred after the Acadian orogeny (F2, 380-340 m.a.), which produced large isoclinal folds such as the Burra anticlinorium and the Coletown synclinorium (Fig. 2). These folds have axial plane orientations similar to those folds produced by F1. Most workers now believe that the thermal peak, hence F2, was attained during the Taconic and not the Acadian (Butler, 1972; Fullagar & Bottino, 1970; Dallmeyer, 1975a; Dallmeyer, 1975b; Hatcher, Butler, Fullagar, Secor & Snoke, 1980). A Barrovian sequence of metamorphic mineral assemblages was produced during M2. The biotite isograd is located ~9 km west of Ducktown (Carpenter, 1970), and grade increases progressively to the east through garnet, staurolite and kyanite isograds. Maximum grade in the mine area is middle amphibolite facies and is characterized by the assemblage staurolite ± kyanite. Using a variety of mineral thermobarometers, Nesbitt & Essene (1982) constrained P-T conditions of peak metamorphism to be 6 ± 1 kb and 540° ± 40°C. Brooker, Craig & Rimstidt (1987) used sphalerite geobarometry on sphalerite grains armored by pyrite to obtain a pressure estimate of 6.8 ± 0.8 kb. The M3 event was associated with Alleghanian brittle deformation (F3-F5, 300-250 m.a.) and reached chlorite to biotite grade. These deformation events produced a variety of macroscopic and microscopic structures including small open folds, chevron folds, kink bands and strike-slip faults (Holcombe, 1973; Addy & Ypma, 1977).

In a regional tectonic sense, the Blue Ridge and Inner Piedmont

Provinces form a large allochthon composed of a series of thrust sheets which have been transported up to several hundred kilometers to the northwest (Hatcher & Zietz, 1980). Individual thrust sheets were emplaced at different times throughout the Paleozoic - generally displaying westward younging - and in part probably overlie relatively unmetamorphosed platform sediments whose lateral equivalents are exposed in the Valley and Ridge (Hatcher & Zietz, 1980). Movement along these thrusts document compressional tectonics associated with the closing of Iapetus, beginning in Middle to Late Cambrian time and culminating in continent-continent collision of North America with Africa during the Carboniferous and Permian (Hatcher, 1978).

FLUID INCLUSIONS

Samples were collected at 5 ft intervals from five drill cores that penetrate the ore of the Cherokee orebody and the adjacent wallrock. Samples were also collected from approximately 60 additional drill cores from the Cherokee, Calloway, Boyd and Mary-Polk orebodies (Fig. 2). Hand samples were collected from the south open pit of the Cherokee orebody located just north of the Cherokee Fault (Fig. 2).

Fluid inclusions in ore and host rocks were studied utilizing standard petrographic, microthermometric and Raman spectroscopic techniques. Microthermometric data were collected on a U.S.G.S-type gas-flow stage manufactured by Fluid Inc. and calibrated at the triple point of CO_2 (-56.6°C), the triple point of H_2O (0.0°C) and the critical point of H_2O (374.1°C) with synthetic fluid inclusions (Sterner & Bodnar, 1984). From -198°C to -56.6°C

the accuracy is estimated to decrease in a near-linear manner from ±1°C at -198°C to ±0.1°C at -56.6°C. The estimated accuracy is ±0.1°C from -56.6°C to 100°C and ±2°C at 374.1°C. Reproducibility is in all cases within the estimated accuracy of the temperature determination. Qualitative spectroscopic analyses of the constituent molecular fluid species within fluid inclusions were collected on a ISA U-1000 Raman microprobe equipped with an Ar-ion laser of wavelength 514 nm.

Primary fluid inclusions

Occurrence

Primary fluid inclusions occur in clinopyroxene and rarely in garnet from the Cherokee, Calloway, Boyd and Mary-Polk orebodies (Fig. 2). Pyroxene is generally coarse grained (up to 10 cm), is frequently accompanied by amphibole (in part retrograde) calcite, quartz, pyrrhotite ± garnet ± pyrite ± magnetite ± anhydrite, and is texturally and chemically similar to metasomatic pyroxene found in skarn deposits (see Einaudi, Meinert & Newberry, 1981). Compositionally, pyroxene consists of diopside-hedenburgite-johannsenite solid-solutions with $Di_{55-93}Hd_{42-4}Jo_{7-2}$.

Primary fluid inclusions in pyroxene are usually crystallographically controlled (Fig. 4A) and are elongate along (001). Rods of amphibole commonly have been included during pyroxene growth and are oriented parallel to the *z* axis of pyroxene. In some cases primary fluid inclusions are trapped adjacent to these amphibole inclusions (Fig. 4B) or are pinned between two such crystals. Primary fluid inclusions in garnet occur as random three-dimensional arrays.

Figure 4. Photomicrographs of primary fluid inclusions in clinopyroxene from Ducktown, Tennessee. Scale bar in each picture is 25 μm. A) Crystallographically controlled fluid inclusions; arrow shows direction of (001). B) Fluid inclusion (arrow) trapped at the boundary between pyroxene (p) and crystallographically controlled amphibole (a), which was included during growth of clinopyroxene. C) & D) Inclusions showing evidence for extensive re-equilibration. Note the ghost of the original inclusion wall in D). E) fluid inclusions containing pyrrhotite daughters (po) in addition to calcite (cc) and quartz (qz) daughters, a low salinity aqueous phase and CH_4-rich vapor.

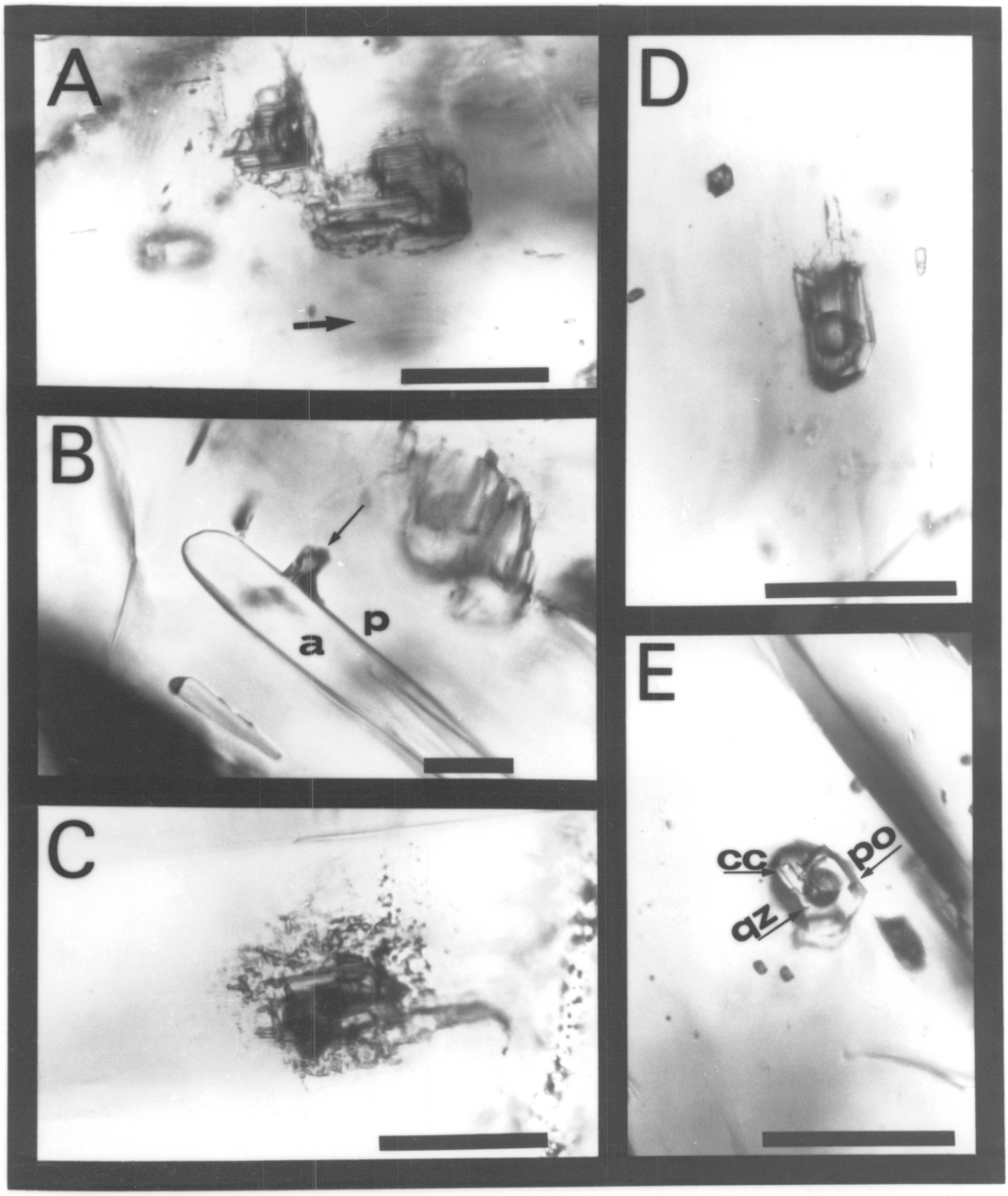
A
B
a
p
C
D
E
cc
po
qz

Primary fluid inclusions in metamorphic pyroxene and garnet are unusual in that they are very large, attaining sizes up to 100 μm, although the average size is 20 μm. Remnants of still larger inclusions are present but these apparently have decrepitated during uplift. Many primary fluid inclusions are highly irregular (Fig. 4C) and show textures which resemble implosion haloes produced during experimental deformation of inclusions in quartz under conditions of external overpressure (Sterner & Bodnar, 1989). This texture is important in constraining the uplift path of the terrane and will be discussed further in a later section. In a number of inclusions, relict ghosts of the original inclusion walls are present several microns into the host (Fig. 4D) and may be located only around certain portions of the inclusion. The possible mechanisms that can generate the above textures include (1) re-action of the host with the trapped fluid resulting in precipitation of pyroxene on the walls of the inclusion during cooling; (2) re-equilibration of inclusions to higher densities during uplift, and (3) migration of inclusions in response to differential stress or temperature. In general, the volume of host affected is too large to have resulted from simple precipitation of pyroxene or garnet on the walls during cooling. In particular, the original inclusion would have had to lose up to 50 percent of its volume by the addition of pyroxene or garnet to the walls of the inclusion, which implies unrealistically high solubilities of these minerals at P-T conditions of peak metamorphism (e.g., 750,000 ppm for diopside). This leaves (1) and (2) as likely mechanisms. Both of these are inferred to have operated.

Primary inclusions contain liquid and vapor, several birefringent daughter crystals and, in some cases, an opaque daughter phase (Fig. 4E). The

birefringent daughter crystals were identified as calcite and quartz using Raman spectroscopy. Calcite occurs as rhombohedral or irregular crystals displaying birefringence in second order colors (blue,green or yellow), while quartz occurs as rounded crystals with undetectable to very low birefringence. Calcite and quartz daughters are present in all primary fluid inclusions (Fig. 4E). The opaque daughter was identified as pyrrhotite with reflected light microscopy and verified with Raman spectroscopy. Pyrrhotite daughters are generally very small and equant and are only visible in ~20 % of the larger inclusions studied (Fig. 4E). Nevertheless, they are interpreted to be true daughters rather than accidental crystals trapped during formation of the fluid inclusions based on their consistent phase ratios when present. Pyrrhotite may be metastably absent from many of the smaller inclusions. With the exception of pyrrhotite, the phases present in primary inclusions are consistent but the proportions of these phases, especially the volume percent vapor, does vary. It is suggested that variable liquid-vapor ratios are the result of re-equilibration of inclusion volumes in response to differential pressure between inclusions and matrix during uplift.

Microthermometry

Heating/freezing tests on primary fluid inclusions coupled with Raman spectroscopy reveal that the fluid portion is aqueous with a salinity of about 3 wt % NaCl equivalent, and approximately 5 mole % CH_4. Upon warming frozen inclusions the first phase transition observed is the homogenization of residual CH_4 [Th(CH_4)] in the presence of clathrate + ice + hydrohalite ± other salts or salt hydrates. Homogenization is to the liquid (L+V->L) at -157°

to -90°C and rarely to the vapor (L+V->V) at -90°C to -83°C. Th(CH_4), especially for the L+V->V mode, is not observed in many inclusions because of optical limitations. The next phase change observed in a very few inclusions is eutectic melting at -22° to -23°C, near the eutectic in the system NaCl-KCl-H_2O (-22.9°C; Linke, 1965). This suggests that NaCl ± KCl is/are the dominant salt(s) dissolved in the aqueous phase. Much of the melt produced at the eutectic is immediately consumed during formation of additional clathrate; however, in some cases the initial melt is armored from the vapor bubble (i.e. the source of CH_4) by existing clathrate. The melting of ice [Tm(ice)] in the presence of clathrate + liquid + vapor occurs at -2.8° to -0.9°C and CH_4 clathrate dissociates [Tm(clath)] at 11.5° to 25.2°C. The temperature of the latter phase change is sensitive to the phases present at Tm(clath), the salt content of the inclusion, the presence of other volatiles such as CO_2 and N_2 and to the internal pressure at Tm(clath). An increase in salinity acts to depress Tm(clath) at constant pressure (Kobayashi, Withrow, Williams & Katz, 1951), whereas an increase in pressure results in elevation of Tm(clath) (Deaton & Frost, 1946). Addition of CO_2 to the CH_4 clathrate structure causes elevation of Tm(clath) at a given pressure (Unruh & Katz, 1949), while addition of N_2 depresses Tm(clath) (Deaton & Frost, 1946).

Thomas & Spooner (1988) present a method of determining the salinity of H_2O-CH_4-NaCl inclusions using Th(CH_4) and Tm(clath). The underlying assumption is that the internal pressure in the inclusion at Tm(clath) can be constrained by the isochore for the vapor phase calculated from Th(CH_4). The problem with this technique is that the formation of ice and CH_4 clathrate both involve volume increases ($\rho_{ice} \approx 0.96$ g/cm^3; $\rho_{clath} \approx 0.91$ g/cm^3)

relative to the aqueous phase in which they form ($\rho_{aqueous} \approx 1.0$ g/cm^3). This results in a decrease in the available volume that the residual CH_4 vapor can occupy and hence in a significant increase in the density of the vapor phase, provided that large quantities of CH_4 are not extracted from the vapor phase during the formation of clathrate. This effect is accentuated as the volume percent vapor decreases. Consequently, Th(CH_4) measured for frozen inclusions will give erroneously high densities and will result in elevated pressure and salinity estimates at Tm(clath). Furthermore, the phases present at Th(CH_4) do not necessarily represent an equilibrium assemblage due to formation of insufficient amounts of clathrate during freezing. The internal pressure may approximately follow the CH_4 isochore below the temperature of first melting, but when melt is generated in the inclusion the pressure decreases due to the negative ΔV of fusion.

Applying the technique of Thomas & Spooner (1988) to micro-thermometric data from primary fluid inclusions from Ducktown results in estimated salinities of 11-14 wt % NaCl equivalent and internal pressures of 400-2000 bars. We believe that both of these estimates are unrealistic. Internal pressures of 2 kb at room temperature imply decrepitation pressures approaching 4 kb. Although the decrepitation behavior of fluid inclusions in pyroxene has not been investigated, 15 μm inclusions in quartz only require about 1400 bars to initiate decrepitation (Bodnar, Binns & Hall, 1989). Also, Tm(ice) in the presence of clathrate (-2.8° to -0.9°C) suggests <u>maximum</u> salinities of less than 5 wt % NaCl equivalent - much lower than the 11-14 wt % implied by the technique of Thomas & Spooner (1988). Using 5 wt % NaCl as an estimated maximum salinity and the data of Kobayashi, Withrow,

Williams & Katz (1951) on the depression of Tm(clath) by NaCl, more realistic internal pressures of 200-600 bars at Tm(clath) are obtained.

Heating above Tm(clath) usually results in decrepitation prior to liquid-vapor homogenization [Th(L-V)] at temperatures of 150°-250°C. Temperatures of liquid-vapor homogenization that could be measured are 200°-250°C. Th(L-V) correlates positively with inclusion size suggesting that re-equilibration toward lower densities has occurred during uplift. The positive correlation results from the fact that larger fluid inclusions re-equilibrate before smaller fluid inclusions and to a greater degree (Bodnar, Binns & Hall, 1989; Sterner & Bodnar, 1989). There is no detectable dissolution of daughter minerals during heating to 250°C.

Bulk composition

Daughter minerals in primary fluid inclusions may be used to determine the bulk composition of the peak metamorphic fluid, assuming no post-trapping compositional changes have occurred. On average, calcite, quartz and pyrrhotite daughters occupy 5, 1 and 0.1 volume % of the inclusion, respectively. As discussed above, microthermometry and Raman spectroscopy indicate that the fluid phase (excluding the daughter crystals) can be adequately represented by the system H_2O-CH_4-NaCl. However, if the solid phases are reintegrated into a homogeneous fluid, assuming that carbonate existed in solution as Ca and CO_2 and that pyrrhotite existed as Fe and H_2S, the estimated composition of the peak metamorphic fluid is:

$X_{H_2O} = 0.93$ Ca = 54,000 ppm

$X_{CH_4} = 0.04$	NaCl = 30,000 ppm
$X_{CO_2} = 0.03$	SiO_2 = 26,000 ppm
$X_{H_2S} = 1 \times 10^{-3}$	Fe = 3,000 ppm

No attempt has been made to charge-balance this composition due to the lack of information on the nature of ionic species in metamorphic fluids; but there must have been appreciable dissolved carbonate or bicarbonate and perhaps chlorine to charge balance calcium and iron. The volatile portion of the calculated fluid composition (which has been normalized to 100 %) exhibits important similarities and differences when compared to theoretical calculations of fluid speciation at elevated pressures and temperatures (Hall, Bodnar & Craig, 1989). The above calculation suggests that the amount of solids dissolved in the peak metamorphic fluid phase exceeded 11 wt. %.

Quartz, calcite and pyrrhotite daughter crystals probably precipitated in response to decreasing temperature. Calcite, which displays retrograde solubility in low salinity, non-alkaline solutions, probably shows prograde solubility at elevated temperatures in saline fluids (Holland & Malinin, 1979). The eroded nature of most calcite daughter crystals suggests that they went through a solubility minimum, in support of prograde solubility of calcite in these fluids at elevated temperatures.

Secondary fluid inclusions in quartz

Immiscible H_2O-CH_4-N_2-NaCl inclusions

The most common type of secondary fluid inclusion was trapped from immiscible H_2O-CH_4-N_2-NaCl fluids. These occur along grain boundaries

between recrystallized quartz (Fig. 5A), along healed intragranular and intergranular microfractures in quartz (Fig. 5B), along radial microfractures in quartz surrounding hexagonal pyrrhotite inclusions (Fig. 5B) and, rarely, as isolated inclusions in quartz. All occurrences have identical compositions. We interpret fluid inclusions which decorate grain boundaries to have been trapped during or after a grain boundary cracking event, which also caused significant intergranular and intragranular fracturing (Fig. 5C), and not during recrystallization of quartz (i.e. M2). This is an important observation because it moves the trapping time from early in the post-peak-metamorphic history, when rocks were behaving ductily, to later in the uplift history during brittle deformation. Grain boundary fluid inclusions in metamorphic rocks are often assumed to have been trapped during recrystallization, but rock mechanics studies have shown that grain boundary cracking occurs before intragranular fracturing, in response to thermal expansion and elastic moduli mismatch between neighboring grains (e.g., Fredrich & Wong, 1986). Fluids present during grain boundary cracking events could be trapped along grain boundaries and texturally appear to have been trapped during recrystallization. This may account for inclusions that are reported in some studies which are texturally early but compositionally and volumetrically late. Grain boundaries in Ducktown rocks are relatively weak and are loci for further fracturing during uplift. As a result, most fluid inclusions along grain boundaries in these rocks have leaked.

Microthermometry and Raman spectroscopy reveal two inclusion types that represent the endmembers of an immiscible fluid and contain (1) CH_4-N_2 with very little H_2O (optically indistinquishable) and (2) H_2O-CH_4-NaCl with

Figure 5. Photomicrographs of secondary fluid inclusions in quartz found at Ducktown Tennessee. Scale bar in each picture is 25 μm. A) H_2O-CH_4-N_2-NaCl inclusions occurring along grain boundaries between recrystallized quartz. B). H_2O-CH_4-N_2-NaCl inclusions occurring along healed intragranular and intergranular microfractures. C) H_2O-CH_4-N_2-NaCl inclusions along radial microfractures associated with second-phase inclusion of pyrrhotite (po). D) Coexisting liquid-rich (L) and vapor-rich (V) H_2O-CH_4-N_2-NaCl inclusions. E) H_2O-CO_2-NaCl inclusions along transgranular fractures. F) randomly oriented H_2O-CO_2-NaCl inclusions G) Low salinity, one-phase aqueous inclusions occurring as an isolated group. H) Low salinity, one-phase aqueous inclusions along interganular fractures. I) Low salinity, one-phase aqueous inclusions showing "sheared" terminations on negative crystals. J) Halite-bearing inclusions along healed fractures; h = halite. K) Late-stage $CaCl_2$-$MgCl_2$-NaCl-H_2O inclusions.

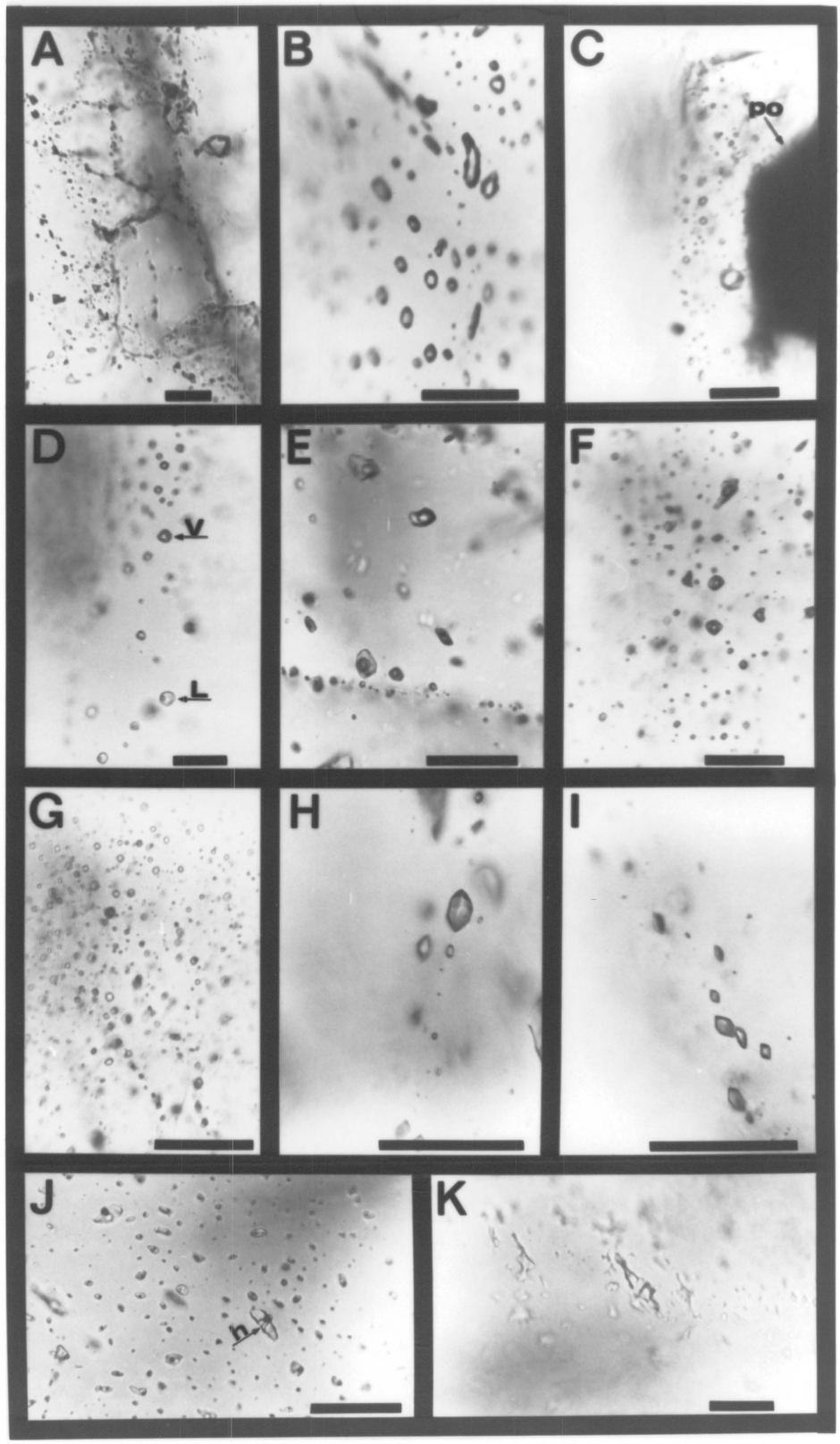
A
B
C
po
D
v
t
E
F
G
H
I
J
n
K

very little N_2. At room temperature these appear as supercritical one phase CH_4-N_2 inclusions and two phase saltwater + CH_4 -rich vapor inclusions, respectively (Fig. 5D). One endmember is usually dominant in a particular sample. In CH_4-N_2 rich inclusions Th(CH_4) occurs over the temperature range -82.2° (homogenization by critical behavior) to -144°C (homogenization to the liquid) with modes at -100° and -127°C. Homogenization is generally to the liquid phase; however, a few inclusions homogenize to the vapor phase at -83° to -87°C. No other phase changes were detected in CH_4-N_2 inclusions, although we suspect that a thin, aqueous film wets the walls of most of the inclusions. Homogenization by critical behavior at -82.2°C in one inclusion compares favorably with the critical temperature of pure CH_4 (-82.6°C). Similar inclusions from another sample homogenize by critical behavior at -88.6° to -90.0°C due to the effect of N_2 as verified by Raman spectroscopy. Data compiled by van den Kerkhof (1988) indicate that ~15 mole % N_2 in CH_4-N_2 inclusions will produce a critical temperature near -90°C. Thus, the vapor-rich endmember of H_2O-CH_4-N_2-NaCl inclusions contains up to at least 15 mole % N_2, relative to N_2 + CH_4.

Upon heating frozen inclusions representing the aqueous endmember, the first phase change observed is eutectic melting in the presence of CH_4 clathrate, ice, hydrohalite(?) and CH_4-rich vapor. Eutectic temperatures are generally -22° to -23°C, suggesting that NaCl ± KCl are the dominant salts in solution. Ice melts at -5° to -11°C in the presence of clathrate, liquid and vapor, and clathrate melts at 6° to 14°C in the presence of liquid and vapor. Tm(ice) in the presence of clathrate provides a maximum salinity estimate of

8-15 wt % NaCl equivalent for these inclusions (Hall, Sterner & Bodnar, 1988). It is likely that true salinities are closer to 5-10 wt % NaCl equivalent, although these cannot be determined microthermometrically. The data of Kobayashi, Withrow, Williams & Katz (1951) suggest internal pressures of 65-200 bars at Tm(clath) for 5-10 wt % NaCl solutions. Addition of N_2 also depresses Tm(clath) (i.e. increases the estimated pressure at a given temperature) (Deaton & Frost, 1946); thus, internal pressures may be slightly higher than quoted above for the H_2O-CH_4-NaCl system.

Total homogenization of aqueous inclusions occurs at temperatures from 200°-265°C (avg. 215°C). However, many inclusions decrepitate at temperatures of 130°-230°C, prior to homogenization, indicating significant internal overpressures. An oriented microfracture array parallel to the trend of the inclusion plane may develop during decrepitation.

A group of variable-sized inclusions was monitored during heating in order to estimate the internal pressures in these inclusions at the temperatures of decrepitation and hence provide constraints on the position of the isochore in P-T space. The approximate volume of each inclusion (modeled as spheres or proloate spheroids) was recorded as was the clathrate dissociation temperature. Inclusions were heated slowly in 5-10°C increments and then slowly cooled to room temperature between each heating step. The clathration temperature for each inclusion was remeasured after each heating increment. As Tm(clath) is sensitive to changes in internal pressure, it provides an indication of density changes due to decrepitation. The equation of Bodnar, Binns & Hall (1988), which relates inclusion size or volume to internal pressure at decrepitation, was used to estimate the internal

pressure at the decrepitation temperature (Td), the latter being defined as the midpoint of the heating increment that caused a decrease in Tm(clath). A well-defined negative correlation between Td and inclusion volume was recorded (Fig. 6), and internal pressures of 1.5-2.5 kb at Td (160-250°C) were calculated. Interpolation to 215°C suggests an internal pressure of ~2.3 kb at Th for this group of inclusions.

Evidence for simultaneous trapping of immiscible fluids is rarely unequivocal in metamorphic rocks. Nevertheless we feel that reasonably good evidence does exist in this case, including:

1) Common co-occurrence of CH_4-N_2 (-H_2O) and H_2O-CH_4-salt (-N_2) inclusions together in a single sample. Both types exist in similar textural settings.

2) Inclusion planes which are dominated by one endmember, but along which the other endmember is randomly interspersed. Mixed inclusions are common near inclusions containing the subordinate endmember (Fig. 5D).

3) When the two types of inclusions coexist, those representing the vapor-rich endmember are distinctly larger than those representing the liquid-rich endmember. This is often the case because of the minimum stable vapor bubble size that may exist. Similar behavior was reported by Bodnar, Burnham & Sterner (1985) for the system H_2O-NaCl.

4) Phase ratios and compositions are qualitatively consistent with what is expected for immiscible fluids in the system H_2O-CH_4-N_2-salt. In other words, the more volatile components CH_4 and N_2 are partitioned into vapor-rich inclusions, while salt is partitioned into aqueous inclusions.

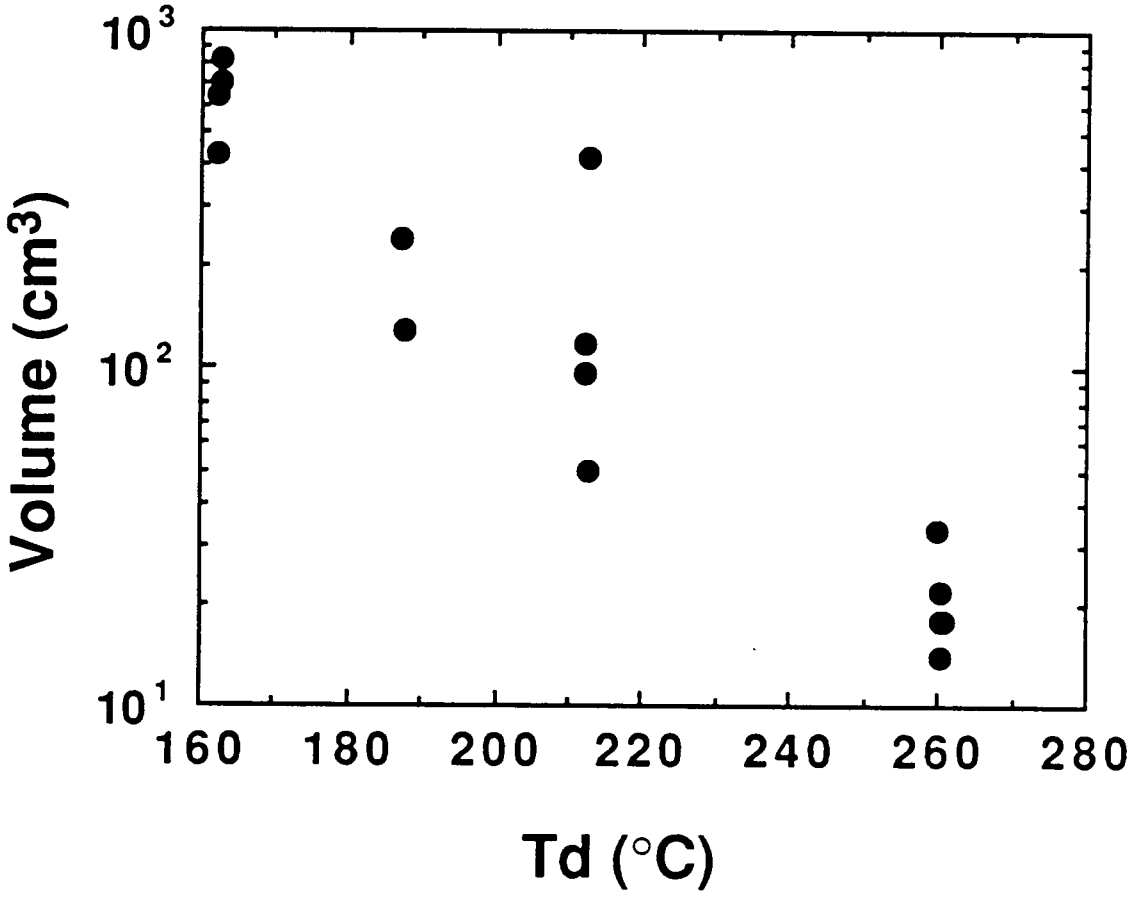

Figure 6. Relationship between inclusion volume and decrepitation temperature (Td) for liquid-rich endmembers of immiscible H_2O-CH_4-N_2-NaCl inclusions.

5) Inclusions of this type are not typical metamorphic inclusions, in that they are not particularly small and do not have "mature" negative crystal shapes. Many are very irregular although decrepitation haloes, common in large inclusions, contribute to their irregularity. The inclusions are similar to hydrothermal inclusions formed at relatively low to moderate P-T conditions, consistent with the inferred P-T conditions of trapping (1-2.3 kb, 215° ± 20°C). The large range in density of the CH_4-N_2 rich phase of the immiscible fluid coupled with the consistency of Th(CH_4) for inclusions representing the coexisting aqueous phase (~215±20°C) implies that immiscible fluids were trapped over a range of pressures but at relatively constant temperature. This observation has significant implications for uplift, as discussed below.

H_2O-CO_2-salt (-CH_4-N_2) inclusions in quartz

Inclusions containing H_2O-CO_2-salt (-CH_4-N_2) were found only in samples of quartzite from wallrock in the south pit. The inclusions occur along transgranular fractures (Fig. 5E) and along grain boundaries in recrystallized quartz or may be randomly oriented (Fig. 5F). They consist of two phases at room temperature, saltwater and CO_2-rich liquid. Raman analyses indicate that detectable amounts of CH_4 and N_2 are present in the CO_2-rich phase of some of these inclusions.

Carbon dioxide melts at -56.6° to -58.9°C in the presence of clathrate + ice + CO_2-rich vapor + CO_2-rich liquid + hydrohalite. These temperatures are consistent with Raman data and suggest small, variable amounts of CH_4 and/or N_2, both of which depress Tm(CO_2) to temperatures below -56.6°C. The depression is attributed to 5-15 mole % CH_4 + N_2 in the CO_2-rich liquid

phase (van den Kerkhof, 1988). "Eutectic" melting of the aqueous phase occurs at -20.5° to -23.0°C, indicating NaCl ± KCl as the dominant salt(s) in solution. It should be noted that this is not a true eutectic because CO_2 is in excess, hence the aqueous melt produced should immediately combine with liquid CO_2 to form more clathrate. In reality however the melt is effectively isolated from liquid CO_2, which is armored by clathrate, allowing a metastable eutectic, applicable to the aqueous portion of the inclusion, to be measured. Ice melts in the presence of clathrate, liquid CO_2 and CO_2-rich vapor at -6.5° to -8.7°C, and CO_2-rich clathrate dissociates at 7.1° to 8.8°C. CO_2 liquid-vapor homogenization to the liquid occurs at -2.2° to +21.7°C in the presence of saltwater. Smaller inclusions homogenize from 250°-292°C and larger inclusions decrepitate over the range 180°-260°C. Frequently, an oriented array of microfractures develops during decrepitation and it is probable that some of the inclusions with highest Th partially decrepitated or stretched during heating. Homogenization temperatures of the smallest inclusions (~250°C) are believed to be most reliable because nearly all large inclusions partially decrepitate before 200°C as evidenced by the decrepitation study described below.

The decrepitation behavior of these inclusions was studied using the technique outlined in the previous section and substituting Th(CO_2) for Tm(clath) as the discriminator for density changes. Again, Td was found to correlate negatively with inclusion volume (Fig. 7) and application of the equation of Bodnar, Binns & Hall (1988) suggests internal pressures of 3 kb at Th (250°C). Although measurement of Th(CO_2) reveals a range in CO_2 densities from 0.76 to 0.94 g/cm^3, a plot of inclusion volume vs. Th(CO_2)

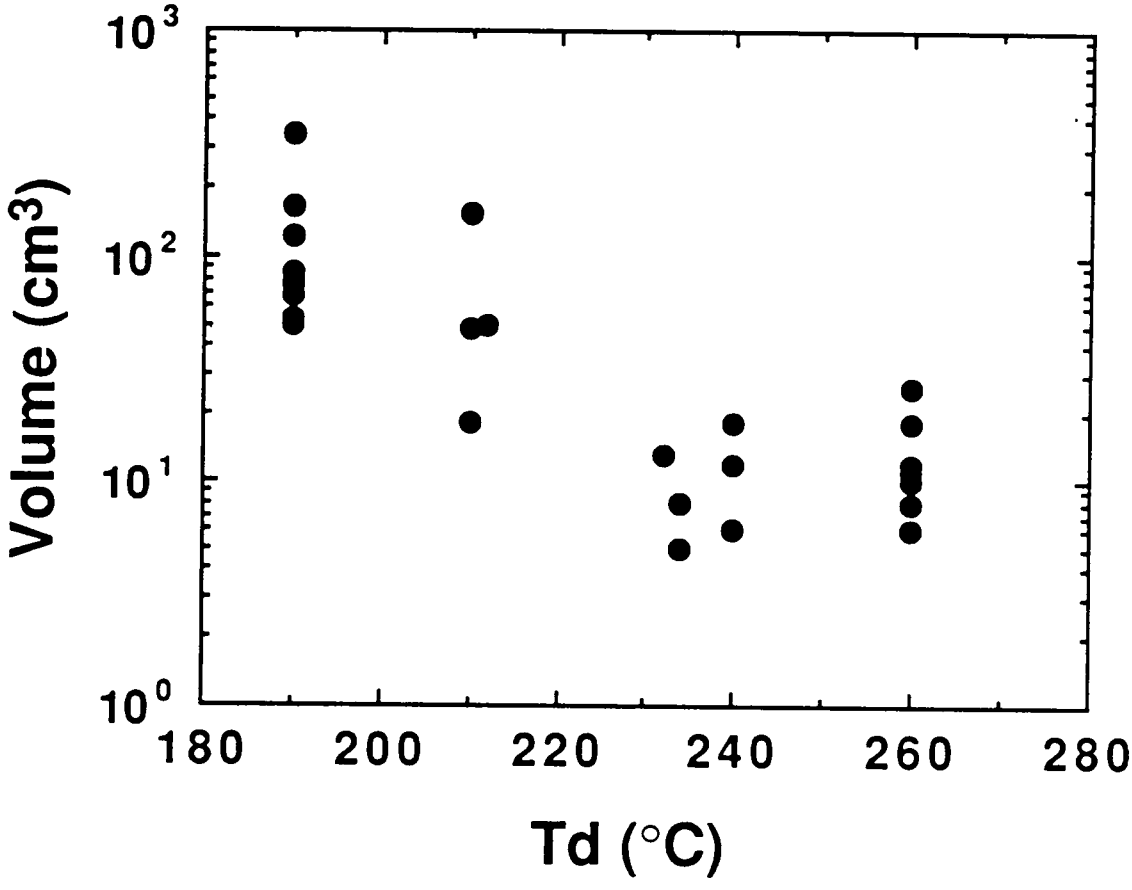

Figure 7. Relationship between inclusion volume and decrepitation temperature (Td) for H_2O-CO_2-NaCl inclusions.

shows no trend (Fig. 8). Hence, except in a very few cases where inclusions have obviously decrepitated there is no evidence to support extensive re-equilibration of these fluid inclusions during uplift. Density variations within a given fracture plane are minimal. It is likely that X_{CO_2} varied in time and space in response to local or external controls on fluid composition. All other parameters being equal, the observed range in density can be explained by an X_{CO_2} variation of only a few mole %.

Salinities of 2.4-5.6 wt % NaCl equivalent were estimated for these inclusions using the method of Collins (1979) and the equation of Bozzo, Chen, Kass & Barduhn (1973). This assumes that the system is adequately represented as H_2O-CO_2-NaCl. Raman analyses and microthermometry indicate that 5-15 mole % $CH_4 + N_2$ may be present in the non-aqueous portion of the inclusions. This translates to roughly 0.5-2 mole % of the total inclusion (X_{CO_2} is calculated to be 0.10-0.15). The effect of both CH_4 and N_2 is to raise the temperature at which clathrate melts in the presence of saltwater, CO_2-rich liquid and CO_2-rich vapor, relative to the pure H_2O-CO_2 system (10°C) (by considering clathrate melting data of Deaton & Frost, 1946 and Unruh & Katz, 1949 and liquid-vapor equilibrium data for CO_2-CH_4 and CO_2-N_2 mixtures compiled by van den Kerkhof). Thus, the actual salinity may be slightly higher, although 0.5-2 mole % $CH_4 + N_2$ is not likely to drastically affect the estimated salinity.

Low-salinity, one-phase, aqueous liquid inclusions

Low-salinity, one-phase, aqueous liquid inclusions are fairly common. They occur as isolated inclusions 2-5 μm in size or as groups of inclusions in

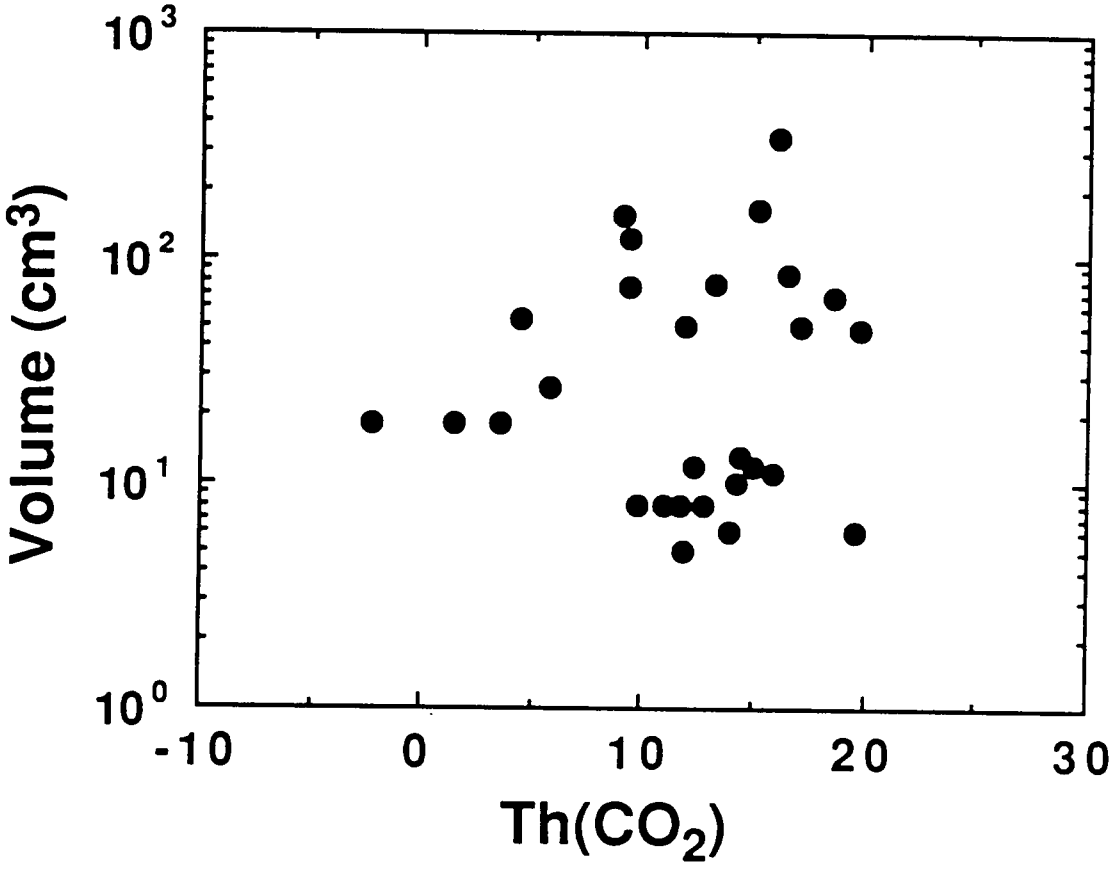

Figure 8. Relationship between inclusion volume and CO_2 homogenization temperature (Th) for H_2O-CO_2-NaCl inclusions.

quartz (Fig. 5G), and more frequently along healed intergranular fractures (Fig. 5H). They almost invariably form negative crystals and some have a sheared appearance with the two terminations of the negative quartz crystal bent in opposite directions (Fig. 5I). A vapor bubble does not nucleate upon cooling and the solution freezes at about -40°C, usually resulting in decrepitation of the inclusion via the process referred to as "freeze-stretching" (Lawler & Crawford, 1983). During decrepitation, oriented microfractures 1-2 inclusion diameters in length develop and emanate from one or both terminations of the negative crystal. After decrepitation these inclusions are two-phase liquid + vapor at room temperature. Subsequent freezing tests give vapor-present ice melting temperatures of 0.0° to -3.8°C, corresponding to salinities of 0-6 wt. % NaCl equivalent (Hall, Sterner & Bodnar, 1988). Reliable eutectic temperatures could not be measured for these inclusions. Upon heating virgin samples, inclusions decrepitate over the range 225-300°C; application of the equation of Bodnar, Binns & Hall (1988) implies internal pressures of ~2.5-3.5 kb at Td. Many of these inclusions have apparently decrepitated during uplift and are two-phase with widely varying liquid-vapor ratios, or are empty. Crushing tests and Raman analyses revealed no noncondensable gas species.

Three-phase, saltwater + vapor + halite inclusions

Three-phase, saltwater + vapor + halite inclusions occur along healed fractures in deformed quartz veins in country rock schists and metagraywackes (Fig. 5J). Many show evidence of necking and display inconsistent liquid/vapor ratios; some lack a vapor phase altogether. The

inclusions do not freeze even when held at liquid nitrogen temperatures for several minutes. Halite dissolution temperatures range from 198° to 202°C , corresponding to 32.5 equivalent wt. % NaCl (Sterner, Hall & Bodnar, 1988a). Inclusions showing no evidence of necking homogenize to the liquid at 160°-190°C. Crushing tests and Raman analyses revealed no noncondensible gases.

$CaCl_2 \pm MgCl_2$ -rich inclusions

$CaCl_2 \pm MgCl_2$ -rich inclusions generally are large and irregularly shaped, and are usually associated with late-stage microfractures in quartz and calcite (Fig. 5K). They are characterized by very low initial melting temperatures (-30° to -70°C) and low final melting temperatures of ice (-9.1° to -43°C). A positive correlation between apparent eutectic temperature and final melting temperature was noted in some samples and probably indicates that the lower eutectic measurements are most nearly correct. It is difficult to detect first melting in fluid inclusions unless significant quantites of melt are produced at the eutectic (i.e. the bulk composition of the inclusion is close to the eutectic composition). Apparent eutectics below -57°C (the eutectic temperature in the system $CaCl_2$-$MgCl_2$-NaCl-H_2O; Linke, 1965) may indicate additional components are present. However, initial melting temperatures as low as -80°C were observed by Davis, Lowentstein & Spencer (1989) in synthetic NaCl-$CaCl_2$-H_2O and NaCl-$MgCl_2$-H_2O inclusions. These authors have attributed initial melting temperatures below those of the stable eutectics of these systems (-35° and -52°C, respectively) to the melting of metastable magnesium and/or calcium salt hydrates.

Most inclusions are one-phase liquids or have very low homogenization temperatures (<100°C). However, in one sample homogenization temperatures of 175° to 265°C were recorded on small inclusions, whereas larger inclusions had still higher Th. In this sample a positive correlation recorded between inclusion size and Th suggests that the inclusions partially decrepitated during uplift. Leakage and partial decrepitation appears to have been intensified by the poorly formed nature of these inclusions. Given the compositional and density variations within this group it is likely that several generations of fluids are represented.

Chronology of Entrapment

Fluid inclusions from Ducktown document a complex post-metamorphic uplift history involving a variety of fluids. Not all fluid inclusion types are found at all sample localities, suggesting that fluid flow was not pervasive or that fluid composition was controlled locally. This is consistent with stable isotope data, which record minimal post metamorphic exchange and imply low integrated fluid/rock ratios (Hall, Wesolowski, Bodnar & Craig, 1989). The restriction of some fluid types to certain areas (e.g. halite-bearing inclusions only in deformed quartz veins) implies that they may have been locally derived or channeled through favorable horizons. As discussed below, the presence of fluid inclusions trapped at various times during the post-metamorphic history provides significant constraints on the uplift path.

Primary fluid inclusions located in pyroxene and garnet from ore zones were trapped during peak metamorphism as the host phases have been shown to have been present and to have equilibrated at peak metamorphic

conditions (Addy & Ypma, 1977; Nesbitt, 1979; 1982). Hence, these inclusions potentially record the compositional and volumetric properties of the peak metamorphic fluid present in oxidized and sulfidized portions of the ore zones (i.e. at fO_2-fS_2 conditions near the Py-Po-Mt buffer) provided that no post-trapping changes in density or composition have occurred. Density variations in primary fluid inclusions have already been noted, and are interpreted to evidence re-equilibration in respose to differential pressure between host and inclusions during uplift. These inclusions may have re-equilibrated compositionally as well, in response to fH_2 gradients established during the early uplift history of the terrane (Hall, Bodnar & Craig, 1989). Nevertheless, their presence does provide useful information on fluid composition, especially of dissolved solids present in the peak metamorphic fluid.

It is inferred, largely from textural evidence, that low salinity, one-phase inclusions record the next oldest fluid. Their deformed nature coupled with their textural maturity, common evidence for movement of inclusions away from the original fracture plane in response to strain in the host quartz (Roedder, 1971), evidence for partial decrepitation or stretching, and their common occurrence as isolated patches in the cores of recrystallized quartz suggest that they were trapped prior to the end of M2.

The next oldest fluid is recorded as CO_2-H_2O-NaCl inclusions in wallrock quartzite. These are moderately texturally mature, show little or no evidence of movement from original planes, and relatively little evidence for volumetric re-equilibration during uplift. The CO_2-H_2O-NaCl inclusions were trapped before immiscible CH_4-N_2-H_2O-NaCl inclusions because the homo-

genization temperatures and pressures of the former, which represent minimum formation conditions, are above the trapping temperatures and pressures of the latter.

Immiscible CH_4-N_2-H_2O-NaCl inclusions are the next fluid recorded and provide a tight constraint on the uplift path because the P-T conditions of homogenization are the trapping conditions (1.0-2.3 kb, 215±20°C). If frequency of inclusion occurrence is any indication, this event appears to have been the most pervasive. Fluid was focussed through favorable horizons, notably ore zones, which acted as conduits for fluid flow. These inclusions are also present throughout the host rocks and in biotite grade rocks to the west of Ducktown.

Three-phase NaCl-H_2O inclusions appear to have been trapped at relatively low P-T conditions. There is substantial evidence for necking in many of these generally texturally immature inclusions. Their occurrence only in deformed (and presumably early) quartz veins in host rock schists and metagraywackes is somewhat problematical as one might expect late-stage fluids to be more pervasive. Also, as is shown below, the isochore calculated for these inclusions does not intersect the uplift path defined by other inclusion isochores.

The youngest fluid inclusions are one-phase, texturally immature $CaCl_2$-$MgCl_2$-NaCl-H_2O inclusions. These are located in poorly healed fractures which transect all other inclusion types and were probably trapped very late in the uplift history from low temperature (<75°C ?) fluids.

Uplift* History

Representative isochores for the above inclusion types were calculated from available experimental and theoretical data, as described below, and are shown in Figure 9A. A theoretical isochore for primary fluid inclusions was constructed from the calculated composition of the fluid present at 6 kb, 550°C and fO_2-fS_2-a_C conditions indicated by sulfide-oxide-silicate assemblages in pyroxene-bearing rocks (pyroxene ± amphibole + calcite + quartz + pyrite + pyrrhotite + magnetite). This peak metamorphic fluid consists essentially of 90 mol% H_2O, 10 mol% CO_2 and 0.1 mol% H_2S. Cooling this trapped fluid isovolumetrically and calculating the P-V-X changes to the trapped fluid produces the isochore shown (Isochore 1; Fig. 9A; see Hall, Bodnar & Craig, 1989, for method). The actual isochore for the fluid portion of primary fluid inclusions is not shown because as discussed above and by Hall, Bodnar & Craig (1989) density and compositional modifications have occurred which make the actual isochore of little value.

The isochore for low-salinity (3 ± 3 wt % NaCl equiv.), one-phase inclusions was extrapolated from the data of Potter & Brown (1977) coupled

---

* The term "uplift path" as used in this paper is synonymous with "decompression- cooling path" and refers to the P-T-time path experienced by the rocks after peak metamorphism during their trip to the surface. It is acknowledged that in a strict sense uplift refers to vertical movement with respect to some datum and does not necessarily involve changes in pressure or temperature.

Figure 9. A) Representative isochores for fluid inclusion types observed at Ducktown. Isochores are enumerated chronologically with (1) corresponding to the earliest inclusions. (1) calculated isochore for the peak metamorphic fluid based on COHS fluid speciation calculations; (2) low salinity one-phase inclusions; (3) H_2O-CO_2-NaCl inclusions; (4A) aqueous endmember, immiscible H_2O-CH_4-N_2-NaCl inclusions; (4B) low density endmember, immiscible H_2O-CH_4-N_2-NaCl inclusions, $Th(CH_4)$ = -127°C, pure CH_4; (4C) as for (4B) except X_{N_2} = 0.15; (4D) low density endmember, immiscible H_2O-CH_4-N_2-NaCl inclusions, $Th(CH_4)$ = -100°C, pure CH_4; (4E) as for (4D) except X_{N_2} = 0.15; (5) halite-bearing inclusions; (6) $CaCl_2$-$MgCl_2$-NaCl-H_2O inclusions. Note that at this scale isochores for (2) and (6) overlap.
B) Suggested uplift path compatible with most fluid inclusion data. Also shown are absolute age constraints based on geochronologic data from the literature.

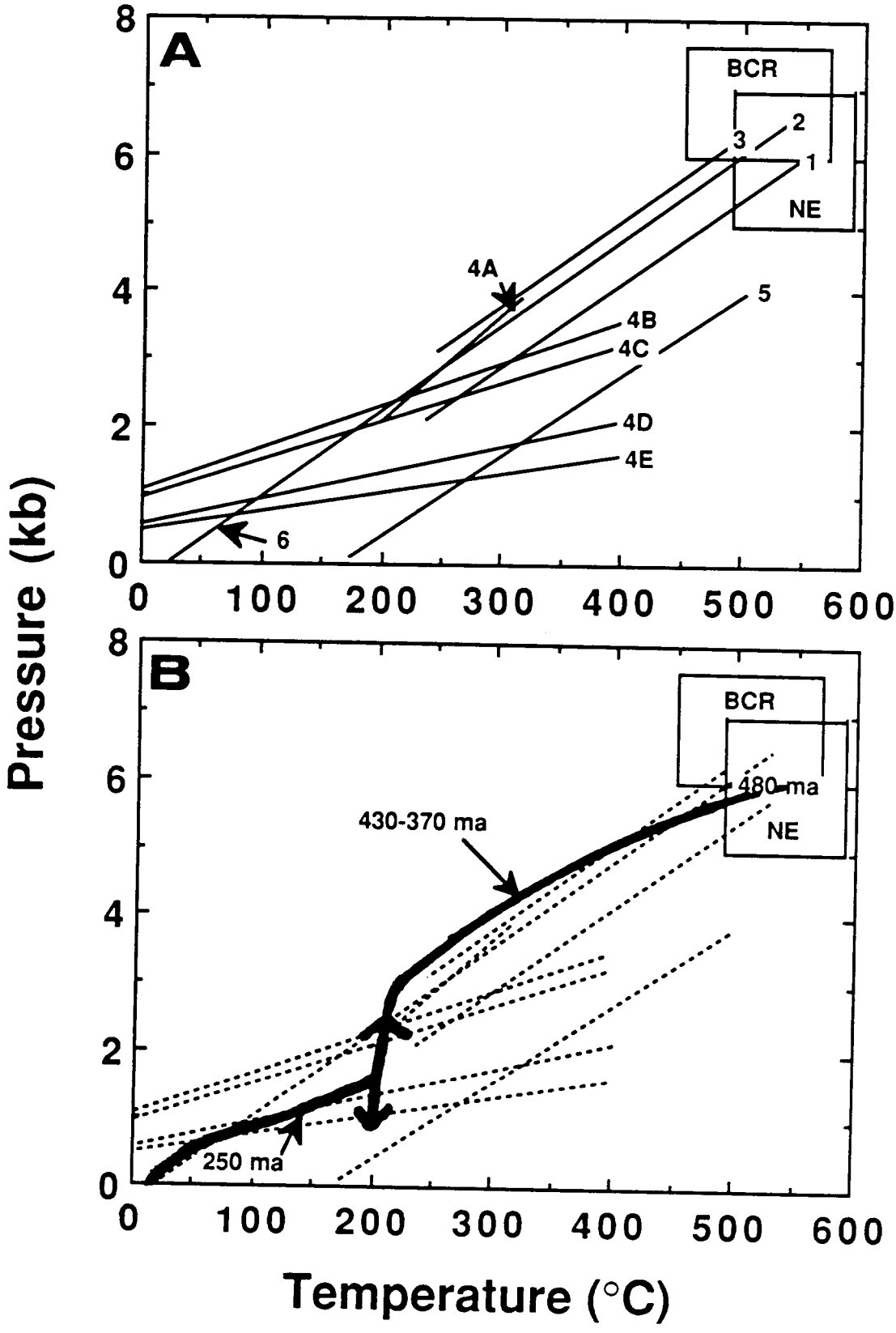
A
BCR
3
2
1
NE
4A
4B
4C
5
4D
4E
6
B
BCR
480 ma
430-370 ma
NE
250 ma
Pressure (kb)
Temperature (°C)
0
2
4
6
8
0
100
200
300
400
500
600

with the decrepitation behavior of these inclusions (Isochore 2; Fig. 9A). The isochore for CO_2-H_2O-NaCl inclusions (Isochore 3; Fig. 9A) was calculated using two independent methods: the decrepitation behavior of the inclusions, and methods and data presented in Brown & Lamb (1989). The two methods produce indistinguishable isochores, which lends support to the decrepitation method for delineating isochores of inclusions which either decrepitate prior to homogenization (Hall & Bodnar, 1986) or have unknown compositions.

Representative isochores for the low density endmember of immiscible CH_4-N_2-H_2O-NaCl inclusions (Isochores 4B-4E; Fig. 9A) were calculated from CH_4 density data of Kleinrahm & Wagner (1986) and a corrected version of Holloway's (1981) ISOCHOR program. The effect of 15 mole % N_2 is also shown with CH_4-N_2 densities taken from van den Kerkhoff (1988) (Isochores 4C and 4E; Fig. 9A). An isochore for the high density (aqueous) endmember was calculated from the decrepitation behavior of one group of inclusions (Isochore 4A; Fig. 9A). The intersection of two isochores, representing coexisting liquid and vapor phases of the immiscible fluid defines a point on the solvus. One such intersection was measured at about 200°C and 2.3 kb (Fig 9A), which is consistent with trapping temperatures of 210°C indicated by Th of the liquid-rich inclusions. As previously mentioned, density variations in CH_4-N_2 inclusions suggest that immiscibility occurred over a range of pressures from 2.3 kb to as low as 1 kb but over a limited temperature range of 215±20°C.

The isochore for halite-bearing inclusions (Isochore 5; Fig. 9A) was estimated from the solubility data of Sterner, Hall & Bodnar (1988a), the volumetric data of Bodnar (1985) and data compiled by Potter & Brown

(1977). The location of this isochore is not tightly constrained because the actual composition of the inclusion could not be determined micro-thermometrically. Only a wt. % NaCl equivalent salinity could be estimated from Tm(halite). Finally, the isochore for one phase $CaCl_2$-$MgCl_2$-NaCl-H_2O inclusions (Isochore 6; Fig. 9A) was approximated from data compiled by Potter & Brown (1977) assuming the inclusions behave as 25 wt % NaCl solutions with homogenization temperatures of 20°C. Note that at the scale of Figure 9A this isochore is indistinguishable from that of low salinity, one-phase inclusions.

An uplift path consistent with the chronology and PVTX properties of fluid inclusions at Ducktown is shown in Figure 9B. The P-T path was initially concave toward the temperature axis, suggesting that the rate of heat conduction exceeded the rate of uplift, but became nearly isothermal at 200°C. The latest stages of uplift may have been temperature-convex. This uplift path implies that the local geotherm decreased from about 24°C/km at peak metamorphic conditions (6 kb, 550°C) to about 18°C/km midway through the uplift path, increased abruptly to about 47°C/km at 200°C and then decreased in the final stages of uplift. These implied gradients assume lithostatic pressure and would of course be less if a hydrostatic component existed at any point along the uplift path. In fact, a significant hydrostatic component probably existed during the final stages of uplift as discussed below.

Why the isochore for halite-bearing inclusions (Isochore 5; Fig. 9A) is located so far off the main trend is unknown. Errors in the estimated volumetric properties cannot account for the deviation. It is possible that

these inclusions were trapped much earlier in the paragenesis than implied by textural relationships. Evidence for early trapping may be the observation that this type of inclusion only occurs in early deformed quartz veins in wallrock lithologies, although the inclusions are secondary with respect to deformation of these veins. None have been found in the ore zones, which contain all other late stage fluid inclusions. It should be noted that an early origin for these inclusions coupled with our suggested uplift path would result in internal underpressures of 2-2.5 kb during uplift - sufficient to produce "implosion haloes" (Sterner & Bodnar, 1989), although none were observed.

The proposed uplift path implies that peak metamorphic fluid inclusions would have become underpressured (internal pressure < external pressure) by as much as a kilobar during uplift (Fig. 9B), and in fact primary fluid inclusions in pyroxene and garnet exhibit textures suggestive of underpressuring (Fig 4D, 4E). The original isochore would have been modified to higher density during development of the observed texture. Subsequent overpressuring during isothermal decompression (Fig. 9B) allowed these inclusions to partially decrepitate, explaining the positive correlation between Th(L-V) and size in some samples.

The uplift path for Ducktown is differs from those modeled by some workers for similar tectonic settings (e.g. Albarede, 1976; England & Richardson, 1977; Oxburgh & England, 1980; England & Thompson, 1984) or implied by some fluid inclusion studies (e.g. Hollister, Burruss, Henry & Hendel, 1979; Schreurs, 1984; Droop, 1985; Casquet, 1986; Santosh, 1987). In most terranes, fluid inclusions suggest that a period of near-isothermal decompression occurs after peak metamorphism,

subsequently requiring a substantial amount of cooling at low pressures and implying high near-surface geothermal gradients (e.g. >100°C/km, assuming lithostatic pressure). Isothermal decompression, which is also predicted by thermal models of overthrust orogenic zones, have been interpreted as resulting from exhumation of tectonically thickened crust in such environments, or alternatively, as related to post- peak metamorphic extension and rapid crustal thinning in an extensional regime (Harris & Holland, 1984; Santosh, 1987).

Despite the abundance of profiles that are convex toward the temperature axis, those suggestive of relatively constant decrease in pressure and temperature (Rudnick, Ashwal & Henry, 1984) or near-isobaric cooling (Swanenberg, 1980; Bohlen, 1987; Hensen & Warren, 1987) have also been described, based on evidence from both fluid inclusions and metamorphic mineral assemblages. The latter profiles, generally recorded in granulite terranes, are usually attributed to development of a thermal dome resulting from magmatically heated crust (Bohlen, 1987; Henson & Warren, 1987), although extensional tectonics has been suggested as a mechanism as well (Harley, 1987). Spear (1987) suggests that isobaric cooling paths can be recorded in upper plates of thrust sheets.

The Ducktown orebodies are located in a subsidiary thrust sheet of the Blue Ridge - Inner Piedmont allochthon (Hatcher and Zietz, 1980). This thrust sheet is bounded by the Alleghanian-age Great Smoky thrust to the west and the Taconic-age Hayesville thrust to the east. According to composite sequential cross sections presented by Hatcher (1978) the package of Ocoee sediments hosting the orebodies was overthrust during the Taconic by

laterally equivalent sedimentary rocks and continental basement, which was moving westward along the Hayesville thrust. During Alleghanian thrusting, Ducktown-bearing sediments were in turn thrust over relatively unmetamorphosed platform sediments to the west along the Great Smoky fault.

According to calculations of England & Thompson (1984), P-T-time paths of tectonically thickened crust are characterized by isobaric heating at peak pressure followed by thermal relaxation along a temperature-convex uplift path. A period of nearly isothermal compression presumably preceeds isobaric heating if the thickening event is rapid. Spear (1987) suggests that P-T-time data from lower plates of thrust sheets should record nearly isothermal compression while upper plates should record nearly isobaric cooling.

Using the above relationships a burial-uplift path has been constructed which, although largely speculative, is consistent with available tectonic data (Fig. 10). The Ducktown orebodies may have been buried beneath as much as 15-17 km of overburden prior to the Taconic (Hatcher, 1978; Glover, Speer, Russell & Farrar, 1983). This suggests that the orebodies underwent burial metamorphism at 4-4.5 kb and 350-400°C prior to deformation. Deformation associated with the Taconic orogeny tectonically thickened the crust to approximately 22 km in the area of the orebodies perhaps resulting in isothermal compression followed by isobaric heating to peak metamorphic conditions (6 kb, 550°C). The uplift path initially may have been characterized by isothermal decompression, as predicted by the model of England and co-workers, but became isobaric at a depth of perhaps 15 km

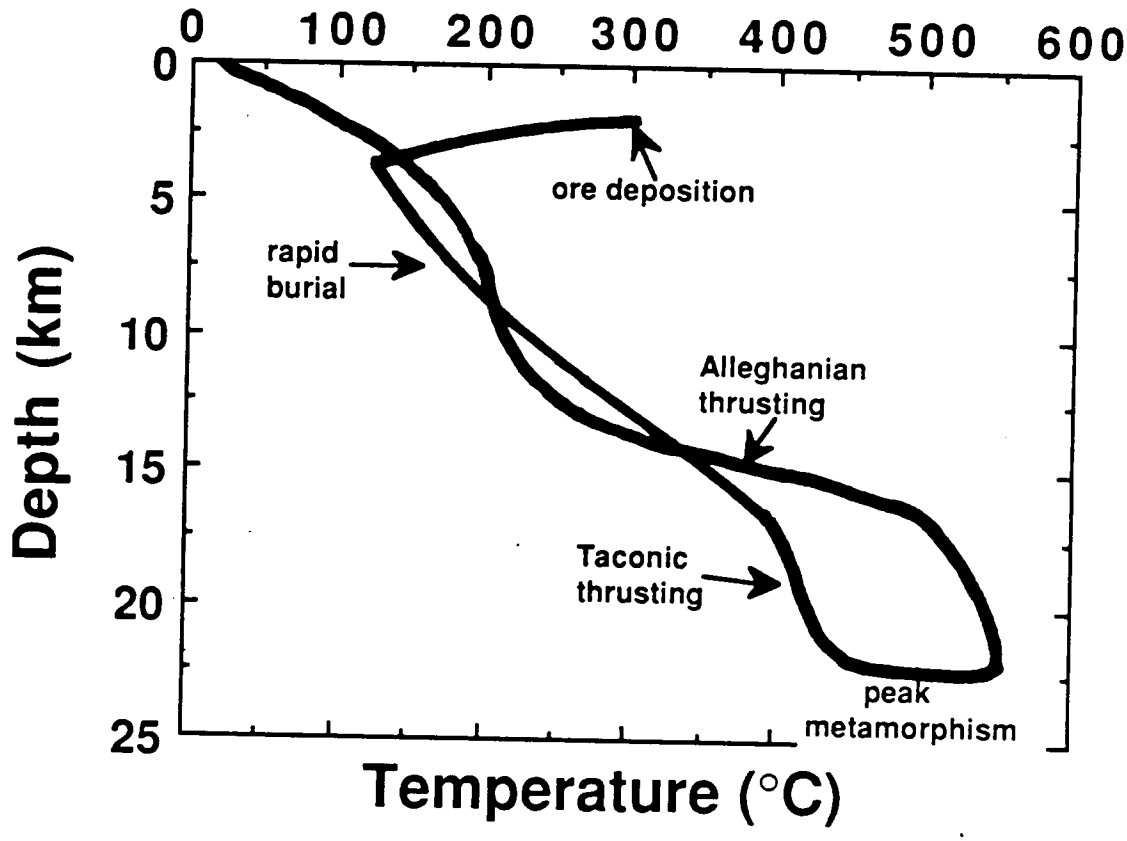

Figure 10. Speculative burial-uplift path consistent with the tectonic history of Ducktown. See text for discussion.

during Alleghanian overthrusting of Ducktown rocks (Fig. 10). Subsequent thermal relaxation produced an isothermal jog in the uplift path followed by post-tectonic cooling along a local geotherm.

The conjectural burial/uplift path shown in Figure 10 is consistent with all fluid inclusion information as well. In particular, the s-shaped uplift path suggested by tectonic considerations is very similar to the uplift path constrained by fluid inclusion data although the mechanism responsible for the isothermal portion is different. We interpret the severe isothermal jog in the uplift path inferred by immiscible H_2O-CH_4-N_2-NaCl inclusions to record fluctuations in fluid pressure during Alleghanian thrusting. It is likely that the pressure variations record oscillations from near lithostatic to near hydrostatic conditions in response to episodic fracturing associated with thrust movement. It is equally as likely that pressure release associated with faulting caused boiling of the H_2O-CH_4-N_2-NaCl fluids. No correlation between age of a plane of inclusions and inclusion density (inferred trapping pressure) could be discerned, early planes being both higher and lower density than later planes. This is consistent with the vassilatory nature of the pressure regime.

Timing and Sources of Fluids

Dallmeyer (1975a) determined $^{40}Ar/^{39}Ar$ incremental gas release ages of 424-435±15 ma. for two biotite samples collected near the margin of the Cherokee orebody and 372±15 ma. for a single sample collected near the center of the orebody. These were interpreted to be cooling ages rather than ages of peak metamorphism, which is placed at 480 ma. on the basis of

Rb-Sr work by Fullagar & Bottino (1970) and other geochronologic data (Dallmeyer, 1975b). Hanson & Gast (1967) have shown that the blocking temperature for argon retention in biotite is 325±25°C. Using this information in conjunction with our uplift path (Fig. 9B) we conclude that at about 430-370 million years ago Ducktown orebodies were experiencing P-T conditions of about 325°C and 4.2 kb. Given that peak metamorphism (6 kb, 550°C) occurred at about 480 ma., we calculate an average uplift rate of 0.13 or 0.06 mm/yr from Middle Ordovician to Middle Silurian or Late Devonian, depending on which retention age is used. The younger cooling age, recorded by biotite in the ore zone, implies either that the orebody cooled slower than the host rocks or that the interior of the orebody was subjected to a later thermal event, both of which imply slightly different P-T-time paths for orebodies and host rocks. Fluid inclusion evidence presented earlier suggests that the orebodies may have been channels for fluid flow during uplift. This presumably resulted from rheological contrasts between the sulfide bodies and surrounding silicate rocks, which allowed development of fractures near orebodies. It is possible that fluids circulated through the orebodies during the Acadian (380-340 ma.) and caused argon to be lost from biotite in ore zones. This hypothesis is consistent with the Rb-Sr work of Fullagar & Bottino (1970) who report that samples away from the ore zones approximate an isochron corresponding to 475 ma., which is interpreted to be the age of peak metamorphism, but that samples collected near the orebodies suggest significantly younger ages. These authors interpreted the younger ages to have resulted from loss of radiogenic and common Sr from the ore zones.

An additional constraint on uplift comes from the Jamieson & Beaumont model (1988), which suggests that 4-5 km of erosion has occurred at Ducktown since the end of the Alleghanian (250 ma.). This implies an average uplift rate of 0.06 or 0.09 mm/yr from Middle Silurian or Late Devonian to Late Permian. The calculated average uplift rate from 250 ma. to the present is 0.02 mm/yr.

The age-uplift relationships shown in Figure 9B imply that low salinity, one phase aqueous inclusions were trapped prior to the Acadian (probably late Taconian), and that H_2O-CO_2-NaCl inclusions were trapped during the Acadian. Immiscible H_2O-CH_4-N_2-NaCl inclusions are Alleghanian in age and $CaCl_2$-$MgCl_2$-NaCl-H_2O inclusions are post-Alleghanian.

Although the sources of the fluids represented by secondary fluid inclusions are in most cases unresolved, some generalizations can be made based on the P-T-time relationships established above. The localized nature of early fluids (e.g. primary fluid inclusions and low salinity one phase and H_2O-CO_2-NaCl secondary inclusions) and the pervasive nature of later fluids (e.g. immiscible H_2O-CH_4-N_2-NaCl and $CaCl_2$-$MgCl_2$-NaCl-H_2O inclusions) suggests that early fluids were derived by local devolatilization reactions and later fluids were externally derived.

The composition of H_2O-CO_2-NaCl inclusions, which also contain minor CH_4, combined with inferred trapping conditions near 5 kb and 400°C (Fig. 9B) implies fO_2 conditions approximately one log unit above FMQ. The oxidation state of this fluid is consistent with local derivation from rocks near the orebodies. The orebodies were buffered at fO_2 conditions ranging from FMQ to three log units above FMQ at conditions of peak metamorphism, while

distal host rocks were buffered at fO_2 conditions ranging from FMQ to approximately one log unit below FMQ (Nesbitt & Kelly, 1980; Hall, Bodnar & Craig, 1989).

The compositions of H_2O-CH_4-N_2-NaCl fluids suggest derivation from reduced lithologies buffered at fO_2 conditions significantly below FMQ. These fluids were probably formed by expulsion of pore fluids and maturation of organic material during thrusting of Ducktown orebodies over unmetamorphosed sediments. Episodic fracturing allowed these fluids to "boil" and circulate upward from the lower plate.

SUMMARY

Primary fluid inclusions trapped in peak metamorphic clinopyroxene and garnet contain H_2O-CH_4-NaCl fluids and daughter crystals of calcite, quartz and pyrrhotite. Although post-trapping volumetric and compositional changes have occurred, significant quantities of dissolved solids must have been present in the peak metamorphic fluids which formed pyroxene and garnet in the ore zones.

Secondary fluid inclusions in quartz from ore zones and country rocks document a complex uplift history involving a variety of fluids in the system C-O-H-N-salt. Early fluids were formed by local devolatilization reactions while late fluids were more pervasive and were externally derived. The ore zones appear to have acted as conduits for fluid flow during the later stages of uplift.

Secondary fluid inclusions constrain uplift to have been temperature-concave from 6 kb and 550°C to 2.3 kb and 215°±20°C and then nearly

isothermal at 215°±20°C over the pressure range 2.3-1.0 kb. The latest stages of uplift appear to have been temperature-convex. This P-T-time path is consistent with the tectonic history of the Ducktown area. Temperature-concave uplift occurred from 480 ma. to 427-372 ma. implying average uplift rates of 0.13 to 0.06 mm/yr. Uplift rates of 0.06-0.09 mm/yr from 424-372 ma. to 250 ma. are implied by our data.

Isothermal decompression is documented by immiscible H_2O-CH_4-N_2-NaCl fluids that were emplaced during Alleghanian thrusting and which were derived by expulsion of pore fluids and maturation of organic material in lower plate sediments. Episodic movement along the Great Smoky and related faults caused these fluids to "boil" and move upward.

REFERENCES

Addy, S. K. & Ypma, P. J. M., 1977. Origin of massive sulfide deposits at Ducktown, Tennessee: An oxygen, carbon, and hydrogen isotope study. *Economic Geology*, **72**,1245-1268.

Albarede, F., 1976. Thermal models of post-tectonic decompression as exemplified by the Haut-Allier granulites (Massif Central, France). *Bulletin Soc. Geol. Fr.*, **18**, 1023-1032.

Bodnar, R. J., 1985. P-V-T properties of the system NaCl-H_2O. *Unpubl. PhD Thesis, The Pennsylvania State University, University Park, PA.*

Bodnar, R. J., Burnham, C. W. & Sterner, S. M., 1985. Synthetic fluid inclusions in natural quartz. III. Determination of phase equilibrium properties in the system H_2O-NaCl to 1000°C and 1500 bars. *Geochimica et Cosmochimica Acta*, **49**, 1861-1873.

Bodnar, R. J., Binns, P. R. & Hall, D. L., 1989. Synthetic fluid inclusions. VI. Quantitative evaluation of the decrepitation behavior of fluid inclusions in quartz at one atmosphere confining pressure. *Journal of Metamorphic Geology*, **6**, 229-242.

Bohlen, S. R., 1987. Pressure-temperature-time paths and a tectonic model for the evolution of granulites. *Journal of Geology*, **95**, 617-632.

Bozzo, A. T., Chen, H-S, Kass, J. R. & Barduhn, A. J., 1973. The properties of the hydrates of chlorine and carbon dioxide. *4th International Symposium on Fresh Water from the Sea*, **3**, 437-451.

Brooker, D. D., Craig, J. R. & Rimstidt, J. D., 1987. Ore metamorphism and pyrite porphyroblast development at the Cherokee Mine, Ducktown, Tennessee. *Economic Geology*, **82**, 72-86.

Brown, P. E. & Lamb, W. M., 1989. P-V-T properties of fluids in the system $H_2O \pm CO_2 \pm$NaCl: New graphical presentations and implications for fluid inclusion studies. *Geochimica et Cosmochimica Acta* (in press).

Butler, J. R., 1972. Age of Paleozoic metamorphism in the Carolinas, Georgia, and Tennessee Southern Appalachians. *American Journal of Science*, **272**, 319-333.

Carpenter, R. H., 1970. Metamorphic history of the Blue Ridge province of Tennessee ade North Carolina. *Geological Society of America Bulletin*, **81**, 749-762.

Casquet, C., 1986. C-O-H-N fluids in quartz segregations from a major ductile shear zone: the Berzosa fault, Spanish Central System. *Journal of Metamorphic Geology*, **4**, 117-130.

Collins, P. L. F., 1979. Gas hydrates in CO_2-bearing fluid inclusions and the use of freezing data for the estimation of salinity. *Economic Geology*, **74**, 1435-1444.

Craig, J. R., 1983. Metamorphic features in Appalachian massive sulfides. *Mineralogical Magazine*, **47**, 515-525.

Dallmeyer, R. D., 1975a. $^{40}Ar/^{39}Ar$ incremental release ages of biotite from the Cherokee orebody, Ducktown, Tennessee: their bearing on the age of sulfide mineralization. *Economic Geology*, **70**, 341-345.

Dallmeyer, R. D., 1975b. Incremental $^{40}Ar/^{39}Ar$ ages of biotite and hornblende from retrograded basement gneisses of the Southern Blue Ridge: their bearing on the age of Paleozoic metamorphism. *American Journal of Science*, **275**, 444-460.

Davis, D. W., Lowenstein, T. K. & Spencer, R. J., 1989. Melting behavior of fluid inclusions in laboratory-grown halite crystals in the systems $NaCl-H_2O$, $NaCl-KCl-H_2O$, $NaCl-MgCl_2-H_2O$, & $NaCl-CaCl_2-H_2O$. *Geochimica et Cosmochimica Acta* (in press).

Deaton, W. M. & Frost, E. M., Jr., 1946. Gas hydrates and their relation to the operation of natural gas pipelines. *U. S. Bureau of Mines Monograph*, **8**, 103p.

Droop, G. T. R., 1985. Alpine metamorphism in the south-east Tauern Window, Austria: 1. P-T variations in space and time. *Journal of Metamorphic Geology*, **3**, 371-402.

Dubessy, J., 1984. Simulation des equilibres chimiques dans le systeme COH. Consequences methodologiques pour les inclusions fluides. *Bull. Mineral.*, **107**, 155-168.

Einaudi, M. T., Meinert L. D. & Newberry, R. J., 1981. Skarn deposits. *Economic Geology 75th Anniversary Volume*, 317-391.

Emmons, W. H. & Laney, F. B., 1926. Geology and ore deposits of the Ducktown mining district, Tennessee. *U. S. Geological Survey Professional Paper*, **139**, 114p.

England, P. C. & Richardson, S. W., 1977. The influence of erosion upon the mineral facies of rocks from different metamorphic environments. *J. Geol. Soc. London*, **134**, 201-213.

England, P. C. & Thompson, A. B., 1984. Pressure-temperature-time paths of regional metamorphism I. Heat transfer during the evolution of regions of thickened crust. *Journal of Petrology*, **25**, 894-928.

Eugster, H. P. & Skippen, G. B., 1967. Igneous and metamorphic reactions involving gas equilibria. In *Researches in Geochemistry, II* (ed Abelson, P. H.). New York, John Wiley and Sons, 942-520.

Fredrich, J. T. & Wong, T., 1986. Micromechanics of thermally induced cracking in three crustal rocks. *Journal of Geophysical Research,* **91**, 12,743-12,764.

French, B. M., 1966. Some geological implications of equilibrium between graphite and a C-H-O gas phase at high temperatures and pressures. *Reviews of Geophysics*, **4**, 223-253.

Fullagar, P. D. & Bottino, M. L., 1970. Sulfide mineralization and rubidium-strontium geochronology at Ore Knob, North Carolina, and Ducktown, Tennessee. *Economic Geology*, **65**, 541-550.

Gair, J. E. & Slack, J. F., 1984. Deformation, geochemistry, and origin of massive sulfide deposits, Gossan Lead District, Virginia. *Economic Geology*, **79**, 1483-1520.

Giletti, B. J. & Anderson, T. F., 1975. Studies in diffusion, II. Oxygen in phlogopite mica. *Earth and Planetary Science Letters*, **28**, 225-238.

Gilletti, B. J. & Yund, R. A., 1984. Oxygen diffusion in quartz. *Journal of Geophysical Research*, **89**, 4039-4046.

Giletti, B. J., Semet, M. P. & Yund, R. A., 1978. Studies in diffusion, III. Oxygen in feldspars, an ion microprobe determination. *Geochimica et Cosmochimica Acta*, **42**, 45-57.

Glover, L., III, Speer, J. A., Russell, G. S. & Farrar, S. S., 1983. Ages of regional metamorphism and ductile deformation in the central and southern Appalachians. *Lithos*, **16**, 223-245.

Hadley, J. B., 1970. The Ocoee Series and its possible correlatives. In *Studies of Appalachian Geology - Central and Southern* (eds Fisher, G. W. and others). New York, Interscience Publishers, 247-259.

Hadley, J. B. & Goldsmith, R., 1963. Geology of the eastern Great Smoky Mountains, North Carolina and Tennessee. *U. S. Geological Survey Professional Paper*, **349-B**, 118 p.

Hall, D. L. & Bodnar, R. J., 1986. Determination of isochoric P-T paths for fluid inclusions which decrepitate prior to homogenization (abstr.). *Geological Society of America Abstracts with Programs*, **18**, 625.

Hall, D. L. & Bodnar, R. J., 1989. Methane in fluid inclusions from granulites: A product of hydrogen diffusion?. *Geochimica et Cosmochimica Acta* (in review).

Hall, D. L., Bodnar, R. J. & Craig, J. R., 1989. Fluid evolution during metamorphism and uplift of the massive sulfide deposits at Ducktown, Tennessee, U.S.A. II. Evidence for compositional changes to fluid inclusions via hydrogen diffusion. *American Mineralogist* (in preparation).

Hall, D. L., Wesolowski, D., Bodnar, R. J. & Craig, J. R., 1989. Fluid evolution during metamorphism and uplift of the massive sulfide deposits at Ducktown, Tennessee, U.S.A. III. Stable isotope systematics. *Economic Geology* (in preparation).

Hall, D. L., Sterner, S. M. & Bodnar, R. J., 1988. Freezing point depression of NaCl-KCl-H_2O solutions. *Economic Geology*, **83**, 197-202.

Hall, D. L., Sterner, S. M. & Bodnar, R. J., 1989. Fluid inclusions in regional metamorphic rocks: experimental evidence for post-entrapment volumetric and compositional modifications (abstr.). *10th European Current Research on Fluid Inclusions, Royal School of Mines, Imperial College, University of London*, 44.

Hanson, G. N. & Gast, P. W., 1967. Kinetic studies in contact metamorphic zones. *Geochimica et Cosmochimica Acta*, **31**, 1119-1153.

Harley, S., 1987. Isobaric cooling in high grade terranes: constraints and inferences (abstr.). *Metamorphic Studies Group Joint meeting with IGCP Project 235, Evolution of Metamorphic Belts, Dublin, Ireland, 1987.*, 10.

Harris, N. B. W. & Holland, T. J. B., 1984. The significance of cordierite-hypersthene assemblages from the Beitbridge region of the central Limpopo belt: evidence for rapid decompression in the Archaen?. *American Mineralogist*, **69**, 1036-1049.

Hatcher, R. D., Jr., 1978. Tectonics of the western Piedmont and Blue Ridge, Southern Appalachians: review and speculations. *American Journal of Science*, **278**, 276-304.

Hatcher, R. D., Jr. & Zietz, I., 1980. Tectonic implications of regional aeromagnetic and gravity data from the Southern Appalachians. In *Proceedings the Caledonides in the U.S.A., IGCP Project 27: Caledonide Orogen* (ed Wones, D. R.), 235-244.

Hatcher, R. D., Jr., Butler, J. R., Fullagar, P. D., Secor, D. T. & Snoke, A. W., 1980. Geologic Synthesis of the Tennessee-Carolinas-Northeast Georgia Southern Appalachians. In *Proceedings the Caledonides in the U.S.A., IGCP Project 27: Caledonide Orogen* (ed Wones, D. R.), 83-90.

Henry, D. K., Craig, J. R. & Gilbert, M. C., 1979. Ore mineralogy of the Great Gossan Lead, Virginia. *Economic Geology*, **74**, 645-656.

Hensen, B. J. & Warren, R. G., 1987. The P-T evolution of the Proterozoic Arunta block, Central Australia (abstr.). *Metamorphic Studies Group Joint meeting with IGCP Project 235, Evolution of Metamorphic Belts, Dublin, Ireland, 1987.*, 10.

Holcombe, R. J., 1973. Mesoscopic and microscopic analysis of deformation and metamorphism near Ducktown, Tennessee. Ph. D. Thesis, Stanford University, 225 p.

Holland, H. D. & Malinin, S. D., 1979. The solubility and occurrence of non-ore minerals. In *Geochemistry of Hydrothernal Ore Deposits, 2nd Edition* (ed. Barnes, H. L.). New York, Wiley-Interscience, 461-508.

Hollister, L. S., Burruss, R. C., Henry, D. L. & Hendel, E., 1979. Physical conditions during uplift of metamorphic terranes, as recorded by fluid inclusions. *Bulletin de Mineralogie*, **102**, 555-561.

Holloway, J. R., 1977. Fugacity and activity of molecular species in supercritical fluids. In *Thermodynamics in Geology* (ed Fraser, D. G.). Dordrecht, D. Reidel Publishing Company, 161-181.

Holloway, J. R., 1981. Compositions and volumes of supercritical fluids in the earth's crust. In *Short Course in Fluid Inclusions: Applications to Petrology* (eds Hollister, L. S. and Crawford, M. L.). *Mineral. Assoc. Canada*, **6**, 13-38.

Jamieson R. A. & Beaumont, C., 1988. Orogeny and metamorphism: a model for deformation and pressure-temperature-time paths with applications to the central and southern Appalachians. *Tectonics*, **7**, 417-445.

Kerkhof, A. M., van den 1988. The system CO_2-CH_4-N_2 in fluid inclusions: Theoretical modelling and geological applications. Ph.D. Thesis, Free University - Amsterdam, 206p.

Kleinrahm, R. & Wagner, W., 1986. Measurement and correlation of the equilibrium liquid and vapour densities and the vapour pressure along the coexistence curve of methane. *Journal of Chemical Thermodynamics*, **18**, 739-760.

Kobayashi, R., Withrow, H. J., Williams, G. B. & Katz, D. L., 1951. Gas hydrate formation with brine and ethanol solutions. *Proceedings of the 30th Annual Convention Natural Gasoline Association of America*, 27-31.

Kreulen, R., 1987. Thermodynamic calculations of the C-O-H system applied to fluid inclusions: Are fluid inclusions unbiased samples of ancient fluids? *Chemical Geology*, **61**, 59-64.

Kronenberg, A. K., Kirby, S. H., Aines, R. D. & Rossman, G. R., 1986. Solubility and diffusional uptake of hydrogen in quartz at high water pressures: Implications for hydrolytic weakening. *Journal of Geophysical Research*, **91**, 12723-12744.

Lawler, J. P. & Crawford, M. L., 1983. Stretching of fluid inclusions resulting from a low-temperature microthermometric technique. *Economic Geology*, **78**, 527-529.

Lawson, L. S. & Misra, K. C., 1985. Geochemistry and tectonic significance of amphibolites of the Ducktown Mining District, Tennessee (abstr.). *Geological Society of America Abstracts with Programs*, **17**, 640.

Linke, W. F., 1965. *Solubilities of inorganic and metal organic compounds.* American Chemical Society, **2**, Van Nostrand, 1914 p.

Magee, M., 1968. Geology and ore deppsits of the Ducktown district, Tennessee. In *Ore deposits of the United States: 1933-1967* (ed Ridge, J. D.). *American Institute of Mining, Metallurgical, and Petroleum Engineers, Inc.*, 207-241.

Muelenbachs, K. & Kushiro, I., 1974. Oxygen isotope exchange and equilibrium of silicates with CO_2 and O_2. *Carnegie Institute Washington, D. C., Yearbook*, **73**, 232-236.

Mullis, J., 1979. The system methane-water as a geologic thermometer and barometer from the external part of the Central Alps. *Bulletin de Mineralogie*, **102**, 526-536.

Nesbitt, B. E., 1979. Regional metamorphism of the Ducktown, Tennessee massive sulfides and adjoining portions of the Blue Ridge Province. Ph. D Thesis. Univerisity of Michigan, 216 p.

Nesbitt, B. E., 1982. Metamorphic sulfide-silicate equilibria in the massive sulfide deposits at Ducktown, Tennessee. *Economic Geology*, **77**, 364-378.

Nesbitt, B. E. & Essene, E. J., 1982. Metamorphic thermometry and barometry of a portion of the southern Blue Ridge province. *American Journal of Science*, **282**, 701-729.

Nesbitt, B. E. & Kelly, W. C., 1980. Metamorphic zonation of sulfides, oxides and graphite in and around the orebodies at Ducktown, Tennessee. *Economic Geology*, **75**, 1010-1021.

Ohmoto, H. & Kerrick, D., 1977. Devolatilization equilibria in graphitic systems. *American Journal of Science*, **277**, 1013-1044.

Oxburgh, E. R. & England, P. C., 1980. Heat flow and the metamorphic evolution of the eastern Alps. *Eclogae. Geol. Helv.*, **73**, 379-398.

Pasteris, J. D. & Wanamaker, B. J., 1988. Laser raman microprobe analysis of experimentally re-equilibrated fluid inclusions in olivine: Some implications for mantle fluids. *American Mineralogist*, **73**, 1074-1088.

Popp, R. D., Gilbert, M. C. & Craig, J. R., 1977. Stability of Fe-Mg amphiboles with respect to sulfur fugacity. *American Mineralogist*, **62**, 13-20.

Potter, R. W., II & Brown, D. L., 1977. The volumetric properties of aqueious sodium chloride solutions from 0° to 500°C and pressures up to 2000 bars based on a regression of available data in the literature. *U. S. Geological Survey Bulletin*, **1421-C**, 36p.

Rankin, D. W., 1975. The continental margin of eastern North America in the Southern Appalchians: the opening and closing of the proto-Atlantic ocean. *American Journal of Science*, **275-A**, 298-336.

Rankin, D. W., 1976. Appalachian salients and recesses: Late Precambrian continental breakup and the opening of the Iapetus Ocean. *Journal of Geophysical Research*, **81**, 5605-5619.

Rodgers, J., 1972. Latest Precambrian (post-Grenville) rocks of the Appalachian region. *American Journal of Science*, **272**, 507-520.

Roedder, E., 1971. Metastability in fluid inclusions. *Soc. Mining Geol. Japan, Spec. Issue*, **3**, 327-334.

Roedder, E., 1984. *Fluid inclusions*. Mineralogical Society of America, Reviews in Mineralogy, **12**, 644 p.

Roedder, E. & Skinner, B. J., 1968. Experimental evidence that fluid inclusions do not leak. *Economic Geology*, **63**, 715-730.

Rudnick, R. L., Ashwal, L. D. & Henry, D. J., 1984. Fluid inclusions in high-grade gneisses of the Kapaskasing structural zone, Ontario: metamorphic fluids and uplift/erosion path. *Contributions to Mineralogy and Petrology*, **87**, 399-406.

Santosh, M., 1987. Cordierite gneisses of southern Kerala, India: Petrology, fluid inclusions and implication for crustal uplift history. *Contributions to Mineralogy and Petrology*, **96**, 343-356.

Schreurs, J., 1984. The amphibolite-granulite facies transition in West Uusimaa, S. W. Finland. A fluid inclusion study. *Journal of Metamorphic Geology*, **2**, 327-341.

Slater, R., 1982. Massive sulfide deposits of the Ducktown mining district, Tennessee. In *Exploration for Metallic Resources in the Southeast.* University of Georgia, Department of Geology and Center for Continuing Education, 91-99.

Spear, F., 1987. Relative thermobarometry, P-T paths and the tectonic evolution of metamorphic belts (abstr.). *Metamorphic Studies Group Joint meeting with IGCP Project 235, Evolution of Metamorphic Belts, Dublin, Ireland, 1987.*, 20.

Sterner, S. M. & Bodnar, R. J., 1984. Synthetic fluid inclusions I: Compositional types synthesized and applications to experimental geochemistry. *Geochimica et Cosmochimica Acta*, **48**, 2659-2668.

Sterner, S. M. & Bodnar, R. J., 1989. Synthetic fluid inclusions - VII. Re-equilibration of fluid inclusions in quartz during laboratory-simulated burial and uplift. *Journal of Metamorphic Geology*,**7**, 243-260.

Sterner, S. M., Hall, D. L. & Bodnar, R. J., 1988a. Synthetic fluid inclusions V: solubility relations in the system NaCl-KCl-H_2O under vapor-saturated conditions. *Geochimica et Cosmochimica Acta*, **52**, 989-1005.

Sterner, S. M., Hall, D. L. & Bodnar, R. J., 1988b. Post-entrapment compositional changes in fluid inclusions: Experimental evidence for water diffusion in quartz (abstr.). *Geological Society of America Abstracts with Programs*, **20**, A100.

Swanenberg, H. E. C., 1980. Fluid inclusions in high-grade metamorphic rocks from S. W. Norway. *Geologica Ultraiectina, Univ. Utrecht.*, **25**, 147p.

Thomas, A. V. & Spooner, E. T. C., 1988. Fluid inclusions in the system H_2O-CH_4-NaCl-CO_2 from metasomatic tourmaline within the border unit of the Tanco zoned granitic pegmatite, S. E. Manitoba. *Geochimica et Cosmochimica Acta*, **52**, 1065-1076.

Tso, J. L., Gilbert, M. C. & Craig, J. R., 1979. Sulfidation of synthetic biotite. *American Mineralogist*, **64**, 304-316.

Unruh, C. H. & Katz, D. L., 1949. Gas hydrates of carbon dioxide and methane mixtures. *Journal of Petroleum Technology*, **1**, 83-86.

Warren, R. G. & Shaw, R. D., 1985. Volcanogenic Cu-Pb-Zn bodies in granulites of the central Arunta Block, central Australia. *Journal of Metamorphic Geology*, **3**, 481-499.

CHAPTER III

FLUID SPECIATION CALCULATIONS AND EVIDENCE FOR HYDROGEN DIFFUSION

INTRODUCTION

In part I of the present study primary fluid inclusions in pyroxene in ore zones were found to contain an H_2O-CH_4-NaCl fluid with 3 wt% NaCl and 5 mol% CH_4. These inclusions also contain daughter crystals of calcite, quartz and pyrrhotite. Re-integration of all fluid and solid components into a homogeneous fluid, assuming that carbon in carbonate and sulfur in pyrrhotite were present in the peak metamorphic fluid as CO_2 and H_2S, respectively, results in a normalized volatile composition of 93 mol% H_2O, 4 mol% CH_4, 3 mol% CO_2 and 0.1 mol% H_2S (Hall et al., 1989a). In the present communication, the volatile composition presented above is compared to C-O-H-S fluid speciation calculations, and a model for hydrogen diffusion into primary fluid inclusions is presented to explain the discrepancies in calculated and observed fluid compositions.

GEOLOGIC SETTING

Details of the geology and tectonic setting of the Ducktown, Tennessee massive sulfide deposit were presented in part I of this study and will not be duplicated here. The following is a condensed version describing the salient features of the orebodies.

The deposit is located in the southeast corner of Tennessee in the Blue Ridge Province of the southern Appalachians (Fig. 1), and consists of eight

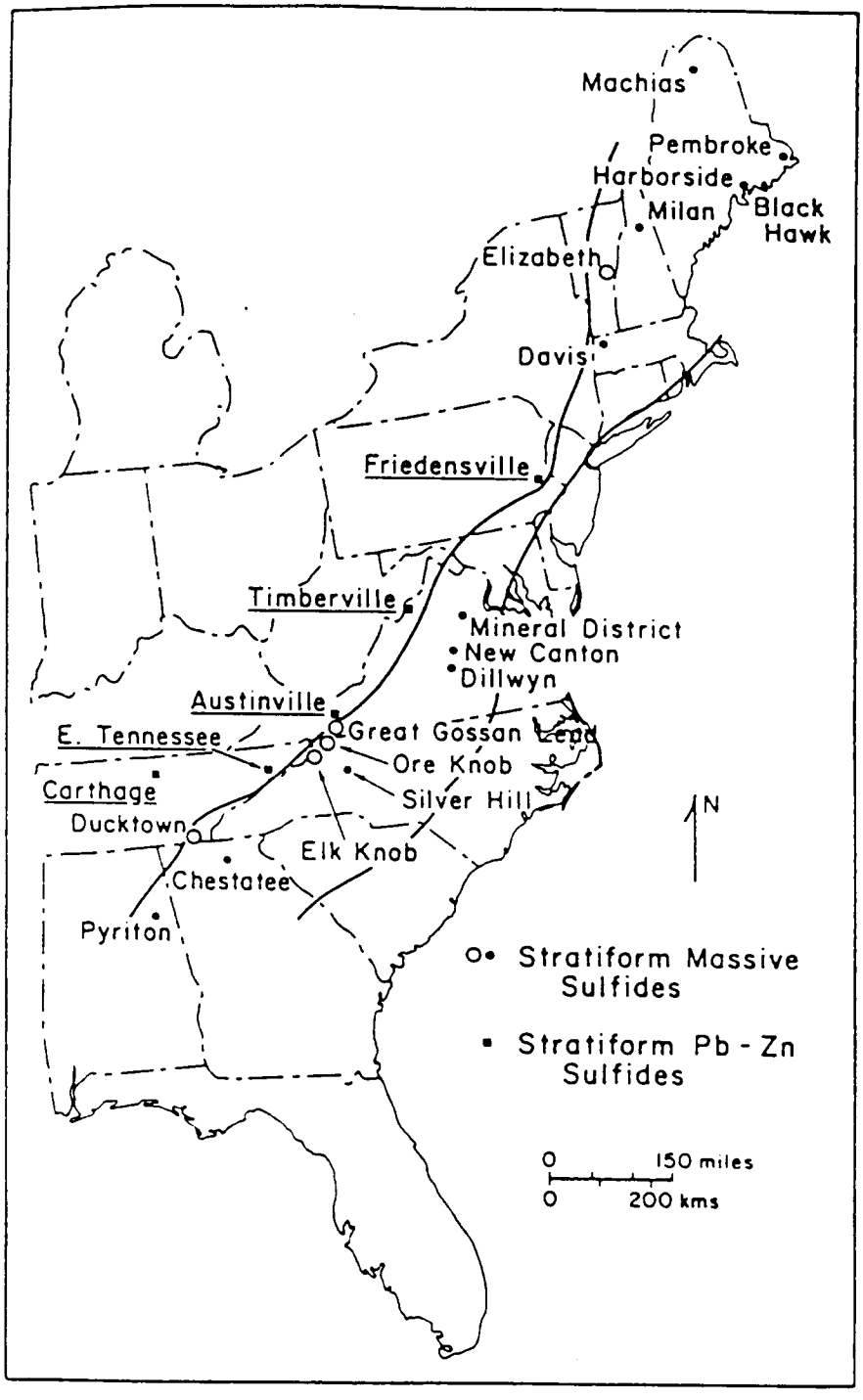

Figure 1. Index map of the eastern U. S. showing the locations of stratiform ore deposits in the Appalachians. From Craig (1983).

major pyrrhotite-rich bodies containing subordinate pyrite, chalcopyrite, sphalerite, galena, magnetite and traces of other ore minerals. The country rocks hosting the orebodies are dominantly metagraywackes and quartz-mica schists with lesser quartzite, metaconglomerate and calc-silicate hornfels.

The orebodies were formed in a rift environment by a sea floor hydrothermal system associated with the opening of Iapetus in the Late Precambrian (Mauger, 1972; Addy, 1973; Nesbitt, 1979). The deposit was metamorphosed and deformed twice in the Taconic (480-440 Ma) and metamorphosed once and deformed several times in the Alleghanian (300-250 Ma) (Holcombe, 1973; Addy and Ypma, 1977). Peak metamorphism occurred at 6-7 kbar and 525-550°C (Nesbitt and Essene, 1982; Brooker et al., 1987; Hall et al., 1989c). Metamorphism and deformation was in response to the closing of Iapetus during the Paleozoic.

C-O-H-S FLUID CALCULATIONS

Method

Speciation in the peak metamorphic fluids was calculated using the "equilibrium constants - mass balance" technique (French, 1966; Eugster and Skippen, 1967; Holloway, 1977; Ohmoto and Kerrick, 1977; Ferry and Baumgartner, 1987). The general procedure of Ohmoto and Kerrick (1977) was modified to allow for carbon activity less than one and for non-ideal mixing in the fluid phase. In a homogeneous C-O-H-S fluid five variables must be specified for the system to be invariant. However, if graphite is present then the system is invariant when four parameters are defined. By

fixing the fluid pressure (P_{fluid}), temperature (T), oxygen fugacity (fO_2), sulfur fugacity (fS_2) and the activity of carbon (a_C), the system is completely constrained. We have assumed that the species present are H_2, O_2, S_2, H_2O, H_2S, CO_2, COS, CO, SO_2 and CH_4, which are related through the linearly independent reactions

$$C + O_2 = CO_2 \quad (1)$$

$$CO + 1/2O_2 = CO_2 \quad (2)$$

$$H_2 + 1/2O_2 = H_2O \quad (3)$$

$$CH_4 + 2O_2 = CO_2 + 2H_2O \quad (4)$$

$$1/2S_2 + O_2 = SO_2 \quad (5)$$

$$CO + 1/2S_2 = COS \quad (6)$$

$$1/2S_2 + H_2O = H_2S + 1/2O_2 \quad (7)$$

and the constraint that

$$\Sigma X_i = 1 \quad (8).$$

(see Table 1 for all notation). If real mixing in the fluid is assumed for the 10 species then the mole fractions of these species at constant P_{fluid} and T are related to their fugacities by the equation

$$(f_i)_{Pfluid,T} = \Gamma_i X_i \gamma_i P_{fluid} \quad (9).$$

If species are assumed to mix ideally then equation (9) reduces to

Table 1. Notation

a	empirical coefficient of the RK	Mt	magnetite
a_C	activity of carbon	Musc	muscovite
Act	actinolite	n_i	initial number of moles
An	anorthite	n_f	final number of moles
Anhy	anhydrite	P_{fluid}	fluid pressure
b	empirical coefficient of the RK	Po	pyrrhotite
Cc	calcite	Py	pyrite
Czo	clinozoisite	Qtz	quartz
Di	diopside	R	gas constant
f	fugacity	Rut	rutile
Gt	garnet	Spn	sphene
Graph	graphite	T	temperature
i	fluid component	Trem	tremolite
ij	interaction between unlike molecules	V	mean molar volume
Ilm	ilmenite	X	mole fraction
j	fluid component	Zo	zoisite
k	iteration number	γ	fugacity coefficient
Ksp	K-feldspar	Γ	activity coefficient
m	pertaining to the fluid mixture		

$$(f_i)_{Pfluid,T} = X_i \gamma_i P_{fluid} \qquad (10).$$

Functions describing the equilibrium constants for reactions (1)-(7) are presented in Ohmoto and Kerrick (1977). Fugacity coefficients for ideal mixing were taken from Burnham et al. (1969) for H_2O, Wall and Burnham (1974) for CO_2, Shaw and Wones (1964) for H_2 below 3 kbar and from the reduced variable equations of Ryzhenko and Volkov (1971) for CO, CH_4, SO_2, COS and H_2S and for H_2 above 3 kbar. Following Ohmoto and Kerrick (1977) γS_2 was assumed to be unity. Fugacities for real mixing were calculated from the equation

$$\ln(f_i) = \ln[V/(V-b_m)] + b_i/(V-b_m) - [2\Sigma X_j a_{ij}/(RT^{1.5}b_m)]\ln[(V+b_m)/V] + (a_m b_i/b_m^2 RT^{1.5})\{\ln[(V+b_m)/V] - b_m/(b_m+V)\} - \ln(V/RT) \qquad (11)$$

(Flowers and Helgeson, 1983). The *a* and *b* terms were generated from the subroutine MRKMIX (Holloway, 1981). The general Redlich-Kwong equation was then solved explicitly for mean molar volume.

To calculate the mixing terms the mole fractions of the species must be known. These were obtained by assuming ideal mixing to calculate the initial real mixing fugacity coefficients and then using the resulting mole fractions as the new mole fractions to re-calculate the real mixing fugacity coefficients. Convergence is reached in about six iterations. The criteria for convergence is that the relative variation in mole fraction between two successive iterations is less than 10^{-4} for all species:

$$|X_i^k - X_i^{k-1}| \setminus X_i^k < 10^{-4} \quad (12).$$

Mineralogical constraints on fluid composition

Major components

The four reactions:

$$Trem + Cc + Qtz = Di + H_2O + CO_2 \quad (13)$$

$$2Zo + CO_2 = Cc + 3An + H_2O \quad (14)$$

$$Musc + Cc + Qtz = Ksp + An + H_2O + CO_2 \quad (15)$$

$$Rut + Cc + Qtz = Spn + CO_2 \quad (16)$$

constrain X_{CO_2} within the orebodies and country rocks, with the assumption that $X_{H_2O} + X_{CO_2} = 1$. As will be shown, this restriction is generally valid except at the lowest fO_2 and/or highest fS_2 conditions indicated by sulfide-oxide-graphite equilibria at Ducktown. Figure 2 shows the projection of these devolatilization reactions onto T-X_{CO_2} space for P_{fluid} = 6 kbar (see Nesbitt, 1979).

A lower limit for X_{CO_2} in the country rocks is provided by Zo(Czo)-An-Cc-Qtz, typically found in nodules of calc-silicate hornfels within metagraywacke. This assemblage restricts X_{CO_2} to approximately 0.10 at peak metamorphic conditions of 550°C and 6 kbar (Fig. 2); however, in the metagraywackes and schists, which make up the bulk of the country rocks, Cc + An without the presence of epidote minerals suggests X_{CO_2} greater than 0.10. An-Ksp-Musc-Cc-Qtz is common in the country rocks and restricts X_{CO_2} to about 0.15 at 550°C (Fig. 2). Assemblages indicative of $0.10 < X_{CO_2} <$

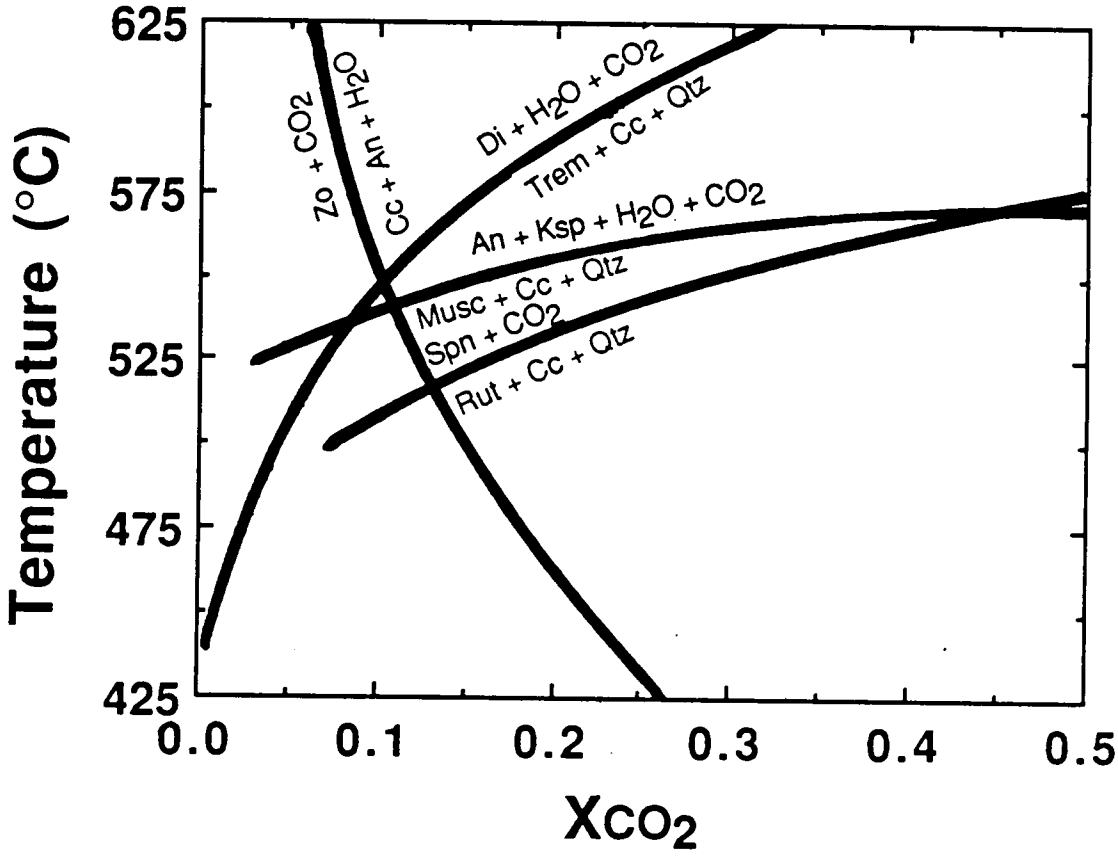

Figure 2. T-XCO_2 relations, calculated for P_{fluid} of 6 kbar, illustrating XCO_2-constraining equilibria pertinent to mineral assemblages at Ducktown. Modified after Nesbitt (1979).

0.15 (e.g. An-Musc-Ksp-Qtz) and $0.15 < X_{CO_2} < 0.85$ (e.g. An-Musc-Cc-Qtz) are also present. Rut-Cc-Qtz is not observed in the country rocks and hence provides an upper limit of approximately 0.35 for X_{CO_2} at 550°C. No systematic spatial variations in the major fluid components H_2O and CO_2 are recorded, as assemblages indicating relatively high X_{CO_2} can be found a few meters from those indicating low X_{CO_2}. It appears that fluid composition was largely controlled by the local metamorphic mineral assemblage and that X_{CO_2} varied between >0.10 and <0.35 within the country rocks.

In the ore zones Di-Trem-Cc-Qtz restricts X_{CO_2} to approximately 0.10 at 550°C. In some cases clinozoisite or zoisite and plagioclase coexist with the above assemblage, a further indication of an X_{CO_2} near 0.10 (Fig. 2). In some samples amphibole is clearly retrograde, plagioclase is missing and the stable peak metamorphic assemblage appears to have been Di-Cc-Qtz; thus, X_{CO_2} was less than 0.10 in these samples. In most of the calc-silicate rocks the stable mineral assemblage is Trem-Cc-Qtz indicating $X_{CO_2} > 0.10$. As in country rocks, samples from the ore zones contain mineral assemblages indicative of X_{CO_2} conditions on either side of equilibrium (15). In addition, Rut-Cc-Qtz is not uncommon, indicating X_{CO_2} in excess of 0.35. Thus, X_{CO_2} conditions in the ore zones appear to have varied from <0.1 to >0.35. As in the country rocks, there is no discernible trend in fluid composition in the ore zones and, again, fluid composition appears to have been locally controlled. This is consistent with centimeter-scale variations in oxide-sulfide mineral assemblages that indicate small-scale variations in fO_2 and fS_2 (see below). Relatively high X_{H_2O} conditions indicated by mineral assemblages in pyroxene-bearing samples are consistent with compositions

of primary fluid inclusions found in pyroxene ($X_{H_2O} \approx 0.9$-0.95) although, as we will show, the original compositions of these inclusions have been modified to slightly higher X_{H_2O}.

The addition of salt to fluid-mineral systems depresses the stability fields of mineral assemblages on the CO_2-bearing sides of reactions (13)-(16) by increasing the activity of CO_2 in the fluid phase (Jacobs and Kerrick, 1981; Bowers and Helgeson, 1983). Thus, the maximum and minimum X_{CO_2} conditions actually experienced by rocks at Ducktown may be significantly less than estimated above. The presence of appreciable amounts of dissolved constituents in peak metamorphic fluids is indicated by primary fluid inclusions in pyroxene, which contain 3 wt% NaCl equivalent and imply over 11 wt% total dissolved solids in the trapped fluid (Hall et al., 1989a).

Estimates of fS_2 and fO_2

Conditions of fO_2 and fS_2 can be reasonably well-constrained using silicate-oxide-sulfide-graphite equilibria. By considering equilibria among Fe-Ti-Ca-C-O-S bearing mineral assemblages, Nesbitt and Kelly (1980) concluded that fO_2 and fS_2 both generally increase as the orebodies are approached. They suggested minimum values of log fO_2 of -22 and log fS_2 of -6.5 for the country rocks and maximum values of log fO_2 of -18.3 and log fS_2 of -2.7 for Py-Po-Mt ore. Relevant phase equilibria in the system Fe-Ti-O-S are shown in Figure 3. Microprobe analyses of sulfide and oxide phases indicate that pyrite, rutile and magnetite are virtually pure end-members, while ilmenite contains an average of 2 mol% Fe_2O_3, 1 mol% MgO and 1 mol% MnO. Pyrrhotite has an average iron content of 47.5 atomic %. The

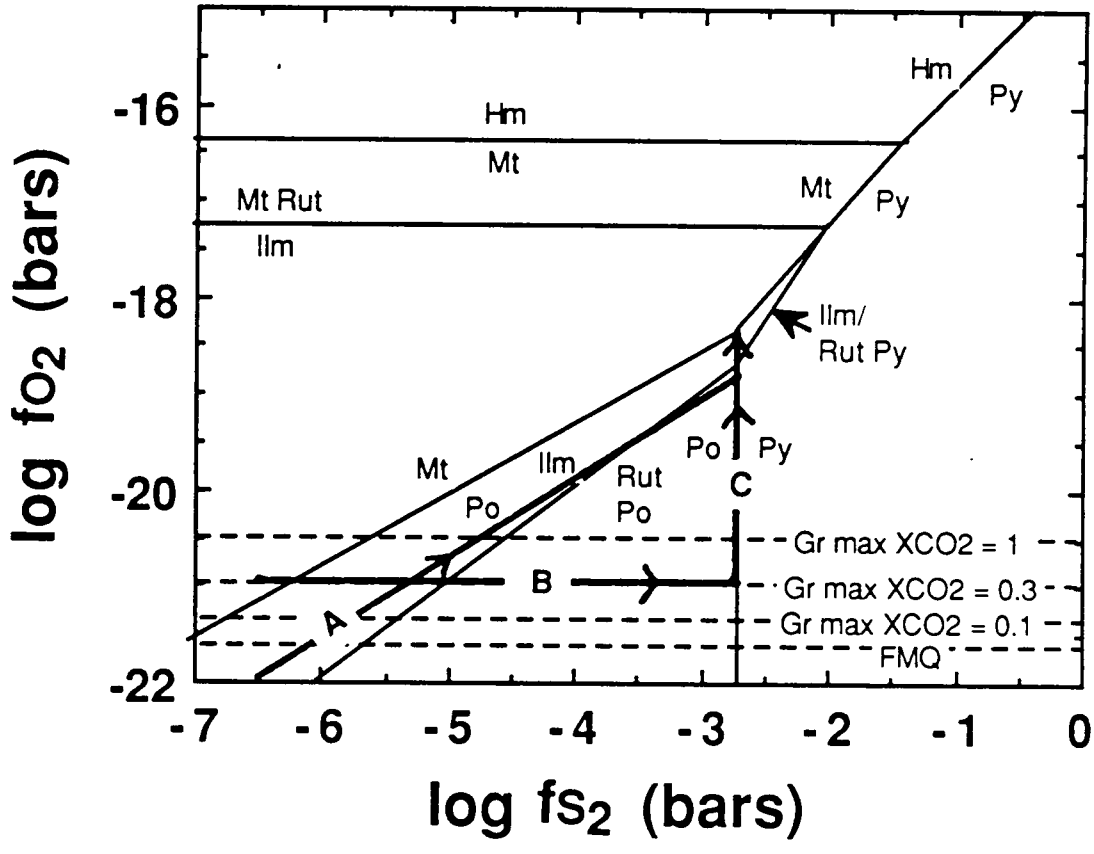

Figure 3. fO_2-fS_2 relations in the system Fe-Ti-O-S at 6 kbar and 550°C. Also shown is the fO_2 of the graphite maximum calculated from equation 1, assuming a maximum XCO_2 of 1.0, 0.3 and 0.1. The fO_2 of FMQ is shown for reference. **A**, **B**, and **C** refer to fO_2-fS_2 trends used to model fluid composition, where **A** is the trend suggested by Nesbitt & Kelly (1980). Data from Toulmin and Barton (1964), Robie et al. (1978), and Barton and Skinner (1979).

effects of solid solution have been ignored in constructing Figure 3.

Away from the orebodies, within staurolite grade country rocks, the common sulfide-oxide-graphite assemblage is pyrrhotite-ilmenite-graphite, however, pyrrhotite-pyrite-ilmenite was also noted. As the orebodies are approached, primary graphite disappears and rutile replaces ilmenite as the stable Ti-oxide phase. Within the orebodies themselves the common assemblages are

$$Po \pm Py \pm Mt \pm Rut.$$

However, other apparently stable assemblages were noted including

$$Po + Rut + Graph$$
$$Po + Py + Graph$$
$$Po + Py + Rut + Graph$$

and

$$Po + Py + Mt + Ilm.$$

These assemblages, while not significantly extending the range of fO_2 or fS_2 from that delineated by Nesbitt and Kelly (1980), do suggest that the smooth trend of increasing fS_2 and fO_2 as the orebodies are approached may not hold in general. Specifically, it appears that fO_2 remained low in much of the country rock and wallrock and attained values approaching pyrrhotite-

pyrite-magnetite only in certain portions of the orebodies. The presence of native bismuth in galena and the rare occurrence of primary graphite with calcite indicate low fO_2 conditions in these portions of the ore zones. A similar conclusion was reached by Nesbitt (1982) while investigating sulfide-silicate equilibria. He found that, in general, the X_{Fe} of biotite, garnet, staurolite and chlorite decreased toward the ore and that the distribution and composition of these phases were consistent with a progressive increase in fS_2 toward the ore, but that a decrease in fO_2 was required within the wallrocks and ore zones.

The foregoing indicates that fO_2 and fS_2 were variable within ore zones and country rocks. This is consistent with our T-XCO_2 analysis which suggests that fluid composition was locally controlled.

Activity of carbon

In the country rocks, where graphite is common, the activity of carbon is unity. The general absence of primary graphite in the orebodies and wallrock implies reduced a_C, consistent with the location of the graphite maximum at log fO_2 of -20.5 as calculated from reaction (1) at 6 kbar and 550°C (Fig. 3). At the graphite maximum the fluid is essentially pure CO_2; however, mineral assemblages in the country rocks fix maximum XCO_2 near 0.3. Therefore, a better estimate of the graphite maximum is obtained by setting XCO_2 equal to 0.3 and calculating fO_2 from reaction (1), which results in an estimated log fO_2 of -20.96 (Fig. 3). At fO_2 conditions above that of the estimated graphite maximum, fluid composition is dependent on the activity of carbon. Figure 4 shows fluid composition as a function of a_C 6 kbar, 550°C, log fO_2 = -20 and

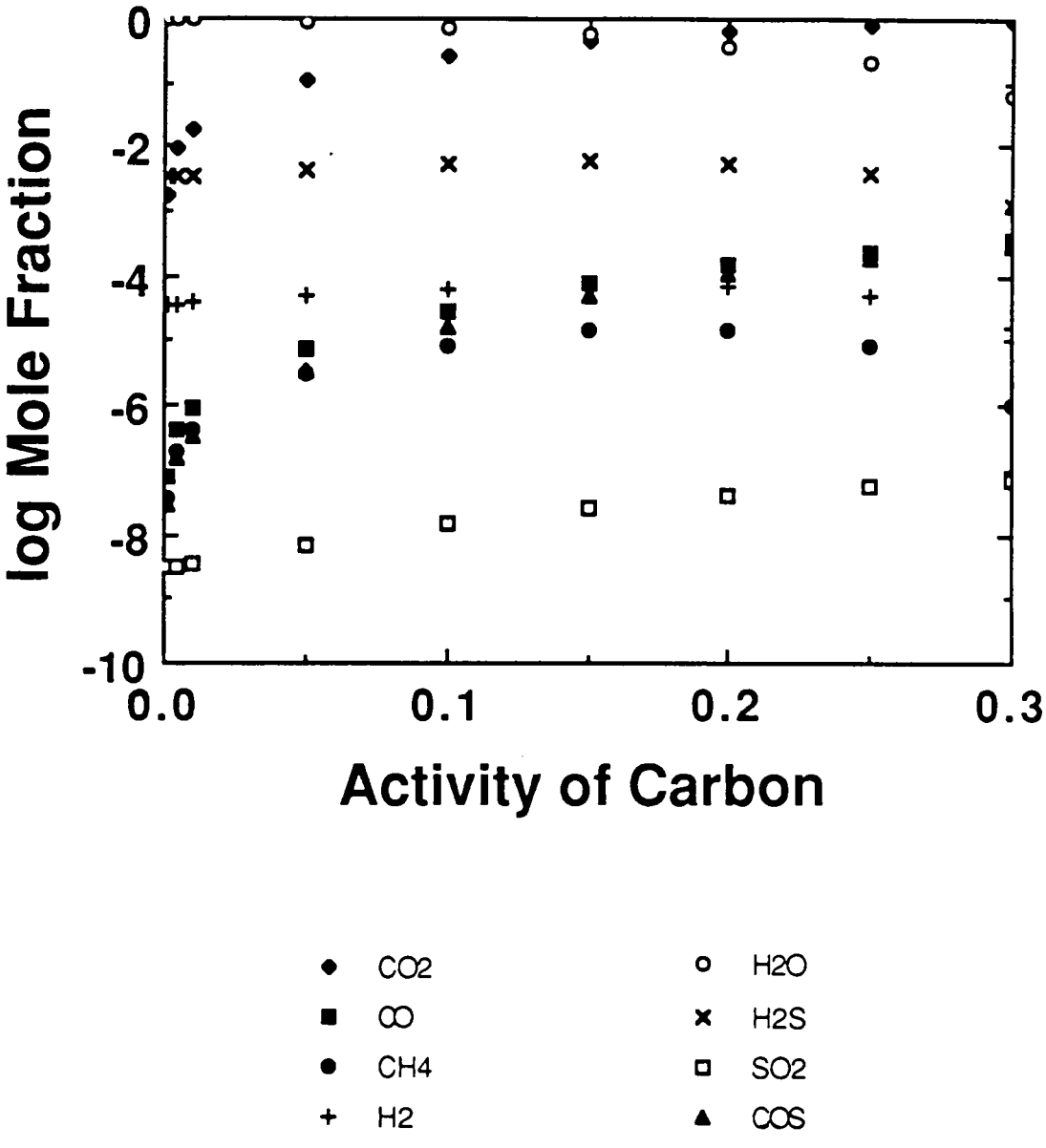

Figure 4. Log X_i-a_C diagram calculated for 6 kbar, 550°C log fO_2 = -20 and log fS_2 = -3, showing the variation in fluid composition with the activity of carbon.

log fS_2 = -3. XCO_2 increases as a_C increases at constant fO_2, and depending on the activity of carbon, at any fO_2 above the graphite maximum the fluid composition varies from virtually pure H_2O to pure CO_2 at P-T-fS_2 conditions considered here (Fig. 4).

Within the ore zones, the most oxidized mineral assemblages (i.e. those containing Py-Po-Mt) invariably indicate the lowest XCO_2 conditions ($\leq$0.10). When graphite is found with low XCO_2 assemblages it is always secondary (precipitated by retrograde fluids). Primary graphite, present during peak metamorphsm, does occur rarely in the ore zones, but, the accompanying silicate-oxide-sulfide assemblages are consistent with relatively low fO_2, high XCO_2 conditions ($0.1<XCO_2<0.4$). As previously mentioned there is no systematic trend in XCO_2 in the wallrocks or ore zones. Because the ranges of XCO_2 recorded in the country rocks and ore zones are similar, we have arbitrarily chosen to model the activity of carbon along the fO_2-fS_2 trend of Nesbitt and Kelly (1980) by 1) assuming it is constant above the graphite maximum for XCO_2 = 0.3 (log fO_2 = -20.96) and is equal to 0.001, thereby producing a fluid with XCO_2 = 0.10 at the fO_2-fS_2 conditions indicated by Py-Po-Mt; and 2) assuming it varies above the graphite maximum for XCO_2 = 0.1 (log fO_2 = -21.35) in order to maintain an XCO_2 of 0.1. The latter requires that a_C decrease fairly regularly from 1 at log fO_2 of -21.35, to 0.001 at Py-Po-Mt. Considering the nonsystematic local control of fluid composition within the country rocks and ore zones it is improbable that a_C varied smoothly from country rock to ore zones, but, rather, oscillated in response to the same local controls of fluid composition.

Results

Fluid speciation was calculated for points along the suggested fO_2-fS_2 trend of Nesbitt and Kelly (1980) with a_C modeled as described above (Fig. 5). Results indicate that H_2O and CO_2 were generally the dominant molecular species, comprising 94-100 mol% of the peak metamorphic fluid. At the low fO_2-fS_2 end of the trend, CH_4 reaches 1 mol%, but the lower limit of fO_2 is not well-constrained by the oxide-sulfide mineral assemblages and significantly larger proportions of CH_4 are possible at lower fO_2 (e.g. 7 mol% CH_4 at log fO_2 = -23, log fS_2 = -6.5). However, if XCO_2 was everywhere ≥0.10, as suggested by silicate mineral assemblages, the minimum log fO_2 was -21.35 and the maximum XCH_4 was less than 1 mol%. Above the graphite maximum H_2O and CO_2 dominate, and the ratio of these two species is completely dependent on the value chosen for a_C. If a_C is constant at 0.001 (Fig 5A) then the fluid varies from pure H_2O just above the graphite maximum, to H_2O + CO_2 with XCO_2 = 0.1 at the Po-Py-Mt buffer. At higher fO_2-fS_2 conditions, XH_2O, XCH_4 and XH_2 decrease, XCO_2, XCO, XSO_2 and XCOS increase and XH_2S remains relatively constant (Fig. 5A). If XCO_2 is constant at 0.10 along the same trend [i.e. model (2) for a_C], XH_2O, XCO_2, XH_2S and XCOS remain approximately constant, XCH_4, XCO and XH_2 decrease and XSO_2 increases (Fig. 5B). While fluid composition is reasonably well-constrained at both ends of trend **A** (Fig. 3) it is poorly constrained in the middle due to uncertainties associated with a_C. Nevertheless, the calculations do imply that the peak metamorphic fluid was essentially a binary H_2O-CO_2 mixture above the graphite maximum along the fO_2-fS_2 trend of Nesbitt and Kelly (1980).

Figure 5. X_i- fO_2 relations calculated for 6 kbar and 550°C with fO_2 and fS_2 constrained by trend **A** (Fig. 3). A) a_C = 0.001 above log fO_2 of -20.96, which produces a maximum XCO_2 of 0.3. B) XCO_2 = 0.10 (a_C = 1-0.001). The graphite maximum is located at fO_2 = -21.35, which corresponds to a maximum XCO_2 of 0.1.

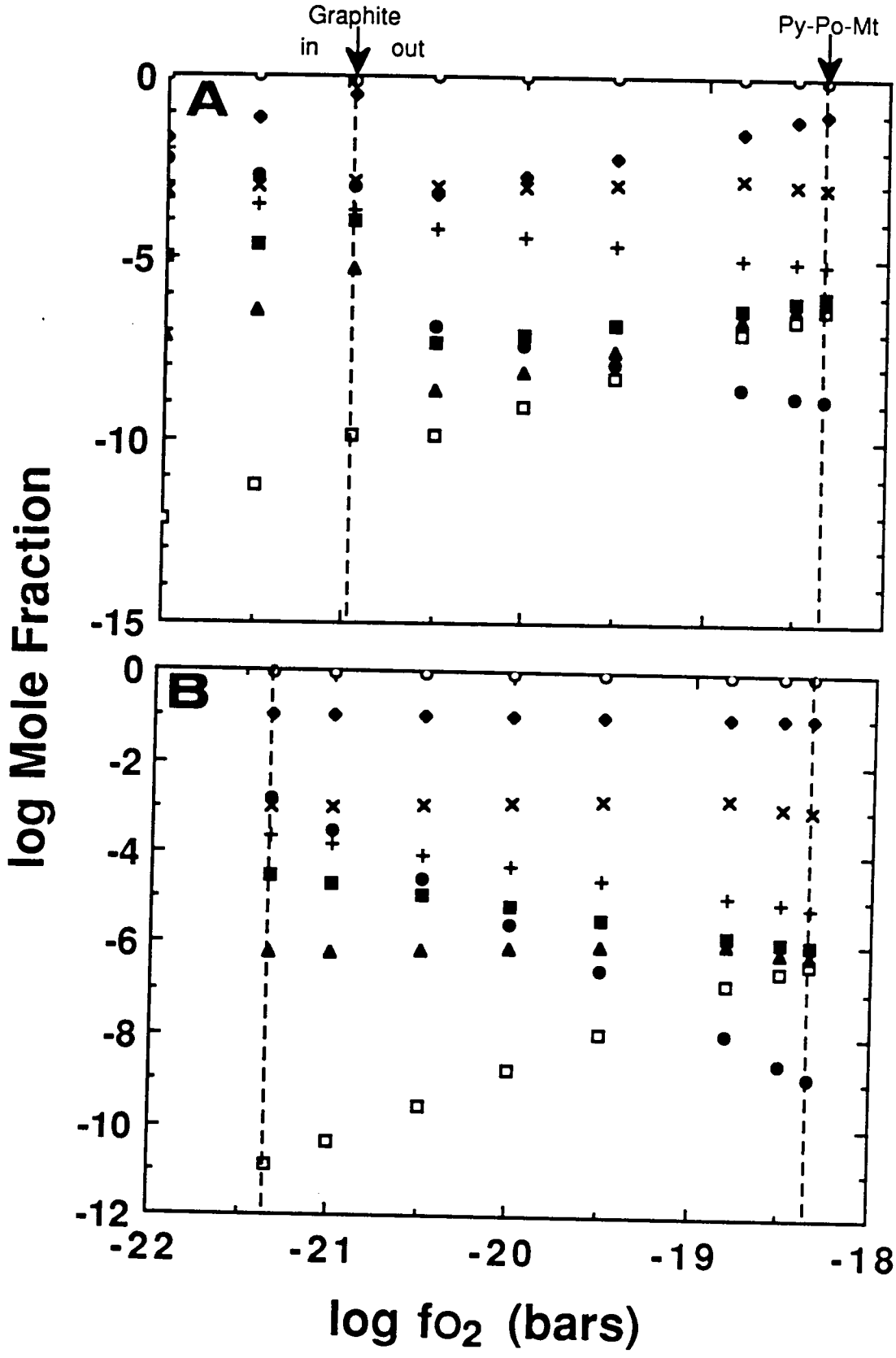
Graphite
in
out
Py-Po-Mt
A
B
0
-5
-10
-15
-2
-4
-6
-8
-12
-22
-21
-20
-19
-18
log Mole Fraction
log fO2 (bars)

As previously mentioned, mineral assemblages suggest that in some areas fO_2-fS_2 conditions deviated significantly from trend **A**, specifically, that low fO_2 - high fS_2 conditions prevailed in some rocks (trend **B**, Fig. 3). The apparent equilibrium assemblage Po + Py + Graph ± Spn is observed infrequently within the wallrocks, constraining log fS_2 to be -2.7 and log fO_2 to be as low as -22 (Fig. 3). At these conditions the metamorphic fluid is composed of approximately 90 mol% H_2O, 7 mol% H_2S 2.5 mol% CO_2, and 0.5 mol% CH_4. Fluid composition was calculated assuming constant log fO_2 = -20.96 (XCO_2 ~ 0.3) and variable log fS_2 between -6.5 and -2.7 (trend **B**, Fig. 3). Results, presented in Figure 6, indicate that as fS_2 increases CH_4 is replaced by H_2S as the third most abundant species, but that everywhere along trend **B** $XCO_2 + XH_2O \geq 0.97$. As expected, mole fractions of all sulfur species increase as fS_2 increases. Mole fractions of other species do not change appreciably.

Many mineral assemblages imply buffering of fS_2 by Py-Po at log fO_2 conditions between -20.96 (assuming a maximum XCO_2 of 0.3 and a_C=1) and -18.34 (Py-Po-Mt). As mentioned above, mineral assemblages in ore zones indicating the lowest fO_2 also imply the highest XCO_2. Fluid compositions calculated along this trend (**C** in Fig. 3) are presented in Figure 7 and assume a linear decrease in XCO_2 from 0.3 at log fO_2 = -20.96 to 0.1 at log fO_2 = -18.34. H_2S may have comprised up to 3 mol% of the fluid at low fO_2; XH_2O increases while mole fractions of all other species decrease as log fO_2 increases (Fig. 7).

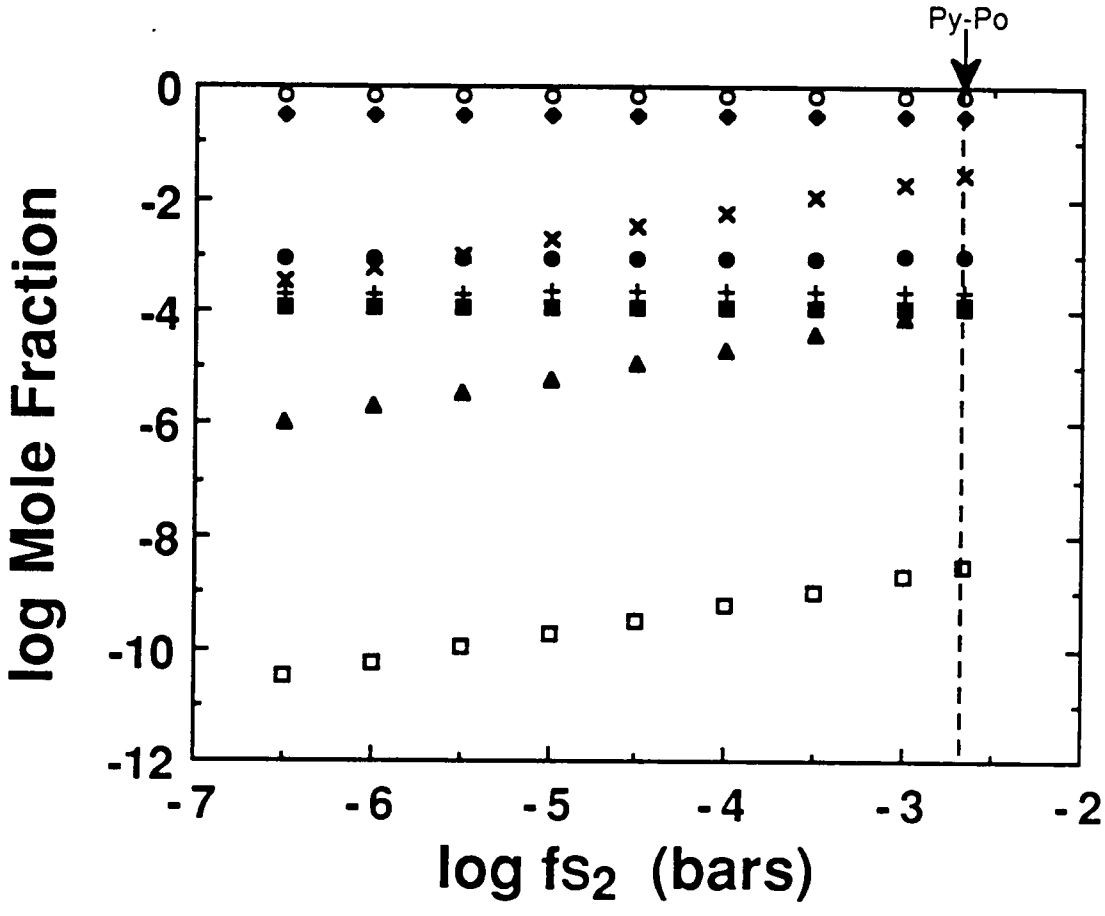

Figure 6. X_i- fS_2 relations calculated for 6 kbar and 550°C with fO_2 constant at -20.96 (trend **B**, Fig. 3). An fO_2 of -20.96 corresponds to an XCO_2 of 0.3.

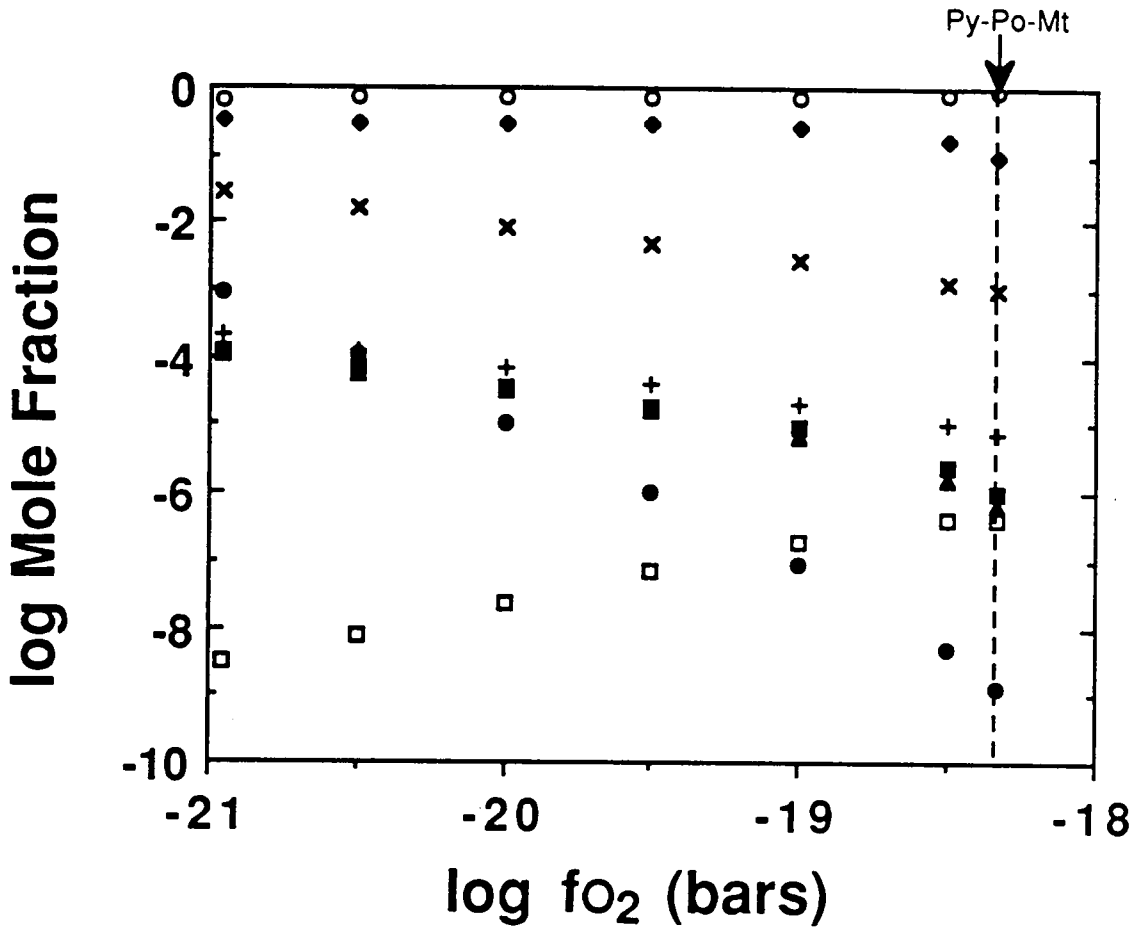

Figure 7. X_i- fO_2 relations calculated for 6 kbar and 550°C with fS_2 constant at -2.7 (trend C, Fig. 3). An fS_2 of -2.7 corresponds to the Py-Po equilibrium boundary.

Comparison of calculated fluid compositions with primary fluid inclusions

Clinopyroxene is generally coarse grained (up to 10 cm) and is accompanied by tremolite-actinolite, calcite, quartz, pyrrhotite ± garnet ± pyrite ± magnetite ± anhydrite. Primary fluid inclusions in clinopyroxene contain an aqueous liquid phase with a salinity of 3 wt% NaCl equivalent, a CH_4-rich vapor phase and daughter crystals of calcite, quartz and pyrrhotite at room temperature. These phases were re-integrated into a single homogeneous fluid phase to provide an estimated normalized volatile composition of 93 mol% H_2O, 4 mol% CH_4, 3 mol% CO_2 and 0.1 mol% H_2S (Hall et al., 1989a).

Comparison of calculated peak metamorphic fluid compositions, constrained by mineral assemblages coexisting with clinopyroxene, with the estimated compositions of primary fluid inclusions in clinopyroxene indicate significant similarities and differences (Table 2). Both compositions imply that water was the dominant molecular fluid species during peak metamorphism and that CO_2 was a significant species as well. Also, both predict comparable quantities of H_2S. However, the calculated composition suggests that CH_4 was present in negligible amounts while observed compositions of primary fluid inclusions reveal that CH_4 is present in proportions subequal to, or greater than CO_2. In order to reconcile the calculated speciation with fluid inclusion data would require very reducing conditions during trapping, specifically, log fO_2 of ~-22.8 and log fS_2 of <~-6.5, within the Po-Ilm-Graph or Po-Rut-Graph stability fields (Fig. 3). This is inconsistent with the equilibrium mineral assemblages coexisting with

Table 2. Observed and calculated fluid compositions

Observed			Calculated		
X_{H_2O}	=	0.93	X_{H_2O}	=	0.90
X_{CH_4}	=	0.04	X_{CH_4}	=	10^{-9}
X_{CO_2}	=	0.03	X_{CO_2}	=	0.10
X_{H_2S}	=	0.001	X_{H_2S}	=	0.001

pyroxene containing primary fluid inclusions, which indicate trapping at log fO_2 near -18.3 and log fS_2 near -2.7 (i.e. defined by Py-Po-Mt). The discrepancy cannot be explained by any reasonable errors in the determination of P-T-fO_2-fS_2-a_C conditions attending pyroxene growth or in the calculation of fluid speciation. Even a 50 % uncertainty in the fugacity coefficients of H_2O, CO_2 and CH_4 would only increase X_{CH_4} by an order of magnitude (eqn. 4).

POST-TRAPPING CHANGES IN FLUID COMPOSITION

Closed system

A mechanism which could account for the disparity between calculated and observed fluid compositions is continued re-equilibration of the molecular species comprising the C-O-H-S fluid during cooling, resulting in a speciation that is substantially different at room temperature than at the conditions of trapping. The change in speciation during cooling of a hypothetical C-O-H-S fluid inclusion can be calculated using methods outlined by Holloway (1981) and Dubessy (1984).

In this procedure, an inclusion is assumed to contain a fluid of known composition and molar volume at some initial P-T condition (e.g. of trapping or observation). By specifying an arbitrary inclusion volume at this pressure and temperature and assuming the system remains isochoric, or by correcting for thermal expansion and compressibility of the host, the new composition, molar volume and internal pressure of the fluid inclusion can be calculated at a specified temperature. The solution requires the functions describing equilibrium constants for reactions (2)-(7) (Ohmoto and Kerrick,

1977), equation (8), and the additional mass balance equations:

$$\Sigma n_i C = \Sigma n_f C \quad (18)$$

$$\Sigma n_i O = \Sigma n_f O \quad (19)$$

$$\Sigma n_i H = \Sigma n_f H \quad (20)$$

$$\Sigma n_i S = \Sigma n_f S \quad (21)$$

Fugacity coefficients for the 10 species considered are computed from Holloway's (1981) program MRKMIX, and the new P-V-X properties of the inclusion are calculated by simultaneously solving the 10 equations (6 describing fluid speciation and 4 describing mass balance) using Newton's method for non-linear equations (Burden and Faires, 1985). The criterion for convergence is that the relative variation in mole fraction between two successive iterations is less than 10^{-4} for all species (equation 11).

Closed system speciation changes that result when the calculated peak metamorphic fluid is trapped and cooled to 400°C are shown in Figure 8. A minimum temperature of 400°C was chosen for several reasons. Holloway's modified Redlich-Kwong equation of state is only applicable above 400°C for aqueous fluids. Furthermore, the kinetics of exchange among carbonic fluid species and graphite are very sluggish below 400°C (Sackett and Chung, 1979; Harting and Maass, 1980; Ziegenbein and Johannes, 1980). Finally, the position of the solvi of C-O-H-S fluids are unknown, but in general probably lie at temperatures below the critical point of water. Thus, a minimum temperature of 400°C restricts calculations to the single fluid phase region.

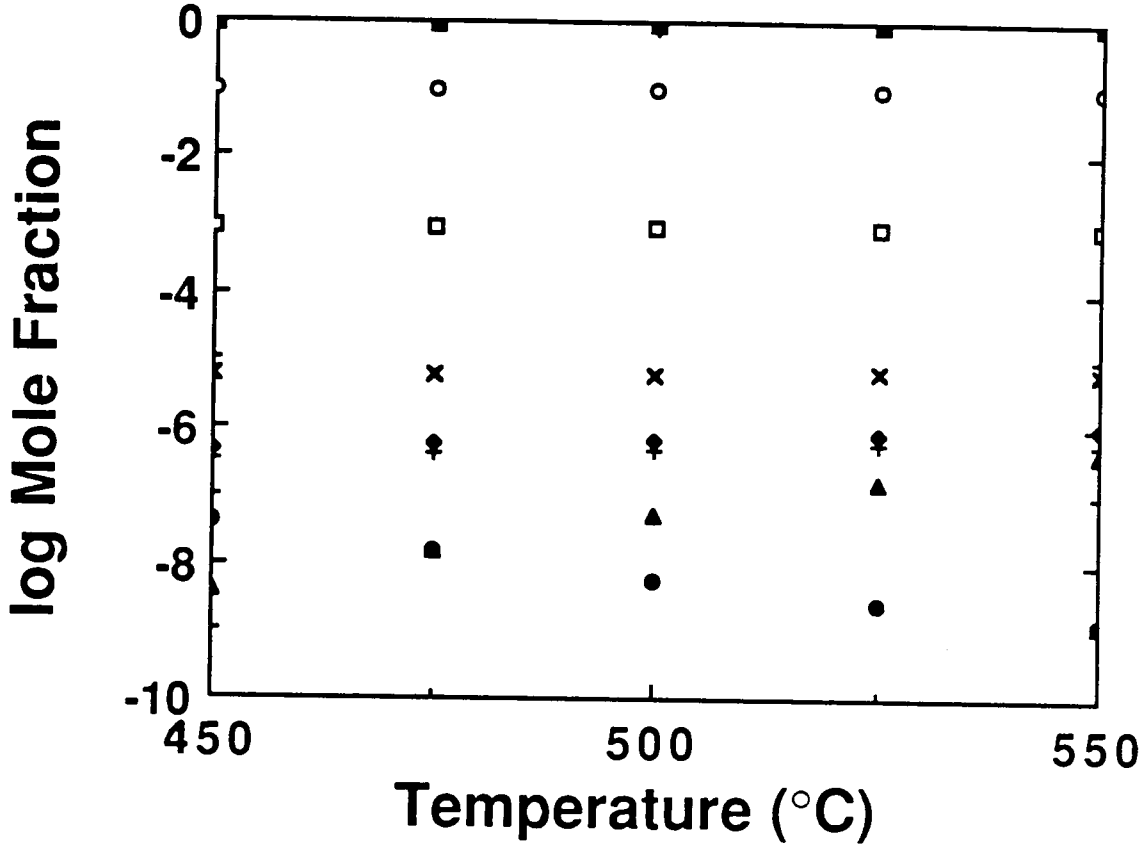

Figure 8. X_i-T relations showing closed system speciation changes obtained by trapping a peak metamorphic fluid at 6 kbar, 550°C, log fO_2 = -18.3, log fS_2 = -2.7 and a_C = 0.001, and cooling it isovolumetrically to 400°C.

The major components of the peak metamorphic fluid, namely H_2O and CO_2, vary insignificantly during cooling, while the minor species O_2, S_2, H_2, SO_2 and CH_4 vary up to several orders of magnitude (Fig. 8). This is in agreement with the conclusion of Dubessy (1984) that it is not possible to render a major fluid component minor or *vice versa* in the absence of a daughter precipitate or a mechanism that preferentially removes one or more component. The fluid was assumed to remain undersaturated with respect to graphite during cooling because graphite was not detected petrographically or during Raman analyses. If graphite were to precipitate in the fluid inclusions during cooling then significant CH_4 may be produced at low temperatures and pressures. Although X_{CH_4} does increase significantly during cooling, the initial quantity of this species is so small (10^{-7} mol%) that an increase of several orders of magnitude leaves CH_4 below detection by any microthermometric or spectroscopic technique.

We conclude that post-entrapment compositional changes in a fluid inclusion which remains a closed system cannot explain the disparity between the calculated peak metamorphic fluid composition and the observed composition of primary peak metamorphic fluid inclusions at Ducktown.

Hydrogen diffusion

Several phenomena observed in fluid inclusions have been attributed to the effects of diffusion. Daughter minerals such as hematite, anhydrite and chalcopyrite which do not dissolve upon heating may have precipitated in response to changes in oxidation state or pH resulting from diffusive loss of

hydrogen (Roedder and Skinner, 1968; Roedder, 1981). Tiny, ubiquitous fluid inclusions in quartz from high grade metamorphic rocks may form by diffusive exsolution of "water" from the quartz structure during cooling and decompression of the terrane (White, 1973; Wilkins and Barkas, 1978), and water precipitation and diffusion in wet quartz and berlinite as the result of annealing has been documented (Cordier et al., 1988). Similarly, Sterner et al. (1988), Hall et al. (1989b) and Hall et al. (unpub. data) have shown that preferential loss of H_2O from fluid inclusions in quartz can occur in response to differential pressure between inclusion and matrix. These authors have also documented hydrogen gain by CO_2-H_2O fluid inclusions in quartz, resulting in reduction of CO_2 to $CH_4 + H_2O$ at temperatures as low as 650°C. Diffusive loss of water from C-O-H inclusions has been suggested as a possible explanation for nearly pure CO_2 inclusions in granulites and other high-grade rocks (Roedder, 1981), while diffusive gain of hydrogen and reduction of CO_2 may explain the common occurrence of appreciable CH_4 in fluid inclusions from granulites (Hall and Bodnar, 1989).

The driving force for hydrogen diffusion out of, or into, a fluid inclusion is the fH_2 gradient between the host (or imposed by the fluid circulating through the rock) and the fluid inside the inclusion. These gradients may become appreciable during cooling and decompression. Diffusion rates of hydrogen through minerals are sufficiently rapid above 600°C (Kats, 1962; Kats et al., 1962; Kronenberg et al., 1986) that over geologic time appreciable gradients in hydrogen fugacity could not be maintained. It is unclear, however, what the effective "blocking temperature" is for hydrogen diffusion over geologic time. The extent or importance of hydrogen diffusion depends on the

P-T-time path as well as the compositions of the inclusion and matrix fluid and crystal chemistry.

We have calculated the changes in the fugacity of hydrogen in the matrix and in model peak metamorphic fluid inclusions during uplift. The inclusions trapped the fluid composition calculated for 6 kbar, 550°C, log fO_2 = -18.3, log fS_2 = -2.7 and a_C = 0.001 (Table 2). The uplift path chosen for the matrix was constrained by paragenetic and microthermometric data from secondary fluid inclusions in quartz (Hall et al., 1989a) and is slightly concave toward the temperature axis (Fig. 9) over the temperature range considered here (550-400°C). The "pseudo-isochore" calculated by cooling the peak metamorphic fluid isovolumetrically, but taking into account P-V-T variations due to speciation changes, indicates that the hypothetical inclusions are underpressured (i.e. $P_{ext} > P_{int}$) during uplift (Fig. 9). At 400°C the pressure differential is about 750 bars.

The fH_2 gradient established during the post-metamorphic history is presented in Figure 10. For these calculations it is assumed that the matrix fluid composition (i.e. fO_2 and fS_2) is buffered by Py-Po-Mt. Two fH_2-T curves were calculated for the matrix, one with a_C constant at 0.001 (Matrix 1; Fig. 10) and the other with a_C varying from 0.001 at 6 kbar and 550 °C to 0.159 at 5 kbar and 400°C, so that XCO_2 is constant at 0.10 (Matrix 2; Fig. 10). These calculations indicate that fH_2 in the matrix is greater than that in the fluid inclusion, and in fact is 4 times that in the inclusion at 450°C, although both fugacities are low, thus the gradient is only approximately 0.3 bars (Fig. 10). Thus, a small fH_2 gradient may have been established during uplift and this gradient theoretically could have promoted hydrogen diffusion into primary

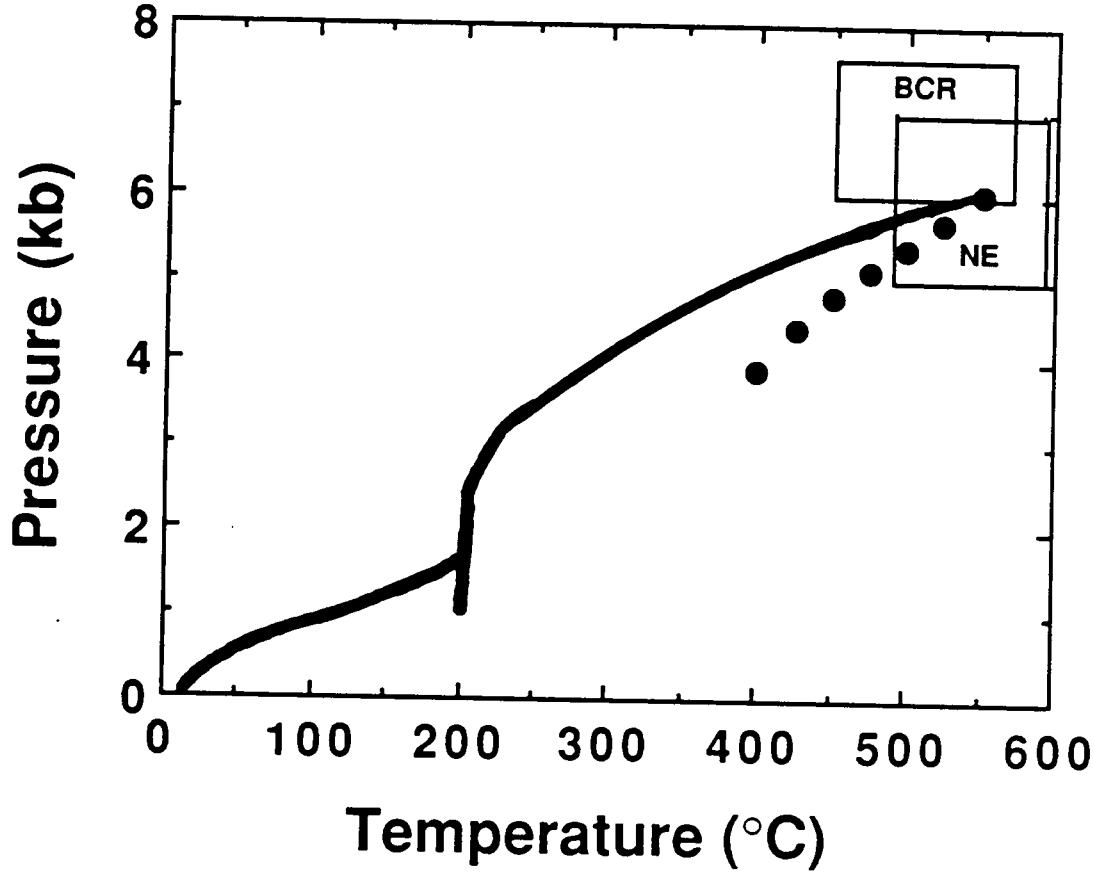

Figure 9. P-T diagram illustrating the uplift path delineated by Hall, et al. (1989a) for Ducktown rocks (line), and the calculated P-T path (pseudoisochore) traversed by hypothetical peak metamorphic fluid inclusions during cooling (dots).

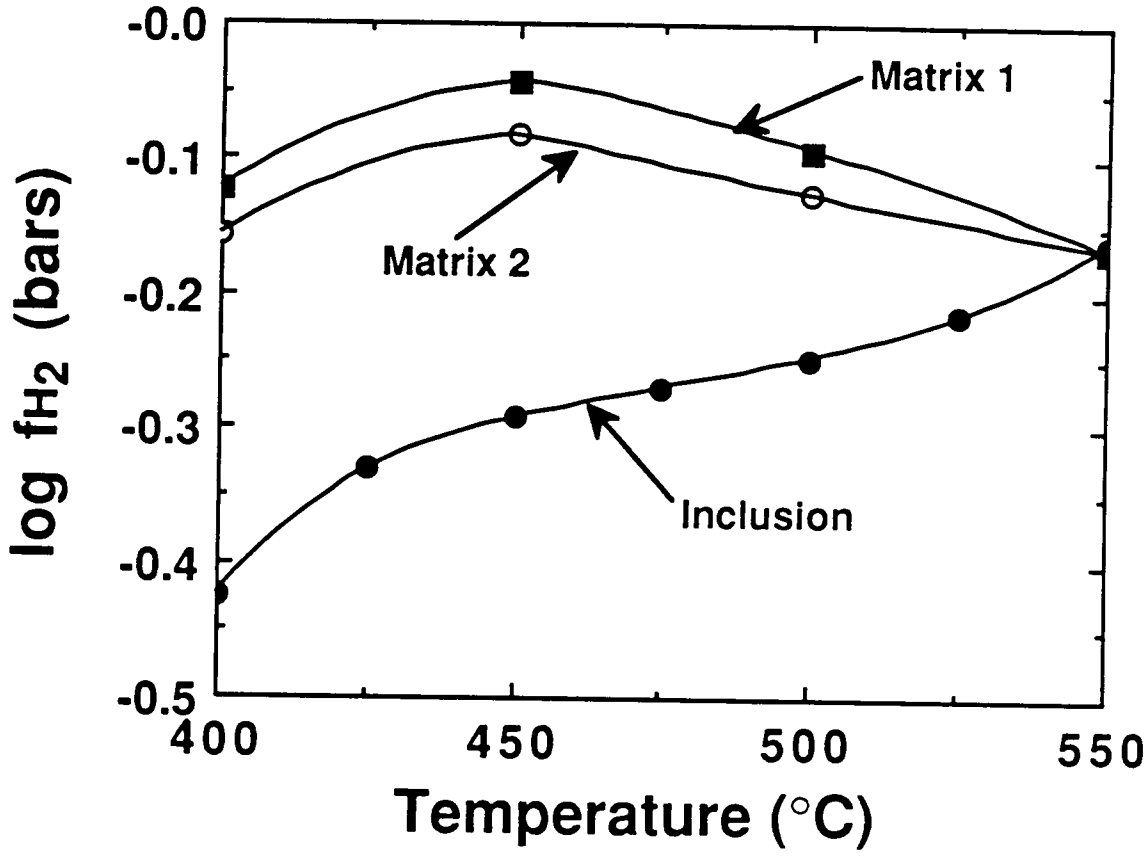

Figure 10. fH_2-T relationships calculated for matrix fluids and a hypothetical peak metamorphic fluid inclusion trapped at 6 kbar, 550°C, log fO_2 = -18.3, log fS_2 = -2.7 and a_C = 0.001. Pressures in the matrix during uplift were constrained by Figure 9 and fO_2-fS_2 conditions are buffered at Py-Po-Mt. The internal pressure of the fluid inclusion is dictated by the P-V-T-X properties of the trapped fluid and the assumption that the inclusion behaves isovolumetrically. Matrix 1 was calculated assuming a_C is constant and equal to 0.001 while Matrix 2 assumes that XCO_2 is constant and equal to 0.10.

fluid inclusions.

The difference in fH_2 between matrix and inclusion is magnified by an order of magnitude if the fluid in "hydrogen communication" with primary fluid inclusions is not controlled by Py-Po-Mt but by a more reduced assemblage, such as Po-Ilm-Graph or FMQ. This may have occurred if fluid in equilibrium with the bulk of the host metagraywackes and quartz-mica schists, or reduced portions of ore zones, infiltrated high fO_2 (pyroxene-bearing) portions of the orebodies after peak metamorphism. The fH_2 gradient resulting from infiltration of a fluid with fO_2 buffered by FMQ and fS_2 buffered by pyrrhotite with $X_{FeS} = 0.95$, relative to $FeS\text{-}S_2$, is shown in Figure 11. If this fluid comes into diffusive communication with primary fluid inclusions an fH_2 gradient of 15-30 bars will result, again promoting hydrogen diffusion into primary fluid inclusions. Secondary fluid inclusions in quartz indicate that influx of post-peak metamorphic fluids into ore zones from external sources did occur, and at least one such fluid was responsible for precipitation of secondary graphite and replacement of sulfides by graphite in ore zones. The observed replacement of magnetite by pyrrhotite may be mineralogical evidence for influx of low-fO_2 fluids.

We have calculated the amount of hydrogen diffusion necessary to equilibrate the fH_2 gradient between inclusions and matrix at 450°C. If the matrix fluid is buffered by Py-Po-Mt, diffusion of much less than 0.1 mol% of the total hydrogen originally present in the inclusion will negate the fH_2 gradient. If the matrix fluid is buffered by FMQ, however, an amount of hydrogen approximately equivalent to 12.5 mol% of the hydrogen originally present in the inclusion must diffuse into the fluid inclusion to equilibrate fH_2.

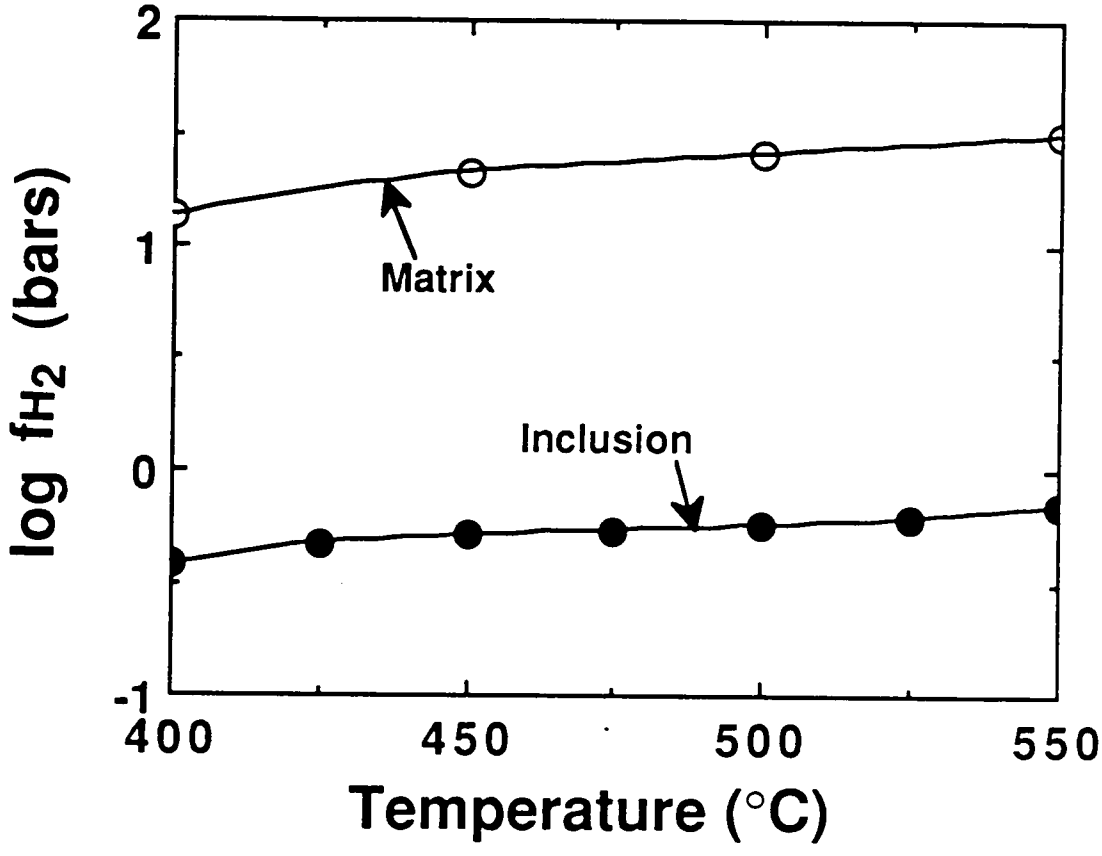

Figure 11. fH_2-T relationships calculated for matrix fluids and a hypothetical peak metamorphic fluid inclusion. Conditions are the same for the inclusion as in Figure 10. Here, the fO_2 of the matrix fluid is buffered by FMQ and fS_2 is buffered by Po with $X_{FeS} = 0.95$.

Diffusion of this much hydrogen into a fluid inclusion has significant effects on the P-V-X properties. The mole fraction of methane increases over seven orders of magnitude from 10^{-9} to 0.03; the fluid is essentially 90 mol% H_2O, 7 mol% CO_2 and 3 mol% CH_4 after diffusion of 12.5 mol% hydrogen (Fig. 12). Methane has become an important component, which may be detectable during routine microthermometric studies and spectroscopically. Furthermore, the above fluid composition compares favorably with the actual composition estimated for primary fluid inclusions (Table 2).

After 12.5 % diffusion the molar volume of the fluid has decreased from 22.81 to 21.60 cm^3 (Fig. 13) and the internal pressure has increased from 4.8 to 6.4 kbar (Fig. 14). Because the matrix is at about 5.5 kbar at 450°C (Fig. 9; Fig. 14), hydrogen diffusion results in approximately 900 bars of internal overpressure inside the inclusions, which may be enough to cause the inclusions to stretch (Sterner and Bodnar, 1989). Variable liquid-vapor ratios have been observed in primary fluid inclusions in pyroxene, and clathrate dissociation temperatures suggest a range of internal pressures at room temperature, perhaps due to equilibration toward lower densities during uplift (Hall et al., 1989a). It is important to emphasize that in the absence of hydrogen diffusion the primary inclusions should be underpressured during uplift and may tend toward higher densities (Fig. 14). Although the appearance of the inclusions may be qualitatively similar, in the latter case the lowest rather than highest density inclusions would most closely approximate the original isochore, and a negative rather than positive correlation between inclusion size and homogenization temperature should be observed. In fact, textures indicative of internal underpressuring have

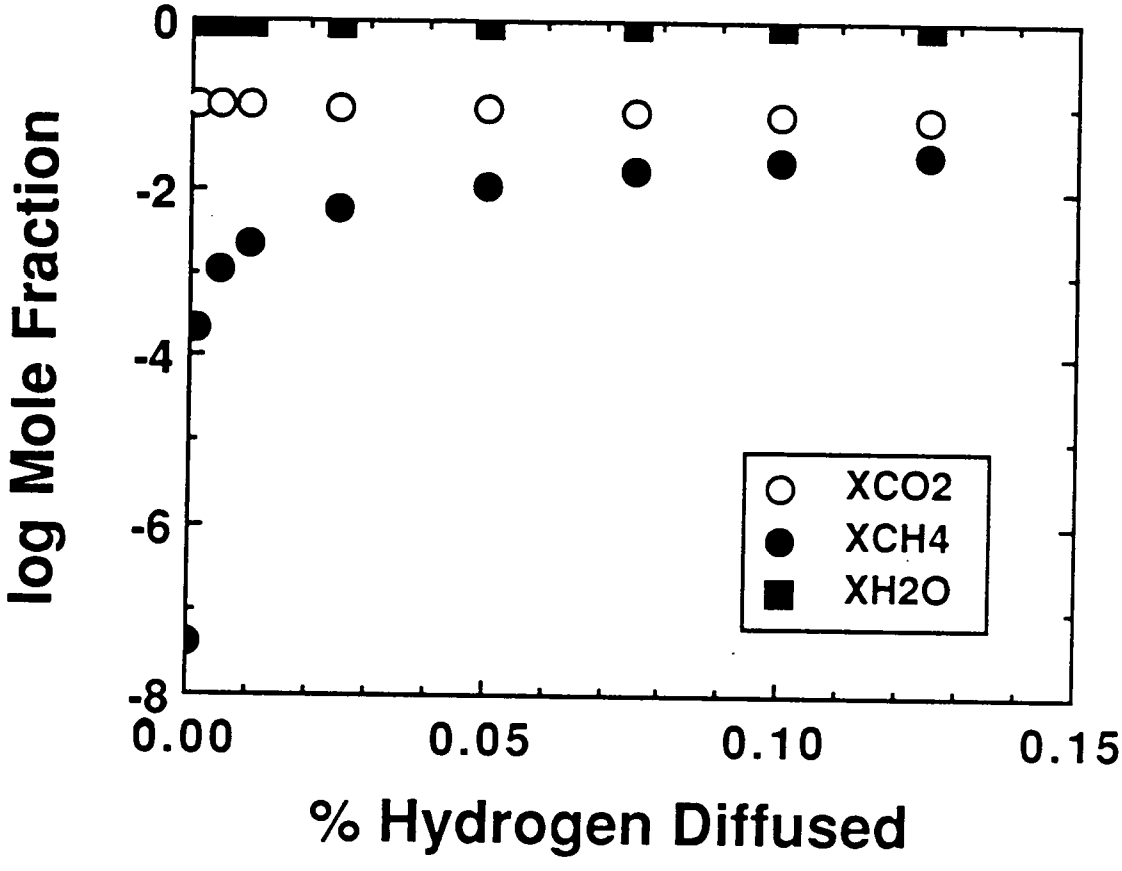

Figure 12. Variation in X_{H_2O}, X_{CO_2} and X_{CH_4} during hydrogen diffusion at 450°C. The percent of hydrogen diffused is referenced to the total amount of hydrogen originally contained within the inclusion prior to diffusion; in other words contributed from H_2O, CH_4, H_2 and H_2S.

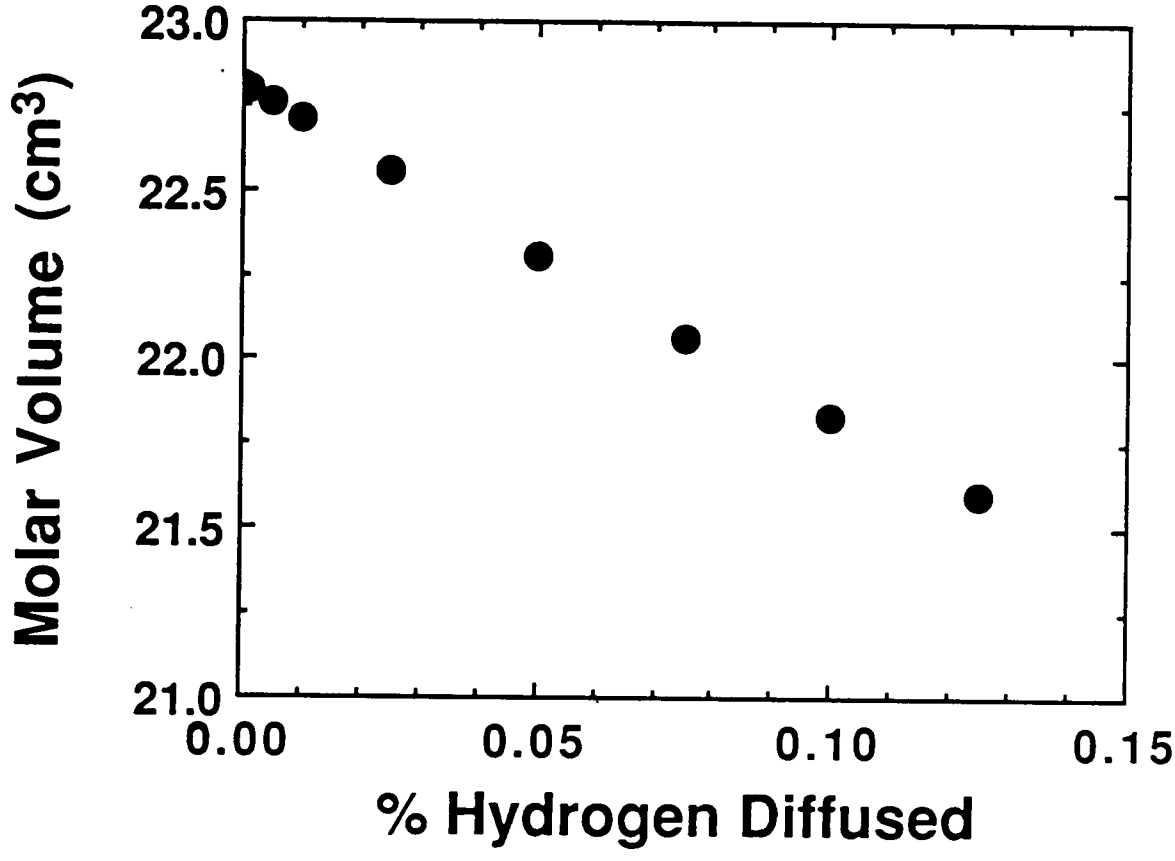

Figure 13. Variation in the molar volume of the fluid inclusion during hydrogen diffusion at 450°C.

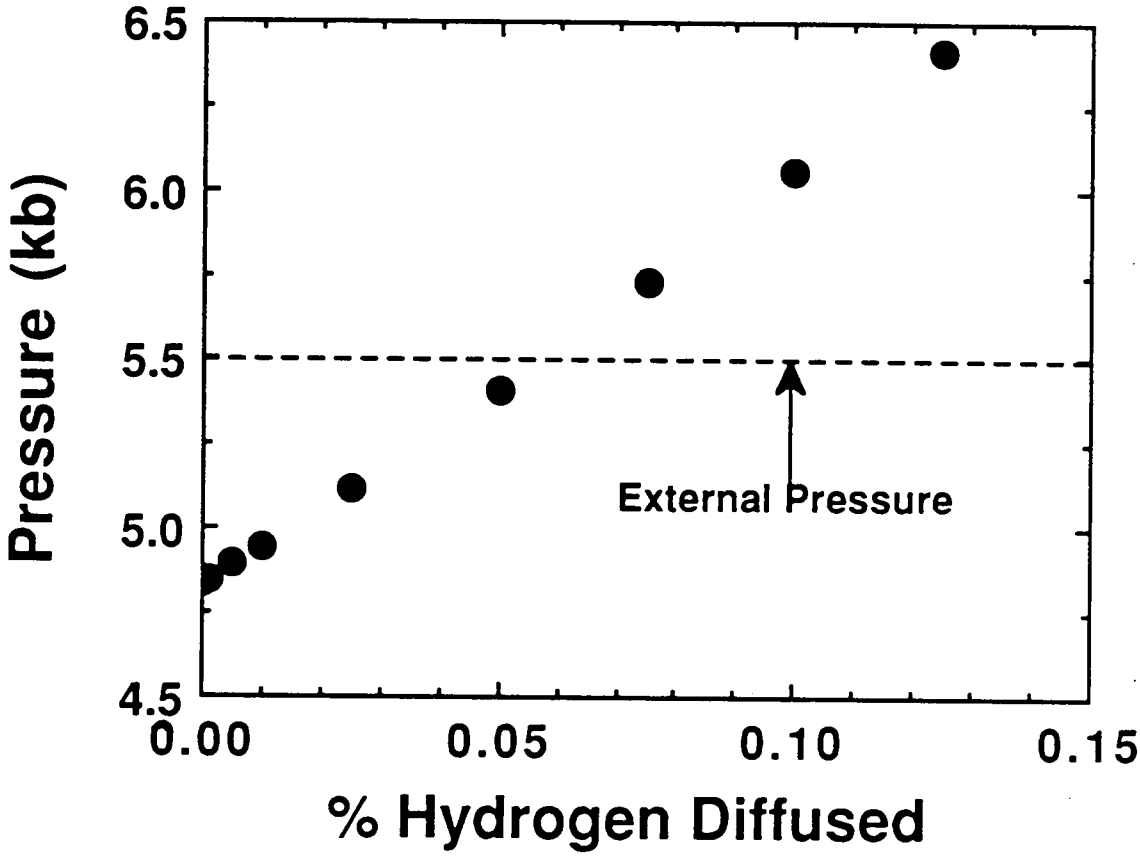

Figure 14. Variation in the internal pressure of the fluid inclusion during hydrogen diffusion at 450°C. The external pressure at 450°C is taken from Figure 9.

been noted in primary fluid inclusions (Hall et al., 1989a) suggesting that inclusions were initially underpressured, and re-equilibrated to higher densities prior to the hydrogen diffusion event. If the inclusions were to begin stretching during hydrogen diffusion, the effect would be to reduce the fugacity of hydrogen in the inclusions by reducing the total pressure, perhaps resulting in further hydrogen diffusion to equilibrate fH_2. This in turn would result in higher CH_4/CO_2 in the final inclusion fluid.

δD values of primary fluid inclusions

Bulk δD values of primary fluid inclusions range from -96 to -104 per mil (Hall et al., 1989c). However the δD of water in equilibrium with local hydrous phases was -33 to -42 per mil during peak metamorphism (Addy and Ypma, 1977; Hall et al., 1989c). Low δD primary fluid inclusions are consistent with a diffusion model because isotopically light hydrogen would preferentially enter the inclusions due to the fractionation between H_2 and H_2O in the matrix fluid, and the faster rate of diffusion through pyroxene of H relative to D. Mass balance calculations (Hall et al., 1989c) suggest that 16-18 percent diffusion would account for the D-depletion, which compares favorably to the 12.5 percent required to produce the necessary chemical changes.

CONCLUSIONS

Primary fluid inclusions in pyroxene, which formed at peak metamorphic conditions of 6 kbar and 550°C with fO_2-fS_2 values buffered near Py-Po-Mt, contain a normalized volatile composition of 93 mol% H_2O, 4 mol% CH_4, 3 mol% CO_2 and 0.1 mol% H_2S. Fluid speciation calculations and silicate

mineral assemblages suggest that the trapped fluid should consist of 90 mol% H_2O, 10^{-7} mol% CH_4, 10 mol% CO_2 and 0.1 mol% H_2S. Methane was not a significant component of peak metamorphic fluids in ore zones.

Post-trapping speciation changes can account for the discrepancy in the CH_4/CO_2 ratio only if the inclusions behaved as open systems and hydrogen diffused into the inclusions causing reduction of CO_2 to CH_4. This has been shown to be feasible if fluids from the bulk of the country rocks infiltrated the ore zones after peak metamorphism. Country rock fluids are buffered at fO_2 approximately 3 log units below oxidized portions of ore zones. An fH_2 gradient is established between inclusions and grain boundary fluids which would promote diffusion into primary fluid inclusions.

δD values of primary fluid inclusions ar 65 per mil lower than equilibrium values at peak metamorphism. Hydrogen diffusion would drastically lower δD by addition of isotopically light hydrogen. Mass balance calculations suggest that the amount of hydrogen necessary to lower δD will also result in sufficient compositional changes to reconcile calculated and observed fluid compositions. Hence, hydrogen diffusion is presently the best explanation for discrepancies between calculated and observed fluid compositions in primary fluid inclusions from Ducktown.

REFERENCES

Addy, S.K. (1973) The problem of ore genesis at Ducktown, Tennessee. Interpretation of stable isotopes (18O/16O, 13C/12C and D/H), micoprobe, and textural data. Ph.D. thesis, Columbia University, New York.

Addy, S.K., and Ypma, P.J.M. (1977) Origin of massive sulfide deposits at Ducktown, Tennessee: An oxygen, carbon, and hydrogen isotope study. Economic Geology, 72, 1245-1268.

Barton, P.B., and Skinner, B.J. (1979) Sulfide mineral stabilities. In H.L. Barnes, Ed., Geochemistry of hydrothermal ore deposits 2nd edition, p. 278-403. Wiley and Sons, New York.

Bowers, T.S., and Helgeson, H.C. (1983) Calculation of the thermodynamic and geochemical consequences of nonideal mixing in the system H_2O-CO_2-NaCl on phase relations in geologic systems: metamorphic equilibria at high pressures and temperatures. American Mineralogist, 68, 1059-1075.

Brooker, D.D., Craig, J.R., and Rimstidt, J.D. (1987) Ore metamorphism and pyrite porphyroblast development at the Cherokee Mine, Ducktown, Tennessee. Economic Geology, 82, 72-86.

Burden, R.L., and Faires, J.D. (1985) Numerical Analysis, 3rd ed. Prindle, Weber and Schmidt, Boston, 676p.

Burnham, C.W., Holloway, J.R., and Davis, N.F. (1969) Thermodynamic properties of water to 1,000°C and 10,000 bars. Geological Society of America Special Paper, 132, 96p.

Cordier, P., Boulogne, B., and Doukhan, J. (1988) Water precipitation and diffusion in wet quartz and wet berlinite $AlPO_4$. Bulletin de Mineralogie, 111, 113-137.

Craig, J.R. (1983) Metamorphic features in Appalachian massive sulfides. Mineralogical Magazine, 47, 515-525.

Dubessy, J. (1984) Simulation des equilibres chimiques dans le systeme COH. Consequences methodologiques pour les inclusions fluides. Bulletin de Mineralogie, 107, 155-168.

Eugster, H.P., and Skippen, G.B. (1967) Igneous and metamorphic reactions involving gas equilibria. In P.H. Abelson, Ed., Researches in geochemistry, II, p. 942-520, John Wiley and Sons, New York.

Ferry, J.M., and Baumgartner, L. (1987) Thermodynamic models of molecular fluids at the elevated pressures and temperatures of crustal metamorphism. In I. S. E. Carmichael and H. P. Eugster, Eds., Thermodynamic modeling of geological materials: Minerals, fluids and melts. Mineralogical Society of America Reviews in Mineralogy, 17, 323-366.

Flowers, G.C., and Helgeson, H.C. (1983) Equilibrium and mass transfer during progressive metamorphism of siliceous dolomites. American Journal of Science, 283, 230-286.

French, B.M. (1966) Some geological implications of equilibrium between graphite and a C-H-O gas phase at high temperatures and pressures. Reviews of Geophysics, 4, 223-253.

Hall, D.L., and Bodnar, R.J. (1989) Methane in fluid inclusions from granulites: A product of hydrogen diffusion?. Geochimica et Cosmochimica Acta (in press).

Hall, D.L., Bodnar, R.J., and Craig, J.R. (1989a) Fluid evolution during metamorphism and uplift of the massive sulfide deposits at Ducktown, Tennessee, U.S.A. I. Constraints from Fluid Inclusions. Journal of Metamorphic Geology (in review).

Hall, D.L., Sterner, S.M., and Bodnar, R.J. (1989b) Fluid inclusions in regional metamorphic rocks: experimental evidence for post-entrapment volumetric and compositional modifications (abstr.). 10th European Current Research on Fluid Inclusions, Royal School of Mines, Imperial College, University of London, 44.

Hall, D.L., Wesolowski, D., Bodnar, R.J., and Craig, J.R. (1989c) Fluid evolution during metamorphism and uplift of the massive sulfide deposits at Ducktown, Tennessee, U.S.A. III. Stable isotope systematics. Economic Geology (in review).

Harting, P., and Maass, I. (1980) Neue Ergebnisse zum Kohlenstoff-Isotopenaustausch im system CH_4-CO_2. In: Mitteilungen zur z. Arbeitstagung "Isotope in der Natur", 26, Leipzig, 13-24.

Holcombe, R.J. (1973) Mesoscopic and microscopic analysis of deformation ond metamorphism near Ducktown, Tennessee. Unpub. Ph.D. thesis, Stanford University, 225 p.

Holloway, J.R. (1977) Fugacity and activity of molecular species in supercritical fluids. In D.G. Fraser, Ed., Thermodynamics in Geology, p. 161-181, D. Reidel Publishing Company, Dordrecht.

Holloway, J.R. (1981) Compositions and volumes of supercritical fluids in the earth's crust. In L.S. Hollister and M.L.Crawford, Eds., Short course in fluid inclusions: Applications to petrology. Mineralogical Association of Canada, 6, 13-38.

Jacobs, G.K., and Kerrick, D.M. (1981) Devolatilization equilibria in H_2O-CO_2 and H_2O-CO_2-NaCl fluids: an experimental and thermodynamic evaluation at elevated pressures and temperatures. American Mineralogist, 66, 1135-1153.

Kats, A. (1962) Hydrogen in alpha-quartz. Philips Research Report, 17, 1-31, 133-279.

Kats, A., Haren, Y., and Stevels, J. M. (1962) Hydroxyl groups in β-quartz. Physical Chemistry of Glasses, 3, 69-75.

Kronenberg, A.K., Kirby, S.H., Aines, R.D., and Rossman, G. R. (1986) Solubility and diffusional uptake of hydrogen in quartz at high water pressures: Implications for hydrolytic weakening. Journal of Geophysical Research, 91, 12723-12744.

Mauger, R.L. (1972) A sulfur isotope study of the Ducktown Tennessee District, U.S.A. Economic Geology, 67, 497-510.

Nesbitt, B.E. (1979) Regional metamorphism of the Ducktown, Tennessee massive sulfides and adjoining portions of the Blue Ridge Province. Unpublished Ph. D. Thesis, University of Michigan, 216 p.

Nesbitt, B.E. (1982) Metamorphic sulfide-silicate equilibria in the massive sulfide deposits at Ducktown, Tennessee. Economic Geology, 77, 364-378.

Nesbitt, B.E., and Kelly, W.C. (1980) Metamorphic zonation of sulfides, oxides and graphite in and around the orebodies at Ducktown, Tennessee. Economic Geology, 75, 1010-1021.

Nesbitt, B.E., and Essene, E. J. (1982) Metamorphic thermometry and barometry of a portion of the southern Blue Ridge province. American Journal of Science, 282, 701-729.

Ohmoto, H., and Kerrick, D. (1977) Devolatilization equilibria in graphitic systems. American Journal of Science, 277, 1013-1044.

Robie, R.A., Hemingway, B.S., and Fisher, J.R. (1978) Thermodynamic properties of minerals and related substances at 298.15 K and 1 bar (10^5 Pascals) pressure and at higher temperatures. U.S. Geological Survey Bulletin 1452, 456 pp.

Roedder, E. (1981) Origin of fluid inclusions and changes that occur after trapping. In L.S. Hollister and M.L.Crawford, Eds., Short course in fluid inclusions: Applications to petrology. Mineralogical Association of Canada, 6, 103-137.

Roedder, E., and Skinner, B.J. (1968) Experimental evidence that fluid inclusions do not leak. Economic Geology, 63, 715-730.

Ryzhenko B.N., and Volkov V.P. (1971) Fugacity coefficients of some gases in a broad range of temperatures and pressures. Geochemistry International, 468-481.

Sackett, W.M., and Chung, H.M. (1979) Experimental confirmation of the lack of carbon isotope exchange between methane and carbon oxides at high temperatures. Geochimica et Cosmochimica Acta, 43, 273-276.

Shaw, H.R., and Wones, D.R. (1964) Fugacity coefficients for hydrogen gas between 0°-1000°C for pressures to 3000 atm. American Journal of Science, 262, 918-929.

Sterner, S.M., and Bodnar, R.J. (1989) Synthetic fluid inclusions - VII. Re-equilibration of fluid inclusions in quartz during laboratory-simulated burial and uplift. Journal of Metamorphic Geology, 7, 243-260.

Sterner, S.M., Hall, D.L., and Bodnar, R.J. (1988) Post-entrapment compositional changes in fluid inclusions: Experimental evidence for water diffusion in quartz (abstr.). Geological Society of America Abstracts with Programs, 20, A100.

Toulmin, P., III, and Barton, P.B. (1964) A thermodynamic study of pyrite and pyrrhotite. Geochimica et Cosmochimica Acta, 28, 641-671.

Wall, V.J., and Burnham, C.W. (1974) NATO conference.

White, S. (1973) Dislocations and bubbles in vein quartz. Nature, Physical Sciences, 243, 11-14.

Wilkins, R.W.T., and Barkas, J.P. (1978) Fluid inclusions, deformation and recrystallization in granite tectonites. Contributions to Mineralogy and Petrology, 65, 293-299.

Ziegenbein, D., and Johannes, N. (1980) Graphite in C-H-O fluids: an unsuitable compound to buffer fluid composition at temperatures up to 700° C. N. Jb. Miner. Abh., 7, 289-305.

CHAPTER IV
STABLE ISOTOPES

INTRODUCTION

Metamorphosed pyrrhotite-pyrite-rich massive sulfide deposits, some of the largest and best studied of which are located at Ducktown, Tennessee, occur throughout the Appalachian-Caledonian orogen (Fig. 1). Despite the importance of these ores and their long history of exploitation, many questions remain unanswered regarding the origin of these bodies and their behavior during metamorphism. Many of the questions concerning the origin and evolution of these deposits could be addressed if the temporal and spatial chemical evolution history of fluids attending burial, metamorphism and uplift of these deposits were known. Furthermore, the Appalachian deposits, as well as their Caledonian equivalents, show many similarities in mineralogy, chemistry, occurrence and metamorphic grade, suggesting that a comprehensive study of fluid evolution in one deposit would be applicable to others as well.

In this study, we have collected C-O isotope data on quartz and calcite from the Cherokee and Calloway ore bodies, two of the largest sulfide occurrences in the Ducktown deposit. In addition, we present carbon isotope data from primary and secondary graphite from the ore zones and country rocks, and C-O-H isotope data from primary and secondary fluid inclusions. The petrology and significance of the fluid inclusions have been addressed by Hall et al. (1989a). These new isotope data are combined with previous silicate C-O-H isotope data of Addy and Ypma (1977), more recent

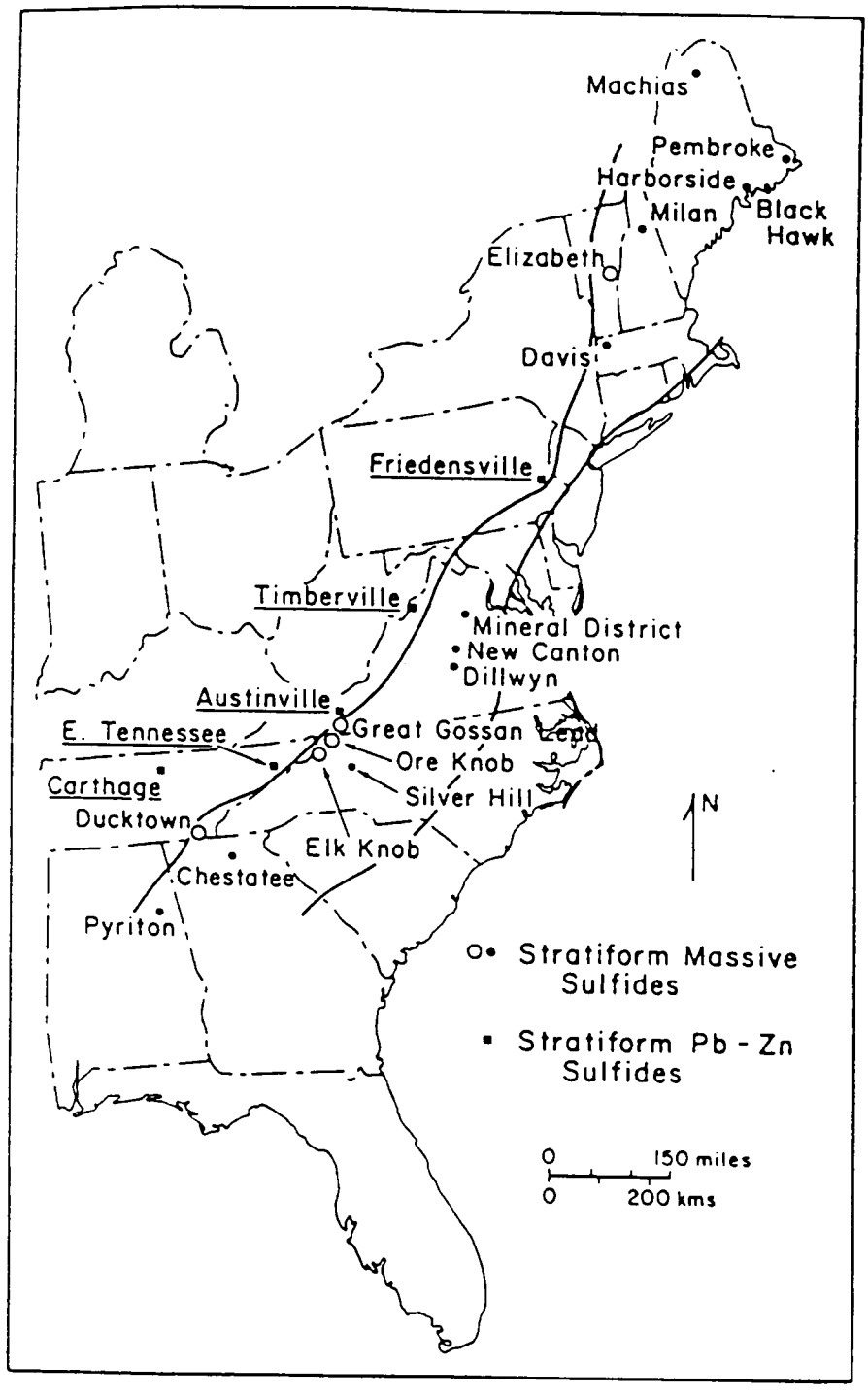

Figure 1. Index map of the eastern U. S. showing the locations of stratiform ore deposits in the Appalachians (from Craig, 1983).

information on the fractionation of oxygen between metamorphic minerals, new insights on the origin of Ducktown-type deposits, and the conclusions reached Hall et al. (1989a, b) to develop a model for fluid evolution during metamorphism and uplift of this deposit.

Geological Setting

The Ducktown mining district is located in the southeast corner of Tennessee (N35 01 lat. and W084 26 long.) in the Blue Ridge Province of the Southern Appalachians (Fig. 1). Eight major orebodies ranging in size from 0.25 million to 70 million tons (180 million tons total) are contained within the Late Precambrian Copperhill Formation of the Great Smoky Group within the Ocoee Series (Fig. 2). It is now generally accepted that the massive sulfides were deposited syngenetically with enclosing sediments during sea-floor hydrothermal activity (Mauger, 1972; Addy, 1973; Nesbitt, 1979). Consequently, they are classified as volcanogenic massive sulfide (VMS) deposits, although some aspects of their genesis are not clear.

Detailed stratigraphic studies have been conducted by Emmons and Laney (1926), Magee (1968) and Holcombe (1973). The orebodies are located within one to three stratigraphic horizons but are difficult to correlate due to the effects of deformation (Fig. 2). The host rocks are dominantly metagraywackes and quartz-mica schists with lesser quartzite, metaconglomerate and calc-silicate hornfels. The hornfels contains plagioclase, quartz, calcite, clinozoisite, hornblende, garnet and sphene; it occurs as irregular podlike masses within metagraywacke, and may represent metamorphosed calcareous concretions (Hadley and Goldsmith,

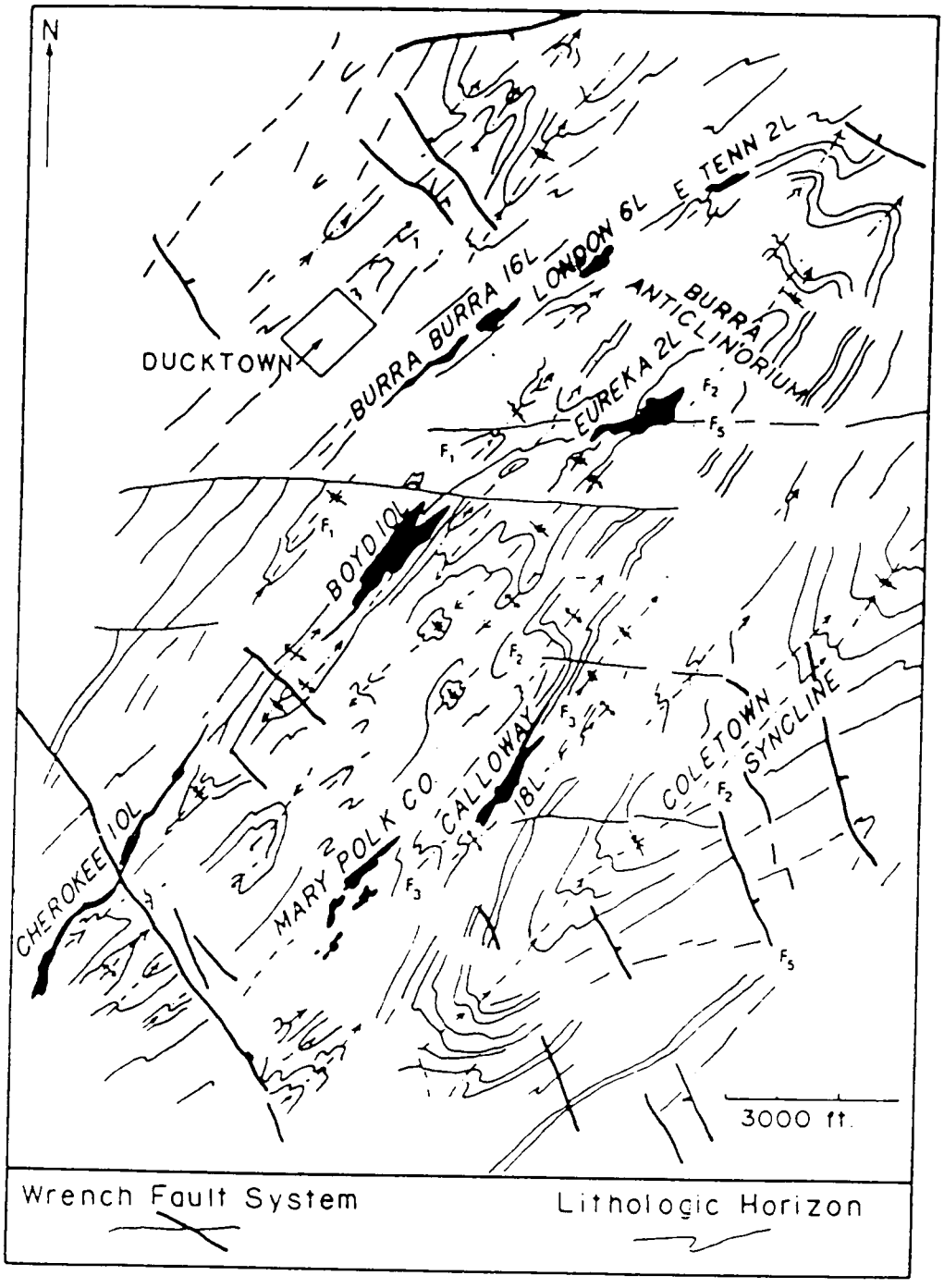

Figure 2. Detailed structural map of the Ducktown mining district showing the distribution of the orebodies (black) and lithologic units (thin lines). Also shown are megascopic structural features (heavy lines). F1-F5 correspond to the deformation events shown in Figure 3. (From Addy and Ypma, 1977).

1963). In addition, several lithologies have been recorded only near the orebodies, including chlorite schist containing dominantly chlorite, muscovite schist consisting dominantly of fine grained muscovite, biotite schist, plagioclase-rich rock and spessartine-rich rock. Similar lithologies have been recorded near other metamorphosed massive sulfides (e.g., Gair and Slack, 1984) and have been interpreted to represent either metamorphosed volcaniclastic rocks, or metamorphosed equivalents of alteration zones and exhalites typically found around unmetamorphosed volcanogenic massive sulfide deposits (Henry et al., 1979; Gair and Slack, 1984).

The orebodies vary from massive to disseminated but consist on average of 65 vol% massive sulfide and 35 vol% gangue. The massive sulfide ranges from pyrrhotite-rich to pyrite-rich but consists in general of 60 vol% pyrrhotite, 30 vol% pyrite, 4 vol% chalcopyrite, 4 vol% sphalerite and 2 vol% magnetite (Magee, 1968). Other reported metallic phases include galena, molybdenite, tetrahedrite, native bismuth, cubanite, stannite, bornite, rutile and ilmenite. Traces of gold and silver have been reported from assays but the mineralogic hosts for these metals remain unknown as no discrete precious-metal-bearing phase has ever been reported. Assays of samples from ore zones average 35.4 wt% Fe, 24.3 wt% S, 1.04 wt% Cu, and 0.89 wt% Zn (Slater, 1982). Gangue minerals include tremolite-actinolite, cummingtonite, biotite, muscovite, stilpnomelane, chlorite, quartz, calcite, dolomite, rhodochrosite, talc, clinopyroxene, plagioclase, garnet, epidote group minerals, anhydrite and rhodonite.

The Ocoee Series consists of at least 12 km of marine clastic rocks deposited in a large, rapidly subsiding basin while adjacent areas were

being uplifted (Rogers, 1972). The Great Smoky Group, within which the massive sulfides were deposited, represent deep water turbidites with source areas to the northeast (Hadley, 1970). Evidence for cogenetic volcanism during sedimentation of the Ocoee Series is sparse, as little volcanic or volcaniclastic material is recognized in the statigraphic record (Rankin, 1976). Rankin (1975) has suggested that the absence of volcanic rocks in the Ocoee reflects deposition in a series of grabens to the west (cratonward) of the actual opening of the Precambrian Iapetus ocean. Thus, no *in situ* production of oceanic crust occurred within these grabens. However, amphibolite bodies that have been found have been interpreted to be metamorphosed synsedimentary diabase sills and dikes (Slater, 1982). These amphibolites have the geochemical signature of olivine tholeiites and are thought to have been emplaced during intracratonic rifting in the early stages of development of Iapetus (Lawson and Misra, 1985).

In a regional tectonic sense, the Blue Ridge and Inner Piedmont Provinces form a large allochthon composed of a series of thrust sheets which have been transported up to several hundred kilometers to the northwest (Hatcher and Zietz, 1980). Individual thrust sheets were emplaced at different times throughout the Paleozoic - generally displaying westward younging - and in part probably overlie relatively unmetamorphosed platform sediments whose lateral equivalents are exposed in the Valley and Ridge (Hatcher and Zietz, 1980). Movements along these thrusts document compressional tectonics associated with the closing of Iapetus, beginning in Middle to Late Cambrian time and culminating in continent-continent collision of North America with Africa during the Carboniferous and Permian (Hatcher,

1978).

The Ducktown orebodies and their host rocks have undergone polyphase regional metamorphism associated with the closing of Iapetus during the Paleozoic. Holcombe (1973) and Addy and Ypma (1977) have recognized at least five episodes of deformation (F1-F5) and three episodes of metamorphism (M1-M3) (Fig. 3). The M1-F1 event, which reached garnet grade and produced large open folds in lower grade areas and tight isoclinal folds in higher grade areas, occurred during the Taconic orogeny (480-440 m.a.). Axial planes strike north-northeast and dip 30°-35° southeast (Holcombe, 1973). The M2 metamorphic event attained staurolite-kyanite grade and was interpreted by Addy and Ypma (1977) to have occurred after the Acadian orogeny (F2, 380-340 m.a.), which produced large isoclinal folds such as the Burra anticlinorium and the Coletown synclinorium (Fig. 2). These folds have axial plane orientations similar to those folds produced by F1. Most workers now believe that the thermal peak, hence F2, was attained during the Taconic and not the Acadian (Butler, 1972; Fullagar and Bottino, 1970; Dallmeyer, 1975a; Dallmeyer, 1975b; Hatcher, Butler, Fullagar, Secor and Snoke, 1980). A Barrovian sequence of metamorphic mineral assemblages was produced during M2. The biotite isograd is located ~9 km west of Ducktown (Carpenter, 1970), and grade increases progressively to the east through garnet, staurolite and kyanite isograds. Maximum grade in the mine area is middle amphibolite facies and is characterized by the assemblage staurolite ± kyanite. Using a variety of mineral thermobarometers, Nesbitt and Essene (1982) constrained P-T conditions of peak metamorphism to be 6 ± 1 kb and 540° ± 40°C. Brooker et al. (1987)

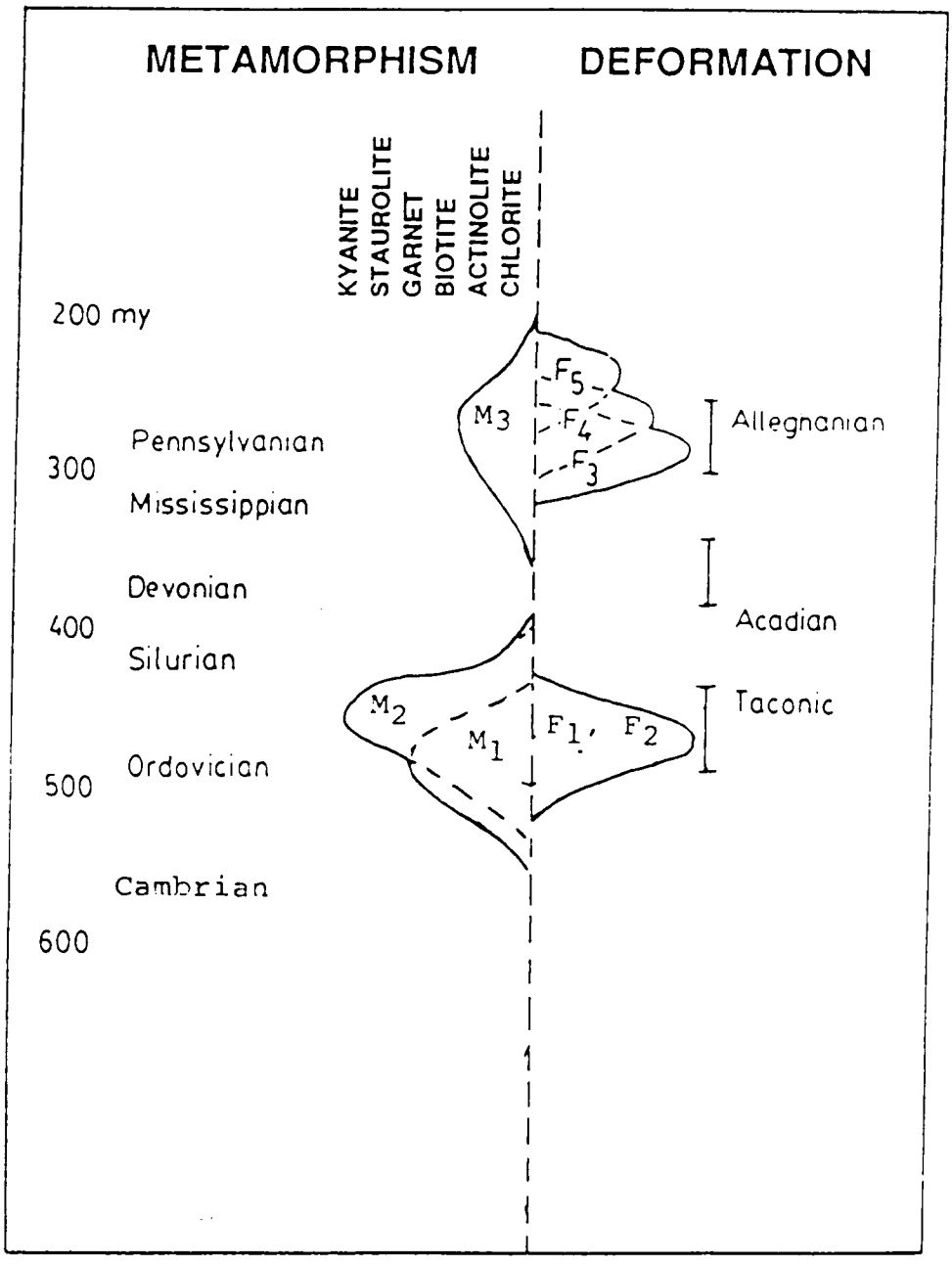

Figure 3. Schematic diagram showing the sequence of deformation and metamorphism (Modified after Addy and Ypma, 1977).

used sphalerite geobarometry on sphalerite grains armored by pyrite to obtain a pressure estimate of 6.8 ± 0.8 kb. The M3 event was associated with Alleghanian brittle deformation (F3-F5, 300-250 m.a.) and reached chlorite to biotite grade. These deformation events produced a variety of macroscopic and microscopic structures including small open folds, chevron folds, kink bands and strike-slip faults (Holcombe, 1973; Addy and Ypma, 1977).

The orebodies at Ducktown exhibit important similarities to active seafloor hydrothermal deposits, such as are forming in the Red Sea and Guaymas Basin, to younger, relatively undisturbed VMS deposits such as the Kuroko and Besshi deposits, and to older massive sulfide deposits such as the Jerome deposit. Most recent and ancient VMS deposits have chlorite-rich stockworks in their footwalls, which display ^{18}O-depletions due to interaction of high temperature (300-400°C) fluids (dominantly seawater) with the host rocks. Continued hydrothermal activity after ore deposition has been suggested to explain hanging wall alteration in these deposits. Although no stockwork structures have been recognized at Ducktown, this may be the result of metamorphism, as it has been recognized that in deformed VMS deposits stockwork zones may be sheared to the point of being laterally conformable with the orebodies (Lydon, 1988). Copper and zinc distributions at Ducktown generally do not follow the typical pattern of Cu-enriched footwall and Zn-enriched hanging wall; both Zn and Cu rich zones occur near the footwall, hanging wall and central portions of the orebodies - perhaps due to metamorphic remobilization and deformation as well. However, Slater (1982) reports Cu-rich footwall and Zn-rich hanging wall mineralization in some areas, and Allison (1984) has used trace element

distributions and the common occurrence of Cu-rich mineralization and chlorite schist on the present hanging wall of the Cherokee orebody to postulate that it has been overturned. Muscovite schist occurs in beds up to 10 meters thick in both hanging wall and footwall rocks, but is more common at shallower levels (Magee 1968), while chlorite schist, attaining thicknesses of 200 meters, appears to be more abundant in the footwalls and deeper portions of the orebodies. Muscovite in the footwall may form thin selvages between ore and chlorite schist (Magee, 1968).

Lydon (1988) has suggested two genetically distinct subcategories of VMS deposits: Cu-Zn and Zn-Pb-Cu, reflecting mafic volcanic and felsic volcanic hosts, respectively, or their sedimentary derivatives. This classification implies that the ultimate source of the metals is the underlying host rocks. Ducktown orebodies generally have Cu/Zn ratios greater than 1 and low lead contents (<0.1%). Thus, the deposits can be categorized as Cu-Zn type, consistent with the relatively mafic metagraywackes, which make up the bulk of the country rock. The lack of barite (or barium-rich minerals), rarity of anhydrite and low sulfur isotopic ratios ($\delta^{34}S$ average < 5 ‰, Mauger, 1972) noted at Ducktown are typical of Cu-Zn type VMS deposits. Au and Au/Ag ratios are usually higher in Cu-Zn type deposits than in the Zn-Pb-Cu type, but precious metal contents of Ducktown ore are uniformly low.

To separate Cu and Zn from Pb and to explain the general lack of Ba in Cu-Zn type VMS deposits, Lydon (1988) has called upon neutral to alkaline ore fluids and metal transport as bisulfide complexes. However, the Red Sea deposits, which bear striking similarities to the those at Ducktown, are Zn-Cu-rich, Pb-poor, contain no barite and are currently being formed by

highly saline brines. These brines are slightly acidic, are low in total sulfur and contain large quantities of dissolved Fe, all of which preclude significant transport of metals as bisulfide complexes (Pottorf and Barnes, 1983). The low Pb and Ba contents reflect the paucity of these elements in the source rocks (basalts) rather than some geochemical winnowing process. It is likely that the same argument applies to the Ducktown deposit as well.

Previous Stable Isotope Work

Addy and Ypma (1977) conducted an extensive study of C-O isotopes at Ducktown. The results of their study can be summarized as follows.

(1) Rocks proximal to the orebody, which are dominantly chlorite and muscovite schists, have bulk compositions that are ^{18}O-depleted relative to distal rocks (dominantly metagraywackes and biotite schists). This is reflected in the $\delta^{18}O$ values of mineral separates, which are systematically lower by about 2-3 per mil near the ore zones.

(2) Limited hydrogen isotope data suggest that biotite and muscovite have nearly identical δD values throughout the deposit.

(3) $\delta^{13}C$ values of calcite in both country rock and ore zones are similar and range from -13.9 to -20.2 per mil PDB.

From these data Addy and Ypma (1977) reached the following conclusions.

(1) Isotopic fractionations between quartz and magnetite in the ore zones provide the most reliable thermometers and suggest isotopic temperatures of 492° to 541°C. Other potential oxygen isotope thermometers such as quartz-biotite, quartz-muscovite, quartz-garnet, quartz-calcite and

calcite-magnetite give larger ranges and in many cases suggest geologically unreasonable temperatures, although average quartz-biotite and quartz-muscovite temperatures from the alteration zones and country rock are near 500°C. Isotopic disequilibrium, resulting in unreasonable temperature estimates, is postulated to have resulted from post-metamorphic retrogression.

(2) Interaction of organic matter with sedimentary carbonate during metamorphism caused the low values of $\delta^{13}C$ in calcite.

(3) Depletion of ^{18}O from ore zones is the result of interaction with isotopically light hydrothermal solutions, which invaded the ore zones *during* peak metamorphism. The similarity of δD and $\delta^{13}C$ values among minerals in country rocks and ore zones suggested to Addy and Ypma (1977) that a single, isotopically homogeneous fluid was present away from ore zones during metamorphism. Escape of this fluid through the ore zones with preferential loss of CO_2 (presumably due to fluid immiscibility?) was suggested as the mechanism by which the aqueous portion of this fluid became ^{18}O-depleted and caused lowering of $\delta^{18}O$ values in the ore zones.

Mauger (1972) investigated sulfur isotopes in samples of Calloway and Cherokee ore. His data show that ore types (e.g. pyrite-rich, pyrrhotite-rich, and magnetite-rich) and accompanying $\delta^{34}S$ patterns are broadly conformable to the orebody contacts. Although grain scale equilibration of sulfur isotopes occurred during metamorphism, original larger scale isotopic inhomogeneities are preserved. Variable $\delta^{34}S$ values resulted from bulk differences in $\delta^{34}S$ related to original depositional patterns and were preserved through metamorphism.

The Present Investigation

We have collected C-O isotope data from calcite and quartz mineral separates from the Calloway and Cherokee orebodies (Table 1). Carbonate mineral separates were analyzed for oxygen and carbon isotopes using the phosphoric acid technique of McCrea (1950). Quartz mineral separates were analyzed for oxygen isotopes using the bromine pentafluoride technique of Clayton and Mayeda (1963). Carbon isotope data from primary and secondary graphite from the ore zones and country rocks, and C-O-H isotope data from primary fluid inclusions in peak metamorphic clinopyroxene and secondary CH_4-(CO_2)-N_2-H_2O-NaCl inclusions in quartz were also collected (analyses by Isotope Specialists Inc.) (Tables 1, 2). Inclusion fluids were liberated from the host minerals by crushing *en vacuo*. Water, carbon-dioxide and methane were cryogenically separated and their isotope ratios were analyzed. Isotope values are reported in standard δ-notation with $\delta^{18}O$ referenced to Standard Mean Ocean Water (SMOW) and $\delta^{13}C$ referenced to a belemnite guard from the Peedee Formation in North Carolina (PDB). The isotopic fractionations between two minerals or fluid species are reported in standard Δ-notation.

Isotope Geothermometry

Mineral pairs

Availability of more recent fractionation factors between some mineral pairs warrants re-assessment of the metamorphic temperatures estimated by Addy and Ypma (1977). Nesbitt and Essene (1982) and Brooker et al. (1987)

Table 1. Oxygen and carbon isotope data from the Ducktown deposits (this study).

Sample	Description	$\delta^{18}O$*			$\delta^{13}C$#	
		Cc	Pl	Qz	Graph	Cc
CH7-green	cg Cc intergrown w/ Am	7.38				-17.63
CH7-white	cg Cc w/ above, later generation	7.30				-15.77
CH12-core	cg gry Cc pod in Po-Py-Cpy-rich ms	7.59				-12.67
CH12-rim	fg rexlized wht Cc tail on above	7.56				-13.83
CH15	Px+Am+Cc	7.05				-13.59
CHP100	large gry Cc pod in Py-rich ms	7.66				-14.03
CHP101	large cg gry Cc pod in foliated Po-rich ms	7.37				-13.01
CHP102	cg gry Cc pod in Po-rich ms	8.43				-15.92
CHP103	large gry Cc pod in Py-rich ms	7.62				-14.34
CHP104A	large wht Cc pod w/ Py-Po-Bi-rich schist	9.35				-12.20
CHP104B	dark gry Cc intergrown with above	9.32				-12.30
CHP105	clear Qz eye (boudined) in Po-rich ms			9.25		
CHP106	clear Qz pod in Po-rich ms			8.74		
CHP107	clear Qz pod in Po-rich ms			8.73		
CH827-54	Px+Qt+Cc+sulfide			8.71		
CH1214-175	Qz+Px			8.63		
CH1226-390	Qz+Px+Cc+minor sulfide			8.46		
CH1227-222	Qz+Px, very little sulfide			8.75		
CH1461-186	Pl+Am+Bi schist, minor Po		7.47			
CH1461-223	Po+Py+Qz			8.19		
CH1461-275	fg Po+Qz			9.20		
CH1464-257	Am+Qz+Pl schist		6.87			
CH1464-259	foliated Po-rich ms w/ Pl+Bi+Ct		7.18			
CH4164-313	large Qz pod in banded fg schist			8.40		
CH1464-344	Qz segregation in Am+Qz+Cc+sulfide schist			8.32		
CH1466-267	coarse wht Cc w/ Am in Po-rich ms	9.66				-13.81
CH1466-339	qtz boudin in Bi-Mu-Ct schist			9.00		
CH1466-380	Qt-rich lens in Po-Py-Cpy-rich ms			8.77		
CH1477-339	Gt-Bi-Pl schist			9.14		
			6.40			
CH1504-125	gry Cc pod in ms	8.09				-12.78
CH1577-280	fg saccharoidal sulfide-poor Qz vein			9.15		
CH1582-490	cg sulfide-poor Gt-Bi-Pl-Qz schist			9.10		
CH1594-144	Am-Bi-Pl-Qz schist w/ Po+Py+Cpy		7.60			
CH1594-187	foliated Po-rich ms w/ Am+Bi+Py+Cc	8.15				-14.27
CH1594-208	Px w/ Po-rich ms	7.40				-15.30
CH1594-220	cg Cc eye in Po-rich ms	7.29				-15.18
CH1594-237	gry Cc with Qz and Po-Py-Mt-rich ms	7.06		8.21		-14.14
CL425-126	Cc w/ Py+Po+Mt inclusions	9.47				-14.28
CL795-129	Cc w/ Po-rich ms	8.32				-15.67
CL826-9	Cc w/ Po-rich ms	7.84				-13.59
B770-2272B	graph schist w/ chloritized garnet				-23.1	
Mile 446.6	graph-rich phyllite, biotite zone				-20.1	
MP1154-5.5	graph-rich schist in country rock				-24.2	
MP1154-43	secondary graph replacing sulfides in ms				-25.6	

* per mil SMOW; # per mil PDB; *Ct* chlorite; *Cc* calcite; *Pl* Plagioclase; *Qz* quartz; *Mu* muscovite; *Am* amphibole; *Po* pyrrhotite; *Py* pyrite; *Cpy* chalcopyrite; *Mt* magnetite; *Bi* biotite; *Px* pyroxene; *Gt* garnet; *cg* coarse-grained; *fg* fine-grained; *gry* gray; *wht* white; *ms* massive sulfide; *Graph* graphite; *CH* Cherokee; *CL* Calloway; *B* Boyd; *MP* Mary-Polk

Table 2. C-O-H isotope analyses (‰) of inclusion fluids (this study).

Ratio	Host							
	Px	Px	Px	Px	Qtz	Qtz	Qtz	Qtz
$\delta^{18}O_{H_2O}$	-15.4	-15.6	-16.2	-15.8	-15.2	-13.9	-14.1	-18.0
δD_{H_2O}	-97	-98	-103	-94	-52	-80	-69	-69
$\delta^{18}O_{CO_2}$	NA	NA	NA	NA	26.2	26.6	30.7	29.5
$\delta^{13}C_{CO_2}$	NA	NA	NA	NA	-15.8	-11.5	-13.2	-12.9
δD_{CH_4}	-103	NA	NA	-115	-103	-107	-98	NA
$\delta^{13}C_{CH_4}$	-20.4	-21.7	-16.2	-17.4	-22.1	-25.9	-27.3	NA
δD_{bulk}*	-97	-98	-104	-96	-55	-81	-70	-70
$\delta^{18}O_{bulk}$#	-15.4	-15.6	-16.2	-15.8	-14.3	-13.1	-13.1	-17.1
$\delta^{13}C_{bulk}$#	-20.4	-21.7	-16.2	-17.4	-21.5	-24.5	-25.9	-------

NA not analyzed; *assumes X_{CH_4} = 0.1 for Px and 0.05 for Qtz; #assumes X_{CH_4} = 1.0 in Px and $X_{CH_4}/(X_{CO_2}+X_{CH_4})$ = 0.9 in Qtz

have constrained P-T conditions of peak metamorphism to have been 540±40°C and 6-7 kb utilizing a variety of mineralogic thermobarometers. Therefore, isotopic temperature estimates provide an indication of the degree of isotopic equilibrium attained during peak metamorphism, and the extent of retrograde exchange. Temperatures indicated by fractionation of ^{18}O between quartz, calcite, magnetite, garnet, muscovite, biotite and chlorite, calculated using appropriate fractionation factors and the oxygen isotope data of Addy and Ypma (1977), are presented in Table 3. A variety of experimental and/or empirical fractionations are available for the mineral pairs considered here, and these are compared in Table 3.

Quartz and magnetite form one of the more useful mineral pairs for thermometry because of the large fractionation between the two minerals and because both are fairly resistant to retrograde isotopic exchange (O'Neil, 1986). Not surprisingly, isotopic temperatures obtained for quartz-magnetite pairs utilizing the fractionation factors of Downs et al. (1981) or Mathews et al. (1983) are the most consistent of all mineral pair thermometers investigated in this study and suggest average equilibration temperatures of 533° and 549°C, respectively - in excellent agreement with mineral thermobarometers. Other mineral pairs are much less consistent, but quartz-biotite, quartz-muscovite and quartz-chlorite pairs give respective average temperatures of 501°, 490° and 530°C (Table 3), suggesting that these minerals equilibrated at or near peak metamorphic temperatures as well.

The isotopic temperatures suggested by quartz-chlorite fractionations are important because they imply that chlorite was present during peak metamorphism and equilibrated with coexisting phases. The presence of

Table 3. Summary of oxygen isotope temperatures obtained using isotope data of Addy and Ypma (1977)

Mineral pair	Reference	Temperature (°C)		Number of Analyses
		Average	Range	
Qz-Mt	Downs et al. (1981)	533	506-574	5
	Mathews et al. (1983)	549	529-580	
Qz-Mu	Matsuhisa et al. (1979) + O'Neil & Taylor (1969)	336	291-370	8
	Matsuhisa et al. (1979) + Bottinga & Javoy (1973)	379	342-407	
	Javoy (1977)	490	451-520	
	Mathews & Schliestedt (1984)	426	383-458	
Qz-Bi	Bottinga & Javoy (1975)	501	446-559	20
Qz-Gt	O'Neil (1986), for qtz-pyrope	538	436-654	6
	Javoy (1977)	581	494-676	
Qz-Ct	Matsuhisa et al. (1979) + Field & Fifarek (1985)	530	500-561	6
	Wenner & Taylor (1971)	419	387-453	
	Javoy (1977)	561	540-583	
Qz-Cc	Matsuhisa et al. (1979) + O'Neil et al. (1969)	424	155-736	11
	Mathews et al. (1983)	314	116-517	

large amounts of chlorite adjacent to the orebodies led earlier workers to postulate that it resulted from retrograde hydration of peak metamorphic minerals and hence that ore zones may have been loci for post metamorphic fluid flow, or that the orebodies themselves were formed after metamorphism by hydrothermal fluids (Brown, 1961; Tung, 1968; Addy and Ypma, 1977). However, Nesbitt (1982) concluded that most chlorite near the ore zones equilibrated compositionally and texturally with other peak metamorphic phases, hence was present during metamorphism. Quartz-chlorite isotope temperatures presented here support this conclusion. Minor replacement of biotite and garnet by chlorite did occur after peak metamorphism, but this secondary chlorite is volumetrically insignificant compared to primary chlorite.

Quartz and garnet should form a good isotope thermometer due to the resistance to re-equilibration of these two minerals (Garlick and Epstein, 1967); however, a temperature range of over 200°C was obtained for this mineral pair (Table 3). Taylor and O'Neil (1977) have shown that at 600°C the fractionation between grossular and andradite is 1.6 per mil, and it appears that pyrope concentrates ^{18}O more than grossular (see Fig. 2 of O'Neil, 1986). The large oxygen isotope fractionation between grossular and andradite appears to be related to the substitution of Al^{3+} for Fe^{3+} in the octahedral site, while the smaller fractionation between pyrope and grossular is presumably related to the substitution of Ca^{2+} for Mg^{2+} in the eight coordinated triangular dodecahedral site. Consequently, almandine and spessartine probably exhibit isotopic fractionations similar to pyrope, given the similarity in cation sizes among Mg^{2+}, Fe^{2+} and Mn^{2+} relative to Ca^{2+}, although the actual fractionations have not been determined. Mathews et al.

(1983) found no significant fractionation between diopside and hedenbergite and concluded that substitution of Fe^{2+} for Mg^{2+} in the octahedral sites of these minerals had little effect on isotopic fractionation. In light of the above discussion, variable compositions can produce significant variations in apparent temperatures if only a single fractionation factor is employed.

Ducktown garnets are compositionally variable. In the country rocks garnet contains, on the average, 75-80 mole % almandine and 10 mole % grossular with the remaining 10-15 mole % dominated by pyrope (Nesbitt, 1982). Spessartine rarely exceeds 10 mole %. Near the ore zones iron is replaced by manganese so that the spessartine component averages about 30 mole % while almandine decreases to 40 mole %. Grossular remains essentially the same and the pyrope component increases slightly (Nesbitt, 1982). During the present study, garnet coexisting with clinopyroxene in the Mary-Polk orebody was found to have an average composition of $Gr_{62}And_{16}Sp_{12}Alm_{10}$. Coexisting pyroxene is more iron-rich (average $Di_{57}Hd_{39}Jo_4$) than most pyroxene in samples without garnet (average $Di_{75}Hd_{21}Jo_4$). Furthermore, electron microprobe traverses across garnets from both ore zones and country rocks indicate that they are compositionally zoned, generally from Mn-Ca-rich cores to Fe-Mg-rich rims. Thus, $\delta^{18}O$ values on bulk grains represent an average value for an average garnet composition. These complex garnet substitutions coupled with the significant compositional effects on oxygen isotope fractionations between garnet endmembers may account for some of the spread in the isotopic temperature data.

Quartz-calcite and calcite-magnetite pairs give very large ranges in

apparent temperatures (Table 3) and in some cases are obviously not in equilibrium (e.g. those pairs analyzed by Addy and Ypma that display negative values of $\Delta_{qtz\text{-}cc}$). Much of the calcite appears to have been present during the metamorphic event. This is supported by the apparent textural equilibrium among quartz, calcite, amphibole and pyroxene in the ore zones, and by calcite deformation textures, which are concordant with those of surrounding rocks. Furthermore, Nesbitt and Essene (1982) have used calcite-dolomite geothermometry to obtain inferred temperatures of peak metamorphism of 540°±40°C.

Retrograde exsolution of dolomite from calcite, as noted by Nesbitt and Essene (1982), is a possible source of scatter in calculated temperatures. Dolomite concentrates ^{18}O relative to calcite. If exsolution occurs the remaining calcite will be lighter and $\Delta_{qtz\text{-}cc}$ will be larger, resulting in low temperature estimates. Most quartz-calcite pairs analyzed by Addy and Ypma (1977) do in fact indicate low temperatures. Reaction times with phosphoric acid in both the present study and that of Addy and Ypma (1977) were intentionally short, to avoid liberation of significant amounts of CO_2 from dolomite; hence, only CO_2 from calcite was analyzed. In reality, however, the effect of dolomite exsolution on $\delta^{18}O$ values is probably insignificant. Nesbitt and Essene (1982) found that re-integrated $MgCO_3$ contents of calcite average 5 mole %. Assuming a maximum $\Delta_{dol\text{-}cc}$ of 1.5 per mil (i.e. equilibration at about 300°C) the maximum effect of exsolution would be to lower $\delta^{18}O$ (i.e. increase $\Delta_{qtz\text{-}cc}$) by 0.08 per mil. If the original quartz-calcite equilibrium temperature was 550°C ($\Delta_{qtz\text{-}cc}$ = 1.1 ‰), dolomite exsolution could only account for temperatures up to 50°C lower than equilibrium.

Obviously retrograde exchange, or a late stage origin for calcite must be invoked, especially for samples with negative $\Delta_{qtz\text{-}cc}$. Calcite is very susceptible to retrograde isotopic exchange, even below 300°C (Clayton et al., 1968). This, coupled with the relative temperature insensitivity of the quartz-calcite pair (i.e. $\Delta_{qtz\text{-}cc}$ is small and does not vary much over a large temperature range) make this mineral pair a poor geothermometer but a sensitive indicator of retrograde exchange. Cathodoluminescence reveals textures, such as calcite microveins in fractured silicates, suggestive of a late origin or of late stage remobilization of calcite. In these cases calcite would not likely be in equilibrium with coexisting quartz. The source of C-O variability in carbonates is discussed further under "Coupled O-C Isotope Trends in Calcite".

Mineral triplets

One test of isotopic equilibrium and validity of isotopic temperatures is concordancy among three or more coexisting minerals for which fractionation factors are known (Deines, 1977). Concordancy is demonstrated if temperatures for all possible mineral pairs are within the combined temperature uncertainty arising from isotopic analysis of the individual mineral pairs (generally ± 0.3 ‰). Table 4 shows the samples of Addy and Ypma (1977) in which three or more minerals were analyzed and also shows our calculated temperature and uncertainty associated with the individual mineral pairs. Pairs involving calcite and garnet have been excluded due to the problems of re-equilibration and uncertain origin of calcite, and large compositional effects on isotopic fractionation between garnet endmembers,

Table 4. Isotope temperatures indicated by mineral triplets. Concordant samples are bolded. Isotope data from Addy and Ypma (1977)

Sample	Qt-Mu	Qt-Bi	Qt-Ct	Mu-Bi	Mu-Ct	Bi-Ct
C186-460AZ		**503±20**	**500±20**			**488+79 -60**
CHSA-21AZ		**509±20**	**529±23**			**567+109 -79**
CHSA-11AZ	478±29		561±26		685+44 -38	
CHSA-10CR	460±27	503±20		582+70 -56		
CHSA-18CR	451±26	559±24		868+184 -125		
C190-461AZ	**509±33**	**522±24**	**537±24**	**543+61 -49**	**598+82 -73**	**538+97 -71**
C248-461AZ	498±31	551±22		652+91 -70		
C287-461AZ	**498±31**		**529±23**		**598+82 -73**	
CSA-26CR	520±34	484±18		440+39 -33		

Sources of isotopic fractionation factors: *Qt-Mu* Javoy (1977); *Qt-Bi* Bottinga and Javoy (1975); *Qt-Ct* Qt-H_2O of Matsuhisa et al. (1979) combined with Ct-H_2O of Field and Fifarek (1985); *Mu-Bi*, *Mu-Ct* and *Bi-Ct* were derived from their respective Qt-mineral fractionations.

as discussed above. Of the 15 samples in which three or more minerals were analyzed, only four show mutual overlap of temperatures calculated from three or more Δ's. One sample shows temperature concordance among the minerals quartz, biotite, muscovite and chlorite (i.e., 6 possible Δ's). Not surprisingly, the samples showing temperature concordance also plot closest to best-fit equilibrium curves on Δ-Δ plots (Fig. 4), a further indication that they approached and maintained isotopic equilibrium (Deines, 1977). All four of these samples are from "alteration zones", using the terminology of Addy and Ypma (1977), which envelope the orebodies and consist largely of chlorite and muscovite schist and calc-silicate minerals. These zones correspond roughly to the "pyrrhotite-rutile" zones of Nesbitt and Kelly (1980).

The temperature range of overlap among mineral triplets or quadruplets for each of the four concordant samples is shown in Figure 5. Note that no area of mutual overlap exists for all samples; however, three overlap in the temperature range 525°-529°C. If the temperature indicated by the muscovite-chlorite pair in two samples is ignored, mutual overlap is generated for all four samples over the temperature range 515-520°C. Equilibrium temperatures of 515-529°C are consistent with the estimate of 540±40°C obtained by Nesbitt and Essene (1982) with mineral thermobarometry, and are also consistent with average isotope temperature estimates of 530-550°C derived from quartz-magnetite pairs (Table 3). As previously mentioned, this mineral pair may be the most reliable; however, absence of other useful coexisting minerals preclude verification of quartz-magnetite temperatures by the mineral-triplet method. Combining all available petrologic and isotopic data, we conclude that a peak metamorphic

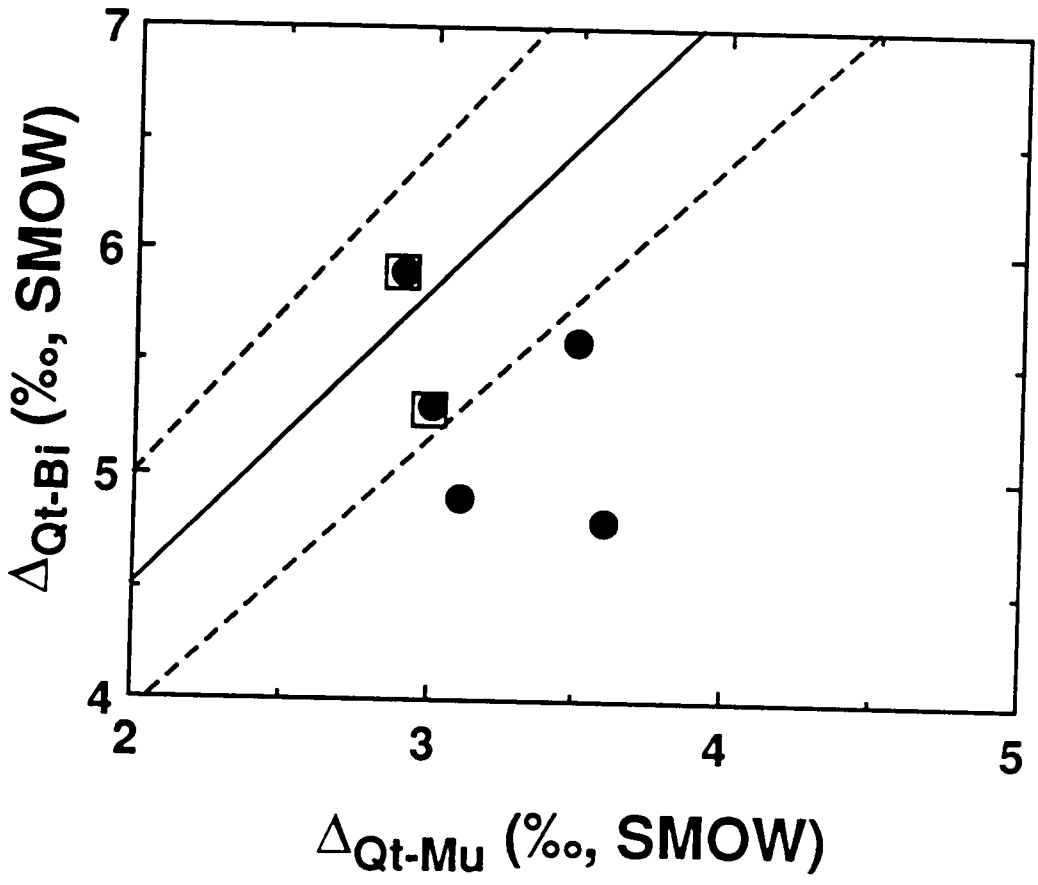

Figure 4. Approach to isotopic equilibrium of samples indicating temperature concordance among the minerals quartz, biotite and muscovite. The solid line is the best correlation regression of naturally observed fractionations from Deines (1977). Dashed lines show approximate limits of acceptable deviations due to experimental uncertainties. The five data points represent samples in which these three minerals were analyzed. Boxed data points are two of the four samples which show temperature concordance. Data from Addy and Ypma (1977).

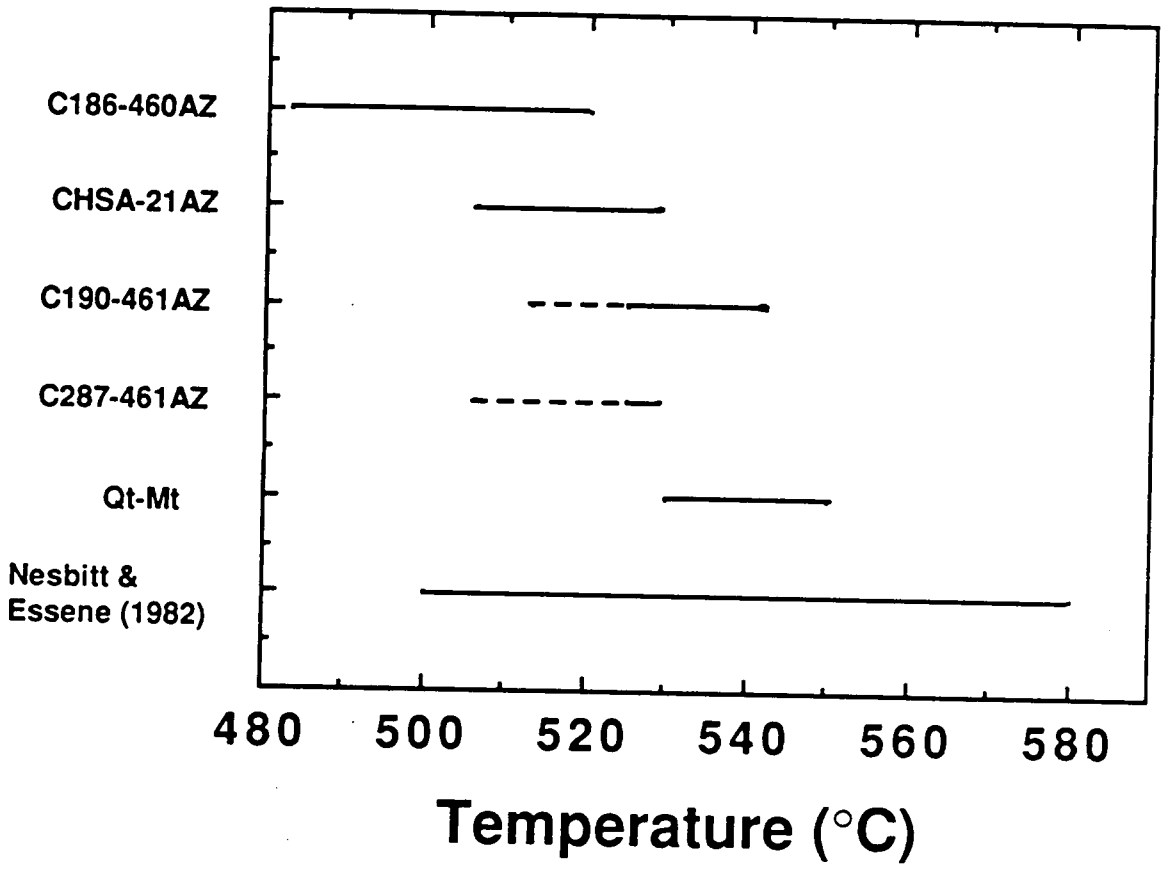

Figure 5. Isotopic temperatures indicated by the four concordant samples (solid lines). Temperature ranges are extended for two samples as indicated by dashed lines if two muscovite-chlorite pairs are ignored. Also shown is the temperature range indicated by quartz-magnetite mineral pairs (Qt-Mt) and the temperature estimated by Nesbitt & Essene (1982) via mineral thermobarometers. Data from Addy and Ypma (1977).

temperature near 530°C is most likely.

$\delta^{18}O_{qtz}$ - $\delta^{18}O_{mineral}$ Relationships

Addy and Ypma (1977) recognized that $\delta^{18}O$ values for quartz, garnet, biotite and muscovite form two discrete populations - one for samples collected near the orebodies and the other for samples collected from the country rocks (Fig. 6). Their data indicate that quartz coexisting with muscovite, garnet, biotite and chlorite in ore zones has $\delta^{18}O$ values of 8.4-9.7 per mil, while quartz in the country rocks has $\delta^{18}O$ values of 10.3-11.4 per mil (Fig. 6A). Quartz coexisting with magnetite in ore zones has intermediate $\delta^{18}O$ values of 9.2-10.3 per mil. Garnet and biotite in ore zones are ^{18}O-depleted by 2 per mil, on the average, compared to corresponding minerals in country rocks while muscovite in ore zones shows a 3 per mil depletion. No trend is seen between individual orebodies (Fig. 6B). Our $\delta^{18}O$ values for quartz near the orebodies range from 8.2 to 9.3 per mil (Table 1) consistent with the data of Addy and Ypma (1977).

The $\delta^{18}O$ values for quartz coexisting with calcite in country rocks are higher than values from near orebodies, but the $\delta^{18}O$ relationship between quartz-calcite pairs is not as distinct as for other quartz-mineral pairs. Also, the $\delta^{18}O$ values of quartz with calcite in ore zones vary continuously from country rock values to more typical ore zone values with no distinct hiatus, as was found for other mineral pairs. Thus, as discovered by Addy and Ypma (1977), $\delta^{18}O$ of all minerals with the exception of calcite are lower by several per mil in the ore zones. Average calculated and analyzed whole-rock $\delta^{18}O$ values for country rock metagraywackes are approximately 9 per mil.

Figure 6. $\delta_{mineral}$ vs. δ_{qtz} diagram for coexisting mineral pairs. A) plotted as a function of location. Open symbols = country rocks, closed symbols = ore zones. Triangles = quartz-calcite, squares = quartz-muscovite, circles = quartz-garnet, diamonds = quartz-biotite, X = quartz-chlorite and crosses = quartz-magnetite. All chlorite and magnetite is from the orebodies. Constant $\Delta_{qtz\text{-}min}$ lines, corresponding to an equilibrium temperature of 530°C, are shown for each mineral pair. B) Same data plotted to delineate mineral pairs from different orebodies. Filled circles = Cherokee, open circles = Calloway, filled square = Mary-Polk and open square = Boyd. Data from Addy and Ypma (1977).

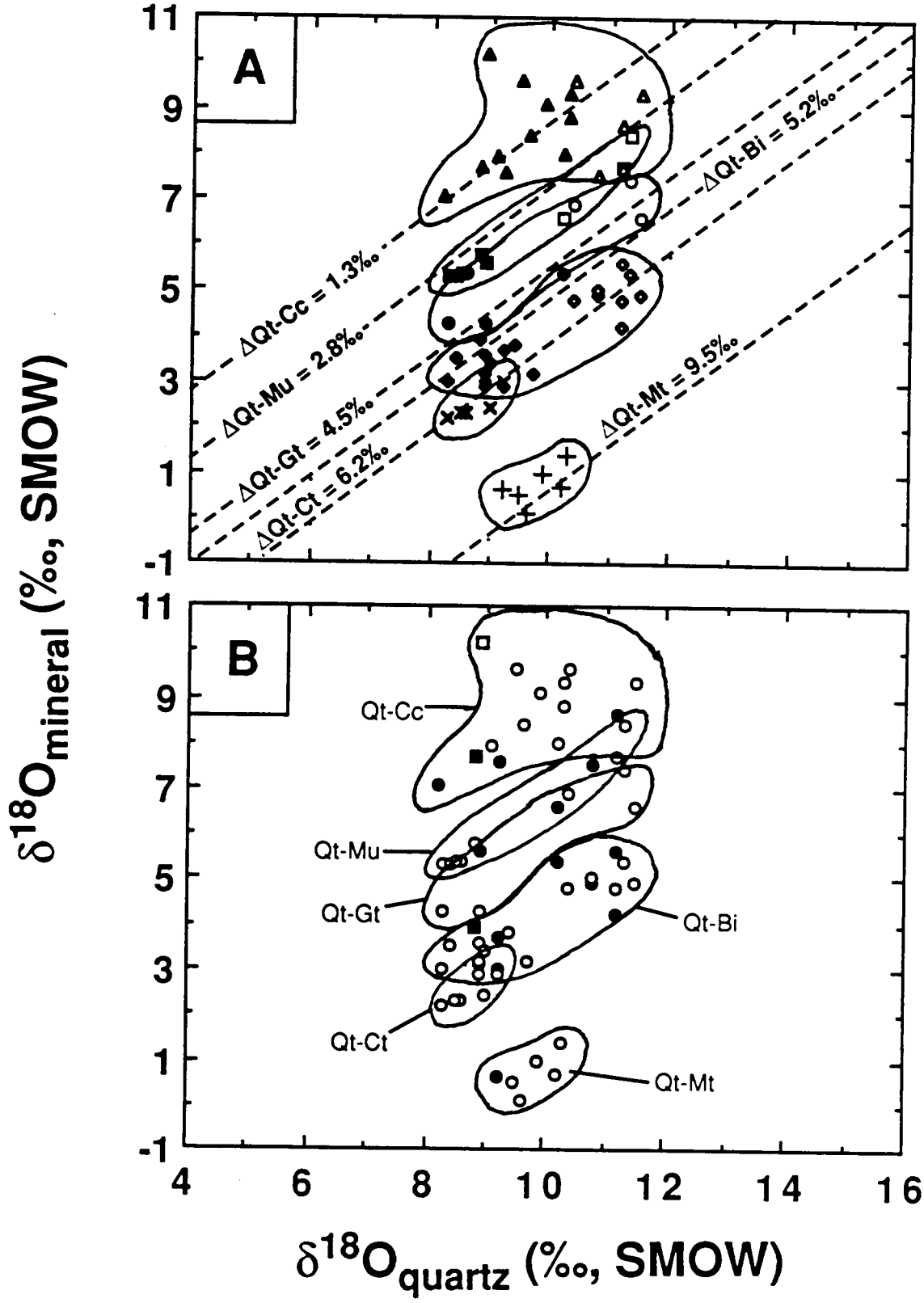
A
B
ΔQt-Cc = 1.3‰
ΔQt-Mu = 2.8‰
ΔQt-Gt = 4.5‰
ΔQt-Ct = 6.2‰
ΔQt-Bi = 5.2‰
ΔQt-Mt = 9.5‰
Qt-Cc
Qt-Mu
Qt-Gt
Qt-Ct
Qt-Bi
Qt-Mt
11
9
7
5
3
1
-1
4
6
8
10
12
14
16
δ18Omineral (‰, SMOW)
δ18Oquartz (‰, SMOW)

Calculated average whole-rock $\delta^{18}O$ values for schists surrounding the orebodies are 4 per mil for chlorite-rich lithologies and 6-7 per mil for muscovite-rich lithologies. Whole-rock depletions are obviously a function of modal mineralogy and are most pronounced in those samples containing large modal abundances of the ^{18}O-depleted mineral chlorite. The source of ^{18}O-depletion in the ore zones is discussed below.

Plots of the oxygen isotope composition of quartz versus those of biotite, garnet and muscovite are best fit by straight lines with approximate slopes of 1 - in other words, constant $\Delta_{qtz\text{-}min}$ (Fig. 6A). These represent isotherms in δ-δ space, suggesting that minerals in ore zones and country rocks approached isotopic equilibrium during metamorphism. A less distinct trend is noted for chlorite and magnetite. These minerals were only stable in the ore zones during metamorphism and hence the large isotopic shift between ore zone and country rock minerals, which best delineates the constant Δ lines, is not present. The ultimate positions attained along these lines are a function of a variety of parameters such as bulk isotopic compositions of the fluid + mineral systems, water/rock ratios, and the mechanisms of exchange. Scatter about the lines indicates either that some samples did not reach equilibrium during metamorphism or that post-metamorphic exchange has altered peak metamorphic $\delta^{18}O$ values. Isothermal compositional effects on fractionation may also account for some scatter. The fact that both high and low $\delta^{18}O$ groups cluster around the same line indicates that the minerals in all lithologies were subjected to the same thermal event. Assigning temperatures to constant Δ lines requires information on isotopic fractionation between minerals. Appropriate fractionation factors (Table 3) were used to

plot constant Δ lines for 530°C (Fig. 6A), which is our best estimate for the temperature of peak metamorphism based on isotopic thermometry and mineralogic thermobarometry (Fig. 5).

Ducktown rocks were completely recrystallized during peak metamorphism and most minerals grew or equilibrated compositionally at peak metamorphic pressures and temperatures (Nesbitt, 1979) and probably equilibrated isotopically as well. Thus, deviations from the constant Δ lines, which represent equilibration at 530°C, evidence post-metamorphic disequilibrium and/or equilibrium isotopic exchange rather than failure to attain equilibrium during metamorphism. Most of the analyzed quartz-biotite, quartz-muscovite and quartz-chlorite pairs have larger $\Delta_{qtz\text{-}min}$ than that of the 530°C isotherm, suggesting exchange at lower temperatures.

Recent studies have shown that by interpreting stable isotope data in terms of temperature, mass balance and kinetics of isotopic exchange it is often possible to distinguish between fluid absent, closed system and open system environments (Gregory, 1986; Gregory and Criss, 1986; Gregory and Taylor, 1986; Criss et al., 1987). In this context, closed systems are defined as those in which minerals and fluid are present in constant relative proportions so that the integrated water/rock ratio is constant, while in open systems externally derived fluid is allowed to enter and leave the system so that the integrated water/rock ratio increases with time. Differences in exchange mechanisms may be resolved into predictable patterns if isotopic compositions of coexisting minerals are plotted in δ-δ space, and many suites of rocks show disequilibrium arrays indicative of open system exchange (e.g., Gregory and Taylor, 1986; Gregory et al., 1986). In some cases it is possible

to place constraints on the water/rock ratio, temperature of exchange and isotopic compositions of fluid and rock.

The $\delta^{18}O_{qtz}$- $\delta^{18}O_{bi}$ data of Addy and Ypma (1977) are re-plotted in Figure 7. In this diagram schematic exchange trajectories are shown for fluid-absent, closed system and buffered open system exchange at 400°C, the latter of which is characterized by a large flux of isotopically homogeneous fluid. Although the general shapes of these trajectories are correct (see Gregory and Criss, 1986 and Criss et al., 1987), no attempt has been made to calculate actual values as these are dependent on several parameters, some of which are not available.

From Figure 7 we conclude that it is impossible to resolve which post-metamorphic exchange mechanisms operated on the rocks. Data lying between the 530° and 400°C isotherms are consistent with partial exchange at 400°C under fluid absent conditions or closed system conditions with an extremely low mole fraction of water. This requires that several bulk isotopic compositions or modal mineralogies be involved within the country rocks and ore zones. Alternatively, data points lying above the 530°C isotherm, as well as all other data, are consistent with various closed system and open system models (Fig. 7). If the data pattern was produced by closed system exchange, then the mole fraction of water must have been fairly low. If general open system conditions prevailed, then the fluid flux must have been low. Finally, if buffered open system conditions caused isotopic re-distribution, then the $\delta^{18}O$ value of the fluid could not have been very different from the fluid in equilibrium with the rocks at peak metamorphism.

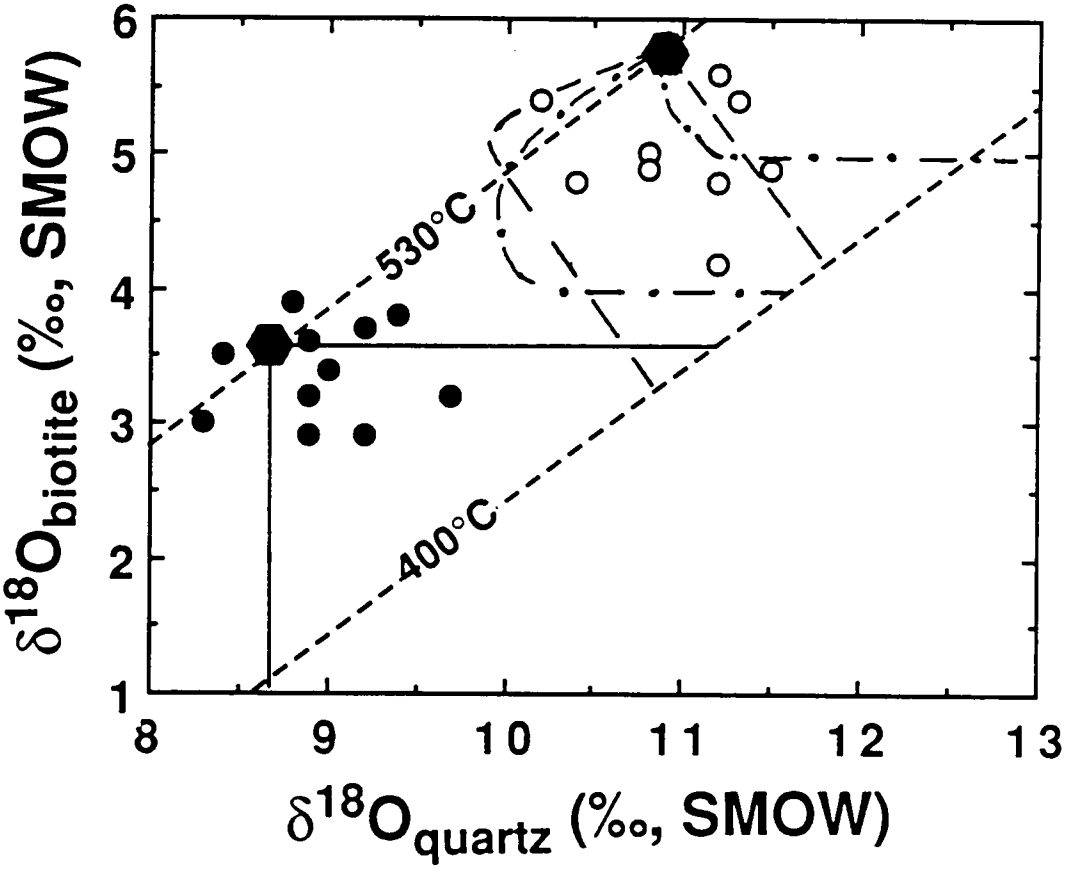

Figure 7. δ_{bi} vs δ_{qtz} diagram showing schematic fluid-absent (solid lines), closed system (dashed lines) and buffered open system (dot-dashed lines) exchange trajectories (Gregory and Criss, 1986; Criss et al., 1987) emanating from hypothetical initial isotopic compositions (hexagons). A value of $\Delta_{qtz\text{-}bi}$ of 5.2 per mil corresponds to equilibrium at 530°C, while 7.6 per mil corresponds to equilibrium at 400°C (Javoy, 1977). Data from Addy and Ypma (1977). Data symbols are the same as in Figure 6A.

There is a slight indication that oxygen isotopes in the ore zone re-equilibrated at constant $\delta^{18}O_{bi}$ while country rock oxygen re-equilibrated at relatively constant $\delta^{18}O_{qtz}$. This could be interpreted as evidence for post-metamorphic exchange of all lithologies with the same fluid, implying open system conditions. The final isotopic composition of the fluid would have been around 7 per mil if exchange occurred at 400°C (Fig. 7).

Coupled O-C Isotope Trends in Calcite

Oxygen and carbon isotopic ratios for calcite measured during this study and by Addy and Ypma (1977) range from 7.1-10.2 per mil in $\delta^{18}O$ and -12.2 to -20.2 per mil in $\delta^{13}C$ (Table 1; Fig. 8). The average $\delta^{13}C$ for calcite in the ore zones is 2 per mil higher than calcite in the country rocks, although data for the latter are limited (Fig 8B). There is a tendency for calcite from the Calloway orebody to be enriched in ^{18}O by an average of 1.5 per mil relative to calcite from the Cherokee orebody, but no trend is seen in $\delta^{13}C$ (Fig 8A). No pattern was recognized for oxygen or carbon as a function of calcite type (gray, white or green) during this study (Table 1). Samples containing two apparent generations or types of calcite, indicated by tie-lines in Figure 8, show negligible differences in $\delta^{18}O$ and only small differences in $\delta^{13}C$ (1-2 ‰; Table 1). This suggests that carbon and oxygen isotopes were homogenized on a local scale. Regional variations in $\delta^{18}O$ of calcite is suggested by the 1.5 per mil difference in $\delta^{18}O$ between the Calloway and Cherokee orebodies (Fig. 8A) and the large overall range in $\delta^{13}C$.

The low $\delta^{13}C$ values obtained for calcite suggest interaction with low $\delta^{13}C$ fluids derived from organic material (Fig. 9). Low $\delta^{13}C$ rocks may be

Figure 8. $\delta^{13}C$ vs $\delta^{18}O$ diagram for calcites. A) data sorted according to orebody and calcite type. Filled circles = Cherokee, open circles = Calloway, filled square = Mary-Polk and open square = Boyd. Horizontally-ruled hexagons = gray calcite in massive sulfide, vertically-ruled hexagons = white calcite in massive sulfide, vertically-ruled triangle = calcite with amphibole, horizontally-ruled triangle = calcite with amphibole and pyroxene and open triangle = calcite with pyroxene. Tie-lines connect coexisting generations of calcite. B) Data sorted according to location. Open circles = country rocks, filled circles = ore zones. Data from this study and Addy and Ypma (1977).

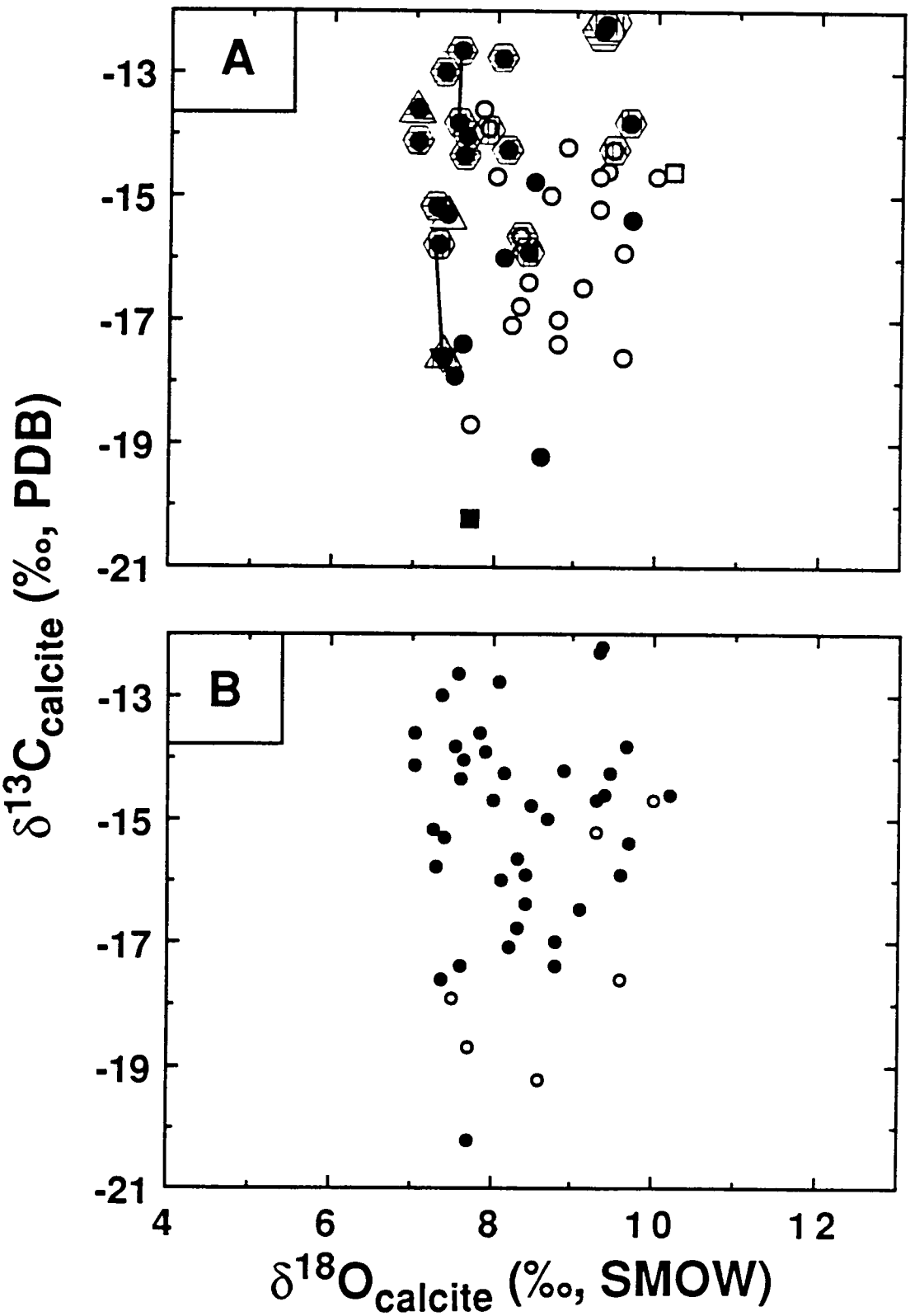
A
B
-13
-15
-17
-19
-21
4
6
8
10
12
δ13Ccalcite (‰, PDB)
δ18Ocalcite (‰, SMOW)

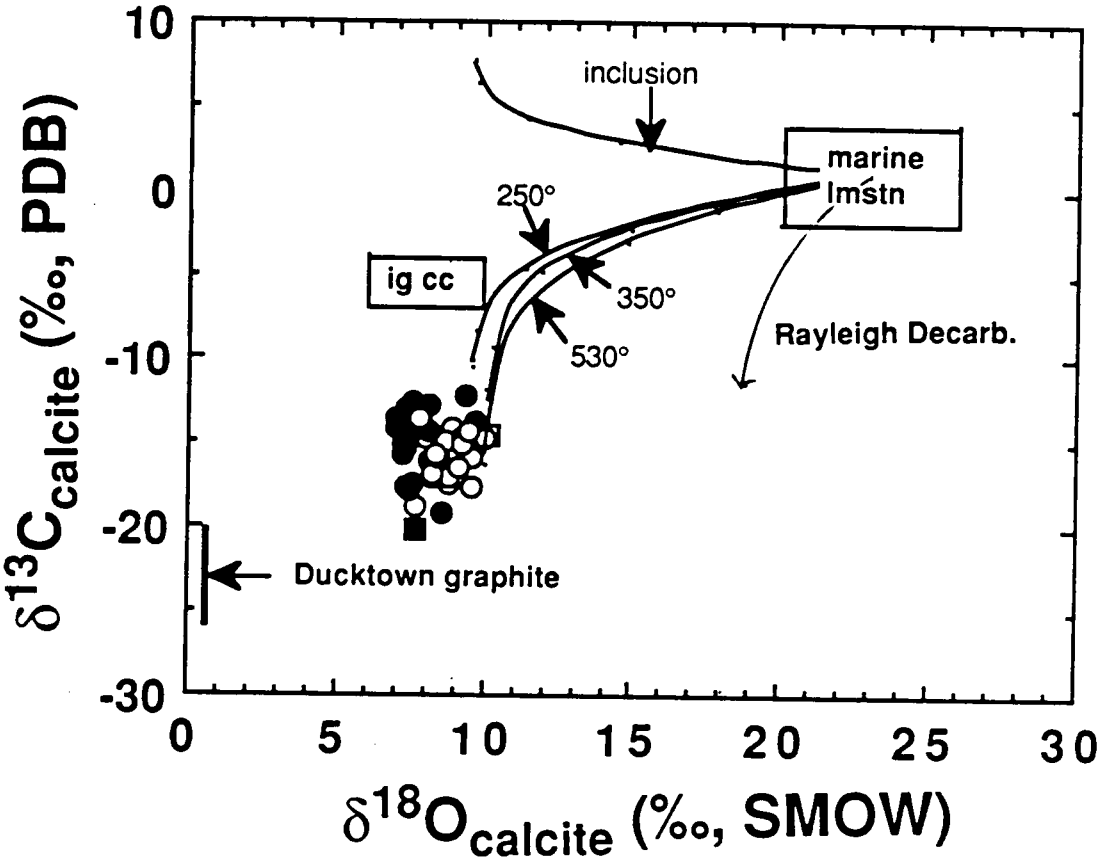

Figure 9. $\delta^{13}C$ vs $\delta^{18}O$ diagram showing carbon and oxygen isotopic values of Ducktown calcites from this study and Addy and Ypma (1977) in relation to marine limestone, igneous calcite and graphite from Ducktown. The path of progressive Rayleigh decarbonation at 530°C is shown for marine limestone with initial $\delta^{13}C$ of +1per mil and $\delta^{18}O$ of +23 per mil. Also shown are exchange trajectories representing interaction of marine limestone with a CO_2-H_2O fluid at 350° to 530°C, a CH_4-H_2O fluid at 250°C, and CH_4-H_2O fluid with the $\delta^{13}C$ signature of secondary CH_4-N_2-H_2O-NaCl fluid inclusions at 250°C. See text for discussion.

produced by simple Rayleigh decarbonation, in which infinitely small aliquots of fluid are evolved, exchange, and then leave the system (Fig. 9). However, large depletions require that decarbonation nears completion, in other words, that most carbonate is converted to CO_2 and removed from the rock. Only limited ^{18}O-depletion can be achieved because, even in the event of complete decarbonation, most oxygen remains in the rock in the form of calc-silicate minerals. Our limited data indicate that there is no trend of $\delta^{13}C$ or $\delta^{18}O$ as a function of the extent of decarbonation. In particular, samples containing no calc-silicate minerals, amphibole bearing samples and pyroxene bearing samples, representing progressive decarbonation, show no pattern (Fig. 8A). This suggests that the low $\delta^{13}C$ values, and the $\delta^{18}O$ values as well, are not simply the result of decarbonation, but originate either from pre- syn- or post-metamorphic fluid-mineral exchange. No primary graphite is present in the ore zones. Hence, exchange of calcite in ore zones with organic material or low $\delta^{13}C$ fluids must have involved externally derived fluids, implying that the ore zone-country rock system was open to carbon isotope exchange prior-to, during or after peak metamorphism.

An average bulk $\delta^{13}C$ value of -11.5 per mil was calculated from measured $\delta^{13}C$ of methane in primary fluid inclusions (Table 2) and by reintegrating the carbon from calcite daughters contained within these inclusions. Primary fluid inclusions originally contained H_2O and CO_2 as the dominant fluid species, but underwent compositional changes due to diffusive addition of hydrogen (Hall et al., 1989b). The $\delta^{13}C$ values of CO_2 in equilibrium with two samples of calcite coexisting with pyroxene (-13.6 and -15.3 ‰; Table 1) are -10.8 and -12.5 per mil at 530°C (Bottinga, 1969).

These values compare favorably with the bulk $\delta^{13}C$ value of primary fluid inclusions (-11.5 ‰), and suggests that low $\delta^{13}C$ values were attained by carbonate during or before peak metamorphism, prior to growth of pyroxene.

The fact that an indistinct trend is produced by $\delta^{18}O$ values of coexisting calcite and quartz (Fig. 6) suggests that post-metamorphic exchange with externally derived fluids may have affected peak metamorphic $\delta^{18}O$ and perhaps $\delta^{13}C$ values. Coupled O-C isotope exchange trajectories were calculated using Taylor's (1979) equation for open system exchange

$$\text{water/rock} = \ln[(\delta^{i}_{water} + \Delta_{rock\text{-}water} - \delta^{i}_{rock})/(\delta^{i}_{water} - \delta^{f}_{rock} + \Delta_{rock\text{-}water})] \quad (1),$$

where *i* and *f* refer to initial and final values and $\Delta_{rock\text{-}water}$ is the temperature-dependent fractionation between rock and water. The trajectories (Fig. 9) show the effects of progressive interaction of an infiltrating fluid with marine limestone ($\delta^{18}O$ = +23 ‰; $\delta^{13}C$ = +1 ‰). The original (pre-metamorphic) isotopic composition of the carbonate is unknown. However, the values representing maximum exchange at a given temperature (i.e. at large w/r) are dependent only on the fractionation between water and rock, and the fluid composition, and are independent of the initial rock composition (eqn. 1). The fluid inclusion record indicates that CH_4 was the dominant carbonic fluid species below 250°C, whereas CO_2 was the dominant carbonic fluid species above 250°C. Hence the model fluid was chosen to be CH_4-H_2O with XCH_4 = 0.1 at 250°C and CO_2-H_2O with XCO_2 = 0.1 at 350°, 450° and 530°C. The carbon and/or oxygen isotopic ratios of CH_4 and CO_2 were assumed to be in equilibrium with local graphite (avg. -23 ‰; Table 1). The $\delta^{18}O$ value of H_2O

was assumed to be in equilibrium with country rock quartz (avg. 11 ‰; Fig. 6A; see also Addy and Ypma, 1977) at the temperature of interest.

The trajectories indicate that the magnitude and direction of exchange is consistent with an infiltration model, and model exchange trajectories for a CO_2-H_2O fluid at 350-530°C predict the $\delta^{18}O$ and $\delta^{13}C$ values of many of the carbonates. Exchange with CH_4-H_2O fluids at low temperatures does not result in sufficient ^{13}C-depletion to account for observed $\delta^{13}C$ values. Furthermore, exchange with CH_4-N_2-H_2O-NaCl fluid inclusions (Bulk $\delta^{13}C$ = -21.5 to -25.9 ‰; Table 2) at 250°C would result in ^{13}C-enrichment (Fig. 9). The lowest $\delta^{13}C$ values cannot have been derived from interaction with CO_2-H_2O fluids at a peak metamorphic temperature of 530°C unless CO_2 was in equilibrium with graphite with lower $\delta^{13}C$ than the present values of Ducktown graphite, or the fractionation between graphite and CO_2 was smaller than the value we used (14 ‰; Bottinga, 1969). The presence of graphite with lower $\delta^{13}C$ values seems unlikely because if CO_2 is produced by oxidation of carbon during progressive metamorphism, the residual carbon will become more depleted in ^{13}C (Bottinga, 1969). For instance, a sample of graphite from biotite-grade rocks to the west of the Ducktown orebodies has $\delta^{13}C$ = -20.1 per mil, whereas two samples of peak metamorphic graphite near the orebodies have $\delta^{13}C$ = -23.1 and -24.2 per mil (Table 1). A sample of secondary graphite replacing sulfides in the Mary-Polk orebody has $\delta^{13}C$ = -25.6 per mil. This graphite may have been precipitated from late-stage CH_4-bearing solutions recorded in secondary fluid inclusions. Thus, peak metamorphic graphite may have had slightly higher $\delta^{13}C$, which would produce less ^{13}C-depletion in carbonates if CO_2

was in equilibrium with local graphite. Fluid inclusions and petrographic considerations (Hall et al. 1989a, b) suggests that early (e.g. CO_2 bearing) fluids were locally-derived, hence CO_2 is expected to be in equilibrium with local graphite. Fluids responsible for precipitation of secondary graphite may have affected $\delta^{13}C$ and $\delta^{18}O$ values of calcite and might explain the additional observed ^{13}C-depletion.

In summary, the data and computed trends in Figure 9 suggest that the calcites in the ore zones and country rocks probably formed by either precipitation from peak metamorphic fluids which had previously equilibrated with country rock graphite, or by exchange of carbonate of more normal marine-limestone isotopic composition with such fluids during peak metamorphism. Further minor depletion in ^{13}C and ^{18}O and homogenization of $\delta^{18}O$ between ore zone and country rock carbonates probably occurred during minor retrograde interaction with country rock fluids. The fact that $\delta^{18}O$ in ore zone silicates did not respond to this late stage, minor retrograde exchange is probably due to very low water/rock ratios and/or the much more sluggish exchange kinetics of silicates relative to calcite at temperatures below 500°C (Cole and Ohmoto, 1986).

Hydrogen Isotopes

Addy and Ypma (1977) found no difference between δD values of biotite and muscovite from the ore zones and unaltered country rocks, although their data set is small. Their reported δD values of biotite, muscovite and chlorite range from -68 to -77 per mil, -49 to -54 per mil and -62 to -69 per mil, respectively. The hydrogen isotopic compositions of the peak metamorphic

(530°C) fluid implied by δD of biotite, muscovite and chlorite, using the fractionation factors of Suzuoki and Epstein (1976) and Graham et al. (1987) are -33 to -42 per mil SMOW. Calculated δD values for H_2O are nearly identical for all three minerals, implying that these minerals equilibrated hydrogen isotopes at peak metamorphic temperatures. Thus, the present δD values have not been significantly affected by infiltration of low temperature fluids.

Conversely, the fluid inclusion record implies that fluid infiltrated the orebodies and surrounding rocks after metamorphism. In addition, there is evidence for large-scale mobility of hydrogen during early uplift (Hall et al., 1989b), which would tend to homogenize δD in minerals from the ore zones and country rocks. Graham (1981) has shown that closure temperatures for hydrogen isotopic exchange among most hydrous minerals are below 300°C if an aqueous phase is present. Despite these observations, it appears that peak metamophic δD values were retained during infiltration of post-peak metamorphic fluids. This probably indicates that, in spite of the abundance of secondary fluid inclusions and the variety of fluids trapped during uplift, post-metamorphic integrated fluid/rock ratios were small.

Isotopic Disequilibrium

Our new data and temperature calculations and analysis of Δ-Δ relationships support the conclusion of Addy and Ypma (1977) regarding the degree of isotopic disequilibrium. Minor apparent disequilibrium is noted in all minerals and larger departures from equilibrium are seen in calcite - to the point of isotopic reversals in a few quartz-calcite pairs. Apparent

disequilibrium is most pronounced in mineral pairs whose relative fractionations are small (e.g. quartz-calcite and mica-mica pairs). However, in general, large departures from isotopic equilibrium are absent. Furthermore, it is not clear how much apparent isotopic disequilibrium (e.g. deviations from colinearity on Δ-Δ plots) can be attributed to compositional variations within each mineral phase or how much temperature variability is introduced by departure of mineral compositions at Ducktown from those of the minerals used in establishing fractionation factors. Compositional effects should be minimal in pairs involving quartz, calcite and magnetite as these phases are compositionally uniform at Ducktown. However, other phases show significant compositional variability (Nesbitt, 1979). Evidence for small-scale retrograde exchange is consistent with data from fluid inclusions which indicate that several compositionally distinct fluids invaded the area during uplift (Hall et al., 1989a).

Isotopic Compositions of Fluid Inclusions

C-O-H isotope analyses of primary fluid inclusions in peak metamorphic clinopyroxene are presented in Table 2. The bulk $\delta^{18}O$ values do not reflect peak metamorphic values because the fluids have exchanged with the host pyroxene and quartz daughters during cooling. Calculation of the bulk $\delta^{13}C$ requires reintegration of carbon from calcite daughters. This was accomplished by estimating the volume percent of calcite and CH_4 in primary fluid inclusions (average 5 vol% and 15 vol%, respectively) and assuming a final isotopic equilibration temperature of 100°C for calcite and CH_4. As discussed above, the reconstructed $\delta^{13}C$ values are in equilibrium with local

carbonate at peak metamorphic temperatures. There are no hydrous phases within these inclusions, hence the δD values should be peak metamorphic values.

Bulk δD values of -96 to -104 per mil were obtained from these inclusions. These values are significantly lower than estimated δD for water in equilibrium with biotite, muscovite and chlorite at Ducktown (-33 to -42 ‰). As the fluid present in primary fluid inclusions was produced by local devolatilization reactions it is unlikely that it would not be in isotopic equilibrium with local hydrous phases during metamorphism. Hall et al. (1989b) proposed that the CH_4 in primary fluid inclusions was formed by reduction of CO_2 to $CH_4 + H_2O$ during diffusive addition of hydrogen to these inclusions. This diffusion event occurred during early uplift ($T \geq 450°C$) in response to an fH_2 gradient between the inclusions and fluids present in the host rock (e.g. along grain boundaries). The isotopic data presented above is consistent with this model. Molecular hydrogen diffusing into these inclusions would have very low δD values with respect to the δD of aqueous grain boundary fluids. Fractionation of hydrogen isotopes between hydrogen and water in the parent aqueous solution may have been as high as that for H_2 gas in equilibrium with water vapor ($\Delta H_2O\text{-}H_2$ = 360 ‰ at 450°C; Bottinga, 1969). During diffusion, additional fractionation would result from the faster rate of diffusion of H relative to D; thus, the net fractionation between hydrogen reaching the inclusion and H_2O in the parent solution may have been significantly greater than $\Delta H_2O\text{-}H_2$. Using a minimum fractionation of 360 per mil, approximately 16-18 percent of the hydrogen present in these inclusions would have to be added during diffusion. This value compares

favorably with an estimate of 13 percent based on constraints imposed by the inclusion compositions and mineral equilibria at Ducktown (Hall et al., 1989b). The difference between these two numbers may reflect the additional fractionation between H and D caused by diffusion through pyroxene.

The average bulk δD value obtained for secondary CH_4-N_2-H_2O-NaCl inclusions, which were trapped at 215° ± 20°C and 1.0-2.3 kb (Hall et al., 1989a) is -70 per mil (Table 2). At 250°C this fluid is in equilibrium with biotite, muscovite and chlorite with δD values of -150, -127 and -105 per mil, respectively. Hence, these inclusion fluids are not in equilibrium with local hydrous phases. Likewise, at 250°C CO_2 in these inclusions is in equilibrium with calcite with $\delta^{13}C$ of -10 to -15 per mil and CH_4 is in equilibrium with calcite with $\delta^{13}C$ of +5 to -1 per mil (Bottinga, 1969). Hence, while CO_2 may be in carbon isotopic equilibrium with local carbonate, CH_4 is strongly out of equilibrium with calcite in country rocks and ore zones, and CO_2 and CH_4 are not in equilibrium with each other despite having been trapped together for at least 250 my.

Hall et al. (1989a) postulated that CH_4-N_2-H_2O-NaCl fluids were externally derived and attained their CH_4 and N_2 from maturation of organic matter. The $\delta^{13}C$ values of CH_4 produced by thermal cracking are typically between -35 and -55 per mil (Schoell, 1984), which is significantly lower than $\delta^{13}C$ values of analyzed fluid inclusions (Table 2). However, this does not preclude subsequent exchange of thermogenic CH_4 with carbonate, or reduction of CO_2 produced by thermal cracking (-10 to -30 ‰; Ohmoto and Rye, 1979) to CH_4 during transport through low fO_2 lithologies. Isotopic

disequilibrium between these fluids and local minerals is consistent with external derivation of the fluids.

Origin of the Low ^{18}O Zones Around the Orebodies

Addy and Ypma (1977) discovered that minerals from samples near orebodies are depleted in ^{18}O by 2-3 per mil relative to the same minerals in the country rock. As mentioned earlier, they interpreted this phenomenon to have been the result of syn-metamorphic channelling of immiscible metamorphic fluids through the ore zones. Their interpretation was influenced by the common localization of shear zones within orebodies and the prevalence near the ore zones of the minerals chlorite and muscovite, typically formed by retrograde hydration reactions.

More recent studies (Beaty and Taylor, 1982; Woodruff et al., 1984; Munha et al., 1986; Aggarwal and Longstaffe, 1987) have noted similar zones (both enriched and depleted in ^{18}O) and chlorite-muscovite rich lithologies in other metamorphosed massive sulfide bodies. In these studies, the isotopic halos were interpreted to be relict features produced by sea-floor hydrothermal alteration by fluids responsible for ore deposition and subsequently preserved through the metamorphic event(s).

Several observations argue against development of the low $\delta^{18}O$ zones near Ducktown orebodies during peak metamorphism. Firstly, minerals were shown to have equilibrated isotopically (Fig. 6) and chemically (Nesbitt, 1982) at peak metamorphic pressures and temperatures. Mineralogical variations within the orebodies indicate small-scale variations in fO_2, fS_2 and XCO_2 during peak metamorphism and imply local control of fluid composition

(Nesbitt and Kelly, 1980; Hall et al., 1989b). It is unlikely that an isotopically homogeneous fluid (indicated by similar $\delta^{18}O$ of minerals from all alteration zones) could infiltrate the ore zones at relatively high integrated water/rock ratios (to allow equilibration of all minerals with the fluid) without destroying the mineralogic evidence for previous fluid heterogeneity. The preservation in both country rock and ore zones of small $\delta^{18}O$ differences between adjacent lithologies, and petrologic evidence for bed to bed variations in fluid composition argue against large-scale oxygen isotopic homogenization during metamorphism.

Secondly, immiscibility was cited by Addy and Ypma (1977) to account for ^{18}O-depletion and concentration of chlorite and muscovite, which they felt was retrograde, near ore zones. As was shown by Nesbitt (1979) and isotopic temperatures presented in this study, chlorite and muscovite surrounding the orebodies equilibrated mineralogically and isotopically at peak metamorphic conditions and therefore were not formed by retrograde hydration reactions. It is likely that these minerals, or their precursors (e.g., sericite or illite) were always present near the orebodies and are the result of sea-floor hydrothermal alteration of graywacke. Furthermore, primary fluid inclusions in pyroxene from the Cherokee, Calloway, Boyd and Mary-Polk orebodies are compositionally uniform. Although these inclusions have experienced post- peak metamorphic volumetric and compositional changes (Hall et al., 1989a,b), there is no evidence that immiscible fluids were ever present during peak metamorphism. In particular, the nearly constant salinity observed in all primary fluid inclusions (3 ± 2 wt % NaCl equivalent) argues against immiscibility as widely varying salinities should be seen (Sterner et

al., in prep.). In addition, the daughter minerals pyrrhotite, calcite and quartz, present in most primary fluid inclusions, suggest that peak metamorphic fluids were near saturation with the local mineral assemblage (pyroxene, calcite, quartz, pyrrhotite, ± amphibole, ± pyrite, ± magnetite), consistent with local rather than exotic derivation of the fluids.

Finally, subtle variations in $\delta^{34}S$ of pyrrhotite, pyrite and chalcopyrite were recorded by Mauger (1972) and were interpreted to represent, in part, original depositional variability, which was retained through metamorphism. It is unlikely that local $\delta^{34}S$ variations could survive a pervasive fluid infiltration event.

The sea-floor hydrothermal system proposed to be responsible for ^{18}O depletion of wall rocks should have had a measurable effect on δD values as well. For instance, in both the Kuroko and Cyprus VMS deposits altered rocks have average δD values of -40 to -45 per mil while host rocks have average δD values of -60 per mil (Heaton and Sheppard, 1977; Hattori and Sakai, 1979; Ohmoto and Rye, 1974). The enrichment of deuterium in alteration zones reflects the higher temperatures attending ore deposition.

The uniformity of the limited δD data from minerals from Ducktown ore zones and country rocks suggests that any original spatial variations in the hydrogen isotopic compositions of hydrous phases were homogenized during or prior to metamorphism. As in the case of carbonates in the ore zones and country rocks, the re-equilibration of the hydrogen in hydrous minerals at or slightly below peak metamorphic conditions could have occurred via fluid infiltration with preservation of $\delta^{18}O$ disequilibrium between ore and host rocks. This is because a) the atom% of hydrogen in rocks, even

those composed of pure muscovite or chlorite, is very low compared to an equivalent amount of water on an equal oxygen basis, and b) rates of D/H exchange between hydrous silicates and water are orders of magnitude greater than oxygen exchange. Thus, the δD homogenization could have occurred at or near peak metamorphic conditions, and at very low fluid/rock ratios, while still maintaining a significant disequilibrium in $\delta^{18}O$ between the ore zone and host rock silicates.

Water/rock Ratios During Metamorphism

If the ^{18}O-depletion near ore zones did occur during peak metamorphism, an estimate of the water/rock ratio necessary to produce the observed $\delta^{18}O$ values can be calculated from equation (1). If all minerals equilibrated with the fluid, and if the isotopic composition of the system was buffered by the fluid, we can replace δ_{rock} and $\Delta_{rock\text{-}water}$ with $\delta_{mineral}$ and $\Delta_{mineral\text{-}water}$, respectively. Then, using average $\delta^{18}O$ values for quartz in the country rock and ore zones for δ^{i}_{qtz} and δ^{f}_{qtz}, respectively, and a $\Delta_{qtz\text{-}H2O}$ of 2 per mil at 530°C (Matsuhisa et al., 1979) it is possible to calculate water/rock ratios as a function of the initial $\delta^{18}O$ value of the fluid. The results of these calculations indicate that the observed depletion in the ore zones can be produced at low water/rock ratios (Fig. 10). However, the infiltrating fluid could not have been in equilibrium with the country rocks and would have had to have been depleted in ^{18}O by about 2 per mil. Considering the relative molar volumes of quartz and water at 530°C and 6 kb, a water/rock ratio of 1.0 implies that each cm^3 of rock interacted with about 2 cm^3 of fluid. As the instantaneous water/rock ratio (related to rock permeability) was probably closer to 0.01,

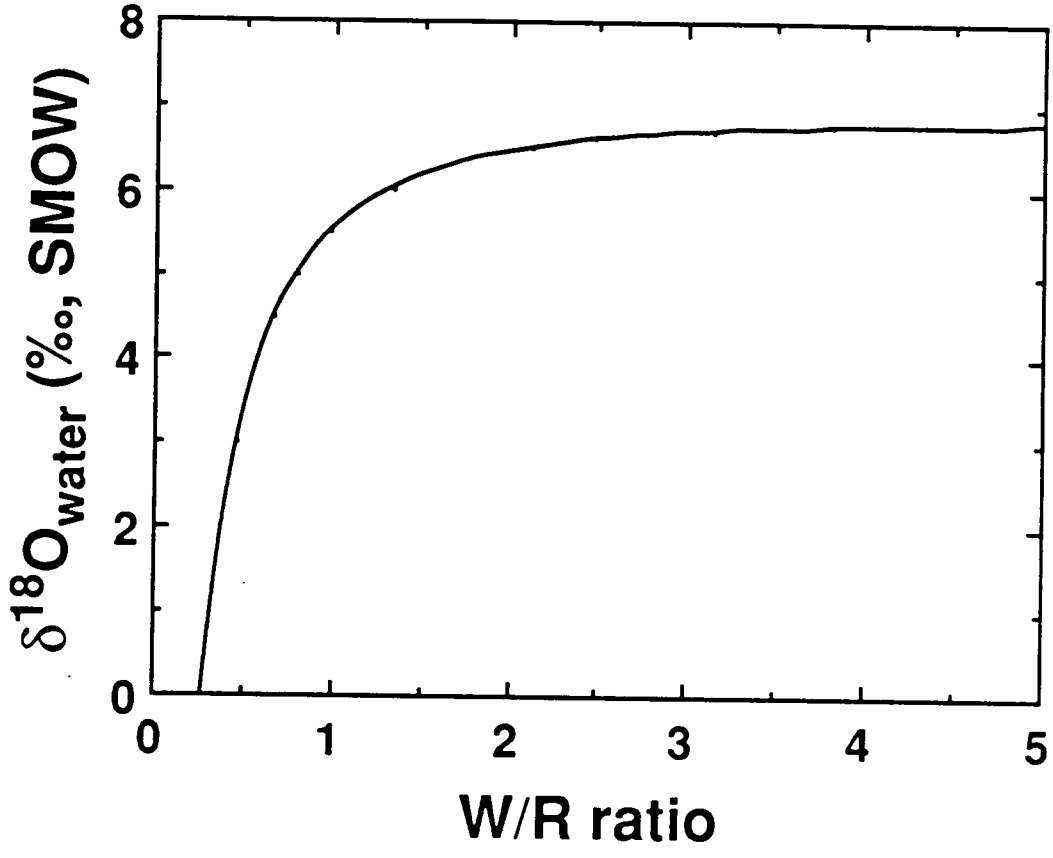

Figure 10. Diagram showing the water/rock ratio, on an atomic % oxygen basis, as a function of the $\delta^{18}O$ of the infiltrating fluid. Values were calculated assuming Taylor's (1979) open system model, and by assuming that $\Delta_{qtz\text{-}water}$ adequately models $\Delta_{rock\text{-}fluid}$.

each cm^3 of altered rock would have had to have passed on the order of a hundred instantaneous volumes of fluid. Unless the isotopically distinct fluid was introduced instantaneously, however, we are left with the problem of transporting ^{18}O-depleted fluid long distances through country rocks to the ore zones without allowing it to equilibrate along the way. In any case, the incoming fluid should have left an even greater signature on distal rocks; however, such channelways have not been reported, and the low $\delta^{18}O$ zones are restricted to the rocks immediately surrounding the orebodies.

It appears, then, that depletion of ^{18}O in ore zones during peak metamorphism, while theoretically possible, is mechanistically unlikely and is not supported by most petrologic data. Depletion after peak metamorphism is likewise improbable. Both high and low $\delta^{18}O$ lithologies were shown to have locally equilibrated at around 530°C (Fig. 6A) and although some post-metamorphic re-equilibration has occurred, $\delta^{18}O$ relations in silicates are closely tied to peak metamorphic mineralogic variations. No low $\delta^{18}O$ zones have been found in country rocks. Although secondary fluid inclusions suggest that fluids may have infiltrated the ore zones late in the uplift history, the country rocks saw similar fluids. These fluids do not appear to have affected $\delta^{18}O$ values in silicates appreciably because Δ values for quartz-mineral pairs from ore zones do not deviate significantly further from peak Δ values than those for country rocks (Fig. 6A).

Conversely, depletion prior to metamorphism is consistent with most petrologic observations. The local control of fluid composition during metamorphism suggests that integrated water/rock ratios during metamorphism were low and that at that time the rocks may have behaved

essentially as a closed system with respect to oxygen except on a small scale (centimeters to meters). The low $\delta^{18}O$ zones at Ducktown are consistent with reports from other massive sulfide bodies, some weakly metamorphosed, and with the genetic model evolving from these studies that suggests that the isotopic halos formed during sea-floor hydrothermal activity. The depletions result from a combination of high temperatures, low $\delta^{18}O$ fluids (largely seawater) and formation of large quantities of the low ^{18}O mineral chlorite in the alteration halos or stockworks of VMS deposits. Calculated whole-rock $\delta^{18}O$ values of 4-7 per mil, obtained for chlorite-rich and muscovite-rich lithologies at Ducktown compare favorably with $\delta^{18}O$ values of 4.5-8 per mil obtained for chlorite-sericite zone rocks in the Kuroko deposits (Green et al., 1983).

$\delta^{18}O$ Value of the Ore Fluid

Using the average $\delta^{18}O$ values of mineral separates in the ore zone coupled with modal mineralogies, we have calculated whole-rock $\delta^{18}O$ values for chlorite-rich and muscovite-rich schists, and have compared these values to those for the country rock metagraywacke in order to estimate the $\delta^{18}O$ of the ore fluid. This calculation assumes that the whole-rock $\delta^{18}O$ values and modal mineralogies of chlorite-rich and muscovite-rich schists did not change significantly during metamorphism. This assumption may not be strictly valid. However, fluid inclusion, petrographic and stable isotope data presented above (e.g., local derivation of peak metamorphic fluids, local control of fluid composition, and preservation of premetamorphic $\delta^{18}O$ signatures) suggest that integrated water/rock ratios during and after

metamorphism were small, and that the ore and host rocks probably behaved as closed systems with respect to oxygen on scales larger than cm to m. Therefore, we believe that the whole-rock $\delta^{18}O$ values did not change more than 1 per mil. Small variations in the modal mineralogies of these rocks do not appreciably affect this calculation.

The computation follows that of Beaty and Taylor (1982). An initial whole-rock value for country rock metagraywacke is estimated to be 9 per mil (Addy and Ypma, 1977). The compositions of the most chlorite-rich and muscovite-rich lithologies can be approximated to within 10 % by a binary mixture of muscovite or chlorite and quartz, with 25 volume % quartz. Average $\delta^{18}O$ values for chlorite, muscovite and quartz in these rocks are 2.5 , 5.5 and 8.9 per mil, respectively. Thus, the calculated whole-rock $\delta^{18}O$ is 4.1 per mil for chlorite schist and 6.3 per mil for muscovite schist. We have chosen to use the empirical relationship for $\Delta_{qtz\text{-}ct}$ of Wenner and Taylor (1971) because it was specifically developed for use at lower temperatures. We have recalculated this relationship using the more recent data of Matsuhisa et al. (1979) for $\Delta_{qtz\text{-}H2O}$, to get $\Delta_{qtz\text{-}ct} = 1.62(10^6/T^2) - 0.98$ for the temperature range 250°-500°C. The likely temperature of alteration and ore deposition is 250°-350°C based on temperatures of active sea-floor hydrothermal vents. Thus, the original $\Delta_{qtz\text{-}ct}$ was 4.9-3.2 per mil at 250-350°C. Substituting this information into the equation used to calculate the whole-rock $\delta^{18}O$ and utilizing a $\Delta_{qtz\text{-}H2O}$ of 8.9-5.3 per mil at 250-350°C we calculate a $\delta^{18}O_{H_2O}$ of -1.1 to +1.2 per mil for the temperature range 250°-300°C. Uncertainties in the whole-rock isotopic composition of the chlorite schist, due to ambiguities related to the effects of metamorphism on

whole-rock values or to variations in modal mineralogy and bulk composition, can be related to uncertainties in $\delta^{18}O_{H_2O}$. For instance, a rock containing 50 % chlorite and 50 % quartz has a calculated whole-rock value of 5.7 per mil. The calculated $\delta^{18}O_{H_2O}$ values are -0.7 to +2.0 per mil for alteration temperatures of 250°-350°C. A change in whole-rock values of ±1 per mil, due to the effects of devolatilization during metamorphism, causes a direct ±1 per mil uncertainty in the calculated $\delta^{18}O_{H_2O}$ values. Combining the above results and using 300°C as an average estimated temperature of ore deposition, the likely range in $\delta^{18}O_{H_2O}$ is -1 to +2 per mil.

Fluid with this range of $\delta^{18}O$ overlaps the fields of present day seawater (-1.0 to +0.5 ‰; Epstein and Mayeda, 1953), and formation waters from sedimentary basins consisting of marine rocks (-10 ‰ to +10 ‰; Sheppard, 1984). The latter fluids generally consist of seawater or meteoric water which has been modified by water-rock interaction (Clayton et al., 1966; Hitchon and Friedman, 1969; Flesicher et al., 1977), and there is a general trend of increasing salinity with increasing deviation from meteoric or seawater values. The small metal carrying capacity of relatively unmodified seawater flowing through graywacke at 350°C (e.g., 6 ppm Fe, 0.11 ppm Cu and 1.5 ppm Zn; Bischoff et al., 1981) requires enormous water/rock ratios to deposit significant massive sulfide, assuming transport as chloride complexes. However, saline fluids, perhaps $\delta^{18}O$-shifted to more positive values through water-rock interaction, may carry considerably more metal and calculated water/rock ratios are proportionally smaller and more realistic. Brines responsible for ore deposition in the Red Sea contain in excess of 25 wt. % total dissolved salts, 81 ppm Fe, 0.26 ppm Cu and 5.4 ppm Zn (Brewer and

Spencer, 1969), and have $\delta^{18}O$ values of +1 to +3 per mil (Craig, 1969; Schoell and Faber, 1978). These brines appear to have originated from Red Sea paleowaters (Schoell and Faber, 1978). As described below, the metal contents of these brines are sufficient to have transported and deposited the massive sulfides at Ducktown with reasonable water/rock ratios (10^3) and the $\delta^{18}O$ values of the Red Sea brines are within the calculated range of $\delta^{18}O$ values for fluids responsible for ore deposition at Ducktown.

Water/rock Ratios During Ore Deposition

Using estimated $\delta^{18}O$ values for the ore fluid of -1 to +2 per mil at 300°C, we have calculated the water/rock ratio necessary to cause observed depletions in quartz-muscovite-chlorite lithologies. This calculation is somewhat speculative (and circular) in that fluid/mineral equilibrium (implying appreciable water/rock ratios) was assumed in order to calculate the $\delta^{18}O$ of the ore fluid, which in turn is used in this water/rock calculation. We assumed that these rocks, which have whole-rock $\delta^{18}O$ values of 4-7 per mil, originally had $\delta^{18}O$ values near the average country rock value of 9 per mil. The results of these calculations for both open and closed system conditions are shown in Figure 11. Water/rock ratios assuming open system conditions were calculated from equation (1), whereas, those for closed system conditions were calculated from the relationship

$$\text{water/rock} = (\delta^{f}_{rock} - \delta^{i}_{rock})/(\delta^{i}_{water} - \delta^{f}_{rock} + \Delta_{rock\text{-}water}) \qquad (2)$$

(Taylor, 1979), where the symbols are the same as for equation (1). The

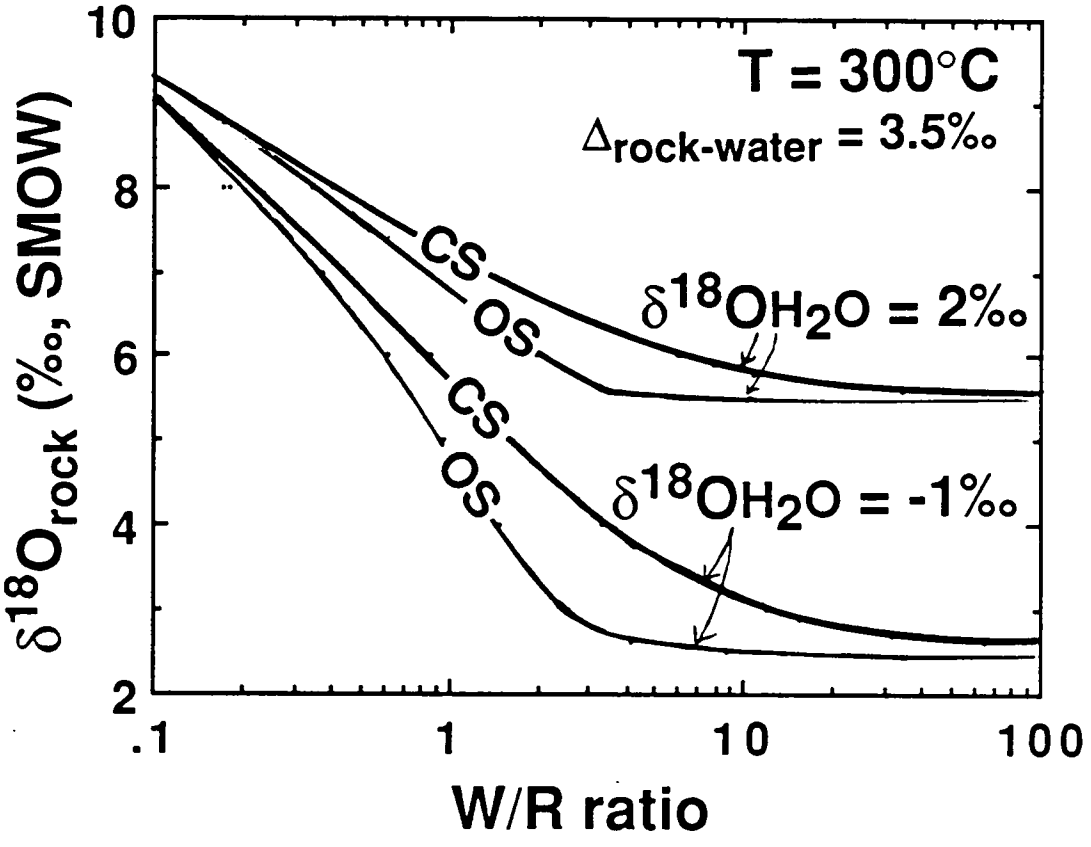

Figure 11. Diagram showing the water/rock ratio, on an atomic % oxygen basis, required to produce the given final whole-rock $\delta^{18}O$ values at 300°C. The initial whole-rock $\delta^{18}O$ value is 9 per mil and the isotopic fractionation between rock and water is assumed to be 3.5 per mil. Calculations were done for both open (OS) and closed system (CS) conditions and for $\delta^{18}O_{H_2O}$ of +2 per mil and -1 per mil.

fractionation between basalt and seawater at 300°C, measured by Cole et al. (1987), was used for $\Delta_{rock\text{-}fluid}$. This value (3.5 ‰) is near the average theoretical value for $\Delta_{rock\text{-}fluid}$ calculated from initial and final modal mineralogies of altered rocks (i.e. graywacke and chlorite schist). Problems associated with the quantification of water/rock ratios have been discussed by Ohmoto (1986), who suggests that open system exchange in natural hydrothermal systems may require much larger water/rock ratios than those calculated using Taylor's open system model (eqn. 1). Thus, the water/rock ratios presented here represent minimum values. Figure 11 indicates that large water/rock ratios may have been required to produce the maximum whole-rock ^{18}O-depletions, depending on the isotopic composition of the fluid. Maximum depletions cannot be attained with $\delta^{18}O$ values greater than approximately +1 per mil at 300°C, but are possible at higher temperatures. At lower temperatures, a given whole-rock ^{18}O-depletion requires a greater water/rock ratio, due to the increase in $\Delta_{rock\text{-}water}$.

An independent method of approximating integrated water/rock ratios is to compare a given mass of altered rock to the mass of fluid necessary to transport and deposit the ore contained in that packet of rock. We have done this, given a 500-750 foot alteration zone (hanging wall + footwall) containing a slab of ore 50-100 feet thick consisting of 35 % Fe, 1.04 % Cu and 0.89 % Zn by weight (Slater, 1982). The ore fluid is assumed to carry 100-1000 ppm Fe, 1-10 ppm Cu and 1-10 ppm Zn, which are typical values measured for hot brines circulating through graywacke (Bischoff et al., 1981). If we assume that the ore fluid is 100 % efficient at precipitating metals in the ore zone and that the only rock that the fluid sees is the packet considered, water/rock

ratios (atomic % oxygen basis) on the order of 10^2-10^3 are calculated. This is obviously an imprecise estimate because the actual volume of rock seen by the ore fluid is unknown, and possibly much greater than indicated by the volume of muscovite and chlorite schist. Likewise a given volume of rock may have seen more fluid than just that responsible for ore deposition. Finally, the efficiency of ore deposition at submarine hydrothermal vents is variable depending on the density of the ore fluid. If the density of the ore solution is less than that of the surrounding seawater, then most of the metal may be carried away from the vent and widely dispersed. In the Red Sea deposits, however, the exiting brines are so dense that they do not mix appreciably with overlying seawater, but remain pooled in topographic depressions where most of the metal is deposited during cooling. In spite of these unknowns, these calculations produce water/rock ratios that are within an order of magnitude of those calculated from $\delta^{18}O$ relationships, and suggest that high water/rock ratios accompanied ore deposition at Ducktown.

Summary and Conclusions

Oxygen isotope analyses of Addy and Ypma (1977) indicate that minerals in ore zones are depleted in ^{18}O by 2-3 per mil, relative to minerals in country rocks, and whole rocks in the ore zones are depleted by 2-5 per mil. Temperature estimates of concordant mineral triplets suggest that minerals in all lithologies equilibrated during peak metamorphism at temperatures of 530° ± 20°C. Integration of isotopic data with information on mineral assemblages, mineral chemistry, and fluid inclusions suggest that the low $\delta^{18}O$ zones surrounding the orebodies must have formed prior to

metamorphism, probably during sea-floor hydrothermal alteration and massive sulfide deposition.

Integrated water/rock ratios may have been as high as 10^2-10^3 during ore deposition and the ore fluid appears to have been largely seawater or slightly modified seawater. Subsequent metamorphism occurred at low integrated water/rock ratios and the rocks behaved as closed systems with respect to oxygen except on small scales. δD values of biotite and muscovite are similar in the ore zones and country rocks and biotite, muscovite and chlorite equilibrated with the same fluid (δD = -33 to -42 ‰) at peak metamorphism. As the sea-floor hydrothermal system responsible for ^{18}O-depletion of ore zones should have had a similar effect on δD values it is concluded that homogenization of hydrogen isotopes in country rocks and ores zones occurred during or prior to peak metamorphism. $\delta^{13}C$ values of primary fluid inclusions are in equilibrium with local carbonate at peak metamorphic temperatures. This carbonate has low $\delta^{13}C$ values indicative of interaction with organic matter, and there is no difference in $\delta^{13}C$ between ore zones and country rocks. These observations suggest that low $\delta^{13}C$ values in carbonate were attained prior to or during peak metamorphism. Influx of post- peak metamorphic fluids, recorded as secondary fluid inclusions, does not appear to have affected $\delta^{18}O$ values of silicates appreciably, but may be responsible for small changes in $\delta^{18}O$ and $\delta^{13}C$ of calcite.

Primary fluid inclusions have bulk δD values of -96 to -104 per mil. These values are approximately 60 to 65 per mil depleted in deuterium compared to the δD of peak metamorphic fluids. Diffusive addition of isotopically light hydrogen to primary fluid inclusions during uplift would result in lower bulk δD

values. This hypthesis is consistent with the conclusion of Hall et al. (1989b) that hydrogen diffusion into peak metamorphic fluid inclusions is required to explain discrepancies between calculated and observed inclusion compositions.

REFERENCES

Addy, S. K., 1973, The problem of ore genesis at Ducktown, Tennessee. Interpretation of stable isotopes ($^{18}O/^{16}O$, $^{13}C/^{12}C$ and D/H), microprobe, and textural data: Ph.D. thesis, Columbia Univ., New York.

Addy, S. K., and Ypma, P. J. M., 1977, Origin of massive sulfide deposits at Ducktown, Tennessee: An oxygen, carbon, and hydrogen isotope study: Econ. Geol., v. 72, p. 1245-1268.

Aggarwal, P. K., and Longstaffe, F. J., 1987, Oxygen-isotope geochemistry of metamorphosed, massive sulfide deposits of the Flin Flon - Snow Lake Belt, Manitoba: Contrib. Mineral. Petrol., v. 96, p. 314-325.

Allison, M. C., 1984, Trace element distribution in pyrite and pyrrhotite from the Ducktown Mining District, Tennessee: Unpub. M.S. Thesis, Univ. Tennessee, Knoxville, 150p.

Beaty, D. W., and Taylor, H. P., Jr., 1982, Some petrologic and oxygen isotopic relationships in the Amulet Mine, Noranda, Quebec, and their bearing on the origin of Archean massive sulfide deposits: Econ. Geol., v. 77, p. 95-108.

Bischoff, J. L., Radtke, A. S., and Rosenbauer, R. J., 1981, Hydrothermal alteration of graywacke by brine and seawater: Roles of alteration and chloride complexing on metal solubilization at 200° and 350°C: Econ. Geol., v. 76, p. 659-676.

Bottinga, Y., 1969, Calculated fractionation factors for carbon and hydrogen isotope exchange in the system calcite-carbon dioxide-graphite-methane-hydrogen- water vapor: Geochim. Cosmochim. Acta, v. 33, p. 49-64.

Bottinga, Y., and Javoy, M., 1973, Comments on oxygen isotopic geothermometry: Earth Planet. Sci. Letters, v. 20, p. 250-265.

Bottinga, Y., and Javoy, M., 1975, Oxygen isotope partitioning among the minerals in igneous and metamorphic rocks: Rev. Geophysics Space Physics, v. 13, p. 401-418.

Brewer, P. G., and Spencer, D. W., 1969, A note on the chemical composition of the Red Sea brines, *in* Degens, E. T., and Ross, D. A., eds., Hot brines and recent heavy metal deposits in the Red Sea: New York, Springer-Verlag, p. 174-179.

Brooker, D. D., Craig, J. R., and Rimstidt, J. D., 1987, Ore metamorphism and pyrite porphyroblast development at the Cherokee Mine, Ducktown, Tennessee: Econ. Geol., v. 82, p. 72-86.

Brown, H. S., 1961, Wall rock alteration at Calloway Mine, Ducktown, Tennessee: Tennessee Copper Company, Unpub. Report.

Butler, J. R., 1972, Age of Paleozoic metamorphism in the Carolinas, Georgia, and Tennessee Southern Appalachians: Am. Jour. Sci., v. 272, p. 319-333.

Carpenter, R. H., 1970, Metamorphic history of the Blue Ridge province of Tennessee and North Carolina: Geol. Soc. Am. Bull., v. 81, p.749-762.

Clayton, R. N., and Mayeda, T. K., 1963, The use of bromine pentafluoride in the extraction of oxygen from oxides and silicates for isotopic analysis: Geochim. et Cosmochim. Acta, v. 27, p. 43-52.

Clayton, R. N., Friedman, I., Graf, D. L., Mayeda, T. K., Meents, W. F., and Shimp, N. F., 1966, The origin of saline formation waters, 1. Isotopic composition: Jour. Geophys. Res., v. 71, p. 3869-3882.

Clayton, R. N., Muffler, L. J. P., and White, D. E., 1968, Oxygen isotope study of calcite and silicates of the River Ranch No. 1 Well, Salton Sea geothermal field, California: Am. Jour. Sci., v. 266, p. 968-979.

Cole, D. R., and Ohmoto, H., 1986, Kinetics of isotopic exchange at elevated temperatures and pressures, *in* Valley, J. W., Taylor, H. P., Jr., and O'Neil, J. R., eds., Stable isotopes in high temperature geological processes: Mineral. Soc. Am., Reviews in Mineralogy, v. 16, p. 41-90.

Cole, D. R., Mottl, M. J., and Ohmoto, H., 1987, Isotopic exchange in mineral-fluid systems. III. Oxygen and hydrogen isotopic investigation of the experimental basalt-seawater system: Geochim. et Cosmochim Acta, v. 51, p. 1523-1538.

Craig, H., 1969, Geochemistry and origin of the Red Sea brines, *in* Degens, E. T., and Ross, R. A., eds., Hot brines and recent heavy metal deposits in the Red Sea: New York, Springer-Verlag, p. 208-242.

Craig, J. R., 1983, Metamorphic features in Appalachian massive sulfides: Mineral. Mag., v. 47, p. 515-525.

Criss, R. E., Gregory, R. T., and Taylor, H. P., Jr., 1987, Kinetic theory of oxygen isotope exchange between minerals and water: Geochim. et Cosmochim. Acta, v. 51, p. 1099-1108.

Dallmeyer, R. D., 1975a, $^{40}Ar/^{39}Ar$ incremental release ages of biotite from the Cherokee orebody, Ducktown, Tennessee: their bearing on the age of sulfide mineralization: Econ. Geol., v. 70, p. 341-345.

Dallmeyer, R. D., 1975b, Incremental $^{40}Ar/^{39}Ar$ ages of biotite and hornblende from retrograded basement gneisses of the Southern Blue Ridge: their bearing on the age of Paleozoic metamorphism: Am. Jour. Sci., v. 275, p. 444-460.

Deines, P., 1977, On the oxygen isotope distribution among mineral triplets in igneous rocks: Geochim. et Cosmochim. Acta, v. 41, p. 1709-1730.

Downs, W. F., Touysinhthiphonexay, Y., Deines, P., 1981, A direct determination of the oxygen isotope fractionation between quartz and magnetite at 600° and 800°C and 5 kbar. Geochim. et Cosmochim. Acta, v. 45, p. 2065-2072.

Emmons, W. H., and Laney, F. B., 1926, Geology and ore deposits of the Ducktown mining district, Tennessee: U. S. G. S. Prof. Paper, no. 139, 114p.

Epstein, S., and Mayeda, T., 1953, Variations of O^{18} content of waters from natural sources: Geochim. et Cosmochim. Acta, v. 4, p. 213-224.

Field, C. W., and Fifarek, R. H., 1985, Light stable-isotope systematics in the epithermal environment, *in* Berger, B. R., and Bethke, P. M., eds., Geology and geochemistry of epithermal systems: Rev. Econ. Geol., v. 2, p. 99-128.

Fleischer, E., Goldberg, M., Gat, J. R., and Magaritz, M., 1977, Isotopic composition of formation waters from deep drillings in southern Israel: Geochim. et Cosmochim. Acta, v. 41, p. 511-525.

Fullager, P. D., and Bottino, M. L., 1970, Sulfide mineralization and rubidium-strontium geochronology at Ore Knob, North Carolina, and Ducktown, Tennessee: Econ. Geol., v. 65, p. 541-550.

Gair, J. E., and Slack, J. F., 1984, Deformation, geochemistry, and origin of massive sulfide deposits, Gossan Lead District, Virginia: Econ. Geol., v. 79, p. 1483-1520.

Garlick, G. D., and Epstein, S., 1967, Oxygen isotope ratios in coexisting minerals of regionally metamorphosed rocks. Geochim. et Cosmochim. Acta, v. 31, p. 181-214.

Graham, C. M., 1981, Experimental hydrogen isotope studies III: Diffusion of hydrogen in hydrous minerals and stable isotope exchange in metamorphic rocks: Contrib. Mineral. Petrol., v. 76, p. 216-228.

Graham, C. M., Viglino, J. A., and Harmon, R. S., 1987, Experimental study of hydrogen-isotope exchange between aluminous chlorite and water and of hydrogen diffusion in chlorite: Am. Mineral., v. 72, p. 566-579.

Green, G. R., Ohmoto, H., Date, J., and Takahashi, T., 1983, Whole-rock oxygen isotope distribution in the Fukuzawa-Kosaka area, Hokuroku district, Japan, and its potential application to mineral exploration: Econ. Geol. Mon. 5, p. 395-411.

Gregory, R. T., 1986, Oxygen isotope systematics of quartz-magnetite pairs from Precambriam iron formations: evidence for fluid-rock interaction during diagenesis and metamorphism, *in* Walther, J. V., and Wood, B. J., eds., Fluid-rock interactions during metamorphism: New York, Springer, p.132-153.

Gregory, R. T., and Criss, R. E., 1986, Isotopic exchange in open and closed systems, in Stable Isotopes *in* Valley, J. W., Taylor, H. P., Jr., and O'Neil, J. R., eds., Stable isotopes in high temperature geological processes: Mineral. Soc. Am., Reviews in Mineralogy, v. 16, p. 91-128.

Gregory, R. T., and Taylor, H. P., Jr., 1986, Possible non-equilibrium oxygen isotope effects in mantle nodules, an alternative to the Kyser-O'Neil-Carmichael $^{18}O/^{16}O$ geothermometer: Contrib. Mineral. Petrol., v. 93, p. 114-119.

Hadley, J. B., 1970, The Ocoee Series and its possible correlatives, *in* Fisher, G. W., et al., eds., Studies of Appalachian geology - central and southern: New York, Interscience Publishers, p. 247-259.

Hadley, J. B., and Goldsmith, R., 1963, Geology of the eastern Great Smokey Mountains, North Carolina and Tennessee: U. S. G. S. Prof. Paper, no. 349-B, 118 p.

Hall, D. L., Bodnar, R. J., and Craig, J. R., 1989a, Fluid evolution during metamorphism and uplift of the massive sulfide deposits at Ducktown, Tennessee, U.S.A. I. Evidence from fluid inclusions: Jour. Metamorphic Geol. (submitted).

Hall, D. L., Bodnar, R. J., and Craig, J. R., 1989b, Fluid evolution during metamorphism and uplift of the massive sulfide deposits at Ducktown, Tennessee, U.S.A. II. Evidence for compositional changes to fluid inclusions via hydrogen diffusion: Am. Jour. Sci. (submitted).

Hatcher, R. D., Jr., 1978, Tectonics of the western Piedmont and Blue Ridge, Southern Appalachians: review and speculations: Am. Jour. Sci., v. 278, p. 276-304.

Hatcher, R. D., Jr., and Zietz, I., 1980, Tectonic implications of regional aeromagnetic and gravity data from the Southern Appalachians, *in* Wones, D. R., ed., Proceedings the Caledonides in the U.S.A., IGCP project 27: Caledonide Orogen, p. 235-244.

Hatcher, R. D., Jr., Butler, J. R., Fullagar, P. D., Secor, D. T., and Snoke, A. W., 1980, Geologic synthesis of the Tennessee-Carolinas-Northeast Georgia southern Appalachians, *in* Wones, D. R., ed., Proceedings the Caledonides in the U.S.A., IGCP project 27: Caledonide Orogen, p. 83-90.

Hattori, K., and Sakai, H., 1979, D/H ratios, origins and evolution of the ore-forming fluids for the Neogene veins and Kuroko deposits of Japan: Econ. Geol, v. 74, p. 535-555.

Heaton, T. H. E., and Sheppard, S. M. F., 1977, Hydrogen and oxygen isotope evidence for sea water hydrothermal alteration and ore deposition, Troodos Complex, Cyprus, *in* Volcanic processes in ore genesis: Geol. Soc. London, Spec. Paper 7, p. 42-57.

Henry, D. K., Craig, J. R., and Gilbert, M. C., 1979, Ore mineralogy of the Great Gossan Lead, Virginia: Econ. Geol., v. 74, p. 645-656.

Hitchon, B., and Friedman, I., 1969, Geochemistry and origin of formation waters in the western Canada sedimentary basin I. Stable isotopes of hydrogen and oxygen. Geochim. et Cosmochim. Acta, v. 33, p. 1321-1349.

Holcombe, R. J., 1973, Mesoscopic and microscopic analysis of deformation and metamorphism near Ducktown, Tennessee: Unpub. Ph. D. Thesis, Stanford University, 225 p.

Javoy, M., 1977, Stable isotopes and geothermometry: Jour. Geol. Soc. London, v. 133, p. 609-636.

Lawson, L. S., and Misra, K. C., 1985, Geochemistry and tectonic significance of amphibolites of the Ducktown Mining District, Tennessee (abstr.): Geol. Soc. Am. Abstr. Programs, v. 17, p. 640.

Lydon, J. W., 1988, Ore deposit models #14. Volcanogenic massive sulphide deposits part 2: genetic models: Geoscience Canada, v. 15, p. 43-65.

Magee, M., 1968, Geology and ore deposits of the Ducktown district, Tennessee, *in* Ridge, J. D., ed., Ore deposits of the United States: 1933-1967: Am. Inst. Mining, Metal., and Petrol. Eng., Inc., p. 207-241.

Mathews, A., and Schliestedt, M., 1984, Evolution of the blueschist and greenschist facies rocks of Sifnos, Cyclades, Greece. A stable isotope study of subduction-related metamorphism: Contrib. Mineral. Petrol., v. 88, p. 150-163.

Mathews, A., Goldsmith, J. R., and Clayton, R. N., 1983, Oxygen isotope fractionations involving pyroxenes: the calibration of mineral-pair geothermometers: Geochim. et Cosmochim. Acta, v. 47, p. 631-644.

Matsuhisa, Y., Goldsmith, J. R., and Clayton, R. N., 1979, Oxygen isotopic fractionation in the system quartz-albite-anorthite-water: Geochim. et Cosmochim. Acta, v. 43, p. 1131-1140.

Mauger, R. L., 1972, A sulfur isotope study of the Ducktown Tennessee District, U.S.A: Econ. Geol., v. 67, p. 497-510.

McCrea, J. M., 1950, The isotopic chemistry of carbonates and a paleotemperature scale: Jour. Chem. Phys., v. 18, p. 849-857.

Munha, J., Barriga, F. J. A. S., and Kerrich, R., 1986, High ^{18}O ore-forming fluids in volcanic-hosted base metal massive sulfide deposits: geologic, $^{18}O/^{16}O$, and D/H evidence from the Iberian Pyrite Belt; Crandon, Wisconsin; and Blue Hill, Maine: Econ. Geol., v. 81, p. 530-552.

Nesbitt, B. E., 1979, Regional metamorphism of the Ducktown, Tennessee massive sulfides and adjoining portions of the Blue Ridge Province. Unpub. Ph. D. Thesis, Univerisity of Michigan, 216 p.

Nesbitt, B. E., 1982, Metamorphic sulfide-silicate equilibria in the massive sulfide deposits at Ducktown, Tennessee: Econ. Geol., v. 77, p. 364-378.

Nesbitt, B. E., and Kelly, W. C., 1980, Metamorphic zonation of sulfides, oxides and graphite in and around the orebodies at Ducktown, Tennessee: Econ. Geol., v. 75, p. 1010-1021.

Nesbitt, B. E., and Essene, E. J., 1982, Metamorphic thermometry and barometry of a portion of the southern Blue Ridge province: Am. Jour. Sci., v. 282, p. 701-729.

Ohmoto, H., 1986, Stable isotope geochemistry of ore deposits, *in* Valley, J. W., Taylor, H. P., Jr., and O'Neil, J. R., eds., Stable isotopes in high temperature geological processes: Mineral. Soc. Am., Reviews in Mineralogy, v. 16, p. 491-559.

Ohmoto, H., and Rye, R. O., 1974, Hydrogen and oxygen isotopic compositions of fluid inclusions in the Kuroko deposits, Japan: Econ. Geol., v. 69, p. 947-953.

Ohmoto, H., and Rye, R. O., 1979, Isotopes of sulfur and carbon, *in* Barnes, H. L., ed., Geochemistry of hydrothermal ore deposits, 2nd edition: J. Wiley and Sons, New York, p. 509-567.

O'Neil, J. R., 1986, Theoretical and experimental aspects of isotopic fractionation,*in* Valley, J. W., Taylor, H. P., Jr., and O'Neil, J. R., eds., Stable isotopes in high temperature geological processes: Mineral. Soc. Am., Reviews in Mineralogy, v. 16, p. 1-40.

O'Neil, J. R., and Taylor, H. P., Jr., 1969, Oxygen isotope equilibrium between muscovite and water: Jour. Geophys. Res., v. 74, p. 6012-6022.

Pottorf, R. J., and Barnes, H. L., 1983, Mineralogy, Geochemistry, and ore genesis of hydrothermal sediments from the Atlantis II Deep, Red Sea: Econ Geol. Monograph 5, p. 198-223.

Rankin, D. W., 1975, The continental margin of eastern North America in the Southern Appalachians: the opening and closing of the proto-Atlantic ocean: Am. Jour. Sci., v. 275-A, p. 298-336.

Rankin, D. W., 1976, Appalachian salients and recesses: Late Precambrian continental breakup and the opening of the Iapetus Ocean: Jour. Geophys. Res., v. 81, p. 5605-5619.

Rogers, J., 1972, Latest Precambrian (post-Grenville) rocks of the Appalachian region: Am. Jour. Sci., v. 272, p. 507-520.

Schoell, M., 1984, Stable isotopes in petroleum research, *in* Brooks, J., and Welte, D., eds., Advances in petroleum geochemistry, volume 1: Academic Press, London, p. 215-243.

Schoell, M., and Faber, E., 1978, New isotopic evidence for the origin of the Red Sea brines: Nature, v. 275, p. 436-438.

Sheppard, S. M. F., 1984, Stable isotope studies of formation waters and associated Pb-Zn hydrothermal ore deposits, *in* Durand, B., ed., Thermal phenomena in sedimentary basins: Editions Technip., Paris, p. 301-317.

Slater, R., 1982, Massive sulfide deposits of the Ducktown mining district, Tennessee, *in* Exploration for metallic resources in the southeast: University of Georgia, Dept. Geol. Center Contin. Ed., p. 91-99.

Sterner, S. M., Hall, D. L., and Bodnar, R. J., 1989, Fluid immiscibility in geologic environments: Interpretation of fluid inclusion data using available fluid phase equilibria: Contrib. Mineral. Petrol. (in preparation).

Suzuoki, T., and Epstein, S., 1976, Hydrogen isotope fractionation between OH-bearing minerals and water: Geochim. et Cosmochim. Acta, v. 40, p. 1229-1240.

Taylor, H. P., Jr., 1979, Oxygen and hydrogen isotope relationships in hydrothermal mineral deposits, *in* Barnes, H. L., ed., Geochemistry of hydrothermal ore deposits: New York, Wiley-Interscience, p. 236-277.

Taylor, B. E., O'Neil, J. R., 1977, Stable isotope studies of metasomatic skarns and associated metamorphic and igneous rocks, Osgood Mountains, Nevada: Contrib. Mineral. Petrol., v. 63, p. 1-49.

Tung, J. P., 1968, A study of the wall rocks and their relationship to the ore body at the Calloway Mine Ducktown, Tennessee: Unpub. M.S. Thesis, Univ. Tenn., Knoxville, 67p.

Wenner, D. B., and Taylor, H. P., Jr., 1971, Temperatures of serpentinization of ultramafic rocks based on O^{18}/O^{16} fractionation between coexisting serpentine and magnetite: Contrib. Mineral. Petrol., v. 32, p. 165-185.

Woodruff, L. G., Gair, J. E., and Slack, J. F., 1984, Sulfur and oxygen isotope study of the Great Gossan Lead, Southwestern Virginia: evidence for a paleohydrothermal system in a regional metamorphic terrane (abstr.): Geol. Soc. Am. Abstr. Programs, v. 16, p. 701.

CHAPTER V
CONCLUSIONS

Primary fluid inclusions trapped in peak metamorphic clinopyroxene and garnet contain H_2O-CH_4-NaCl fluids and daughter crystals of calcite, quartz and pyrrhotite. Although post-trapping volumetric and compositional changes have occurred, significant quantities of dissolved solids must have been present in the peak metamorphic fluids which formed pyroxene and garnet in the ore zones.

Secondary fluid inclusions in quartz from ore zones and country rocks document a complex uplift history involving a variety of fluids in the system C-O-H-N-salt. Early fluids were formed by local devolatilization reactions while late fluids were more pervasive and were externally derived. The ore zones appear to have acted as conduits for fluid flow during the later stages of uplift.

Secondary fluid inclusions constrain uplift to have been temperature-concave from 6 kb and 550°C to 2.3 kb and 215°±20°C and then nearly isothermal at 215°±20°C over the pressure range 2.3-1.0 kb. The latest stages of uplift appear to have been temperature-convex. This P-T-time path is consistent with the tectonic history of the Ducktown area. Temperature-concave uplift occurred from 480 ma. to 427-372 ma. implying average uplift rates of 0.13 to 0.06 mm/yr. Uplift rates of 0.06-0.09 mm/yr from 424-372 ma. to 250 ma. are implied by the data.

Isothermal decompression is documented by immiscible H_2O-CH_4-N_2-NaCl fluids that were emplaced during Alleghanian thrusting and which were

derived by expulsion of pore fluids and maturation of organic material in lower plate sediments. Episodic movement along the Great Smoky and related faults caused these fluids to "boil" and move upward.

Primary fluid inclusions in pyroxene, which formed at peak metamorphic conditions of 6 kbar and 550°C with fO_2-fS_2 values buffered near Py-Po-Mt, contain a normalized volatile composition of 93 mol% H_2O, 4 mol% CH_4, 3 mol% CO_2 and 0.1 mol% H_2S. Fluid speciation calculations and silicate-oxide-sulfide mineral assemblages suggest that the trapped fluid should consist of 90 mol% H_2O, 10^{-7} mol% CH_4, 10 mol% CO_2 and 0.1 mol% H_2S. Methane was not a significant component of peak metamorphic fluids in ore zones.

Post-trapping speciation changes can account for the discrepancy in the CH_4/CO_2 ratio only if the inclusions behaved as open systems and hydrogen diffused into the inclusions causing reduction of CO_2 to CH_4. This has been shown to be feasible if fluids from the bulk of the country rocks infiltrated the ore zones after peak metamorphism. Country rock fluids are buffered at fO_2 approximately 3 log units below oxidized portions of ore zones. An fH_2 gradient is established between inclusions and grain boundary fluids which would promote diffusion into primary fluid inclusions.

δD values of primary fluid inclusions are 65 per mil lower than equilibrium values at peak metamorphism. Hydrogen diffusion would drastically lower δD by addition of isotopically light hydrogen. Mass balance calculations suggest that the amount of hydrogen necessary to lower δD will also result in sufficient compositional changes to reconcile calculated and observed fluid compositions. Hence, hydrogen diffusion is presently the best explanation for

discrepancies between calculated and observed fluid compositions in primary fluid inclusions from Ducktown.

Oxygen isotope analyses of Addy and Ypma (1977) indicate that minerals in ore zones are depleted in ^{18}O by 2-3 per mil, relative to minerals in country rocks, and whole rocks in the ore zones are depleted by 2-5 per mil. Temperature estimates of concordant mineral triplets suggest that minerals in all lithologies equilibrated during peak metamorphism at temperatures of 530° ± 20°C. Integration of isotopic data with information on mineral assemblages, mineral chemistry, and fluid inclusions suggest that the low $\delta^{18}O$ zones surrounding the orebodies must have formed prior to metamorphism, probably during sea-floor hydrothermal alteration and massive sulfide deposition.

Integrated water/rock ratios may have been as high as 10^2-10^3 during ore deposition and the ore fluid appears to have been largely seawater or slightly modified seawater. Subsequent metamorphism occurred at low integrated water/rock ratios and the silicates behaved as closed systems with respect to oxygen except on small scales. δD values of biotite and muscovite are similar in the ore zones and country rocks and biotite, muscovite and chlorite equilibrated with the same fluid (δD = -33 to -42 ‰) at peak metamorphism. As the sea-floor hydrothermal system responsible for ^{18}O-depletion of ore zones should have had a similar effect on δD values it is concluded that homogenization of hydrogen isotopes in country rocks and ores zones occurred during or prior to peak metamorphism. $\delta^{13}C$ values of primary fluid inclusions are in equilibrium with local carbonate at peak metamorphic temperatures. This carbonate has low $\delta^{13}C$ values indicative of interaction

with organic matter, and there is no difference in $\delta^{13}C$ between ore zones and country rocks. These observations suggest that low $\delta^{13}C$ values in carbonate were attained prior to or during peak metamorphism. Influx of post- peak metamorphic fluids, recorded as secondary fluid inclusions, does not appear to have affected $\delta^{18}O$ values of silicates appreciably, but may be responsible for small changes in $\delta^{18}O$ and $\delta^{13}C$ of calcite.

APPENDIX A

LIST OF SAMPLES EXAMINED FOR FLUID INCLUSION ANALYSIS

Sample No.	F.I. Types
B224-108	1
B224-202	1, 4
B503-76	N
B508-159	1
B508-163	1
B509-166	N
B509-232	N
B542-51	4, 5
B567-62	N
B744-131	2
B770-2053	N
B770-2424	N
B770-2529	4
B797-27	N
CH4	3
CH5	4
CH14	4
CH15	1
CH16	1

Sample No.	F.I. Types
CH233-93	4
CH233-317	4
CH233-385	2
CH233-423	4, 5
CH233-480	N
CH233-536	N
CH233-563	4
CH462-26	N
CH462-35	N
CH462-44	N
CH462-45	4
CH462-50	N
CH462-54	N
CH462-63	N
CH462-82	N
CH775-13	4
CH776-3	N
CH776-10	2, 4
CH776-84	N
CH795-5	4
CH795-24	N
CH796-5	1
CH796-12	4

Sample No.	F.I. Types
CH796-25	4
CH855-2	4
CH856-20	5
CH951-60	4, 6
CH951-137	4
CH951-170	2
CH1065-689	N
CH1066-612	4
CH1213-68	N
CH1213-165	N
CH1214-175	1, 2
CH1226-390A	1, 4
CH1226-390B	1, 4
CH1226-432	N
CH1227-221	1
CH1227-222	1
CH1227-288	4
CH1416-238	N
CH1461-186	2
CH1461-199	1
CH1461-223	2
CH1461-275	2
CH1461-298	N

Sample No.	F.I. Types
CH1461-342	N
CH1464-257	N
CH1464-259	N
CH1464-270	4
CH1464-291	2, 4, 5
CH1464-296	N
CH1464-313	2
CH1464-344	2
CH1466-235	5
CH1466-241	N
CH1466-254	N
CH1466-267	N
CH1466-296	N
CH1466-314	4
CH1466-328	1
CH1466-334	2, 3
CH1466-339	2, 4, 5, 6
CH1466-380	4
CH1504-164	N
CH1577-190	2, 4
CH1577-200	4
CH1577-205	2, 4
CH1577-210	4

Sample No.	F.I. Types
CH1577-215	4
CH1577-220	4
CH1577-225	4, 6
CH1577-230	4
CH1577-235	2, 4
CH1577-240	4
CH1577-245	4
CH1577-250	4, 6
CH1577-255	N
CH1577-264	N
CH1577-266	2, 4
CH1577-272	2, 4
CH1577-275	N
CH1577-280	4, 6
CH1577-290	4
CH1582-486	N
CH1582-490	N
CH1594-118	N
CH1594-144	N
CH1594-169	N
CH1594-187	6
CH1594-208	1
CH1594-217	4

Sample No.	F.I. Types
CH1594-226	4
CH1594-237	4
CL628-15	N
CL826-56	N
CL827-2	N
CL827-22	N
CL857-22	N
CL857-111	4
CL908-220	2
CL908-229	4
CL950-47	N
CL950-77	N
MP1154-6	4
MP1154-43	1, 4
MP1156-37	1
MP1174-0	1
MP1174-1	1
MP1177-95	4
PORPH-B	4

B = Boyd orebody; CH = Cherokee orebody; CL = Calloway orebody; MP = Mary-Polk orebody; PORPH-B = quartz eye in pyrite porphyroblast; 1 = primary; 2 = low-salinity, one-phase, NaCl-H_2O; 3 = CO_2-H_2O-NaCl; 4 = immiscible CH_4-N_2-H_2O-NaCl; 5 = halite-bearing; 6 = late-stage $CaCl_2$-rich; N = no inclusions observed, or those present are not diagnostic.

APPENDIX B

FLUID INCLUSION DATA

SAMPLE CH4

$Tm(CO_2)$	Tm(clath)	$Th(CO_2)$	Type
-57.6	7.3	16.8*	3
-57.5	7.8	11.4	3
-57.6	8.0	4.6	3
-57.6	7.4	14.3	3
-58.9	8.8	16.5	3
-58.5	8.3	4.3	3
-58.3	---	16.0	3
-57.6	8.1	8.5	3
-57.6	7.1	6.3	3
-57.6	8.8	8.8	3
-57.5	8.8	18.6	3
-57.5	7.7	21.7	3
-57.5	7.7	19.2	3

*All homogenizations are to the liquid phase unless otherwise noted; V = to the vapor.

SAMPLE CH15

$Th(CH_4)$	Tm(ice)	Tm(clath)	Th	Td	Type
138.8*	-1.9	16.4		179	1
---	-1.5	15.6			1
-125	-2.0	17.2	225		1
---	-1.4	17.3			1
---	-1.4	15.8			1

*All homogenizations are to the liquid phase unless otherwise noted; V = to the vapor.

SAMPLE CH16

$Th(CH_4)$	Tm(ice)	Tm(clath)	Th	Td	Type
	-0.9	17.2		146	1
	-1.0	18.6			1
	-0.9	18.2			1
	---	23.0			1
	-2.0	18.8			1
	-1.3	18.5			1
	-2.2	18.0			1
	-1.1	18.3			1

SAMPLE CH1214-175

$Th(CH_4)$	Te	Tm(ice)	Tm(clath)	Th	Td	Type
-156.7*			23.3		275	1
-142.3			25.2			1
-122.0			25.2	235*	240	1
-91.0		-1.0	18.5	240		1
-93.3			17.8		150	1
-120		-1.2	-----			1
-102.9		-1.0	19.5			1
		-3.4				2
		-3.3				2
		-3.3				2
		-3.4				2
		-2.0				2
		-2.1				2

*All homogenizations are to the liquid phase unless otherwise noted; V = to the vapor.

SAMPLE CH1227-222

$Th(CH_4)$	Te	Tm(ice)	Tm(clath)	Th	Td	Type
		-1.0	-----	230*		1
		-1.3	21.7		187	1
-89.7*		-1.2	14.8		215	1
		-1.2	14.0			1
		-1.4	-----			1
		-1.2	14.8			1
		-1.2	18.5			1
		-6.5	8.5			4A
		-6.0	5.0			4A

*All homogenizations are to the liquid phase unless otherwise noted; V = to the vapor.

SAMPLE CH1226-390A

$Th(CH_4)$	Te	Tm(ice)	Tm(clath)	Th	Td	Type
		-1.4	14.7			1
		-1.2	18.5			1
			23.3			1
		-2.5	-----			4A
		-3.2	-----			4A
		-3.2	7.0			4A

SAMPLE CH1461-275

$Th(CH_4)$	Te	Tm(ice)	Tm(clath)	Th	Td	Type
		-1.2				2
		-1.3				2
		-1.2				2
		-1.3				2
		-1.1				2
		-1.2				2
		-1.3				2
		-1.3				2

SAMPLE CH1464-270

$Th(CH_4)$	Te	Tm(ice)	Tm(clath)	Th	Td	Type
-85 (V)*						4B
-84 (V)						4B
-83 (V)						4B
-90 (V)						4B
-85 (V)						4B
-96.6						4B
-95.7						4B
-93.6						4B
-91.5 (V)						4B
-141						4B
-111						4B
-142						4B
-134						4B
		-3.8	5.5	200*		4A

*All homogenizations are to the liquid phase unless otherwise noted; V = to the vapor.

SAMPLE CH1464-291

$Th(CH_4)$	Te	Tm(ice)	Tm(clath)	Th	Td	Type
-90 (V)*						4B
-95						4B
-93						4B
-87 (V)						4B
		-1.3				2
		-1.6				2
		-1.7				2
		-2.0				2
		-3.2				2

*All homogenizations are to the liquid phase unless otherwise noted; V = to the vapor.

SAMPLE CH1464-313

Th(CH_4)	Te	Tm(ice)	Tm(clath)	Th	Td	Type
		-0.1				2
		-0.4				2
		-0.1				2
		-0.3				2
		-0.8				2
		-0.2				2
		-2.5				2
		-1.9				2
		-0.1				2

SAMPLE CH1464-344

$Th(CH_4)$	Te	Tm(ice)	Tm(clath)	Th	Td	Type
		-1.0				2
		-0.4				2
		-0.7				2
		-0.5				2
		-1.1				2
		-0.5				2
		-0.6				2
		-0.8				2

SAMPLE CH1466-314

$Th(CH_4)$	Te	Tm(ice)	Tm(clath)	Th	Td	Type
	<-26	-8.7	11.0			4A
	<-35	-9.0	12.0			4A
	<-35	-9.8	12.8			4A
	<-35	-10.3	11.9	205*	247	4A

*All homogenizations are to the liquid phase unless otherwise noted; V = to the vapor.

SAMPLE CH1466-328

$Th(CH_4)$	Te	Tm(ice)	Tm(clath)	Th	Td	Type
-82.5 (V)*		-1.8	15.1	201*		1
	-23	-1.8	14.9	205		1
	-22	-1.9	15.0		230	1
		-1.8	15.0	200		1
		-1.8	14.8			1

*All homogenizations are to the liquid phase unless otherwise noted; V = to the vapor.

SAMPLE CH1466-334

$Tm(CO_2)$	Tm(clath)	$Th(CO_2)$	Type
-57.6	8.6	9.3*	3
-56.8	8.0	14.2	3
-57.0	8.3	9.8	3
-57.1	7.8	11.8	3
-56.9	7.8	10.9	3
-57.3	8.7	19.8	3
-57.0	8.5	11.7	3
-57.5	---	9.1	3
-56.6	8.3	16.0	3
-56.6	8.3	14.4	3
-56.7	8.2	15.0	3
-56.6	8.4	12.7	3
-57.3	8.3	12.3	3
-57.1	7.8	14.0	3
-57.1	7.8	19.6	3
-57.3	8.6	15.1	3
-57.4	7.8	13.2	3
-57.3	8.2	18.5	3

SAMPLE CH1466-334 (continued)

$Tm(CO_2)$	Tm(clath)	$Th(CO_2)$	Type
-57.4	7.1	9.3	3
-56.9	8.7	16.5	3
-56.7	8.6	17.1	3
-57.1	8.4	11.9	3
-56.7	7.8	15.8	3
-57.1	8.0	11.2	3
-57.1	8.1	13.0	3
-57.6	---	-3.7	3
-56.6	---	5.2	3
-57.6	8.2	14.1	3
-57.6	---	4.6	3
-57.3	---	-2.2	3

*All homogenizations are to the liquid phase unless otherwise noted; V = to the vapor.

SAMPLE CH1466-339

$Th(CH_4)$	Te	Tm(ice)	Tm(clath)	Tm(halite)	Th	Type
		-2.1				2
		-3.8				2
		-2.5				2
		-2.7				2
		-3.2				2
		0.0				2
		0.0				2
		0.0				2
		0.0				2
		0.0				2
	-71.5	-22.1				6
	-72	-22.0				6
	-72	-17.0				6
		-9.0	11.2			4A
		-8.7	12.5			4A
		-8.9	12.2			4A
				199	190	5
				199	189	5
				201	185	5
				202	190	5

SAMPLE CH1466-380

Th(CH_4)	Te	Tm(ice)	Tm(clath)	Th	Td	Type
	<-25	-10.7	11.2			4A
	<-25	-8.8	12.0			4A
	<-25	-9.2	11.3			4A
	<-25	-7.2	7.5			4A
	<-25	-10.4	6.8			4A
-105.3*						4B
-113.9						4B
-105.1						4B
-99.7						4B
-98.7						4B
-103.4						4B
-104.8						4B
-105.8						4B
-106.8						4B

*All homogenizations are to the liquid phase unless otherwise noted; V = to the vapor.

SAMPLE CH1577-250

$Th(CH_4)$	Te	Tm(ice)	Tm(clath)	Th	Td	Type
	-22	-5.3	11.6			4A
	-23	-6.2	8.0			4A
	-23	-6.2	7.6			4A
	-22.5	-5.6	8.8			4A
	-22	-5.6	8.7			4A
	-22	-5.6	8.7			4A
	-23	-4.7	6.5			4A
	-23	-4.6	6.5			4A
	-23	-4.7	6.4			4A
-103*						4B
-119						4B
-109.5						4B
-86.8 (near crit)						4B
-86.6 (V)						4B
-86.8 (V)						4B
	-60	-43.0				6
	-62	-35.7				6
	-63	-35.5				6

*All homogenizations are to the liquid phase unless otherwise noted. V = to the vapor

SAMPLE CH1577-266

$Th(CH_4)$	Te	Tm(ice)	Tm(clath)	Th	Td	Type
		-2.0	13.5	225*	230	4A
		-2.0	14.2		188	4A
		-2.1	15.6		207	4A
		-3.4	14.3		228	4A
		-2.1	15.2			4A
-105.2*						4B
-144.0						4B
-101.2						4B
-96.2						4B
-99.4						4B
-98.7						4B
-98.6						4B
-97.2						4B
-96.9						4B
-98.6						4B
-102.6						4B
-101.0						4B
-101.3						4B
-96.2						4B

SAMPLE CH1577-266 (continued)

$Th(CH_4)$	Te	Tm(ice)	Tm(clath)	Th	Td	Type
-102.9*						4B
-102.4						4B
-129.1						4B
-127.5						4B
		-0.9				2
		-3.0				2
		-2.7				2

*All homogenizations are to the liquid phase unless otherwise noted. V = to the vapor

SAMPLE CH1577-272

$Th(CH_4)$	Te	Tm(ice)	Tm(clath)	Th	Td	Type
-140*						4B
-132.7						4B
-111.7						4B
-129.1						4B
-129.1						4B
-129.1						4B
-116.6						4B
-109.3						4B
-100.5						4B
-91.2						4B
-87.9						4B
-136.0						4B
-123.2						4B
-132.1						4B
-125.7						4B
-133.1						4B
-88.6 (near crit)						4B
-90.2						4B

*All homogenizations are to the liquid phase unless otherwise noted; V = to the vapor.

SAMPLE CH1577-272 (continued)

$Th(CH_4)$	Te	Tm(ice)	Tm(clath)	Th	Td	Type
-80.3 (V)*						4B
-125.6						4B
-96.0						4B
-95.9						4B
-95.9						4B
-131.6						4B
-131.9						4B
-132.0						4B
-83.3						4B
-88.3						4B
-83.0						4B

*All homogenizations are to the liquid phase unless otherwise noted; V = to the vapor.

SAMPLE CH1577-280

$Th(CH_4)$	Te	Tm(ice)	Tm(clath)	Th	Td	Type
-110.4*						4B
-102.9						4B
-90.4						4B
-86.4						4B
-86.4						4B
-103.6						4B
-100.7						4B
	<-25	-9.1		224*		6
	<-25	-8.5		238		6
		-13.0		186		6
		-12.7		175		6
		-12.9		210		6
	<-29	-11.8		213		6
	<-29	-10.7		195		6
		-11.7		220		6
	<-40	-18.0		265		6
	<-48	-13.5		245		6
		-9.2				6

*All homogenizations are to the liquid phase unless otherwise noted; V = to the vapor.

SAMPLE CH1577-280 (continued)

$Th(CH_4)$	Te	Tm(ice)	Tm(clath)	Th	Td	Type
	<-25	-9.6				6
		-9.1				6
		-11.9				6
	<-30	-11.7				6
		-12.0				6
		-10.7				6
		-20.4				6
		-13.1				6
		-11.5				6
		-10.9				6

SAMPLE CH1594-187

$Th(CH_4)$	Te	Tm(ice)	Tm(clath)	Th	Td	Type
	-59	-15.7				6
	-59	-15.6				6
	-59	-14.1				6
	<-35	-14.8				6

SAMPLE CH1577-280

$Th(CH_4)$	Te	Tm(ice)	Tm(clath)	Th	Td	Type
	<-52	-7.8	11.4			4A
		-7.1	12.5			4A
		-7.2	12.0			4A
		-10.8	---			4A
		-7.3	11.8			4A
		-6.5	9.8	200*		4A
		-8.3	10.2	206		4A
		-7.5	4.0			4A
		-8.1	4.3			4A
		-8.3	4.6			4A
		-8.1	8.6			4A

*All homogenizations are to the liquid phase unless otherwise noted; V = to the vapor.

SAMPLE MP1156-37

$Th(CH_4)$	Te	Tm(ice)	Tm(clath)	Th	Td	Type
-90*		-1.2	11.5			1
		-1.2	15.0			1
-91.7		-1.1	17.0			1

*All homogenizations are to the liquid phase unless otherwise noted; V = to the vapor.

SAMPLE MP1174-1

$Th(CH_4)$	Te	Tm(ice)	Tm(clath)	Th	Td	Type
		-1.0	15.7			1
		-1.0	14.0			1
		-1.2	21.8			1
		-0.9	13.8			1

SAMPLE PORPH-B

$Th(CH_4)$	Te	Tm(ice)	Tm(clath)	Th	Td	Type
-95.5*						4B
-97.2						4B
-90.6						4B
-97.4						4B
-97.4						4B
-90.6						4B
-101.0						4B
-95.3						4B
-82.2 (near crit)						4B
-82.2						4B
-131.0						4B
-133.6						4B
-126.6						4B
-98.0						4B
-97.6						4B
-95.7						4B
-96.3						4B
-99.4						4B

*All homogenizations are to the liquid phase unless otherwise noted; V = to the vapor.

SAMPLE PORPH-B (continued)

$Th(CH_4)$	Te	Tm(ice)	Tm(clath)	Th	Td	Type
-97.6						4B
-94.6						4B
-97.0						4B
-96.0						4B
-95.6						4B
-94.9						4B
-90.4						4B
-88.9						4B
-126.9						4B
-126.3						4B
-125.4						4B
-125.8						4B
-116.8						4B
-127.0						4B
-127.7						4B
-128.0						4B
-132.0						4B
-132.0						4B

*All homogenizations are to the liquid phase unless otherwise noted; V = to the vapor.

SAMPLE PORPH-B (continued)

$Th(CH_4)$	Te	Tm(ice)	Tm(clath)	Th	Td	Type
	<-25	-13.4	6.5			4A
	<-25	-13.8	5.8			4A
	<-25	-14.2	4.8			4A
		-13.8	7.1			4A
		-14.0	7.9			4A
		-12.0	5.9			4A
		-10.5	11.7			4A
		-10.6	11.5			4A
			11.8			4A
			12.2			4A
		-10.4	11.8			4A
		-10.4	11.8			4A
		-10.3	-11.0			4A
		-10.2	-11.0			4A
		-10.5	0.8			4A
		-10.0	12.0			4A
		-10.0	11.7			4A
		-10.1	11.2			4A

SAMPLE PORPH-B (continued)

$Th(CH_4)$	Te	Tm(ice)	Tm(clath)	Th	Td	Type
		-16.4	6.6			4A
		-20.9	8.8			4A
	<-24	-13.4	6.3			4A
	<-24	-13.3	9.6			4A

B = Boyd orebody; CH = Cherokee orebody; CL = Calloway orebody; MP = Mary-Polk orebody; PORPH-B = quartz eye in pyrite porphyroblast; 1 = primary; 2 = low-salinity, one-phase, NaCl-H_2O; 3 = CO_2-H_2O-NaCl; 4 = immiscible CH_4-N_2-H_2O-NaCl; 5 = halite-bearing; 6 = late-stage $CaCl_2$-rich.

APPENDIX C

SOURCE CODE FOR FLUID SPECIATION PROGRAMS

```
C       ********** NEW OHMOTO AND KERRICK PROGRAM ********** 11/9/88
C       **********WRITTEN BY DONALD LEWIS HALL**********
C       CALCULATES FLUID SPECIATION USING THE METHOD OF OHMOTO AND
C       KERRICK (1977) AMER. JOUR. SCI. 277, 1013-1044.  THEIR METHOD HAS
C       BEEN MODIFIED TO ALLOW FOR CARBON ACTIVITIES LESS THAN UNITY
C       AND FOR NON-IDEAL MIXING IN THE FLUID.
C       SPECIES ORDER IS CO2,CO,CH4,H2,H2O,H2S,SO2,O2,S2,COS
        IMPLICIT DOUBLE PRECISION (A-H,O-Z)
        DIMENSION X(10),FUGCOF(10),GAM(10),SLGFUG(10),WW(10)
        CHARACTER*80 ZOUT
        WRITE (9,3003)
 3003   FORMAT(//,'ENTER NAME OF OUTPUT FILE')
        READ (9,3004) ZOUT
 3004   FORMAT (A80)
        OPEN (UNIT=8, FILE=ZOUT)
   44   CONTINUE
        WRITE (9,3002)
 3002   FORMAT(//,'ENTER SAMPLE NUMBER, 99 TO QUIT')
        READ (9,*) SAMPLE
        IF(SAMPLE.EQ.99) GO TO 200
        WRITE (9,1)
     1  FORMAT ('ENTER PRESSURE IN BARS AND TEMP IN DEGREES C')
        READ (9,*) PBARS,TEMPC
         PATM=PBARS/1.01325D0
         TEMPK=TEMPC+273.15D0
        WRITE (9,2)
     2  FORMAT ('ENTER LOG FO2 AND LOG FS2 IN BARS OR ENTER ZERO(S)'/,
     1     'TO SPECIFY BUFFER(S)')
        READ(9,*) SLGFO2,SLGFS2
        IF(SLGFO2.EQ.0.D0) CALL OXYBUF(TEMPK,PBARS,PATM,SLGFO2,JOBF)
         OXFUG=10.0D0**SLGFO2/1.01325D0
        IF(SLGFS2.EQ.0.D0) CALL SLFBUF(TEMPC,TEMPK,PATM,SLGFS2,JSBF)
         SULFUG=10.0D0**SLGFS2
        WRITE(9,3)
     3  FORMAT('ENTER AN ACTIVITY OF CARBON BETWEEN 0 AND 1'/,
     1     'AN ACTIVITY OF 1 IMPLIES THAT GRAPHITE EXISTS')
        READ(9,*) ACTC
C       EQUILIBRIUM CONSTANTS FROM OHMOTO AND KERRICK
         EQA=1.0D0/DSQRT(SULFUG)
         EQB=10.0D0**(20586.0D0/TEMPK+0.0421D0+0.028D0*
     1     (PATM-1.0D0)/TEMPK)
         EQC=10.0D0**(14751.0D0/TEMPK-4.535D0)
         EQD=10.0D0**(12510.0D0/TEMPK-0.979D0*DLOG10(TEMPK)+0.483D0)
         EQE=10.0D0**(41997.0D0/TEMPK+0.719D0*DLOG10(TEMPK)-2.404D0)
         EQF=10.0D0**(18929.0D0/TEMPK-3.783D0)
```

```
      EQG=10.0D0**(4757.0D0/TEMPK-4.096D0)
      EQH=10.0D0**(-8117.0D0/TEMPK+0.188D0*DLOG10(TEMPK)-0.352D0)
      CALL IDEALM(TEMPK,TEMPC,PBARS,PATM,GAM)
      DO 115 I=1,10
      WRITE(9,*) GAM(I)
      WRITE(8,*) GAM(I)
115   CONTINUE
      DO 117 I=1,10
      WW(I)=0.0D0
117   CONTINUE
120   DO 1000 ICOUNT=1,100
      IF(ICOUNT.EQ.1) GO TO 125
      DO 122 I=1,10
      WW(I)=X(I)
122   CONTINUE
125   X(1)=EQB*OXFUG*ACTC/(GAM(1)*PATM)
      IF(X(1).GT.1.0D0) THEN
      WRITE (9,130)
130   FORMAT ('CONDITIONS ARE TOO OXIDIZING FOR GRAPHITE TO'/,
     1  'EXIST; SPECIFY NEW CARBON ACTIVITY BETWEEN 0 AND 1')
      READ (9,*) ACTC
      GO TO 125
      END IF
      X(2)=GAM(1)*X(1)/(EQC*GAM(2)*DSQRT(OXFUG))
      X(7)=EQF*OXFUG/(EQA*GAM(7)*PATM)
      X(8)=OXFUG/(GAM(8)*PATM)
      X(9)=SULFUG/(GAM(9)*PATM)
      X(10)=EQG*GAM(2)*X(2)/(EQA*GAM(10))
      EQ4=GAM(5)/(EQD*GAM(4)*DSQRT(OXFUG))
      EQ5=GAM(1)*(GAM(5)*PATM)**2/(EQE*GAM(3)*OXFUG**2)
      EQ8=EQH*GAM(5)/(EQA*GAM(6)*DSQRT(OXFUG))
C     CALCULATE XH2O USING THE POSITIVE ROOT OF QUADRATIC
      DSCRNT=(EQ4+EQ8+1.0D0)**2-4.0D0*EQ5*X(1)*(X(1)+
     1  X(2)+X(7)+X(8)+X(9)+X(10)-1.0D0)
      A=EQ5*X(1)
      B=EQ4+EQ8+1.0D0
      C=X(1)+X(2)+X(7)+X(8)+X(9)+X(10)-1.0D0
      IF(DSCRNT.EQ.0.0) THEN
      ROOT1=-B/2.0D0*A
      ROOT2=-1.0D0
      ELSE
      SDSCRN=DSQRT(DSCRNT)
      ROOT1=(-1.0D0*B+SDSCRN)/(2.0D0*A)
      ROOT2=(-1.0D0*B-SDSCRN)/(2.0D0*A)
      END IF
      IF(ROOT1.LT.0.0) THEN
      X(5)=ROOT2
      ELSE
      X(5)=ROOT1
      END IF
```

```
      X(4)=EQ4*X(5)
      X(3)=EQ5*X(1)*X(5)**2
      X(6)=EQ8*X(5)
     DO 135 I=1,10
      IF(X(I).LT.0.0D0) THEN
      X(I)=1.0D-30
      END IF
 135  CONTINUE
      CALL NORMAL(X,XTOT)
      DO 140 I=1,10
       SLGFUG(I)=DLOG10(GAM(I)*X(I)*PBARS)
 140  CONTINUE
C     FORMAT STATEMENTS FOR OUTPUT
      WRITE (9,4) SAMPLE,PBARS,TEMPC,JOBF,SLGFO2,JSBF,SLGFS2,
     1 X(5),X(1),X(3),X(6),X(2),X(7),X(10),X(4),X(8),X(9)
     4 FORMAT('SAMPLE #',F10.0,/,5X,'CONDITIONS:',/,
     2    5X,'PRESSURE IN BARS =',F6.0,/,
     3    5X,'TEMPERATURE IN DEGREES C =',F5.0,/,
     3    5X,'OXYGEN BUFFER SPECIFIED; (0=NONE, 1=HM/MT, 2=N/NO,',
     3    '3=QFM, 4=MT/WUST)=',I3,/,
     4    5X,'LOG FO2 IN BARS =',F6.2,/,
     3    5X,'SULFUR BUFFER SPECIFIED; (0=NONE, 1=PY/PO, 2=PO FIELD,',
     3    '3=NOTHING, 4=NOTHING)=',I3,/,
     5    5X,'LOG FS2 IN BARS =',D12.5,/,
     5    5X,'MOLE FRACTION H2O =',D12.5,/,
     6    5X,'MOLE FRACTION CO2 =',D12.5,/,
     7    5X,'MOLE FRACTION CH4 =',D12.5,/,
     8    5X,'MOLE FRACTION H2S =',D12.5,/,
     A    5X,'MOLE FRACTION CO  =',D12.5,/,
     B   5X,'MOLE FRACTION SO2 =',D12.5,/,
     B   5X,'MOLE FRACTION COS =',D12.5,/,
     B   5X,'MOLE FRACTION H2  =',D12.5,/,
     B   5X,'MOLE FRACTION O2  =',D12.5,/,
     B   5X,'MOLE FRACTION S2  =',D12.5,/)
C
      WRITE (8,5) SAMPLE,PBARS,TEMPC,JOBF,SLGFO2,JSBF,SLGFS2,
     1    X(5),X(1),X(3),X(6),X(2),X(7),X(10),X(4),X(8),X(9)
     5 FORMAT('**************************************************',/,
     1  'SAMPLE #',F10.0,/,5X,'CONDITIONS:',/,
     2    5X,'PRESSURE IN BARS =',F6.0,/,
     3    5X,'TEMPERATURE IN DEGREES C =',F5.0,/,
     3    5X,'OXYGEN BUFFER SPECIFIED; (0=NONE, 1=HM/MT, 2=N/NO,',
     3     '3=QFM, 4=MT/WUST)=',I3,/,
     4    5X,'LOG FO2 IN BARS =',F6.2,/,
     3    5X,'SULFUR BUFFER SPECIFIED; (0=NONE, 1=PY/PO, 2=PO FIELD,',
     3     '3=NOTHING, 4=NOTHING)=',I3,/,
     5    5X,'LOG FS2 IN BARS =',D12.5,/,
     5    5X,'MOLE FRACTION H2O =',D12.5,/,
     6    5X,'MOLE FRACTION CO2 =',D12.5,/,
     7    5X,'MOLE FRACTION CH4 =',D12.5,/,
```

```
     8      5X,'MOLE FRACTION H2S =',D12.5,/,
     A     5X,'MOLE FRACTION CO  =',D12.5,/,
     B     5X,'MOLE FRACTION SO2 =',D12.5,/,
     B     5X,'MOLE FRACTION COS =',D12.5,/,
     B     5X,'MOLE FRACTION H2  =',D12.5,/,
     B     5X,'MOLE FRACTION O2  =',D12.5,/,
     B     5X,'MOLE FRACTION S2  =',D12.5,/)
C
      WRITE(8,6) SLGFO2,SLGFS2,SLGFUG(4),(X(I),I=1,10)
    6 FORMAT(//,2X,D12.5,'R',D12.5,'R',D12.5,'R',10(D12.5,'R'))
      CALL ARDVRK(PBARS,TEMPK,X,FUGCOF)
      DO 925 I=1,10
       GAM(I)=FUGCOF(I)
  925 CONTINUE
      IFLAG=0
      DO 950 I=1,10
       IF(DABS(X(I)-WW(I))/X(I).GT.1.0D-4) IFLAG=1
  950 CONTINUE
      IF(IFLAG.EQ.0) GO TO 998
 1000 CONTINUE
  998 GO TO 44
  200 PAUSE
      ENDFILE (UNIT=9)
      CLOSE (UNIT=8)
      STOP
      END
C     ************************************************************
      SUBROUTINE OXYBUF(TEMPK,PBARS,PATM,SLGFO2,JOBF)
      IMPLICIT DOUBLE PRECISION (A-H,O-Z)
      INTEGER JOBF
      WRITE (9,100)
  100 FORMAT ('ENTER 1 FOR H/M, 2 FOR N/NO, 3 FOR QF/M, 4 FOR M/W')
      READ (9,*) JOBF
      IF(JOBF.EQ.1) THEN
        OXFUG=10.D0**(-25632.0D0/TEMPK+14.62D0+0.019D0*
     1    (PBARS-1)/TEMPK)
      ELSE IF(JOBF.EQ.2) THEN
        OXFUG=10.D0**(-24753.5D0/TEMPK+9.141D0+0.046D0*
     1    (PBARS-1)/TEMPK)
      ELSE IF(JOBF.EQ.3) THEN
        OXFUG=(1.0D0/(10.0D0**(25738.0D0/TEMPK-9.0D0-0.092D0*
     1    (PATM-1)/TEMPK)))/1.01325D0
      ELSE
        OXFUG=((1.0D0/(10.0D0**(17157.0D0/TEMPK-7.41D0-0.042D0*
     1    (PATM-1)/TEMPK)))**2)/1.01325D0
      END IF
       SLGFO2=DLOG10(OXFUG)
      RETURN
      END
C     ************************************************************
```

```
      SUBROUTINE SLFBUF(TEMPC,TEMPK,PATM,SLGFS2,JSBF)
      IMPLICIT DOUBLE PRECISION (A-H,O-Z)
      INTEGER JSBF
      WRITE (9,200)
200 FORMAT ('ENTER 1 FOR PY/PO, 2 FOR PO')
      READ (9,*) JSBF
      IF(JSBF.EQ.1) THEN
        SLGFS2=-24.9343D0+0.0545D0*TEMPC-2.693D-5*TEMPC**2
     1    +0.06D0*(PATM-1.0D0)/TEMPK
      ELSE
     WRITE (9,201)
201   FORMAT ('ENTER MOLE FRACTION FES IN PYRRHOTITE')
        READ (9,*) AMFES
        AZ=(70.03D0-85.83D0*AMFES)
        BZ=(1000.0D0/TEMPK-1.0D0)
        CZ=39.3D0*DSQRT(1.0D0-0.9981D0*AMFES)
        SLGFS2=AZ*BZ+CZ-11.91D0
      END IF
      RETURN
      END
C     ************************************************************
      SUBROUTINE IDEALM(TEMPK,TEMPC,PBARS,PATM,GAM)
      IMPLICIT DOUBLE PRECISION (A-H,O-Z)
      REAL*8 TR(10),PR(10),TCR(10),PCR(10),GAM(10)
      DATA TCR/304.25D0,132.95D0,190.55D0,41.25D0,647.25D0,
     1    373.55D0,430.65D0,154.75D0,1313.15D0,378.75D0/
      DATA PCR/73.8D0,35.0D0,46.0D0,21.0D0,221.5D0,90.1D0,
     1    78.8D0,50.8D0,206.7D0,63.5D0/
      DO 10 I=1,10
       TR(I)=TEMPK/TCR(I)
       PR(I)=PBARS/PCR(I)
       IF(TR(I).GT.12.D0) THEN
        GAM(I)=1.D0+1.4986D-2*PR(I)-7.015D-4*TR(I)*PR(I)+
     1    1.024D-5*TR(I)**2*PR(I)+1.0787D-4*PR(I)**2-
     2    6.007D-6*TR(I)*PR(I)**2+8.7D-8*TR(I)**2*PR(I)**2
       ENDIF
       IF(TR(I).GT.3.D0.AND.TR(I).LE.12.D0) THEN
        GAM(I)=1.D0+1.24D-2*PR(I)+2.54D-4*TR(I)*PR(I)-5.104D-5*
     1    TR(I)**2*PR(I)+1.1089D-3*PR(I)**2-1.998D-4*TR(I)*
     2    PR(I)**2+9.393D-6*TR(I)**2*PR(I)**2
       ENDIF
       IF(TR(I).GT.0.D0.AND.TR(I).LE.3.D0) THEN
        GAM(I)=1.D0-2.242D-1*PR(I)+1.4667D-1*TR(I)*PR(I)-2.276D-2*
     1    TR(I)**2*PR(I)+8.899D-3*PR(I)**2-5.119D-3*TR(I)*
     2    PR(I)**2+7.86D-4*TR(I)**2*PR(I)**2
       ENDIF
       IF(I.EQ.4.AND.PBARS.LT.3000.D0) THEN
        SWC1=DEXP(-3.8402D0*TEMPK**0.125D0+0.5410D0)
        SWC2=DEXP(-0.1263D0*DSQRT(TEMPK)-15.980D0)
        SWC3=300.0D0*DEXP(-0.11901D0*TEMPK-5.941D0)
```

```
          ALGMH2=SWC1*PATM-SWC2*PATM**2+SWC3*(DEXP(-PATM/300.0D0)-1)
         GAM(4)=DEXP(ALGMH2)
         ENDIF
         IF(I.EQ.1) THEN
          PKB=PBARS/1000.D0
          CNST=18.703218D0-30.004038D0*PKB+15.782754D0*PKB**2-
     1     3.2421026D0*PKB**3+.24980474*PKB**4
          ATERM=-.083597794D0+.13821708D0*PKB-.070776465D0*
     1     PKB**2+.014457271D0*PKB**3-1.0681165D-3*PKB**4
          BTERM=1.2795747D-4-2.0727426D-4*PKB+1.0505277D-4*
     1     PKB**2-2.1212868D-5*PKB**3+1.5251024D-6*PKB**4
          CTERM=-6.2838D-8+1.0053242D-7*PKB-5.0668132D-8*
     1     PKB**2+1.0140221D-8*PKB**3-7.1638184D-10*PKB**4
          GAM(1)=CNST+ATERM*TEMPC+BTERM*TEMPC**2+CTERM*TEMPC**3
         ENDIF
         IF(I.EQ.5) THEN
          CCNST=.31425026D0-.38594999D0*PKB+.19967493D0*PKB**2-
     1      .051474242*PKB**3+7.1493778D-3*PKB**4-
     2     5.0621009D-4*PKB**5+1.4326474D-5*PKB**6
          AATERM=-4.7919973D-3+6.1915716D-3*PKB-3.2539637D-3*
     1     PKB**2+8.4557946D-4*PKB**3-1.1806683D-4*PKB**4+
     2     8.3852276D-6*PKB**5-2.3779833D-7*PKB**6
          BBTERM=1.2450826D-5-1.4262612D-5*PKB+5.6269161D-6*
     1     PKB**2-9.5662335D-7*PKB**3+7.7368676D-8*
     2     PKB**4-2.3373356D-9*PKB**5
          CCTERM=-2.9718201D-9+1.7106038D-8*PKB-7.6196485D-9*PKB**2+
     1     1.3511195D-9*PKB**3-1.1115976D-10*PKB**4+
     2     3.3487236D-12*PKB**5
          DDTERM=-1.5475286D-11-3.1107153D-12*PKB+2.7666352D-12*
     1     PKB**2-5.5248696D-13*PKB**3+4.7086811D-14*PKB**4-
     2     1.386475D-15*PKB**5
          EETERM=1.0069036D-14-2.8496996D-15*PKB+4.2102278D-16*
     1     PKB**2-4.2332381D-17*PKB**3+2.8545359D-18*PKB**4-
     2     1.1765163D-19*PKB**5
          GAM(5)=CCNST+AATERM*TEMPC+BBTERM*TEMPC**2+CCTERM*TEMPC**3+
     1     DDTERM*TEMPC**4+EETERM*TEMPC**5
         ENDIF
C        CALCULATE FUGACITY COEFFICIENT OF S2
          GAM(9)=1.0
  10    CONTINUE
        RETURN
        END
C       ************************************************************
        SUBROUTINE NORMAL(X,XTOT)
        IMPLICIT DOUBLE PRECISION (A-H,O-Z)
        REAL*8 X(10)
        XTOT=0.0D0
        DO 10 I=1,10
          XTOT=XTOT+X(I)
  10    CONTINUE
```

```
      DO 20 I=1,10
        X(I)=X(I)/XTOT
 20   CONTINUE
      RETURN
      END
C     ********************************************************
      SUBROUTINE ARDVRK(PP,T,X,FUGCOF)
      IMPLICIT DOUBLE PRECISION (A-H,O-Z)
      DIMENSION X(10),ATOT(10),BI(10),FUG(10),FUGCOF(10)
      DATA RBAR/83.137D0/, MIXNUM/10/
      DATA BI/2.97D1,2.738D1,2.9703D1,1.515D1,1.46D1,2.D1,3.94D1,
     1    2.21D1,4.579D1,4.30D1/
      CALL MRKMIX(T,X,BSUM,ASUM,ATOT)
C     CUBIC SOLUTION OF THE MRK FOR VOLUME
      RATM=82.05D0
      RR=RATM
      TCEL=T-273.15
      P=-1.0D0*RR*T/PP
      Q=(BSUM*RR*DSQRT(T**3)+BSUM*BSUM*PP*DSQRT(T)-ASUM)/(-1.0D0*
     1    PP*DSQRT(T))
      R=-1.0D0*ASUM*BSUM/(PP*DSQRT(T))
      A=(3.0D0*Q-P*P)/3.0D0
      B=(2.0D0*P**3-9.0D0*P*Q+27.0D0*R)/27.0D0
      V1=1
      V2=1
      V3=1
      ROOT=B*B/4.0D0+A**3/27.0D0
      IF(ROOT) 90,80,70
 70   C=B/-2.0D0+DSQRT(ROOT)
      IF(C) 71,72,72
 71   C=DABS(C)
      AA=-1.0D0*C**(1.0D0/3.0D0)
      GO TO 73
 72   AA=C**(1.0D0/3.0D0)
 73   CONTINUE
      D=B/-2.0D0-DSQRT(ROOT)
      IF(D) 75,76,76
 75   D=DABS(D)
      BB=-1.0D0*D**(1.0D0/3.0D0)
      GO TO 77
 76   BB=D**(1.0D0/3.0D0)
 77   CONTINUE
      X1=AA+BB
      V1=X1-P/3.0D0
      GO TO 100
 80   C=B/-2.0D0+DSQRT(ROOT)
      IF(C) 81,82,82
 81   C=DABS(C)
      AA=-1.0D0*C**(1.0D0/3.0D0)
      GO TO 83
```

```
 82    AA=C**(1.0D0/3.0D0)
 83    CONTINUE
       D=B/-2.0D0-DSQRT(ROOT)
       IF(D) 85,86,86
 85    D=DABS(D)
       BB=-1.0D0*D**(1.0D0/3.0D0)
       GO TO 77
 86    BB=D**(1.0D0/3.0D0)
 87    CONTINUE
       X1=AA+BB
       V1=X1-P/3.0D0
       X2=(AA+BB)/-2.0D0
       V2=X2-P/3.0D0
       GO TO 100
 90    THETA=DACOS(B/-2.0D0/DSQRT(A**3/-27.0D0))
       X1=2.0D0*DSQRT(A/-3.0D0)*DCOS(THETA/3.0D0)
       X2=2.0D0*DSQRT(A/-3.0D0)*DCOS(THETA/3.0D0+120.0D0)
       X3=2.0D0*DSQRT(A/-3.0D0)*DCOS(THETA/3.0D0+240.0D0)
       V1=X1-P/3.0D0
       V2=X2-P/3.0D0
       V3=X3-P/3.0D0
100    CONTINUE
C      PICK LARGEST OF THE THREE VOLUMES FROM THE CUBIC ROOTS
       VIN=V1-V2
       IF(VIN) 110,110,120
110    VIN=V2
       GO TO 130
120    VIN=V1
130    CONTINUE
       VM=VIN-V3
       IF(VIN) 140,140,150
140    VM=V3
       GO TO 160
150    VM=VIN
160    CONTINUE
C      CALCULATE FUGACITIES FROM CORRECT VERSION OF EQ 108
C      IN FERRY AND BAUMGARNER (REV IN MIN VOL 17)
       AM=ASUM
       BM=BSUM
       DO 180 I=1,MIXNUM
       QA=DLOG(VM/(VM-BM))
       QB=BI(I)/(VM-BM)
       QC=2.0D0*ATOT(I)/X(I)/(RATM*DSQRT(T**3)*BM)
       QD=DLOG((VM+BM)/VM)
       QE=AM*BI(I)/(BM*BM*RATM*DSQRT(T**3))
       QF=QD
       QG=BM/(BM+VM)
       QH=DLOG(PP*VM/(RATM*T))
       FUGCOF(I)=DEXP(QA+QB-QC*QD+QE*(QF-QG)-QH)
180    CONTINUE
```

```
      WRITE(9,*) V1,V2,V3,ASUM,BSUM,PP,T,TCEL
      WRITE(9,*)FUGCOF
      WRITE(9,*)X
      WRITE(8,*) V1,V2,V3,ASUM,BSUM,PP,T,TCEL
      WRITE(8,*)FUGCOF
      WRITE(8,*)X
   89 RETURN
      END
C     ****************************************************************
      SUBROUTINE MRKMIX(T,Y,BSUM,ASUM,ATOT)
      IMPLICIT DOUBLE PRECISION (A-H,O-Z)
      DIMENSION A(10),B(10),Y(10),ATOT(10)
      DATA A/46.D6,16.98D6,31.59D6,3.56D6,35.D6,87.9D6,142.6D6,
     1    17.2D6,887.17D6,128.4D6/
      DATA B/2.97D1,2.738D1,2.9703D1,1.515D1,1.46D1,2.D1,3.94D1,
     1    2.21D1,4.579D1,4.30D1/
      DATA MIXNUM/10/,R/82.05D0/
      IF(T.LT.1.D-4) T=1.D0
      TCEL=T-273.15D0
      R2T=R*R*DSQRT(T**5)
      RT=R*DSQRT(T**3)
      AH2OM=166.8D0-.19308D0*TCEL+.1864D-3*TCEL**2-.71288D-7*TCEL**3
      IF(TCEL.LT.6.D2) AH2OM=4.221D3-3.1227D1*TCEL+8.7485D-2*TCEL**2
     1    -1.07295D-4*TCEL**3+4.86111D-8*TCEL**4
      IF(TCEL.GT.1200.0D0) AH2OM=140.0D0-0.050D0*TCEL
      AH2OM=AH2OM*10.D5
      ACO2M=73.03D0-0.0714D0*TCEL+2.157D-5*TCEL**2
      ACO2M=ACO2M*10.D5
      XK=DEXP(-11.071D0+5953.0D0/T-2.746D6/T**2+4.646D8/T**3)
      CO2H2O=XK*0.5D0*R2T
      CO2H2O=CO2H2O+DSQRT(A(1)*A(5))
      ASUM=0.0
      BSUM=0.0
      DO 102 I=1,MIXNUM
      ASUM=0.0
      BSUM=BSUM+B(I)*Y(I)
      DO 102 J=1,MIXNUM
      IF(I.EQ.J) GO TO 140
      IF(I.EQ.5.AND.J.EQ.1) GO TO 150
      IF(I.EQ.1.AND.J.EQ.5) GO TO 150
      ASUM=ASUM+Y(I)*Y(J)*DSQRT(A(I)*A(J))
      GO TO 101
  140 IF(I.NE.5) GO TO 141
      ASUM=ASUM+Y(I)*Y(J)*AH2OM
      GO TO 101
  141 IF(I.NE.1) GO TO 142
      ASUM=ASUM+Y(I)*Y(J)*ACO2M
      GO TO 101
  142 ASUM=ASUM+Y(I)*Y(J)*A(I)
      GO TO 101
```

```
150   ASUM=ASUM+Y(I)*Y(J)*CO2H2O
101   CONTINUE
      ATOT(I)=ASUM
102   CONTINUE
      ASUM=ATOT(1)+ATOT(2)+ATOT(3)+ATOT(4)+
     1    ATOT(5)+ATOT(6)+ATOT(7)+ATOT(8)+ATOT(9)+ATOT(10)
      RETURN
      END
```

```
C      ************* PROGRAM SUPERFLINC ********************11/13/88
C      *********WRITTEN BY DONALD LEWIS HALL**********************
C      USES OHMOTO AND KERRICK PROGRAM TO CALCULATE INITIAL X(I)
C      THEN USES NEWTON'S METHOD FOR NON-LINEAR SYSTEMS TO SOLVE
C      FOR NEW X(I) AT NEW P-T CONDITIONS
       IMPLICIT DOUBLE PRECISION (A-H,O-Z)
       REAL*8 A(10,10),B(10),X(10),ETOT(4),C(6),XN(10),
     1    XKEQ(6),W(10),GAMMA(10),ALGFUG(10)
       INTEGER INDX(10)
       CHARACTER*80 ZOUT
       N=10
       NP=10
       WRITE(9,5)
    5  FORMAT(//,'ENTER NAME OF OUTPUT FILE')
       READ(9,6) ZOUT
    6  FORMAT(A80)
       OPEN(UNIT=8,FILE=ZOUT)
   44  CONTINUE
C      ORDER OF X IS CO2,CO,CH4,H2,H2O,H2S,SO2,O2,S2,COS
       WRITE (9,50)
   50  FORMAT('ENTER SAMPLE NUMBER, 99 TO QUIT')
       READ (9,*) SAMPLE
       IF(SAMPLE.EQ.99) GO TO 997
       CALL OKSPECN(X,VMM)
       WRITE (8,*) VMM
       WRITE(9,7)
    7  FORMAT('ENTER NEW TEMPERATURE IN DEG. C')
       READ(9,*) TC
       TK=TC+273.15D0
       CALL NORMAL(X,XN,XTOT)
       DO 20 I=1,10
         X(I)=XN(I)
   20  CONTINUE
       VINC=VMM
C      MASS BALANCE EQUATIONS FOR TOTAL C-O-H-S
       ETOT(1)=X(1)+X(2)+X(3)+X(10)
       ETOT(2)=2.0D0*(X(1)+X(7)+X(8))+X(2)+X(5)+X(10)
       ETOT(3)=4.0D0*X(3)+2.0D0*(X(4)+X(5)+X(6))
       ETOT(4)=X(6)+X(7)+2.0D0*X(9)+X(10)
       CALL EQCONST(TK,XKEQ)
C      B(I) = VALUES OF THE 10 EQUATIONS SUBSTITUTING X(I)
C      A(I,J) = JACOBIAN MATRIX
       DO 999 ICOUNT=1,100
         IF(ICOUNT.EQ.100)THEN
         WRITE(9,2)
    2    FORMAT('EXCEEDED 99 ITERATIONS IN NEWTONS METHOD')
         PAUSE
       ELSE
         CONTINUE
         ENDIF
```

```
      CALL FUSER(X,XN,XTOT,TK,VMM,ETOT,B,C,XKEQ,GAMMA,PATM)
      CALL MATRIX(X,XTOT,C,A)
      DO 30 I=1,10
        B(I)=-B(I)
   30 CONTINUE
      CALL LUDCMP(A,N,NP,INDX,D)
C     A(I,J) IS NOW THE DECOMPOSED JACOBIAN MATRIX
      CALL LUBKSB(A,N,NP,INDX,B)
C     B(I) IS NOW THE UPDATED CORRECTION TO X(I)
      IFLAG=0
      DO 35 I=1,10
        W(I)=X(I)
   35 CONTINUE
      X(1)=X(1)+B(7)
      X(2)=X(2)+B(1)
      X(3)=X(3)+B(3)
      X(4)=X(4)+B(2)
      X(5)=X(5)+B(9)
      X(6)=X(6)+B(6)
      X(7)=X(7)+B(4)
      X(8)=X(8)+B(8)
      X(9)=X(9)+B(10)
      X(10)=X(10)+B(5)
      DO 40 I=1,10
       IF(X(I).LE.0.0D0) X(I)=1.0D-31
       IF(DABS(X(I)-W(I))/X(I).GT.1.0D-04)IFLAG=1
   40 CONTINUE
      CALL NORMAL(X,XN,XTOT)
      VMM=VINC/XTOT
      WRITE(9,*)'ITERATION NUMBER ',ICOUNT
      WRITE (9,1) (X(I),B(I),I=1,10)
    1 FORMAT(10(1X,2D12.5/))
      IF(IFLAG.EQ.0) GO TO 998
  999 CONTINUE
  998 PBARS=PATM*1.01325D0
      DO 55 I=1,10
        ALGFUG(I)=DLOG10(GAMMA(I)*XN(I)*PBARS)
   55 CONTINUE
      WRITE(8,3) (XN(I),ALGFUG(I),I=1,10),XTOT,VMM,TC,PBARS
    3 FORMAT(//,10(1X,2D12.5/),/,F8.5,F8.3,F6.0,F7.0)
      WRITE(8,4) ALGFUG(8),ALGFUG(9),ALGFUG(4),(XN(I),I=1,10)
    4 FORMAT(//,2X,D12.5,'R',D12.5,'R',D12.5,'R',10(D12.5,'R'))
      PAUSE
      GO TO 44
  997 STOP
      END
C     ****************************************************************
      SUBROUTINE NORMAL(X,XN,XTOT)
      IMPLICIT DOUBLE PRECISION (A-H,O-Z)
      REAL*8 X(10),XN(10)
```

```
      XTOT=0.0D0
      DO 10 I=1,10
        XTOT=XTOT+X(I)
   10 CONTINUE
      DO 20 I=1,10
        XN(I)=X(I)/XTOT
   20 CONTINUE
      RETURN
      END
C     ********************************************************
      SUBROUTINE EQCONST(TEMPK,E)
      IMPLICIT DOUBLE PRECISION (A-H,O-Z)
      REAL*8 E(6)
C     CALCULATE KEQ FOR RXNS C-H OF OHMOTO AND KERRICK (1977)
       E(1)=10.0D0**((14751.0D0/TEMPK)-4.5350D0)
       E(2)=10.0D0**((12510.0D0/TEMPK)-0.9790D0*DLOG10(TEMPK)+
     1    0.4830D0)
       E(3)=10.0D0**((41997.0D0/TEMPK)+0.7190D0*DLOG10(TEMPK)-
     1   2.4040D0)
       E(4)=10.0D0**((18929.0D0/TEMPK)-3.7830D0)
       E(5)=10.0D0**((4757.0D0/TEMPK)-4.0960D0)
       E(6)=10.0D0**((-8117.0D0/TEMPK)+0.188D0*DLOG10(TEMPK)-
     1   0.352D0)
      RETURN
      END
C     ********************************************************
      SUBROUTINE FUSER(X,XN,XTOT,TK,VMM,ETOT,B,C,XKEQ,GAMMA,PATM)
      IMPLICIT DOUBLE PRECISION (A-H,O-Z)
      REAL*8 X(10),B(10),ATOT(10),GAMMA(10),XKEQ(6),ETOT(4),
     1    C(6),XN(10)
C     BSUM AND ASUM ARE MIXING TERMS CALCULATED FROM HOLLOWAY (1981)
C     ATOT(I) IS THE CONTRIBUTION OF SPECIES 'I' TO ASUM
      CALL MRKMIX(TK,XN,BSUM,ASUM,ATOT)
C     CALCULATE PRESSURE FROM MRK
      R=82.05D0
      PATM=R*TK/(VMM-BSUM)-ASUM/(DSQRT(TK)*(VMM*VMM+BSUM*VMM))
C     CALCULATE GAMMA(I) = FUGACITY COEFFICIENT OF "I"TH SPECIES
      CALL FUGCAL(PATM,TK,XN,ASUM,BSUM,VMM,ATOT,GAMMA)
      DO 676 I=1,10
      WRITE(9,*) GAMMA(I)
  676 CONTINUE
      WRITE(9,*) ASUM,BSUM,PATM,VMM,R,TK
      CALL CONST(GAMMA,XKEQ,PATM,C)
      B(1)=XTOT*C(1)*XN(1)/DSQRT(XN(8))-X(2)
      B(2)=XTOT*C(2)*XN(5)/DSQRT(XN(8))-X(4)
      B(3)=XTOT*C(3)*XN(1)*(XN(5)/XN(8))**2-X(3)
      B(4)=XTOT*C(4)*DSQRT(XN(9))*XN(8)-X(7)
      B(5)=XTOT*C(5)*XN(2)*DSQRT(XN(9))-X(10)
      B(6)=XTOT*C(6)*XN(5)*DSQRT(XN(9)/XN(8))-X(6)
      B(7)=X(1)+X(2)+X(3)+X(10)-ETOT(1)
```

```
      B(8)=X(5)+X(10)+X(2)+2.0D0*(X(8)+X(1)+X(7))-ETOT(2)
      B(9)=2.0D0*(X(5)+X(4)+X(6))+4.0D0*X(3)-ETOT(3)
      B(10)=X(6)+X(10)+X(7)+2.0D0*X(9)-ETOT(4)
      RETURN
      END
C     ******************************************************
      SUBROUTINE MRKMIX(T,Y,BSUM,ASUM,ATOT)
      IMPLICIT DOUBLE PRECISION (A-H,O-Z)
      REAL*8 A(10),B(10),Y(10),ATOT(10)
      DATA A/46.D6,16.98D6,31.59D6,3.56D6,35.D6,87.9D6,142.6D6,
     1    17.2D6,882.17D6,128.4D6/
      DATA B/2.97D1,2.738D1,2.9703D1,1.515D1,1.46D1,2.D1,3.94D1,
     1    2.21D1,4.579D1,4.30D1/
      DATA MIXNUM/10/,R/82.05D0/
      IF(T.LT.1.D-4) T=1.D0
      TCEL=T-273.15D0
      R2T=R*R*DSQRT(T**5)
      RT=R*DSQRT(T**3)
      AH2OM=166.8D0-.19308D0*TCEL+.1864D-3*TCEL**2-
     1    .71288D-7*TCEL**3
      IF(TCEL.LT.6.0D2) AH2OM=4.221D3-3.1227D1*TCEL+8.7485D-2
     1    *TCEL**2-1.07295D-4*TCEL**3+4.86111D-8*TCEL**4
      IF(TCEL.GT.1200.0D0) AH2OM=140.0D0-0.05D0*TCEL
      AH2OM=AH2OM*10.D5
      ACO2M=73.03D0-0.0714D0*TCEL+2.157D-5*TCEL**2
      ACO2M=ACO2M*10.D5
      XK=DEXP(-11.071D0+5953.0D0/T-2.746D6/T**2+
     1  4.646D8/T**3)
      CO2H2O=XK*0.5D0*R2T
      CO2H2O=CO2H2O+DSQRT(A(1)*A(5))
      ASUM=0.0D0
      BSUM=0.0D0
      DO 102 I=1,MIXNUM
       BSUM=BSUM+B(I)*Y(I)
       ASUM=0.0D0
       DO 102 J=1,MIXNUM
        IF(I.EQ.J) GO TO 140
        IF(I.EQ.5.AND.J.EQ.1) GO TO 150
        IF(I.EQ.1.AND.J.EQ.5) GO TO 150
        ASUM=ASUM+Y(I)*Y(J)*DSQRT(A(I)*A(J))
        GO TO 101
140     IF(I.NE.5) GO TO 141
        ASUM=ASUM+Y(I)*Y(J)*AH2OM
        GO TO 101
141   IF(I.NE.1) GO TO 142
        ASUM=ASUM+Y(I)*Y(J)*ACO2M
        GO TO 101
142   ASUM=ASUM+Y(I)*Y(J)*A(I)
        GO TO 101
150   ASUM=ASUM+Y(I)*Y(J)*CO2H2O
```

```
 101   CONTINUE
         ATOT(I)=ASUM
 102 CONTINUE
       ASUM=ATOT(1)+ATOT(2)+ATOT(3)+ATOT(4)+
     1    ATOT(5)+ATOT(6)+ATOT(7)+ATOT(8)+ATOT(9)+ATOT(10)
       RETURN
       END
C      ************************************************************
       SUBROUTINE FUGCAL(PP,T,Y,ASUM,BSUM,VMM,ATOT,FUGCOF)
       IMPLICIT DOUBLE PRECISION (A-H, O-Z)
       REAL*8 Y(10),ATOT(10),BI(10),FUGCOF(10)
       DATA BI/2.97D1,2.738D1,2.9703D1,1.515D1,1.46D1,2.D1,3.94D1,
     1    2.21D1,4.579D1,4.30D1/
       R=82.05D0
       DO 180 I=1,10
        FUGCOF(I)=1.0D0
        IF(Y(I).EQ.0.0D0) GO TO 180
        QA=DLOG(VMM/(VMM-BSUM))
        QB=BI(I)/(VMM-BSUM)
        QC=2.0D0*(ATOT(I)/Y(I))/(R*DSQRT(T**3)*BSUM)
        QD=DLOG((VMM+BSUM)/VMM)
        QE=ASUM*BI(I)/(BSUM*BSUM*R*DSQRT(T**3))
        QF=QD
        QG=BSUM/(BSUM+VMM)
        QH=DLOG(PP*VMM/(R*T))
        FUGCOF(I)=DEXP(QA+QB-(QC*QD)+QE*(QF-QG)-QH)
 180   CONTINUE
       RETURN
       END
C      ************************************************************
       SUBROUTINE CONST(G,E,PATM,C)
       IMPLICIT DOUBLE PRECISION (A-H,O-Z)
       REAL*8 G(10),E(6),C(6)
       C(1)=G(1)/(E(1)*G(2)*DSQRT(G(8)*PATM))
       C(2)=G(5)/(E(2)*G(4)*DSQRT(G(8)*PATM))
       C(3)=G(1)*G(5)**2/(E(3)*G(3)*G(8)**2)
       C(4)=DSQRT(G(9)*PATM)*G(8)*E(4)/G(7)
       C(5)=G(2)*DSQRT(G(9)*PATM)*E(5)/G(10)
       C(6)=E(6)*G(5)*DSQRT(G(9)/G(8))/G(6)
       RETURN
       END
C      ************************************************************
       SUBROUTINE MATRIX(D,XTOT,C,J)
       IMPLICIT DOUBLE PRECISION (A-H,O-Z)
       REAL*8 D(10),C(6),J(10,10)
       DO 15 I=1,10
        DO 15 K=1,10
         J(I,K)=0.0D0
  15   CONTINUE
       DO 17 I=1,6
```

```
      J(I,I)=-1.0D0
   17 CONTINUE
      J(1,7)=DSQRT(XTOT)*C(1)/DSQRT(D(8))
      J(1,8)=-0.5D0*DSQRT(XTOT)*C(1)*D(1)/DSQRT(D(8)**3)
      J(2,8)=-0.5D0*DSQRT(XTOT)*C(2)*D(5)/DSQRT(D(8)**3)
      J(2,9)=DSQRT(XTOT)*C(2)/DSQRT(D(8))
      J(3,7)=C(3)*D(5)**2/D(8)**2
      J(3,8)=-2.0D0*C(3)*D(1)*D(5)**2/D(8)**3
      J(3,9)=2.0D0*C(3)*D(1)*D(5)/D(8)**2
      J(4,8)=C(4)*DSQRT(D(9))/DSQRT(XTOT)
      J(4,10)=0.5D0*C(4)*D(8)/DSQRT(D(9)*XTOT)
      J(5,1)=C(5)*DSQRT(D(9))/DSQRT(XTOT)
      J(5,10)=0.5D0*C(5)*D(2)/DSQRT(D(9)*XTOT)
      J(6,8)=-0.5D0*C(6)*D(5)*DSQRT(D(9))/DSQRT(D(8)**3)
      J(6,9)=C(6)*DSQRT(D(9)/D(8))
      J(6,10)=0.5D0*C(6)*D(5)/DSQRT(D(9)*D(8))
      J(7,1)=1.0D0
      J(7,3)=1.0D0
      J(7,5)=1.0D0
      J(7,7)=1.0D0
      J(8,1)=1.0D0
      J(8,4)=2.0D0
      J(8,5)=1.0D0
      J(8,7)=2.0D0
      J(8,8)=2.0D0
      J(8,9)=1.0D0
      J(9,2)=2.0D0
      J(9,3)=4.0D0
      J(9,6)=2.0D0
      J(9,9)=2.0D0
      J(10,4)=1.0D0
      J(10,5)=1.0D0
      J(10,6)=1.0D0
      J(10,10)=2.0D0
      RETURN
      END
C     ************************************************************
      SUBROUTINE LUDCMP(A,N,NP,INDX,D)
      IMPLICIT DOUBLE PRECISION (A-H,O-Z)
      PARAMETER (NMAX=100,TINY=1.0E-35)
      DIMENSION A(NP,NP),INDX(N),VV(NMAX)
      D=1.0D0
      DO 12 I=1,N
      AAMAX=0.0D0
      DO 11 J=1,N
      IF (DABS(A(I,J)).GT.AAMAX) AAMAX=DABS(A(I,J))
   11 CONTINUE
      IF (AAMAX.EQ.0.0D0) PAUSE 'SINGULAR MATRIX.'
      VV(I)=1.0D0/AAMAX
   12 CONTINUE
```

```
      DO 19 J=1,N
      IF (J.GT.1) THEN
      DO 14 I=1,J-1
      SUM=A(I,J)
      IF (I.GT.1)THEN
      DO 13 K=1,I-1
      SUM=SUM-A(I,K)*A(K,J)
   13 CONTINUE
      A(I,J)=SUM
      ENDIF
   14 CONTINUE
      ENDIF
      AAMAX=0.0D0
      DO 16 I=J,N
      SUM=A(I,J)
      IF (J.GT.1)THEN
      DO 15 K=1,J-1
      SUM=SUM-A(I,K)*A(K,J)
   15 CONTINUE
      A(I,J)=SUM
      ENDIF
      DUM=VV(I)*DABS(SUM)
      IF (DUM.GE.AAMAX) THEN
      IMAX=I
      AAMAX=DUM
      ENDIF
   16 CONTINUE
      IF (J.NE.IMAX)THEN
      DO 17 K=1,N
      DUM=A(IMAX,K)
      A(IMAX,K)=A(J,K)
      A(J,K)=DUM
   17 CONTINUE
      D=-D
      VV(IMAX)=VV(J)
      ENDIF
      INDX(J)=IMAX
      IF(J.NE.N)THEN
      IF(A(J,J).EQ.0.0D0)A(J,J)=TINY
      DUM=1.0D0/A(J,J)
      DO 18 I=J+1,N
      A(I,J)=A(I,J)*DUM
   18 CONTINUE
      ENDIF
   19 CONTINUE
      IF(A(N,N).EQ.0.0D0)A(N,N)=TINY
      RETURN
      END
C     ************************************************************
```

```
      SUBROUTINE LUBKSB(A,N,NP,INDX,B)
      IMPLICIT DOUBLE PRECISION (A-H,O-Z)
      DIMENSION A(NP,NP),INDX(N),B(N)
      II=0
      DO 12 I=1,N
      LL=INDX(I)
      SUM=B(LL)
      B(LL)=B(I)
      IF (II.NE.0)THEN
      DO 11 J=II,I-1
      SUM=SUM-A(I,J)*B(J)
   11 CONTINUE
      ELSE IF (SUM.NE.0.0D0) THEN
      II=I
      ENDIF
      B(I)=SUM
   12 CONTINUE
      DO 14 I=N,1,-1
      SUM=B(I)
      IF(I.LT.N)THEN
      DO 13 J=I+1,N
      SUM=SUM-A(I,J)*B(J)
   13 CONTINUE
      ENDIF
      B(I)=SUM/A(I,J)
   14 CONTINUE.
      RETURN
      END
C     ****************************************************************
      SUBROUTINE OKSPECN(X,VM)
      IMPLICIT DOUBLE PRECISION (A-H,O-Z)
      REAL*8 X(10),FUGCOF(10),GAM(10),XN(10),WW(10)
      WRITE (9,1)
    1 FORMAT ('ENTER PRESSURE IN BARS AND TEMP IN DEGREES C')
      READ (9,*) PBARS,TEMPC
       PATM=PBARS/1.01325D0
       TEMPK=TEMPC+273.15D0
      WRITE (9,2)
    2 FORMAT ('ENTER LOG FO2 AND LOG FS2 IN BARS OR ENTER ZERO(S)'/,
     1    'TO SPECIFY BUFFER(S)')
      READ(9,*) SLGFO2,SLGFS2
      IF(SLGFO2.EQ.0.D0) CALL OXYBUF(TEMPK,PBARS,PATM,SLGFO2,JOBF)
       OXFUG=10.0D0**SLGFO2/1.01325D0
      IF(SLGFS2.EQ.0.D0) CALL SLFBUF(TEMPC,TEMPK,PATM,SLGFS2,JSBF)
       SULFUG=10.0D0**SLGFS2
      WRITE(9,3)
    3 FORMAT('ENTER AN ACTIVITY OF CARBON BETWEEN 0 AND 1'/,
     1    'AN ACTIVITY OF 1 IMPLIES THAT GRAPHITE EXISTS')
      READ(9,*) ACTC
C     EQUILIBRIUM CONSTANTS FROM OHMOTO AND KERRICK
```

```
      EQA=1.0D0/DSQRT(SULFUG)
      EQB=10.0D0**(20586.0D0/TEMPK+0.0421D0+0.028D0*
     1   (PATM-1.0D0)/TEMPK)
      EQC=10.0D0**(14751.0D0/TEMPK-4.535D0)
      EQD=10.0D0**(12510.0D0/TEMPK-0.979D0*DLOG10(TEMPK)+0.483D0)
      EQE=10.0D0**(41997.0D0/TEMPK+0.719D0*DLOG10(TEMPK)-2.404D0)
      EQF=10.0D0**(18929.0D0/TEMPK-3.783D0)
      EQG=10.0D0**(4757.0D0/TEMPK-4.096D0)
      EQH=10.0D0**(-8117.0D0/TEMPK+0.188D0*DLOG10(TEMPK)-0.352D0)
      CALL IDEALM(TEMPK,TEMPC,PBARS,PATM,GAM)
      DO 115 I=1,10
       WRITE(9,*) GAM(I)
       WRITE(8,*) GAM(I)
  115 CONTINUE
      DO 117 I=1,10
       WW(I)=0.0D0
  117 CONTINUE
  120 DO 1000 ICOUNT=1,100
      IF(ICOUNT.EQ.1) GO TO 125
      DO 122 I=1,10
       WW(I)=X(I)
  122 CONTINUE
  125  X(1)=EQB*OXFUG*ACTC/(GAM(1)*PATM)
      IF(X(1).GT.1.0D0) THEN
       WRITE (9,130)
  130  FORMAT ('CONDITIONS ARE TOO OXIDIZING FOR GRAPHITE TO'/,
     1   'EXIST; SPECIFY NEW CARBON ACTIVITY BETWEEN 0 AND 1')
       READ (9,*) ACTC
       GO TO 125
      END IF
       X(2)=GAM(1)*X(1)/(EQC*GAM(2)*DSQRT(OXFUG))
       X(7)=EQF*OXFUG/(EQA*GAM(7)*PATM)
       X(8)=OXFUG/(GAM(8)*PATM)
       X(9)=SULFUG/(GAM(9)*PATM)
       X(10)=EQG*GAM(2)*X(2)/(EQA*GAM(10))
       EQ4=GAM(5)/(EQD*GAM(4)*DSQRT(OXFUG))
       EQ5=GAM(1)*(GAM(5)*PATM)**2/(EQE*GAM(3)*OXFUG**2)
       EQ8=EQH*GAM(5)/(EQA*GAM(6)*DSQRT(OXFUG))
C     CALCULATE XH2O USING THE POSITIVE ROOT OF QUADRATIC
       DSCRNT=(EQ4+EQ8+1.0D0)**2-4.0D0*EQ5*X(1)*(X(1)+
     1   X(2)+X(7)+X(8)+X(9)+X(10)-1.0D0)
      A=EQ5*X(1)
      B=EQ4+EQ8+1.0D0
      C=X(1)+X(2)+X(7)+X(8)+X(9)+X(10)-1.0D0
      IF(DSCRNT.EQ.0.0) THEN
       ROOT1=-B/2.0D0*A
       ROOT2=-1.0D0
      ELSE
       SDSCRN=DSQRT(DSCRNT)
       ROOT1=(-1.0D0*B+SDSCRN)/(2.0D0*A)
```

```
        ROOT2=(-1.0D0*B-SDSCRN)/(2.0D0*A)
       END IF
       IF(ROOT1.LT.0.0) THEN
        X(5)=ROOT2
       ELSE
        X(5)=ROOT1
       END IF
       X(4)=EQ4*X(5)
       X(3)=EQ5*X(1)*X(5)**2
       X(6)=EQ8*X(5)
      CALL NORMAL(X,XN,XTOT)
      DO 920 I=1,10
       X(I)=XN(I)
  920 CONTINUE
      CALL ARDVRK(PBARS,TEMPK,X,VM,FUGCOF)
      DO 925 I=1,10
       GAM(I)=FUGCOF(I)
  925 CONTINUE
      IFLAG=0
      DO 950 I=1,10
       IF(DABS(X(I)-WW(I))/X(I).GT.1.0D-4)IFLAG=1
  950 CONTINUE
        WRITE(9,*)'ITERATION NUMBER ',ICOUNT
        WRITE (9,9) (X(I),I=1,10)
    9   FORMAT(10(1X,D12.5/))
        IF(IFLAG.EQ.0) GO TO 998
 1000 CONTINUE
  998 RETURN
      END
C     ************************************************************
      SUBROUTINE OXYBUF(TEMPK,PBARS,PATM,SLGFO2,JOBF)
      IMPLICIT DOUBLE PRECISION (A-H,O-Z)
      INTEGER JOBF
      WRITE (9,100)
  100 FORMAT ('ENTER 1 FOR H/M, 2 FOR N/NO, 3 FOR QF/M, 4 FOR M/W')
      READ (9,*) JOBF
      IF(JOBF.EQ.1) THEN
        OXFUG=10.D0**(-25632.0D0/TEMPK+14.62D0+0.019D0*
     1   (PBARS-1)/TEMPK)
       ELSE IF(JOBF.EQ.2) THEN
        OXFUG=10.D0**(-24753.5D0/TEMPK+9.141D0+0.046D0*
     1   (PBARS-1)/TEMPK)
       ELSE IF(JOBF.EQ.3) THEN
        OXFUG=(1.0D0/(10.0D0**(25738.0D0/TEMPK-9.0D0-0.092D0*
     1  (PATM-1)/TEMPK)))/1.01325D0
       ELSE
        OXFUG=((1.0D0/(10.0D0**(17157.0D0/TEMPK-7.41D0-0.042D0*
     1  (PATM-1)/TEMPK)))**2)/1.01325D0
      END IF
       SLGFO2=DLOG10(OXFUG)
```

```
      RETURN
      END
C     ************************************************************
      SUBROUTINE SLFBUF(TEMPC,TEMPK,PATM,SLGFS2,JSBF)
      IMPLICIT DOUBLE PRECISION (A-H,O-Z)
      INTEGER JSBF
      WRITE (9,200)
  200 FORMAT ('ENTER 1 FOR PY/PO, 2 FOR PO')
      READ (9,*) JSBF
      IF(JSBF.EQ.1) THEN
        SLGFS2=-24.9343D0+0.0545D0*TEMPC-2.693D-5*TEMPC**2
     1     +0.06D0*(PATM-1.0D0)/TEMPK
      ELSE
      WRITE (9,201)
  201 FORMAT ('ENTER MOLE FRACTION FES IN PYRRHOTITE')
        READ (9,*) AMFES
        AZ=(70.03D0-85.83D0*AMFES)
        BZ=(1000.0D0/TEMPK-1.0D0)
        CZ=39.3D0*DSQRT(1.0D0-0.9981D0*AMFES)
        SLGFS2=AZ*BZ+CZ-11.91D0
      END IF
      RETURN
      END
C     ************************************************************
      SUBROUTINE IDEALM(TEMPK,TEMPC,PBARS,PATM,GAM)
      IMPLICIT DOUBLE PRECISION (A-H,O-Z)
      REAL*8 TR(10),PR(10),TCR(10),PCR(10),GAM(10)
      DATA TCR/304.25D0,132.95D0,190.55D0,41.25D0,647.25D0,
     1   373.55D0,430.65D0,154.75D0,1313.15D0,378.75D0/
      DATA PCR/73.8D0,35.0D0,46.0D0,21.0D0,221.5D0,90.1D0,
     1   78.8D0,50.8D0,206.7D0,63.5D0/
      DO 10 I=1,10
       TR(I)=TEMPK/TCR(I)
       PR(I)=PBARS/PCR(I)
       IF(TR(I).GT.12.D0) THEN
        GAM(I)=1.D0+1.4986D-2*PR(I)-7.015D-4*TR(I)*PR(I)+
     1    1.024D-5*TR(I)**2*PR(I)+1.0787D-4*PR(I)**2-
     2    6.007D-6*TR(I)*PR(I)**2+8.7D-8*TR(I)**2*PR(I)**2
       ENDIF
       IF(TR(I).GT.3.D0.AND.TR(I).LE.12.D0) THEN
        GAM(I)=1.D0+1.24D-2*PR(I)+2.54D-4*TR(I)*PR(I)-5.104D-5*
     1    TR(I)**2*PR(I)+1.1089D-3*PR(I)**2-1.998D-4*TR(I)*
     2    PR(I)**2+9.393D-6*TR(I)**2*PR(I)**2
       ENDIF
       IF(TR(I).GT.0.D0.AND.TR(I).LE.3.D0) THEN
        GAM(I)=1.D0-2.242D-1*PR(I)+1.4667D-1*TR(I)*PR(I)-2.276D-2*
     1    TR(I)**2*PR(I)+8.899D-3*PR(I)**2-5.119D-3*TR(I)*
     2    PR(I)**2+7.86D-4*TR(I)**2*PR(I)**2
       ENDIF
       IF(I.EQ.4.AND.PBARS.LT.3000.D0) THEN
```

```
        SWC1=DEXP(-3.8402D0*TEMPK**0.125D0+0.5410D0)
        SWC2=DEXP(-0.1263D0*DSQRT(TEMPK)-15.980D0)
        SWC3=300.0D0*DEXP(-0.11901D0*TEMPK-5.941D0)
      ALGMH2=SWC1*PATM-SWC2*PATM**2+SWC3*(DEXP(-PATM/300.0D0)-1)
      GAM(4)=DEXP(ALGMH2)
       ENDIF
       IF(I.EQ.1) THEN
        PKB=PBARS/1000.D0
        CNST=18.703218D0-30.004038D0*PKB+15.782754D0*PKB**2-
     1   3.2421026D0*PKB**3+.24980474*PKB**4
        ATERM=-.083597794D0+.13821708D0*PKB-.070776465D0*
     1   PKB**2+.014457271D0*PKB**3-1.0681165D-3*PKB**4
        BTERM=1.2795747D-4-2.0727426D-4*PKB+1.0505277D-4*
     1   PKB**2-2.1212868D-5*PKB**3+1.5251024D-6*PKB**4
        CTERM=-6.2838D-8+1.0053242D-7*PKB-5.0668132D-8*
     1   PKB**2+1.0140221D-8*PKB**3-7.1638184D-10*PKB**4
        GAM(1)=CNST+ATERM*TEMPC+BTERM*TEMPC**2+CTERM*TEMPC**3
       ENDIF
       IF(I.EQ.5) THEN
        CCNST=.31425026D0-.38594999D0*PKB+.19967493D0*PKB**2-
     1    .051474242*PKB**3+7.1493778D-3*PKB**4-
     2     5.0621009D-4*PKB**5+1.4326474D-5*PKB**6
        AATERM=-4.7919973D-3+6.1915716D-3*PKB-3.2539637D-3*
     1  PKB**2+8.4557946D-4*PKB**3-1.1806683D-4*PKB**4+
     2     8.3852276D-6*PKB**5-2.3779833D-7*PKB**6
        BBTERM=1.2450826D-5-1.4262612D-5*PKB+5.6269161D-6*
     1    PKB**2-9.5662335D-7*PKB**3+7.7368676D-8*
     2    PKB**4-2.3373356D-9*PKB**5
        CCTERM=-2.9718201D-9+1.7106038D-8*PKB-7.6196485D-9*PKB**2+
     1    1.3511195D-9*PKB**3-1.1115976D-10*PKB**4+
     2    3.3487236D-12*PKB**5
        DDTERM=-1.5475286D-11-3.1107153D-12*PKB+2.7666352D-12*
     1    PKB**2-5.5248696D-13*PKB**3+4.7086811D-14*PKB**4-
     2    1.386475D-15*PKB**5
        EETERM=1.0069036D-14-2.8496996D-15*PKB+4.2102278D-16*
     1    PKB**2-4.2332381D-17*PKB**3+2.8545359D-18*PKB**4-
     2    1.1765163D-19*PKB**5
        GAM(5)=CCNST+AATERM*TEMPC+BBTERM*TEMPC**2+CCTERM*TEMPC**3+
     1    DDTERM*TEMPC**4+EETERM*TEMPC**5
       ENDIF
C      CALCULATE FUGACITY COEFFICIENT OF S2
        GAM(9)=1.0
   10  CONTINUE
      RETURN
      END
C     ******************************************************
      SUBROUTINE ARDVRK(PP,T,X,VM,FUGCOF)
      IMPLICIT DOUBLE PRECISION (A-H,O-Z)
      DIMENSION X(10),ATOT(10),BI(10),FUG(10),FUGCOF(10)
      DATA RBAR/83.137D0/, MIXNUM/10/
```

```
      DATA BI/2.97D1,2.738D1,2.9703D1,1.515D1,1.46D1,2.D1,3.94D1,
     1    2.21D1,4.579D1,4.30D1/
      CALL MRKMIX(T,X,BSUM,ASUM,ATOT)
C     CUBIC SOLUTION OF THE MRK FOR VOLUME
      RATM=82.05D0
      RR=RATM
      TCEL=T-273.15
      P=-1.0D0*RR*T/PP
      Q=(BSUM*RR*DSQRT(T**3)+BSUM*BSUM*PP*DSQRT(T)-ASUM)/(-1.0D0*
     1    PP*DSQRT(T))
      R=-1.0D0*ASUM*BSUM/(PP*DSQRT(T))
      A=(3.0D0*Q-P*P)/3.0D0
      B=(2.0D0*P**3-9.0D0*P*Q+27.0D0*R)/27.0D0
      V1=1
      V2=1
      V3=1
      ROOT=B*B/4.0D0+A**3/27.0D0
      IF(ROOT) 90,80,70
   70 C=B/-2.0D0+DSQRT(ROOT)
      IF(C) 71,72,72
   71 C=DABS(C)
      AA=-1.0D0*C**(1.0D0/3.0D0)
      GO TO 73
   72 AA=C**(1.0D0/3.0D0)
   73 CONTINUE
      D=B/-2.0D0-DSQRT(ROOT)
      IF(D) 75,76,76
   75 D=DABS(D)
      BB=-1.0D0*D**(1.0D0/3.0D0)
      GO TO 77
   76 BB=D**(1.0D0/3.0D0)
   77 CONTINUE
      X1=AA+BB
      V1=X1-P/3.0D0
      GO TO 100
   80 C=B/-2.0D0+DSQRT(ROOT)
      IF(C) 81,82,82
   81 C=DABS(C)
      AA=-1.0D0*C**(1.0D0/3.0D0)
      GO TO 83
   82 AA=C**(1.0D0/3.0D0)
   83 CONTINUE
      D=B/-2.0D0-DSQRT(ROOT)
      IF(D) 85,86,86
   85 D=DABS(D)
      BB=-1.0D0*D**(1.0D0/3.0D0)
      GO TO 77
   86 BB=D**(1.0D0/3.0D0)
   87 CONTINUE
      X1=AA+BB
```

```
      V1=X1-P/3.0D0
      X2=(AA+BB)/-2.0D0
      V2=X2-P/3.0D0
      GO TO 100
   90 THETA=DACOS(B/-2.0D0/DSQRT(A**3/-27.0D0))
      X1=2.0D0*DSQRT(A/-3.0D0)*DCOS(THETA/3.0D0)
      X2=2.0D0*DSQRT(A/-3.0D0)*DCOS(THETA/3.0D0+120.0D0)
      X3=2.0D0*DSQRT(A/-3.0D0)*DCOS(THETA/3.0D0+240.0D0)
      V1=X1-P/3.0D0
      V2=X2-P/3.0D0
      V3=X3-P/3.0D0
  100 CONTINUE
C     PICK LARGEST OF THE THREE VOLUMES FROM THE CUBIC ROOTS
      VIN=V1-V2
      IF(VIN) 110,110,120
  110 VIN=V2
      GO TO 130
  120 VIN=V1
  130 CONTINUE
      VM=VIN-V3
      IF(VIN) 140,140,150
  140 VM=V3
      GO TO 160
  150 VM=VIN
  160 CONTINUE
C     CALCULATE FUGACITIES FROM CORRECT VERSION OF EQ 108
C     IN FERRY AND BAUMGARNER (REV IN MIN VOL 17)
      AM=ASUM
      BM=BSUM
      DO 180 I=1,MIXNUM
      QA=DLOG(VM/(VM-BM))
      QB=BI(I)/(VM-BM)
      QC=2.0D0*ATOT(I)/X(I)/(RATM*DSQRT(T**3)*BM)
      QD=DLOG((VM+BM)/VM)
      QE=AM*BI(I)/(BM*BM*RATM*DSQRT(T**3))
      QF=QD
      QG=BM/(BM+VM)
      QH=DLOG(PP*VM/(RATM*T))
      FUGCOF(I)=DEXP(QA+QB-QC*QD+QE*(QF-QG)-QH)
  180 CONTINUE
   89 RETURN
      END
```

```
C       ************* PROGRAM SUPERHYDRODIFF ********************11/13/88
C       ************WRITTEN BY DONALD LEWIS HALL**********************
C       USES OHMOTO AND KERRICK PROGRAM TO CALCULATE INITIAL X(I)
C       THEN USES NEWTON'S METHOD FOR NON-LINEAR SYSTEMS TO SOLVE
C       FOR NEW X(I) AT NEW P-T CONDITIONS; THEN ALTERS MASS BALANCE
C       EQUATIONS TO ALLOW FOR HYDROGEN DIFFUSION IN/OUT OF INCLUSION
        IMPLICIT DOUBLE PRECISION (A-H,O-Z)
        REAL*8 A(10,10),B(10),X(10),ETOT(4),C(6),XN(10),
     1     XKEQ(6),W(10),GAMMA(10),ALGFUG(10)
        INTEGER INDX(10),IDIREC
        CHARACTER*80 ZOUT
        N=10
        NP=10
        WRITE(9,5)
    5   FORMAT(//,'ENTER NAME OF OUTPUT FILE')
        READ(9,6) ZOUT
    6   FORMAT(A80)
        OPEN(UNIT=8,FILE=ZOUT)
   44   CONTINUE
C       ORDER OF X IS CO2,CO,CH4,H2,H2O,H2S,SO2,O2,S2,COS
        WRITE (9,50)
   50   FORMAT('ENTER SAMPLE NUMBER, 99 TO QUIT')
        READ (9,*) SAMPLE
        IF(SAMPLE.EQ.99) GO TO 997
        CALL OKSPECN(X,VMM)
        WRITE (8,*) VMM
        WRITE(9,7)
    7   FORMAT('ENTER NEW TEMPERATURE IN DEG. C')
        READ(9,*) TC
        TK=TC+273.15D0
        CALL NORMAL(X,XN,XTOT)
        DO 20 I=1,10
          X(I)=XN(I)
   20   CONTINUE
        VINC=VMM
C       MASS BALANCE EQUATIONS FOR TOTAL C-O-H-S
        ETOT(1)=X(1)+X(2)+X(3)+X(10)
        ETOT(2)=2.0D0*(X(1)+X(7)+X(8))+X(2)+X(5)+X(10)
        ETOT(3)=4.0D0*X(3)+2.0D0*(X(4)+X(5)+X(6))
        ETOT(4)=X(6)+X(7)+2.0D0*X(9)+X(10)
        CALL EQCONST(TK,XKEQ)
C       B(I) = VALUES OF THE 10 EQUATIONS SUBSTITUTING X(I)
C       A(I,J) = JACOBIAN MATRIX
        IDIREC=5
        DELTAH=0.0D0
   25   ICOUNT=0
        DO 999 ICOUNT=1,100
          IF(ICOUNT.EQ.100)THEN
          WRITE(9,2)
    2     FORMAT('EXCEEDED 99 ITERATIONS IN NEWTONS METHOD')
```

```
        PAUSE
      ELSE
        CONTINUE
        ENDIF
        CALL FUSER(X,XN,XTOT,TK,VMM,ETOT,B,C,XKEQ,GAMMA,PATM)
        CALL MATRIX(X,XTOT,C,A)
        DO 30 I=1,10
          B(I)=-B(I)
   30   CONTINUE
        CALL LUDCMP(A,N,NP,INDX,D)
C       A(I,J) IS NOW THE DECOMPOSED JACOBIAN MATRIX
        CALL LUBKSB(A,N,NP,INDX,B)
C       B(I) IS NOW THE UPDATED CORRECTION TO X(I)
        IFLAG=0
        DO 35 I=1,10
          W(I)=X(I)
   35   CONTINUE
        X(1)=X(1)+B(7)
        X(2)=X(2)+B(1)
        X(3)=X(3)+B(3)
        X(4)=X(4)+B(2)
        X(5)=X(5)+B(9)
        X(6)=X(6)+B(6)
        X(7)=X(7)+B(4)
        X(8)=X(8)+B(8)
        X(9)=X(9)+B(10)
        X(10)=X(10)+B(5)
        DO 40 I=1,10
         IF(X(I).LE.0.0D0) X(I)=1.0D-31
         IF(DABS(X(I)-W(I))/X(I).GT.1.0D-04)IFLAG=1
   40   CONTINUE
        CALL NORMAL(X,XN,XTOT)
        VMM=VINC/XTOT
        WRITE(9,*)'ITERATION NUMBER ',ICOUNT
        WRITE (9,1) (X(I),B(I),I=1,10)
    1   FORMAT(10(1X,2D12.5/))
        IF(IFLAG.EQ.0) GO TO 998
  999   CONTINUE
  998   PBARS=PATM*1.01325D0
        DO 55 I=1,10
          ALGFUG(I)=DLOG10(GAMMA(I)*XN(I)*PBARS)
   55   CONTINUE
        WRITE(8,3) (XN(I),ALGFUG(I),I=1,10),XTOT,VMM,TC,PBARS,DELTAH
    3   FORMAT(//,10(1X,2D12.5/),/,F8.5,F8.3,F6.0,F7.0,F8.5)
        WRITE(8,4) ALGFUG(8),ALGFUG(9),ALGFUG(4),(XN(I),I=1,10)
    4   FORMAT(//,2X,D12.5,'R',D12.5,'R',D12.5,'R',10(D12.5,'R'))
        IF(IDIREC.NE.5) GO TO 550
        CALL H2DIFF(ETOT,IDIREC,DELTAH)
        GO TO 25
  550   GO TO 44
```

```
  997  STOP
       END
C      ************************************************************
       SUBROUTINE NORMAL(X,XN,XTOT)
       IMPLICIT DOUBLE PRECISION (A-H,O-Z)
       REAL*8 X(10),XN(10)
       XTOT=0.0D0
       DO 10 I=1,10
         XTOT=XTOT+X(I)
   10  CONTINUE
       DO 20 I=1,10
         XN(I)=X(I)/XTOT
   20  CONTINUE
       RETURN
       END
C      ************************************************************
       SUBROUTINE EQCONST(TEMPK,E)
       IMPLICIT DOUBLE PRECISION (A-H,O-Z)
       REAL*8 E(6)
C      CALCULATE KEQ FOR RXNS C-H OF OHMOTO AND KERRICK (1977)
        E(1)=10.0D0**((14751.0D0/TEMPK)-4.5350D0)
        E(2)=10.0D0**((12510.0D0/TEMPK)-0.9790D0*DLOG10(TEMPK)+
     1    0.4830D0)
        E(3)=10.0D0**((41997.0D0/TEMPK)+0.7190D0*DLOG10(TEMPK)-
     1    2.4040D0)
        E(4)=10.0D0**((18929.0D0/TEMPK)-3.7830D0)
        E(5)=10.0D0**((4757.0D0/TEMPK)-4.0960D0)
        E(6)=10.0D0**((-8117.0D0/TEMPK)+0.188D0*DLOG10(TEMPK)-
     1    0.352D0)
       RETURN
       END
C      ************************************************************
       SUBROUTINE FUSER(X,XN,XTOT,TK,VMM,ETOT,B,C,XKEQ,GAMMA,PATM)
       IMPLICIT DOUBLE PRECISION (A-H,O-Z)
       REAL*8 X(10),B(10),ATOT(10),GAMMA(10),XKEQ(6),ETOT(4),
     1   C(6),XN(10)
C      BSUM AND ASUM ARE MIXING TERMS CALCULATED FROM HOLLOWAY (1981)
C      ATOT(I) IS THE CONTRIBUTION OF SPECIES 'I' TO ASUM
       CALL MRKMIX(TK,XN,BSUM,ASUM,ATOT)
C      CALCULATE PRESSURE FROM MRK
       R=82.05D0
       PATM=R*TK/(VMM-BSUM)-ASUM/(DSQRT(TK)*(VMM*VMM+BSUM*VMM))
C      CALCULATE GAMMA(I) = FUGACITY COEFFICIENT OF "I"TH SPECIES
       CALL FUGCAL(PATM,TK,XN,ASUM,BSUM,VMM,ATOT,GAMMA)
       DO 676 I=1,10
       WRITE(9,*) GAMMA(I)
  676  CONTINUE
       WRITE(9,*) ASUM,BSUM,PATM,VMM,R,TK
       CALL CONST(GAMMA,XKEQ,PATM,C)
       B(1)=XTOT*C(1)*XN(1)/DSQRT(XN(8))-X(2)
```

```
      B(2)=XTOT*C(2)*XN(5)/DSQRT(XN(8))-X(4)
      B(3)=XTOT*C(3)*XN(1)*(XN(5)/XN(8))**2-X(3)
      B(4)=XTOT*C(4)*DSQRT(XN(9))*XN(8)-X(7)
      B(5)=XTOT*C(5)*XN(2)*DSQRT(XN(9))-X(10)
      B(6)=XTOT*C(6)*XN(5)*DSQRT(XN(9)/XN(8))-X(6)
      B(7)=X(1)+X(2)+X(3)+X(10)-ETOT(1)
      B(8)=X(5)+X(10)+X(2)+2.0D0*(X(8)+X(1)+X(7))-ETOT(2)
      B(9)=2.0D0*(X(5)+X(4)+X(6))+4.0D0*X(3)-ETOT(3)
      B(10)=X(6)+X(10)+X(7)+2.0D0*X(9)-ETOT(4)
      RETURN
      END
C     ************************************************************
      SUBROUTINE MRKMIX(T,Y,BSUM,ASUM,ATOT)
      IMPLICIT DOUBLE PRECISION (A-H,O-Z)
      REAL*8 A(10),B(10),Y(10),ATOT(10)
      DATA A/46.D6,16.98D6,31.59D6,3.56D6,35.D6,87.9D6,142.6D6,
     1 17.2D6,882.17D6,128.4D6/
      DATA B/2.97D1,2.738D1,2.9703D1,1.515D1,1.46D1,2.D1,3.94D1,
     1 2.21D1,4.579D1,4.30D1/
      DATA MIXNUM/10/,R/82.05D0/
      IF(T.LT.1.D-4) T=1.D0
      TCEL=T-273.15D0
      R2T=R*R*DSQRT(T**5)
      RT=R*DSQRT(T**3)
      AH2OM=166.8D0-.19308D0*TCEL+.1864D-3*TCEL**2-
     1 .71288D-7*TCEL**3
      IF(TCEL.LT.6.0D2) AH2OM=4.221D3-3.1227D1*TCEL+8.7485D-2
     1  *TCEL**2-1.07295D-4*TCEL**3+4.86111D-8*TCEL**4
      IF(TCEL.GT.1200.0D0) AH2OM=140.0D0-0.05D0*TCEL
      AH2OM=AH2OM*10.D5
      ACO2M=73.03D0-0.0714D0*TCEL+2.157D-5*TCEL**2
      ACO2M=ACO2M*10.D5
      XK=DEXP(-11.071D0+5953.0D0/T-2.746D6/T**2+
     1 4.646D8/T**3)
      CO2H2O=XK*0.5D0*R2T
      CO2H2O=CO2H2O+DSQRT(A(1)*A(5))
      ASUM=0.0D0
      BSUM=0.0D0
      DO 102 I=1,MIXNUM
       BSUM=BSUM+B(I)*Y(I)
       ASUM=0.0D0
       DO 102 J=1,MIXNUM
        IF(I.EQ.J) GO TO 140
        IF(I.EQ.5.AND.J.EQ.1) GO TO 150
        IF(I.EQ.1.AND.J.EQ.5) GO TO 150
        ASUM=ASUM+Y(I)*Y(J)*DSQRT(A(I)*A(J))
        GO TO 101
  140   IF(I.NE.5) GO TO 141
        ASUM=ASUM+Y(I)*Y(J)*AH2OM
        GO TO 101
```

```
  141   IF(I.NE.1) GO TO 142
          ASUM=ASUM+Y(I)*Y(J)*ACO2M
          GO TO 101
  142   ASUM=ASUM+Y(I)*Y(J)*A(I)
          GO TO 101
  150   ASUM=ASUM+Y(I)*Y(J)*CO2H2O
  101   CONTINUE
          ATOT(I)=ASUM
 102 CONTINUE
        ASUM=ATOT(1)+ATOT(2)+ATOT(3)+ATOT(4)+
     1   ATOT(5)+ATOT(6)+ATOT(7)+ATOT(8)+ATOT(9)+ATOT(10)
        RETURN
        END
C       ************************************************************
        SUBROUTINE FUGCAL(PP,T,Y,ASUM,BSUM,VMM,ATOT,FUGCOF)
        IMPLICIT DOUBLE PRECISION (A-H, O-Z)
        REAL*8 Y(10),ATOT(10),BI(10),FUGCOF(10)
        DATA BI/2.97D1,2.738D1,2.9703D1,1.515D1,1.46D1,2.D1,3.94D1,
     1   2.21D1,4.579D1,4.30D1/
        R=82.05D0
        DO 180 I=1,10
         FUGCOF(I)=1.0D0
         IF(Y(I).EQ.0.0D0) GO TO 180
         QA=DLOG(VMM/(VMM-BSUM))
         QB=BI(I)/(VMM-BSUM)
         QC=2.0D0*(ATOT(I)/Y(I))/(R*DSQRT(T**3)*BSUM)
         QD=DLOG((VMM+BSUM)/VMM)
         QE=ASUM*BI(I)/(BSUM*BSUM*R*DSQRT(T**3))
         QF=QD
         QG=BSUM/(BSUM+VMM)
         QH=DLOG(PP*VMM/(R*T))
         FUGCOF(I)=DEXP(QA+QB-(QC*QD)+QE*(QF-QG)-QH)
  180   CONTINUE
        RETURN
        END
C       ************************************************************
        SUBROUTINE CONST(G,E,PATM,C)
        IMPLICIT DOUBLE PRECISION (A-H,O-Z)
        REAL*8 G(10),E(6),C(6)
        C(1)=G(1)/(E(1)*G(2)*DSQRT(G(8)*PATM))
        C(2)=G(5)/(E(2)*G(4)*DSQRT(G(8)*PATM))
        C(3)=G(1)*G(5)**2/(E(3)*G(3)*G(8)**2)
        C(4)=DSQRT(G(9)*PATM)*G(8)*E(4)/G(7)
        C(5)=G(2)*DSQRT(G(9)*PATM)*E(5)/G(10)
        C(6)=E(6)*G(5)*DSQRT(G(9)/G(8))/G(6)
        RETURN
        END
C       ************************************************************
        SUBROUTINE MATRIX(D,XTOT,C,J)
        IMPLICIT DOUBLE PRECISION (A-H,O-Z)
```

```
      REAL*8 D(10),C(6),J(10,10)
      DO 15 I=1,10
       DO 15 K=1,10
        J(I,K)=0.0D0
   15 CONTINUE
      DO 17 I=1,6
       J(I,I)=-1.0D0
   17 CONTINUE
      J(1,7)=DSQRT(XTOT)*C(1)/DSQRT(D(8))
      J(1,8)=-0.5D0*DSQRT(XTOT)*C(1)*D(1)/DSQRT(D(8)**3)
      J(2,8)=-0.5D0*DSQRT(XTOT)*C(2)*D(5)/DSQRT(D(8)**3)
      J(2,9)=DSQRT(XTOT)*C(2)/DSQRT(D(8))
      J(3,7)=C(3)*D(5)**2/D(8)**2
      J(3,8)=-2.0D0*C(3)*D(1)*D(5)**2/D(8)**3
      J(3,9)=2.0D0*C(3)*D(1)*D(5)/D(8)**2
      J(4,8)=C(4)*DSQRT(D(9))/DSQRT(XTOT)
      J(4,10)=0.5D0*C(4)*D(8)/DSQRT(D(9)*XTOT)
      J(5,1)=C(5)*DSQRT(D(9))/DSQRT(XTOT)
      J(5,10)=0.5D0*C(5)*D(2)/DSQRT(D(9)*XTOT)
      J(6,8)=-0.5D0*C(6)*D(5)*DSQRT(D(9))/DSQRT(D(8)**3)
      J(6,9)=C(6)*DSQRT(D(9)/D(8))
      J(6,10)=0.5D0*C(6)*D(5)/DSQRT(D(9)*D(8))
      J(7,1)=1.0D0
      J(7,3)=1.0D0
      J(7,5)=1.0D0
      J(7,7)=1.0D0
      J(8,1)=1.0D0
      J(8,4)=2.0D0
      J(8,5)=1.0D0
      J(8,7)=2.0D0
      J(8,8)=2.0D0
      J(8,9)=1.0D0
      J(9,2)=2.0D0
      J(9,3)=4.0D0
      J(9,6)=2.0D0
      J(9,9)=2.0D0
      J(10,4)=1.0D0
      J(10,5)=1.0D0
      J(10,6)=1.0D0
      J(10,10)=2.0D0
      RETURN
      END
C     ************************************************************
      SUBROUTINE LUDCMP(A,N,NP,INDX,D)
      IMPLICIT DOUBLE PRECISION (A-H,O-Z)
      PARAMETER (NMAX=100,TINY=1.0E-35)
      DIMENSION A(NP,NP),INDX(N),VV(NMAX)
      D=1.0D0
      DO 12 I=1,N
      AAMAX=0.0D0
```

```
      DO 11 J=1,N
      IF (DABS(A(I,J)).GT.AAMAX) AAMAX=DABS(A(I,J))
11    CONTINUE
      IF (AAMAX.EQ.0.0D0) PAUSE 'SINGULAR MATRIX.'
      VV(I)=1.0D0/AAMAX
12    CONTINUE
      DO 19 J=1,N
      IF (J.GT.1) THEN
      DO 14 I=1,J-1
      SUM=A(I,J)
      IF (I.GT.1)THEN
      DO 13 K=1,I-1
      SUM=SUM-A(I,K)*A(K,J)
13    CONTINUE
      A(I,J)=SUM
      ENDIF
14    CONTINUE
      ENDIF
      AAMAX=0.0D0
      DO 16 I=J,N
      SUM=A(I,J)
      IF (J.GT.1)THEN
      DO 15 K=1,J-1
      SUM=SUM-A(I,K)*A(K,J)
15    CONTINUE
      A(I,J)=SUM
      ENDIF
      DUM=VV(I)*DABS(SUM)
      IF (DUM.GE.AAMAX) THEN
      IMAX=I
      AAMAX=DUM
      ENDIF
16    CONTINUE
      IF (J.NE.IMAX)THEN
      DO 17 K=1,N
      DUM=A(IMAX,K)
      A(IMAX,K)=A(J,K)
      A(J,K)=DUM
17    CONTINUE
      D=-D
      VV(IMAX)=VV(J)
      ENDIF
      INDX(J)=IMAX
      IF(J.NE.N)THEN
      IF(A(J,J).EQ.0.0D0)A(J,J)=TINY
      DUM=1.0D0/A(J,J)
      DO 18 I=J+1,N
      A(I,J)=A(I,J)*DUM
18    CONTINUE
      ENDIF
```

```
 19   CONTINUE
      IF(A(N,N).EQ.0.0D0)A(N,N)=TINY
      RETURN
      END
C     ********************************************************

      SUBROUTINE LUBKSB(A,N,NP,INDX,B)
      IMPLICIT DOUBLE PRECISION (A-H,O-Z)
      DIMENSION A(NP,NP),INDX(N),B(N)
      II=0
      DO 12 I=1,N
      LL=INDX(I)
      SUM=B(LL)
      B(LL)=B(I)
      IF (II.NE.0)THEN
      DO 11 J=II,I-1
      SUM=SUM-A(I,J)*B(J)
 11   CONTINUE
      ELSE IF (SUM.NE.0.0D0) THEN
      II=I
      ENDIF
      B(I)=SUM
 12   CONTINUE
      DO 14 I=N,1,-1
      SUM=B(I)
      IF(I.LT.N)THEN
      DO 13 J=I+1,N
      SUM=SUM-A(I,J)*B(J)
 13   CONTINUE
      ENDIF
      B(I)=SUM/A(I,I)
 14   CONTINUE
      RETURN
      END
C     ********************************************************************
      SUBROUTINE OKSPECN(X,VM)
      IMPLICIT DOUBLE PRECISION (A-H,O-Z)
      REAL*8 X(10),FUGCOF(10),GAM(10),XN(10),WW(10)
      WRITE (9,1)
  1   FORMAT ('ENTER PRESSURE IN BARS AND TEMP IN DEGREES C')
      READ (9,*) PBARS,TEMPC
       PATM=PBARS/1.01325D0
       TEMPK=TEMPC+273.15D0
      WRITE (9,2)
  2   FORMAT ('ENTER LOG FO2 AND LOG FS2 IN BARS OR ENTER ZERO(S)'/,
     1    'TO SPECIFY BUFFER(S)')
      READ(9,*) SLGFO2,SLGFS2
      IF(SLGFO2.EQ.0.D0) CALL OXYBUF(TEMPK,PBARS,PATM,SLGFO2,JOBF)
       OXFUG=10.0D0**SLGFO2/1.01325D0
      IF(SLGFS2.EQ.0.D0) CALL SLFBUF(TEMPC,TEMPK,PATM,SLGFS2,JSBF)
```

```
      SULFUG=10.0D0**SLGFS2
      WRITE(9,3)
    3 FORMAT('ENTER AN ACTIVITY OF CARBON BETWEEN 0 AND 1'/,
     1   'AN ACTIVITY OF 1 IMPLIES THAT GRAPHITE EXISTS')
      READ(9,*) ACTC
C     EQUILIBRIUM CONSTANTS FROM OHMOTO AND KERRICK
      EQA=1.0D0/DSQRT(SULFUG)
      EQB=10.0D0**(20586.0D0/TEMPK+0.0421D0+0.028D0*
     1  (PATM-1.0D0)/TEMPK)
      EQC=10.0D0**(14751.0D0/TEMPK-4.535D0)
      EQD=10.0D0**(12510.0D0/TEMPK-0.979D0*DLOG10(TEMPK)+0.483D0)
      EQE=10.0D0**(41997.0D0/TEMPK+0.719D0*DLOG10(TEMPK)-2.404D0)
      EQF=10.0D0**(18929.0D0/TEMPK-3.783D0)
      EQG=10.0D0**(4757.0D0/TEMPK-4.096D0)
      EQH=10.0D0**(-8117.0D0/TEMPK+0.188D0*DLOG10(TEMPK)-0.352D0)
      CALL IDEALM(TEMPK,TEMPC,PBARS,PATM,GAM)
      DO 115 I=1,10
       WRITE(9,*) GAM(I)
       WRITE(8,*) GAM(I)
  115 CONTINUE
      DO 117 I=1,10
       WW(I)=0.0D0
  117 CONTINUE
  120 DO 1000 ICOUNT=1,100
      IF(ICOUNT.EQ.1) GO TO 125
      DO 122 I=1,10
       WW(I)=X(I)
  122 CONTINUE
  125  X(1)=EQB*OXFUG*ACTC/(GAM(1)*PATM)
      IF(X(1).GT.1.0D0) THEN
       WRITE (9,130)
  130  FORMAT ('CONDITIONS ARE TOO OXIDIZING FOR GRAPHITE TO'/,
     1   'EXIST; SPECIFY NEW CARBON ACTIVITY BETWEEN 0 AND 1')
       READ (9,*) ACTC
       GO TO 125
      END IF
       X(2)=GAM(1)*X(1)/(EQC*GAM(2)*DSQRT(OXFUG))
       X(7)=EQF*OXFUG/(EQA*GAM(7)*PATM)
       X(8)=OXFUG/(GAM(8)*PATM)
       X(9)=SULFUG/(GAM(9)*PATM)
       X(10)=EQG*GAM(2)*X(2)/(EQA*GAM(10))
       EQ4=GAM(5)/(EQD*GAM(4)*DSQRT(OXFUG))
       EQ5=GAM(1)*(GAM(5)*PATM)**2/(EQE*GAM(3)*OXFUG**2)
       EQ8=EQH*GAM(5)/(EQA*GAM(6)*DSQRT(OXFUG))
C     CALCULATE XH2O USING THE POSITIVE ROOT OF QUADRATIC
       DSCRNT=(EQ4+EQ8+1.0D0)**2-4.0D0*EQ5*X(1)*(X(1)+
     1   X(2)+X(7)+X(8)+X(9)+X(10)-1.0D0)
       A=EQ5*X(1)
       B=EQ4+EQ8+1.0D0
       C=X(1)+X(2)+X(7)+X(8)+X(9)+X(10)-1.0D0
```

```
      IF(DSCRNT.EQ.0.0) THEN
       ROOT1=-B/2.0D0*A
       ROOT2=-1.0D0
      ELSE
       SDSCRN=DSQRT(DSCRNT)
       ROOT1=(-1.0D0*B+SDSCRN)/(2.0D0*A)
       ROOT2=(-1.0D0*B-SDSCRN)/(2.0D0*A)
      END IF
      IF(ROOT1.LT.0.0) THEN
       X(5)=ROOT2
      ELSE
       X(5)=ROOT1
      END IF

      X(4)=EQ4*X(5)
      X(3)=EQ5*X(1)*X(5)**2
      X(6)=EQ8*X(5)
     CALL NORMAL(X,XN,XTOT)
     DO 920 I=1,10
      X(I)=XN(I)
  920 CONTINUE
     CALL ARDVRK(PBARS,TEMPK,X,VM,FUGCOF)
     DO 925 I=1,10
      GAM(I)=FUGCOF(I)
  925 CONTINUE
     IFLAG=0
     DO 950 I=1,10
      IF(DABS(X(I)-WW(I))/X(I).GT.1.0D-4)IFLAG=1
  950 CONTINUE
       WRITE(9,*)'ITERATION NUMBER ',ICOUNT
       WRITE (9,9) (X(I),I=1,10)
    9  FORMAT(10(1X,D12.5/))
       IF(IFLAG.EQ.0) GO TO 998
 1000 CONTINUE
  998 RETURN
     END
C    ************************************************************
     SUBROUTINE OXYBUF(TEMPK,PBARS,PATM,SLGFO2,JOBF)
     IMPLICIT DOUBLE PRECISION (A-H,O-Z)
     INTEGER JOBF
     WRITE (9,100)
  100 FORMAT ('ENTER 1 FOR H/M, 2 FOR N/NO, 3 FOR QF/M, 4 FOR M/W')
     READ (9,*) JOBF
     IF(JOBF.EQ.1) THEN
       OXFUG=10.D0**(-25632.0D0/TEMPK+14.62D0+0.019D0*
    1   (PBARS-1)/TEMPK)
      ELSE IF(JOBF.EQ.2) THEN
       OXFUG=10.D0**(-24753.5D0/TEMPK+9.141D0+0.046D0*
    1   (PBARS-1)/TEMPK)
     ELSE IF(JOBF.EQ.3) THEN
```

```
        OXFUG=(1.0D0/(10.0D0**(25738.0D0/TEMPK-9.0D0-0.092D0*
     1   (PATM-1)/TEMPK)))/1.01325D0
        ELSE
         OXFUG=((1.0D0/(10.0D0**(17157.0D0/TEMPK-7.41D0-0.042D0*
     1   (PATM-1)/TEMPK)))**2)/1.01325D0
       END IF
        SLGFO2=DLOG10(OXFUG)
       RETURN
       END
C      ***************************************************************
       SUBROUTINE SLFBUF(TEMPC,TEMPK,PATM,SLGFS2,JSBF)
       IMPLICIT DOUBLE PRECISION (A-H,O-Z)
       INTEGER JSBF
       WRITE (9,200)
  200  FORMAT ('ENTER 1 FOR PY/PO, 2 FOR PO')
       READ (9,*) JSBF
       IF(JSBF.EQ.1) THEN
         SLGFS2=-24.9343D0+0.0545D0*TEMPC-2.693D-5*TEMPC**2
     1      +0.06D0*(PATM-1.0D0)/TEMPK
       ELSE
       WRITE (9,201)
  201  FORMAT ('ENTER MOLE FRACTION FES IN PYRRHOTITE')
         READ (9,*) AMFES
         AZ=(70.03D0-85.83D0*AMFES)
         BZ=(1000.0D0/TEMPK-1.0D0)
         CZ=39.3D0*DSQRT(1.0D0-0.9981D0*AMFES)
         SLGFS2=AZ*BZ+CZ-11.91D0
       END IF
       RETURN
       END
C      ***************************************************************
       SUBROUTINE IDEALM(TEMPK,TEMPC,PBARS,PATM,GAM)
       IMPLICIT DOUBLE PRECISION (A-H,O-Z)
       REAL*8 TR(10),PR(10),TCR(10),PCR(10),GAM(10)
       DATA TCR/304.25D0,132.95D0,190.55D0,41.25D0,647.25D0,
     1    373.55D0,430.65D0,154.75D0,1313.15D0,378.75D0/
       DATA PCR/73.8D0,35.0D0,46.0D0,21.0D0,221.5D0,90.1D0,
     1    78.8D0,50.8D0,206.7D0,63.5D0/
       DO 10 I=1,10
        TR(I)=TEMPK/TCR(I)
        PR(I)=PBARS/PCR(I)
        IF(TR(I).GT.12.D0) THEN
         GAM(I)=1.D0+1.4986D-2*PR(I)-7.015D-4*TR(I)*PR(I)+
     1   1.024D-5*TR(I)**2*PR(I)+1.0787D-4*PR(I)**2-
     2    6.007D-6*TR(I)*PR(I)**2+8.7D-8*TR(I)**2*PR(I)**2
        ENDIF
        IF(TR(I).GT.3.D0.AND.TR(I).LE.12.D0) THEN
         GAM(I)=1.D0+1.24D-2*PR(I)+2.54D-4*TR(I)*PR(I)-5.104D-5*
     1     TR(I)**2*PR(I)+1.1089D-3*PR(I)**2-1.998D-4*TR(I)*
     2     PR(I)**2+9.393D-6*TR(I)**2*PR(I)**2
```

```
      ENDIF
      IF(TR(I).GT.0.D0.AND.TR(I).LE.3.D0) THEN
       GAM(I)=1.D0-2.242D-1*PR(I)+1.4667D-1*TR(I)*PR(I)-2.276D-2*
     1   TR(I)**2*PR(I)+8.899D-3*PR(I)**2-5.119D-3*TR(I)*
     2   PR(I)**2+7.86D-4*TR(I)**2*PR(I)**2
      ENDIF
      IF(I.EQ.4.AND.PBARS.LT.3000.D0) THEN
       SWC1=DEXP(-3.8402D0*TEMPK**0.125D0+0.5410D0)
       SWC2=DEXP(-0.1263D0*DSQRT(TEMPK)-15.980D0)
       SWC3=300.0D0*DEXP(-0.11901D0*TEMPK-5.941D0)
      ALGMH2=SWC1*PATM-SWC2*PATM**2+SWC3*(DEXP(-PATM/300.0D0)-1)
      GAM(4)=DEXP(ALGMH2)
      ENDIF
      IF(I.EQ.1) THEN
       PKB=PBARS/1000.D0
       CNST=18.703218D0-30.004038D0*PKB+15.782754D0*PKB**2-
     1   3.2421026D0*PKB**3+.24980474*PKB**4
       ATERM=-.083597794D0+.13821708D0*PKB-.070776465D0*
     1   PKB**2+.014457271D0*PKB**3-1.0681165D-3*PKB**4
       BTERM=1.2795747D-4-2.0727426D-4*PKB+1.0505277D-4*
     1   PKB**2-2.1212868D-5*PKB**3+1.5251024D-6*PKB**4
       CTERM=-6.2838D-8+1.0053242D-7*PKB-5.0668132D-8*
     1   PKB**2+1.0140221D-8*PKB**3-7.1638184D-10*PKB**4
       GAM(1)=CNST+ATERM*TEMPC+BTERM*TEMPC**2+CTERM*TEMPC**3
      ENDIF
      IF(I.EQ.5) THEN
       CCNST=.31425026D0-.38594999D0*PKB+.19967493D0*PKB**2-
     1   .051474242*PKB**3+7.1493778D-3*PKB**4-
     2   5.0621009D-4*PKB**5+1.4326474D-5*PKB**6
       AATERM=-4.7919973D-3+6.1915716D-3*PKB-3.2539637D-3*
     1   PKB**2+8.4557946D-4*PKB**3-1.1806683D-4*PKB**4+
     2   8.3852276D-6*PKB**5-2.3779833D-7*PKB**6
       BBTERM=1.2450826D-5-1.4262612D-5*PKB+5.6269161D-6*
     1   PKB**2-9.5662335D-7*PKB**3+7.7368676D-8*
     2   PKB**4-2.3373356D-9*PKB**5
       CCTERM=-2.9718201D-9+1.7106038D-8*PKB-7.6196485D-9*PKB**2+
     1   1.3511195D-9*PKB**3-1.1115976D-10*PKB**4+
     2   3.3487236D-12*PKB**5
       DDTERM=-1.5475286D-11-3.1107153D-12*PKB+2.7666352D-12*
     1   PKB**2-5.5248696D-13*PKB**3+4.7086811D-14*PKB**4-
     2   1.386475D-15*PKB**5
       EETERM=1.0069036D-14-2.8496996D-15*PKB+4.2102278D-16*
     1   PKB**2-4.2332381D-17*PKB**3+2.8545359D-18*PKB**4-
     2   1.1765163D-19*PKB**5
       GAM(5)=CCNST+AATERM*TEMPC+BBTERM*TEMPC**2+CCTERM*TEMPC**3+
     1   DDTERM*TEMPC**4+EETERM*TEMPC**5
      ENDIF
C     CALCULATE FUGACITY COEFFICIENT OF S2
       GAM(9)=1.0
   10 CONTINUE
```

```
      RETURN
      END
C     ********************************************************
      SUBROUTINE ARDVRK(PP,T,X,VM,FUGCOF)
      IMPLICIT DOUBLE PRECISION (A-H,O-Z)
      DIMENSION X(10),ATOT(10),BI(10),FUG(10),FUGCOF(10)
      DATA RBAR/83.137D0/, MIXNUM/10/
      DATA BI/2.97D1,2.738D1,2.9703D1,1.515D1,1.46D1,2.D1,3.94D1,
     1    2.21D1,4.579D1,4.30D1/
      CALL MRKMIX(T,X,BSUM,ASUM,ATOT)
C     CUBIC SOLUTION OF THE MRK FOR VOLUME
      RATM=82.05D0
      RR=RATM
      TCEL=T-273.15
      P=-1.0D0*RR*T/PP
      Q=(BSUM*RR*DSQRT(T**3)+BSUM*BSUM*PP*DSQRT(T)-ASUM)/(-1.0D0*
     1    PP*DSQRT(T))
      R=-1.0D0*ASUM*BSUM/(PP*DSQRT(T))
      A=(3.0D0*Q-P*P)/3.0D0
      B=(2.0D0*P**3-9.0D0*P*Q+27.0D0*R)/27.0D0
      V1=1
      V2=1
      V3=1
      ROOT=B*B/4.0D0+A**3/27.0D0
      IF(ROOT) 90,80,70
   70 C=B/-2.0D0+DSQRT(ROOT)
      IF(C) 71,72,72
   71 C=DABS(C)
      AA=-1.0D0*C**(1.0D0/3.0D0)
      GO TO 73
   72 AA=C**(1.0D0/3.0D0)
   73 CONTINUE
      D=B/-2.0D0-DSQRT(ROOT)
      IF(D) 75,76,76
   75 D=DABS(D)
      BB=-1.0D0*D**(1.0D0/3.0D0)
      GO TO 77
   76 BB=D**(1.0D0/3.0D0)
   77 CONTINUE
      X1=AA+BB
      V1=X1-P/3.0D0
      GO TO 100
   80 C=B/-2.0D0+DSQRT(ROOT)
      IF(C) 81,82,82
   81 C=DABS(C)
      AA=-1.0D0*C**(1.0D0/3.0D0)
      GO TO 83
   82 AA=C**(1.0D0/3.0D0)
   83 CONTINUE
      D=B/-2.0D0-DSQRT(ROOT)
```

```
      IF(D) 85,86,86
   85 D=DABS(D)
      BB=-1.0D0*D**(1.0D0/3.0D0)
      GO TO 77
   86 BB=D**(1.0D0/3.0D0)
   87 CONTINUE
      X1=AA+BB
      V1=X1-P/3.0D0
      X2=(AA+BB)/-2.0D0
      V2=X2-P/3.0D0
      GO TO 100
   90 THETA=DACOS(B/-2.0D0/DSQRT(A**3/-27.0D0))
      X1=2.0D0*DSQRT(A/-3.0D0)*DCOS(THETA/3.0D0)
      X2=2.0D0*DSQRT(A/-3.0D0)*DCOS(THETA/3.0D0+120.0D0)
      X3=2.0D0*DSQRT(A/-3.0D0)*DCOS(THETA/3.0D0+240.0D0)
      V1=X1-P/3.0D0
      V2=X2-P/3.0D0
      V3=X3-P/3.0D0
  100 CONTINUE
C     PICK LARGEST OF THE THREE VOLUMES FROM THE CUBIC ROOTS
      VIN=V1-V2
      IF(VIN) 110,110,120
  110 VIN=V2
      GO TO 130
  120 VIN=V1
  130 CONTINUE
      VM=VIN-V3
      IF(VIN) 140,140,150
  140 VM=V3
      GO TO 160
  150 VM=VIN
  160 CONTINUE
C     CALCULATE FUGACITIES FROM CORRECT VERSION OF EQ 108
C     IN FERRY AND BAUMGARNER (REV IN MIN VOL 17)
      AM=ASUM
      BM=BSUM
      DO 180 I=1,MIXNUM
      QA=DLOG(VM/(VM-BM))
      QB=BI(I)/(VM-BM)
      QC=2.0D0*ATOT(I)/X(I)/(RATM*DSQRT(T**3)*BM)
      QD=DLOG((VM+BM)/VM)
      QE=AM*BI(I)/(BM*BM*RATM*DSQRT(T**3))
      QF=QD
      QG=BM/(BM+VM)
      QH=DLOG(PP*VM/(RATM*T))
      FUGCOF(I)=DEXP(QA+QB-QC*QD+QE*(QF-QG)-QH)
  180 CONTINUE
   89 RETURN
      END
C     ************************************************************
```

```
      SUBROUTINE H2DIFF(ETOT,IDIREC,DELTAH)
      IMPLICIT DOUBLE PRECISION (A-H,O-Z)
      INTEGER IDIREC
      REAL*8 ETOT(4)
      WRITE(9,10)
10    FORMAT('ENTER ZERO FOR DIFFUSION OUT OF INCLUSION OR'/,
     1     '1 FOR DIFFUSION INTO INCLUSION, AND ENTER THE'/,
     2     'FRACTION OF TOTAL HYDROGEN TO BE DIFFUSED')
      READ(9,*) IDIREC,DELTAH
      IF(IDIREC.EQ.0) THEN
       ETOT(3)=ETOT(3)-ETOT(3)*DELTAH
      ELSE
       ETOT(3)=ETOT(3)+ETOT(3)*DELTAH
      ENDIF
      RETURN
      END
```

The vita has been removed from the scanned document